



SAPIENZA
UNIVERSITÀ DI ROMA

DIPARTIMENTO DI INGEGNERIA STRUTTURALE E GEOTECNICA
DOTTORATO DI RICERCA IN INGEGNERIA GEOTECNICA (20° CICLO)

**SITE CHARACTERIZATION OF ITALIAN RECORDING
STATIONS FOR NEW GROUND MOTION PREDICTIONS**

Giuseppe Scasserra

Tesi per il conseguimento del titolo di “Dottore di Ricerca”

Tutori: Prof. Giuseppe Lanzo (Relatore)
Prof. Beniamino D’Elia
Prof. Fabrizio Mollaioli
Prof. Jonathan Stewart

Roma, Maggio 2008

to Me and to my adorate *Zio Donato*

ACKNOWLEDGMENTS

My first thanks goes to my supervisor prof. Giuseppe Lanzo, for taking me on as a PhD student in geotechnical engineering and for helping me with his knowledge and experience. I also want to thank my italian co-advisors proff. Beniamino D'Elia and Fabrizio Mollaioli for the technical support and precious suggestions.

A special thanks is for prof. Jonathan Stewart, my co-advisor from UCLA, for inspiring, motivating and making me enthusiastic about earthquake engineering and for giving me the chance to work with such a great person he is.

A "Grazie" also to Dr. Paolo Bazzurro for collaborating in this project with his helpful suggestions and support especially in the statistical analyses.

I would like to thank Dr. Robert Kayen for the "lessons" during the SASW campaign in Umbria.

I am glad to meet people like them for which I also have a sincere feeling of friendship.

Ing. Paolo Tommasi, Dr. Copat, Ing. Infantino, Dr. Ponziani from Umbria region administration, Dr. Basili, Dr. Mele and Dr. Castello of INGV are also acknowledged for their help in site and source characterization.

Thanks to my familiy for the patience they always have with me and for supporting me even when I am impossible to support. I hope this thesis can represent reason of pride for my parents, brother, sister and sister in law, so as a motivation for my nephews.

Thanks to my wonderful friends and colleagues Vincenzo and Alessandro for the strong friendship we have.

Thanks to Paolo Compagnone for the wonderful job on the web-site.

Thanks to my *Honeyon*.

INDEX

Chapter 1: INTRODUCTION	1-1
1.1 BACKGROUND AND MOTIVATIONS	1-1
1.2 OBJECTIVE OF THIS THESIS	1-3
1.3 OUTLINE	1-4
Chapter 2: SHORT OVERVIEW ON FACTORS AFFECTING STRONG GROUND MOTION AND MAIN RELATED PARAMETERS	2-1
2.1 INTRODUCTION	2-1
2.2 SOURCE FACTORS	2-1
2.2.1 Magnitude	2-2
2.2.2 Focal Mechanism	2-4
2.2.3 Directivity	2-6
2.2.4 Focal depth	2-7
2.2.5 Hanging wall effect	2-7
2.3 TRAVEL-PATH FACTORS	2-8
2.3.1 Source-to-Site Distance	2-8
2.3.2 Crustal structure	2-9
2.4 SITE FACTORS	2-9
2.5 STRONG MOTION PARAMETERS	2-12
2.5.1 Measures of peak ground motion	2-12
2.5.2 Measures of spectral response	2-14
2.5.3 Measures of energy	2-16
2.5.4 Definitions of ground motion Durations	2-17
Chapter 3: THE ITALIAN ACCELEROMETRIC NETWORK	3-1
3.1 BRIEF NOTES ON THE HISTORICAL DEVELOPMENT OF THE ITALIAN ACCELEROMETRIC NETWORK	3-1
3.2 TYPES OF ACCELEROGRAPHS	3-3
3.3 GEOTECHNICAL AND GEOLOGIC DATA AVAILABLE FOR RECORDING STATIONS	3-8
Chapter 4: GEOTECHNICAL CHARACTERIZATION OF SEVENTEEN UMBRIA- MARCHE RECORDING STATIONS BY THE SASW TECHNIQUE	4-1
4.1 INTRODUCTION	4-1
4.2 THE 1997-98 UMBRIA-MARCHE, ITALY, EARTHQUAKE SEQUENCE AND SELECTED RECORDING STATIONS	4-2

4.3 THE SASW INSTRUMENTATION	4-4
4.4 DISPERSION CURVE EVALUATION AND VELOCITY PROFILE	4-6
Chapter 5: DATABASE OF ITALIAN STRONG MOTION ACCELEROGRAMS	5-1
5.1 INTRODUCTION	5-1
5.2 STRONG MOTION DATASET	5-2
5.2.1 Comparison between corrected data by ESD and PEER processing procedure	5-4
5.3 SOURCE DATABANK	5-7
5.4 SITE DATABANK	5-9
5.4.1 General Consideration	5-9
5.4.2 Estimating velocities for sites without measurements	5-10
5.4.3 EC8 subsoil categories data distribution	5-13
5.5 INSTRUMENT HOUSING	5-9
 Chapter 6: SISMA (Site of Italian Strong Motion Accelerograms): A WEB-DATABASE OF GROUND MOTION RECORDINGS FOR ENGINEERING APPLICATIONS	 6-1
6.1 INTRODUCTION	6-1
6.2 DATABASE SUMMARY	6-2
6.3 SEARCHING; DISPLAYING AND DOWNLOADING DATA	6-3
6.3.1 Earthquake searching	6-3
6.3.2 Station searching	6-6
6.3.3 Recording searching	6-9
 Chapter 7: GROUND MOTION PREDICTION EQUATIONS (GMPEs) FOR ITALY, EUROPE AND WESTERN U.S .	 7-1
7.1 INTRODUCTION	7-1
7.2 GROUND MOTION PREDICTION EQUATIONS	7-4
7.2.1 General formulation and effect of magnitude/distance	7-4
7.3 OVERVIEW OF MOST USED GMPEs	7-6
7.3.1 GMPEs in Italy	7-6
7.3.2 GMPEs in Europe	7-7
7.3.3 The Next Generation of Ground Motion Attenuation Models (NGA)	7-9
 Chapter 8: ADEQUACY OF EMPIRICAL GROUND MOTION MODELS FOR WORLD- WIDE SHALLOW CRUSTAL EARTHQUAKES RELATIVE TO ITALIAN DATA	 8-1
8.1 INTRODUCTION	8-1

8.2 RECENT STUDIES COMPARING EUROPEAN AND CALIFORNIA STRONG GROUND MOTIONS	8-2
8.2.1 Comparison of medians from GMPEs	8-2
8.2.2 Analysis of variance	8-3
8.2.3 Overall goodness-of-fit of model to data	8-4
8.2.4 Interpretation	8-4
8.3 ATTRIBUTES OF NGA AND EUROPEAN GROUND MOTION PREDICTION EQUATIONS	8-5
8.4 DATASET	8-9
8.5 NOTES ON “MIXED RANDOM EFFECT” MODEL FOR REGRESSIONS ANALYSIS	8-11
8.6 DATA ANALYSIS	8-13
8.6.1 Overall GMPE mean and standard deviation terms	8-13
8.7 INTERPRETATION AND CONCLUSIONS	8-27
Chapter 9: SUMMARY AND CONCLUSIONS	8-1
REFERENCES	
APPENDIX A: Results of the SASW testing in Umbria and Marche regions	
APPENDIX B: Sample of recording-station information form	

CHAPTER 1 INTRODUCTION

1.1 BACKGROUND AND MOTIVATIONS

Many engineering seismology and earthquake engineering applications such as attenuation relationships, validation of shaking scenarios and shake maps, dynamic analyses of structural and geotechnical systems require the use of ground motion time histories. In the last twenty years the increasing availability of recorded data (real or natural records), due the development of Internet databases providing free access to a huge number of recordings, resulted in an increasing demand of real accelerograms by the scientific community.

The advantage of using real accelerograms, with respect to synthetic or artificial signals, is that they are genuine records and contain wealth of information about the nature of shaking produced by earthquakes. Specifically real time histories reflect the characteristics of potential ground motions at a specific site. Important characteristics include amplitude of motion, frequency content and duration of shaking. Those are determined by the earthquake source process, the wave propagation effects of the path between the source and the site and the site response.

Site response depend on local site conditions (topography, stratigraphy and geotechnical properties of soil deposits) and it is known to strongly affect seismic ground motion. The variations of ground motion in space, amplitude, frequency content and duration are called “site effects”. Site effects were observed several times during destructive earthquakes based on the intensity and distribution of damages; also real records provided numerous experimental confirmation on the influence of local conditions on the resulting waveforms. Adequate knowledge of local soil conditions is therefore fundamental to the understanding of the modification that a seismic signal undergoes while propagating through a soil deposit up to the surface. Nonlinearity of soil behaviour can also plays an important role in modifying the amplification phenomena with respect to those occurring in linear conditions, the magnitude of these phenomena depending on the intensity of shaking. Subsoil characterization of recording accelerometric stations is therefore a fundamental prerequisite for seismological and engineering applications.

The national strong motion network in Italy consists of analogue and digital accelerographs permanently installed at selected sites distributed in the whole national territory. The first large accelerometer network was realized by ENEL (*Ente Nazionale Energia Elettrica*) between 1975 and 1976. In 1998 the array was acquired by the *Servizio Sismico Nazionale* (SSN) and was named *Rete Accelerometrica*

Nazionale (RAN). The configuration at 2007 includes 298 accelerometers and it is presently operated by *Dipartimento della Protezione Civile* (DPC).

These accelerometers recorded several moderate to large earthquakes in Italy, some of them damaging (e.g., Irpinia earthquake in 1980), thus making the databank of Italian seismic signals one of the richest in the world. The most important source of Italian records is the ESD (European Strong Motion Database) website (<http://www.isesd.cv.ic.ac.uk>) which includes freely downloadable uncorrected and corrected accelerograms, and associated earthquake-, station- and waveform-parameters. However, those records have not been uniformly processed and generally lack the source data. Further, notwithstanding the importance of local soil conditions on the seismic ground motion, site characterization of Italian recording stations is very poor as it has not received much attention in the past.

In particular, level of knowledge of site conditions of recording stations is highly inhomogeneous. Geological information are available for about 300 stations while geophysical and geotechnical data were obtained only for 40 stations (12% of the total number of the stations). For instance, V_s profiles by cross-holes and down-holes measurements are available for some of the stations triggered by the 1976 Friuli and 1980 Irpinia earthquakes. There is therefore an urgent need to improve the geological and geotechnical characterization of the RAN recording stations.

As already stated, the characterization of earthquake loadings for engineering applications generally involves the use of equations based on strong ground motion recorded during previous earthquakes. These equations are often referred to as ground motion prediction equations (GMPEs) or attenuation relations. GMPEs describe the variation of the median and lognormal standard deviation of particular intensity measures (such as peak acceleration, spectral acceleration, or duration) conditional on magnitude, site-source distance, site condition, and other parameters. These equations are crucial to probabilistic seismic hazard analysis and also to deterministic seismic hazard analysis.

The current practice in Italy has been a preference towards the use of local GMPEs derived solely from Italian data. The current national hazard map for Italy ([Working Group, 2004](#)) was developed using slightly modified versions of an Italian GMPEs ([Sabetta and Pugliese, 1996](#)), a European GMPE ([Ambraseys et al., 1996](#)), and GMPEs for particular regions within Italy (e.g., [Malagnini and Montaldo, 2004](#)). These relations are based on relatively small databases; for example the Sabetta and Pugliese (1996) GMPE was derived from an Italian database of 95 recordings from 17 earthquakes. Local databases such as this are naturally smaller than world-wide databases, meaning that error in individual data points have greater influence on the GMPE.

The most recent GMPEs for crustal earthquakes in active regions were developed in United States as part of the Next Generation Attenuation (NGA) project (http://peer.berkeley.edu/products/nga_project.html). These GMPEs are intended to be applicable to geographically diverse regions, the only constraint being that the region is tectonically active and earthquakes occur in the shallow crust.

Because the NGA models represent a major advancement in GMPEs due to the quality and size of the database developed coupled with the relative sophistication of some of the functional forms, it is naturally of interest to determine if the NGA models can be applied in specific geographic regions such as Italy.

1.2 OBJECTIVES OF THIS THESIS

The objective of the research presented here has been focused on different topics. The first was the improvement of the geotechnical characterization of Italian recording stations by means of *ad hoc* in situ investigation. This is aimed at increasing the number of RAN stations for which shear wave velocity profile is available. The ultimate goal was to provide a classification based on synthetic parameter such as V_{S30} (average shear wave velocity in the upper 30 meters) to be used for engineering applications.

The second primary objective was the development of consistent databanks of strong motion accelerograms and their intensity measures, earthquake source parameters and site conditions for recording stations. This consistency, which was one of the major thrusts of the NGA project, means uniform processing of all recordings, classification of geologic site conditions in homogenous format, and systematic compilation of source parameters. This is fundamental for the development of reliable ground motion prediction equations. A second major application of ground motion databases linked to site/source databanks was for dynamic analyses of structural and geotechnical systems. In Italy, dynamic analysis and design using accelerograms has been allowed for civil infrastructure since 2003 (OPCM 3274, 2003), although a recent seismic code (Norme Tecniche per le Costruzioni, 2008) specifically requires the use of natural recordings *in lieu* of synthetic motions for geotechnical applications. There is an urgent need for a database/databank to provide free access to real national accelerograms in order to facilitate such ground motion selection in Italy.

The third objective was related to a broader question of application of world-wide shallow crustal GMPEs in Europe. Specifically this issue was examined by testing the ability of the NGA models to capture the magnitude-scaling, distance-scaling, and site effects represented in the Italian dataset. This testing is of interest for two principal reasons (1) possible application of NGA GMPEs for seismic hazard evaluation in Italy and (2) testing the NGA models against a dataset principally populated by extensional (normal fault) earthquakes, which are poorly represented in the NGA database.

The research work presented in this thesis is the result of a jointed project between the Sapienza University of Rome and University of California Los Angeles (UCLA).

1.3 OUTLINE

The results of this research are organized in nine chapters. Chapter 1 presents the motivation for the current research and the organization of the work.. Many factors are thought to influence strong ground motions and their effects are complex and often interrelated; these factors are discussed in Chapter 2. In the same chapter the identification of parameters that characterize the strong ground motion referred as “intensity measures” (IM) is carried out and most commonly used measures of the seismic motion are reviewed. Chapter 3 describes the Italian accelerometric network (RAN). The development of the RAN is briefly examined with attention essentially devoted to the type of instruments installed and to the geological/geotechnical characterization of the recording stations. For this latter aspect, the need to improve the reliability and the quality of information is recognized. Based on these findings, a site investigation campaign by means of the SASW technique has been conducted in order to obtain the V_S profile in 17 accelerometric stations triggered by the 1997-1998 Umbria –Marche sequence. The results of the tests are illustrated in Chapter 4.

In Chapter 5 the development of an Italian database of strong ground motion recordings and databanks delineating conditions at the instrument sites and characteristics of the seismic sources is presented. The strong motion database consists of 247 corrected recordings from 89 earthquakes and 101 recording stations. Uncorrected recordings were drawn from public web sites and were processed on a record-by record basis using a procedure utilized in the Next-Generation Attenuation (NGA) project. The site databank includes for every recording site the surface geology, a measurement or estimate of average shear wave velocity in the upper 30 m (V_{s30}), and information on instrument housing. Source parameters are drawn from databases maintained (and recently updated) by *Istituto Nazionale di Geofisica e Vulcanologia* (INGV) and include hypocenter location and magnitude for small events ($M \leq 5.5$) and finite source parameters for larger events. Therefore, in this chapter a re-evaluation of the Italian dataset according to standards similar to those utilized for the NGA database is accomplished.

Chapter 6 presents a new website called SISMA, i.e. Site of Italian Strong Motion Accelerograms, which is an Internet site intended to provide freely downloadable high quality Italian strong motion records for engineering applications. This chapter mainly focuses on the principal search criteria being developed within SISMA for the selection of time-histories records involving seismological, ground motion and site parameters.

Chapter 7 summarizes attributes of NGA, European and Italian ground motion prediction equations with respect to magnitude-, distance-, and site-scaling. These GMPEs are formulated with varying degrees of complexity in their functional form as a result of author preference and the size and completeness of the database used in the analysis.

In Chapter 8 the compatibility of NGA models with respect to magnitude-, distance-, and site-scaling implied by Italian strong motion data was investigated by performing the analysis of residuals. Components of the NGA models that are compatible or inadequate relative to the Italian data were

identified. On the basis of these findings, the components of the NGA relations judged to be inadequate were modified while the other features were retained. The modified GMPEs are recommended to be used to evaluate median ground motions for seismic hazard analysis.

Finally Chapter 9 is a summary of the major findings and contributions of this research.

CHAPTER 2 **SHORT OVERVIEW ON FACTORS AFFECTING STRONG GROUND MOTION AND MAIN RELATED PARAMETERS**

2.1 INTRODUCTION

Many factors are considered to affect strong ground motion and a large literature on each of the factors does exist. Traditionally factors are grouped into three categories: source based, travel-path based and those which depend on the local conditions at the site. This separation of factors is followed here in the first part of the chapter.

An overview of some of the most commonly used strong-motion parameters in the technical literature is then reported. These parameters include measures of peak amplitude, spectral response, energy content and duration.

2.2 SOURCE FACTORS

Earthquakes result from the sudden release of elastic strain energy in the Earth's crust because of the rupture on a fault. The rupture begins at one particular point and then propagates along the fault. As the size of an earthquake increases, so does the size of the fault rupture area.

The fault rupture is characterized by a plane or a volume corresponding to the part of the crust from which strain energy is released. The point at which rupture begins is called hypocenter of the earthquake located at some depth below the ground surface (focal or hypocentral depth). The point on the ground surface directly above the hypocenter is called epicenter ([Kramer, 1996](#)).

Fault geometry is intended as the geometrical characterization of the earthquake's source plane, including its orientation. Specifically, the fault plane is well defined if the following parameters are known ([fig. 2.1](#)):

- *width of the fault*, W ;
- *length of the fault*, L ;
- *Top and Bottom depth* - depths of the top edge and bottom edge of the fault, respectively;

- *Strike* - horizontal line produced by the intersection of the fault plane and a horizontal plane; the azimuth of the strike is the orientation of the fault with respect to due North;
- *Dip* - angle between the fault plane and the horizontal plane measured perpendicular to the strike. A vertical fault would have a dip=90°.

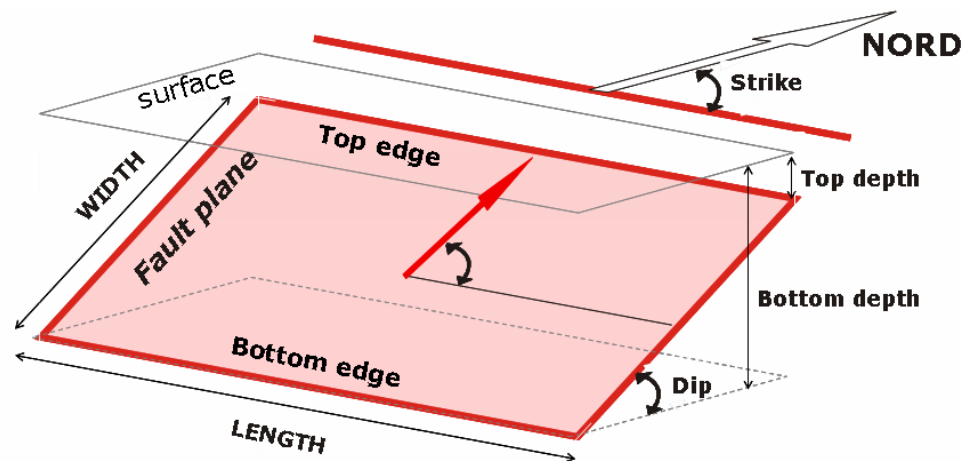


Figure 2.1. Fault plane general scheme and parameters geometric description (Basili et al., 2007)

Magnitude, rupture mechanisms, directivity and focal depth are parameters that define the nature of the resulting motion.

2.2.1 Magnitude

Magnitude is an empirical measurement of the size of an earthquake which is not directly related to a physical quantity but is calculated from some gross characteristic (usually wave amplitudes) of earthquake seismograms, therefore most magnitude measurements are instrumental. Magnitude can be approximately related to the energy released during the earthquake.

The concept of magnitude was first introduced by Richter (1935), who defined a local magnitude scale for southern California. Since then many different magnitude scales have been introduced. The mostly used in practice are :

Local magnitude, M_L . It was originally defined (Richter, 1935) as:

$$M_L = \log_{10} A - \log_{10} A_0(\Delta) \quad (2.1)$$

where A is the maximum recorded amplitude in μm at a distance of 100 km from the earthquake on a Wood-Anderson seismograph (period 0.8 s, magnification 2800, damping 0.8 of critical) and $A_0(\Delta)$ is an empirically derived distance calibration function where Δ is epicentral distance.

Surface Wave Magnitude, M_s . Originally introduced by [Gutenberg and Richter \(1936\)](#) who used the maximum horizontal ground displacement, A_{max} , from waves with periods around 20 s. The surface wave magnitude is obtained from:

$$M_s = \log A + 1.66 \log \Delta + 2.0 \quad (2.2)$$

where A is the maximum ground displacement in microns and Δ is the epicentral distance in degrees.

The surface wave magnitude is most commonly used to describe the size of shallow (less than about 70 km focal depth), distant (further than about 1000 km) moderate to large earthquakes ([Kramer, 1996](#)).

Body Wave Magnitude, m_b . It is based on the amplitude of the first few cycles of p-waves (Gutenberg, 1945) which are not strongly influenced by the focal depth (Bolt, 1989). It is expressed as:

$$m_b = \log A - \log T + 0.01 \Delta + 5.9 \quad (2.3)$$

where A is the p-wave amplitude in micrometers and T is the period of the p-wave, usually about 1s ([Kramer, 1996](#)).

Moment magnitude, M_w . By considering the radiated seismic energy released during earthquakes [Kanamori \(1977\)](#) and [Hanks & Kanamori \(1979\)](#) define a moment-magnitude scale, M_w , by the equation:

$$M_w = (2/3) \log M_0 - 6.03 \quad (2.4)$$

where M_0 is the seismic moment, measured in Nm, defined as follows.

Seismic moment, M_0 . An earthquake fault is mathematically modelled by a shear displacement discontinuity (dislocation) across a surface in an elastic medium. The dislocation is equivalent to a distribution of double couples on this surface whose total moment is ([Kanamori and Anderson, 1975](#)):

$$M_0 = \mu A \bar{D} \quad (2.5)$$

where μ is the rupture strength of the material along the fault, A is fault area and \bar{D} is the average slip along the fault.

M_L , M_s and m_b all saturate, i.e. above a certain level there is no increase in magnitude with increase in earthquake size. Moment magnitude is the only magnitude scale that is not affected by saturation. The latter phenomenon is related to the measured ground-shaking characteristics that for strong earthquakes become less sensitive to the size of the earthquake than for smaller earthquakes. M_w does not saturate because it is based on a direct measure of factors that produce rupture along the fault.

A comparison of the various magnitude scales is reported in [fig. 2.2](#). Saturation effect is evidenced by the flattening of the different curves at higher magnitudes: the m_b , M_L and M_s saturate at magnitude values of about 6, 7 and 8 respectively. From the plot is evident that M_w can be basically assumed equal to M_L for $M_w \leq 6.2$ and to M_s for $6.2 \leq M_w \leq 8.8$. In the figure is also reported for comparison the magnitude M_{JMA} , that is the Japanese local magnitude scale.

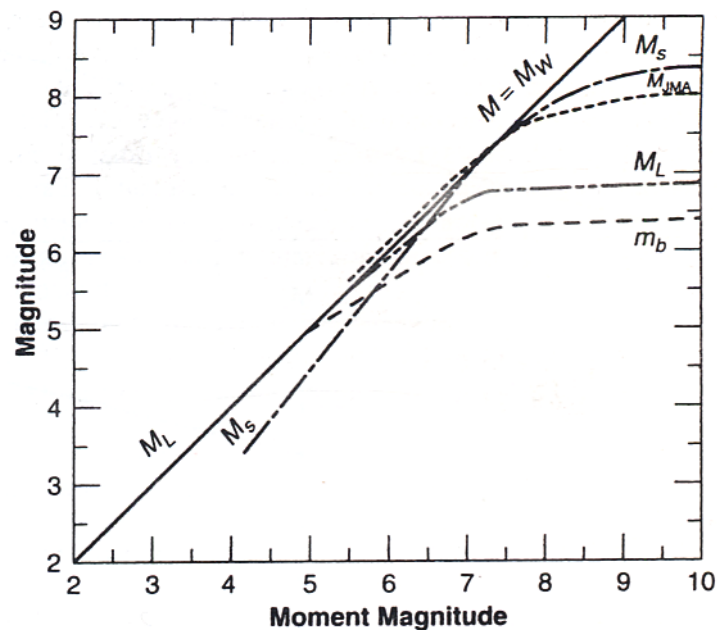


Figure 2.2. Relationship between moment magnitude and the other magnitude definitions (Idriss , 1985).

2.2.2 Focal Mechanism

Focal mechanism indicates the type of movement occurring on a fault. There are two main types of focal mechanism ([Kramer, 1996](#)):

Dip-Slip: Fault movement occurs primarily in direction of slip (or perpendicular to strike). Two types of movement are possible:

Normal - Horizontal component of dip-slip movement is extensional and material above the inclined fault (the hanging wall) moves downwards relative to material below the fault (the foot wall); it is associated with tensile stresses in crust and results in horizontal lengthening of the crust.

Reverse - Horizontal component of dip slip movement is compressional and material above the inclined fault (the hanging wall) moves upwards relative to material below the fault (the foot wall). [Oglesby et al. \(1996\)](#) define all compressional earthquakes with dip angle more than 45° as reverse. Results in horizontal shortening of the crust. A special type of reverse fault is:

Thrust - Occurs when the fault plane has a small dip angle. [Oglesby et al. \(1996\)](#) define all compressional earthquakes with dip angle less than 45° as thrust.

Strike-slip: Fault movement occurs parallel to strike. Usually such faults are nearly vertical and can produce large movements. Two types of movement are possible:

Right lateral strike-slip - Observer standing near such a fault would observe the ground on the opposite side of the fault moving to the right.

Left lateral strike-slip - Observer standing near such a fault would observe the ground on the opposite side of fault moving to the left. The angle between the rupture plane and the surface on the hanging wall side is always acute and it is always obtuse on the foot wall side.

Many earthquakes contain a mixture of dip-slip and strike-slip movements, such focal mechanisms are called *oblique*. The above mentioned focal mechanisms are summarized in [fig. 2.3](#).

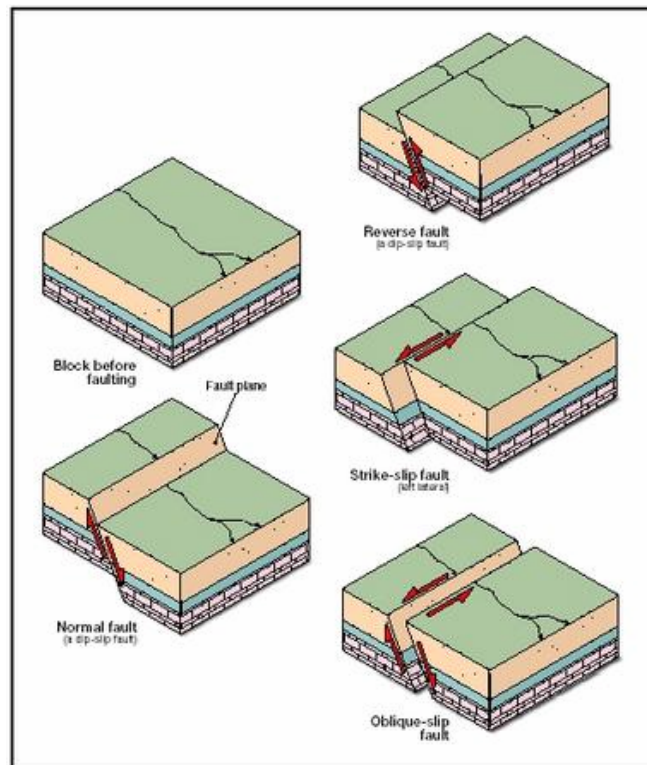


Figure 2.3. Fault ruptures mechanisms

2.2.3 Directivity

Rupture directivity causes spatial variations in ground motion amplitude and duration. This is especially important for the estimation of ground motion in the near-fault zone.

Forward directivity occurs when the ruptures propagates towards a site and the direction of the slip on the fault is also towards the site. It takes place when the velocity of fault rupture is almost as large the shear wave velocity of the rocks near the source. In this situation the wave front arrives as large pulse of motion oriented in the direction perpendicular to the fault. It occurs at the beginning of the record and it is polarized in the strike-normal direction. The pulse of motion is typically characterized by large amplitude at intermediate to long periods and the overall motion is generally of short duration.

Backward directivity occurs when a site is located near the epicentre and it is the condition in which the rupture propagates away from the site. It is characterized by motions with relatively long duration and long amplitude at long periods.

Figure 2.4 shows two near-fault recordings of the Landers 1992 earthquake in which the effects of forward and backward directivity can be appreciated.

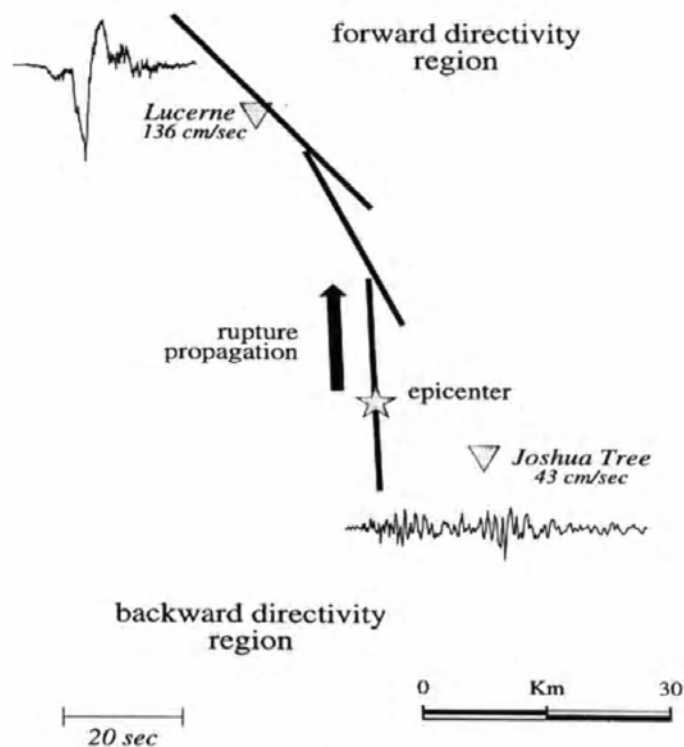


Figure 2.4. Near-field velocity time-histories from accelerograms of 1992 Landers earthquake in California, showing the effect of rupture directivity on the resulting motion (Sommerville et al., 1997)

2.2.4 Focal depth

The usual measure of the depth of an earthquake is the focal (or hypocentral) depth which is the depth at which the rupture begins. The focal depth is only important for small magnitude earthquakes, when the rupture dimensions are small compared to the thickness of the seismogenic layer of the crust; in this case the focal depth is the parameter that controls how deep below the surface the source of energy is located. Conversely, larger earthquakes, which do rupture the entire seismogenic layer, usually nucleate at the base of the seismogenic layer so focal depth is less important.

2.2.5 Hanging wall effect

In recent thrust earthquakes, Northridge (Abrahamson and Somerville, 1996) and Chi-Chi (Shin et al., 2000), it has been found that strong ground motion is often larger at stations on the hanging wall compared with stations on the foot wall.

The most obvious reason is simply that hanging-wall stations are closer to most of the source than foot-wall stations with the same rupture distance (fig. 2.5). Therefore stations on the hanging wall will receive more energy, and hence ground motions will be larger, than stations on the foot wall.

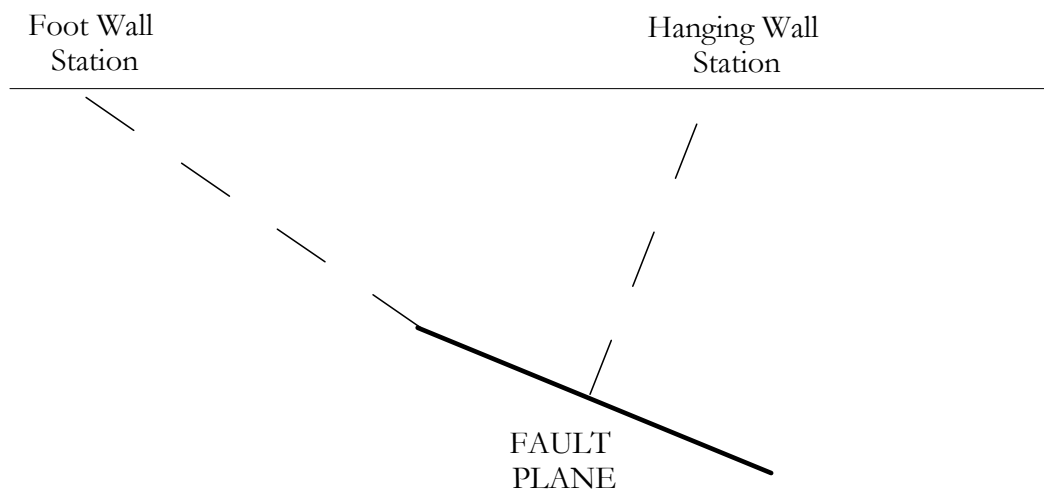


Figure 2.5: Diagram showing how a hanging-wall station is closer to most of the source than a footwall station at the same rupture distance (Douglas, 2001)

2.3 TRAVEL-PATH FACTORS

The travel-path is the particular route that the energy released at the earthquake source will travel along to arrive at a particular site. The travel-path effects include attenuation of wave amplitude, reflection and refraction at the interface of different rock types and wave scattering from small-scale heterogeneities in the crust. The main parameters that characterize the travel-path are the distance and the crustal structure.

2.3.1 Source-to-Site Distance

The distance between the point of occurrence of the earthquake and a given site is a reference parameter. Below the description of the most used distance definitions is illustrated for vertical and dipping faults (fig 2.6):

- *Epicentral distance* (r_{epi}) is the surface distance between site and epicentre of the earthquake;
- *Hypocentral distance* (r_{hypo}) corresponds to the distance between hypocenter and the given site;
- *Joyner & Boore distance* (r_{jb}) is defined as the closest distance, measured on surface, from the projection on surface of the fault plane and the given site;
- *Rupture distance* (r_{rup}) is the buried closest distance between the fault plane and the given site.

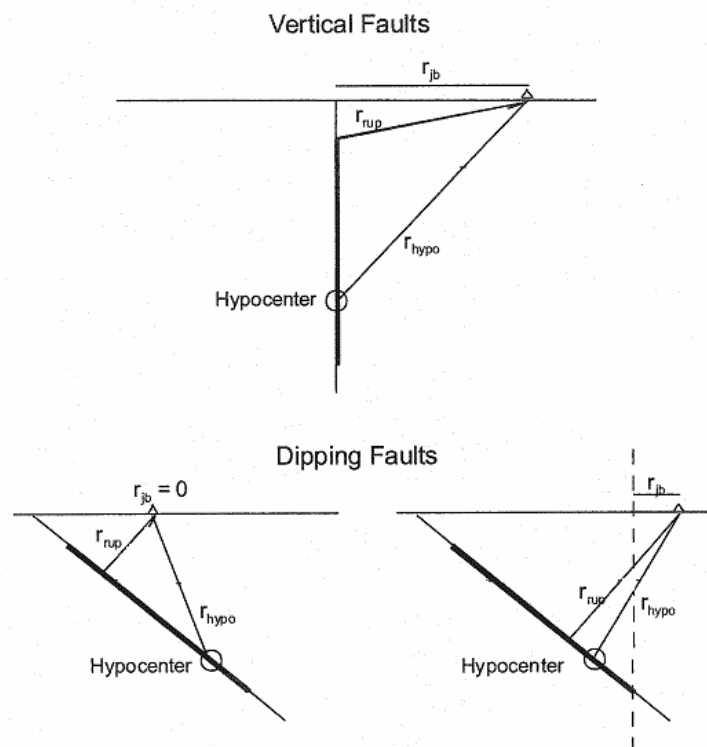


Figure 2.6. Distances geometric definitions for vertical and dipping faults (Abrahamson and Shedlock, 1997)

2.3.2 Crustal structure

Another parameter characterizing the travel-path is the physical composition of the crust and its tendency to transmit or absorb seismic waves energy. When body waves travel through the crust and into the mantle, they encounter boundaries or discontinuities in which they can experience both reflection and refraction.

Waves attenuate due to internal friction, also called intrinsic attenuation, the effect of which can be summarised by the parameter Q . For a volume cycled at a frequency ω , a dimensionless measure of material friction (or anelasticity) is (Aki and Richards, 1980):

$$\frac{1}{Q(\omega)} = \frac{\Delta E}{2\pi E} \quad (2.6)$$

where ΔE is the energy lost in each cycle due to imperfections in elasticity of material and E is the peak strain energy in volume. The Q parameter is related to the damping ratio (D) usually used in soil dynamics by the following equation:

$$\frac{1}{Q(\omega)} = 2D \quad (2.7)$$

where:

$$D = \frac{\Delta E}{4\pi E} \quad (2.8)$$

2.4 SITE FACTORS

When seismic waves approach a site, they undergo modifications while propagating through surface deposits (fig. 2.7). The variations of ground shaking in space, amplitude, frequency content and duration are called “site effects”. Site effects include primarily the effects of impedance contrast of surface soil deposits to the underlying bedrock, or firm soil considered as rock. They also include deep basin effects, and basin edge effects, produced from strong lateral geological discontinuities (e.g. faults). Finally, site effects also include spatial variation of ground shaking characteristics due to surface topography (Lanzo and Silvestri, 1999).

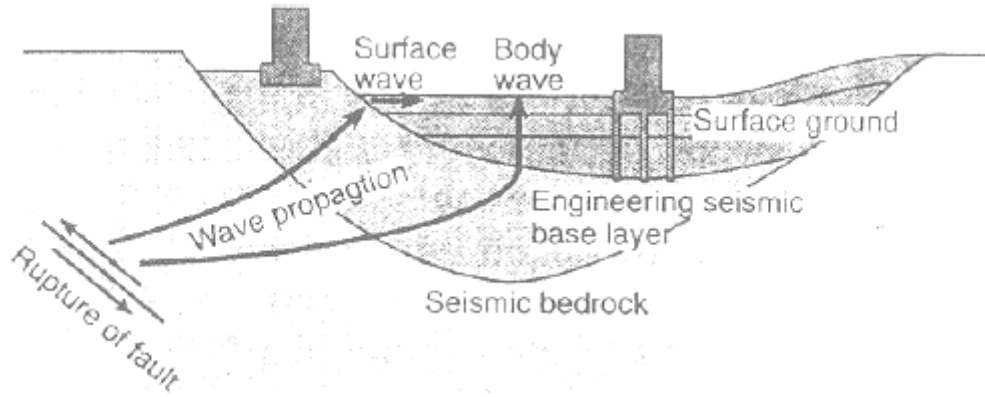


Figure 2.7. Schematic illustration of the wave propagation from fault to ground surface (Pitilakis, 2004)

The fundamental phenomenon responsible for the amplification of motion in soil deposits is the trapping of seismic waves due to impedance contrast. Moreover, the possible interference between the trapped waves leads to resonance effects depending on the geometrical and mechanical characteristics of the soil deposits. For a simple horizontal layered visco-elastic homogeneous soil deposit (1D), resonance effects occur at the natural frequencies of the soil deposit, defined as:

$$f_n = \frac{V_s(2n-1)}{4H} \quad n=1,2,\dots,\infty \quad (2.9)$$

where H is the depth of soil deposit and V_s is the shear wave velocity of the deposit. Specifically, the maximum amplification (A_{\max}) is reached for the *fundamental frequency*

$$f_1 = \frac{V_s}{4H} \quad (2.10)$$

and is given by the expression:

$$A_{\max}(f_1) = \frac{1}{\frac{1}{I} + \frac{\pi D}{2}} \quad (2.11)$$

The term I is defined as *impedance contrast* between soil and the bedrock:

$$I = \frac{\rho_b \cdot V_{s,b}}{\rho_s \cdot V_{s,s}} \quad (2.12)$$

being ρ_b , $V_{s,b}$ and ρ_s , $V_{s,s}$ mass density and shear wave velocity of bedrock and soil respectively, and the product ρV_s the impedance. The amplification due the described phenomenon is also called “stratigraphic or 1D effect”.

On the contrary, the expression “basin effects” is related to the influence of basin configuration on ground motions. Basins generate local surface waves, which subsequently get trapped within the soft layers. Such energy trapping leads in turn to increased amplification with respect to the classical 1D case. Beside those “diffraction” phenomena, basin-edge effects occur as well. Those are caused by constructive interference between direct S waves propagating with an almost vertical travel path through the soil deposits, and diffracted surface waves generated at the basin-edge (Bard and Riepl-Thomas, 1999).

If the semi-length of the soil structure is comparable to its thickness (deep basins), and the reverberating back and forth surface waves are in phase, the waves interfere with each other leading to 2D resonance patterns. The same resonance effects are involved in the seismic wave modulation due to 3D soil structures. The consideration of the second and third lateral dimension in the wave propagation phenomena, in case of 2D and 3D resonance, leads to an increase in ground motion amplification and a shift towards higher values of the peak frequencies (fig. 2.8).

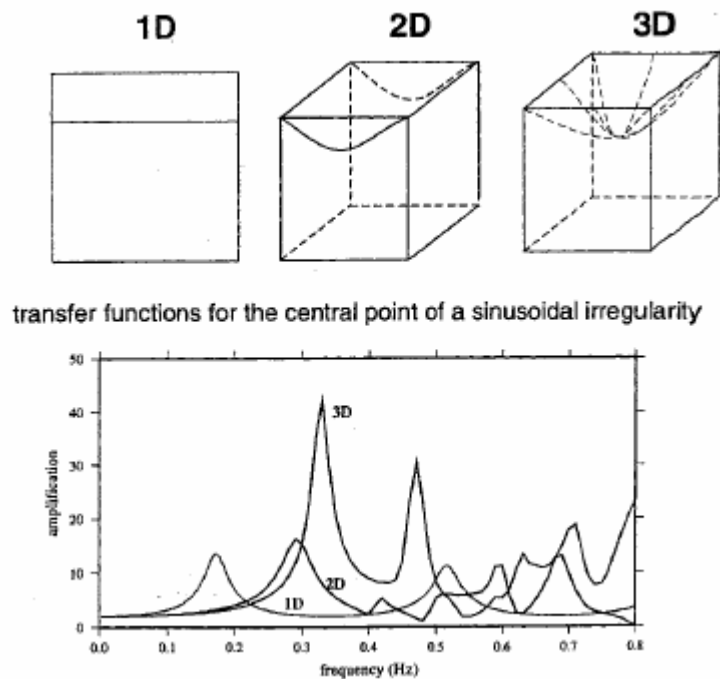


Figure 2.8. Spectral responses computed at the basin center for 1D, 2D and 3D models of semi-shaped basin surface (Riepl, 1997)

In 2D or 3D conditions, amplification can also be enhanced by “topography effects”. The term refers to the variations in ground motion due to the geometry of the ground surface. The damage pattern during earthquakes often shows that most damage tends to concentrate around hilltops and slope crests. Moreover, there are clear instrumental evidence that surface topography affects both the amplitude and frequency content of ground motion (Bard and Riepl-Thomas, 1999). It is generally recognized (Pitilakis, 2004) that the ground motion is amplified at ridge tops increasing with the sharpness of the relief. Moreover, the topographic amplification is band-limited, the maximum effects corresponding to incident wavelengths comparable to the horizontal dimension of the ridge. Regarding the main physical

phenomena responsible of topographic effects, the following factors can be identified: the sensitivity of the surface motion to the incidence angle; the focusing or defocusing of seismic waves reflected along the topographic surface; the diffraction of body and surface waves, leading to interference patterns between the direct and diffracted waves (Bard and Riepl-Thomas, 1999). If topographic amplification is satisfactorily understood from a qualitative point of view, its magnitude is still controversial being the instrumental amplification factors generally appreciable higher than those computed by numerical analyses. This quantitative discrepancy can be explained mainly from the insufficient knowledge of the geological and geotechnical site characteristics which leads to amplification factors that couple both stratigraphic and topographic effects.

Nonlinearity behaviour of soil manifest itself in the form of decreases of shear modulus and increases in material damping as the shear strain is increased. This inelastic behaviour has two main consequences: 1) decreases in fundamental frequency $f_0=1/T_0$, which cause changes in the spectral amplification; 2) substantial reduction in peak acceleration, especially at high frequencies, due to increased damping.

2.5 STRONG-MOTION PARAMETERS

There are many different parameters proposed in the literature to measure the characteristics of the ground shaking. These parameters are reviewed and classified in this section under the sub-headings of:

- measures of peak ground motion;
- measures of spectral response;
- measures of energy;
- definitions of ground-motion duration.

2.5.1 Measures of peak ground motion

Peak ground acceleration (PGA)

Peak ground acceleration is undoubtedly the most widely used parameter for characterising strong motion. It is the maximum absolute value of acceleration in a time-history. However, the use of PGA has many limitations; in particular PGA is generally poorly correlated with damage. Both a short-duration impulse of high-frequency and a long-duration impulse of low frequency may have the same PGA, thus producing very different response in structural or geotechnical systems (fig. 2.9)

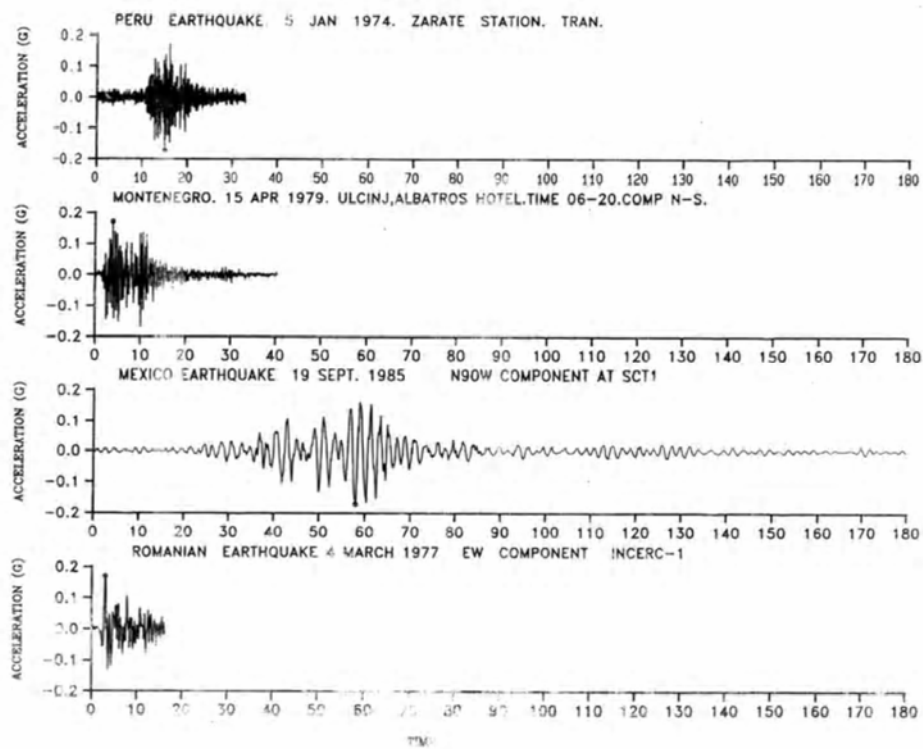


Figure 2.9. Acceleration time-histories with identical values of PGA (Bommer, 1991).

Peak ground velocity (PGV)

The peak ground velocity is the maximum velocity obtained from the ground velocity time-series, which is found by integrating properly filtered and corrected accelerograms. The integration of the accelerogram increases the sensitivity of the PGV to the filtering and correction processes applied to remove the digitisation noise from the record, which tends to attenuate high-frequency components of the motion and enhance low-frequency components.

Peak ground displacement (PGD)

Peak ground displacement is taken from the ground displacement time-series which is obtained by double integration of the acceleration time-series. As the integration process magnifies errors the ground displacement time-series is more sensitive to filtering techniques than ground acceleration or velocity time-series. An additional issue is that, without other data such as Global Positioning System (GPS) measurements, it is impossible to determine if there is any permanent ground deformation recorded by analogue accelerographs as they do not record the start of the ground motion. This has led to the common practice of adjusting the base-line of accelerograms to ensure a zero initial and final displacement.

2.5.2 Measures of spectral response

Elastic response spectra

The elastic response parameters are derived from the solution of the equations of motion for a viscously damped elastic Single Degree of Freedom (SDOF) system:

$$ma + cv + ku = -ma_g \quad (2.13)$$

where m is the mass, a is the absolute acceleration of the mass, c is the viscous damping, v is the relative velocity between the mass and the ground, k is the elastic stiffness, u is the relative displacement between the mass and the ground and a_g is the acceleration of the ground. It is generally more convenient to express the characteristics of the system in terms of its natural period, T_0 , or natural frequency, ω_0 , and damping ratio, β :

$$T_0 = \frac{1}{2\pi} \sqrt{\frac{m}{k}} \quad (2.14)$$

$$\omega_0 = \sqrt{\frac{k}{m}} = \frac{2\pi}{T_0} \quad (2.15)$$

$$\beta = \frac{c}{2m\omega_0} \quad (2.16)$$

Substituting these into equation (2.9) yields:

$$a + \beta 2\omega_0 v + \omega_0^2 u = -a_g \quad (2.17)$$

Equation (2.13) can be solved to find the relative displacement $u(t)$ under the action of an arbitrary ground acceleration time-series by integration or by solving Duhamel's convolution integral. Duhamel's integral describes the response in terms of the input ground-motion amplitude and the time of the motion. The response at any given time is found by multiplying the ground-motion amplitude at each instant by a harmonic transfer function and a weighting function that decreases the influence of the ground motion on the response amplitude with time:

$$u(t) = -\frac{1}{\omega_d} \int_0^t a_g(\tau) e^{-\beta\omega_0(t-\tau)} \sin[\omega_d(t-\tau)] d\tau \quad (2.18)$$

where ω_d is the damped circular frequency $\omega_d = \omega_0(1-\beta^2)$ and τ is the time of the ground acceleration. The relative velocity is found by differentiating equation (2.14) and the absolute acceleration found using equation (2.13).

Response spectra of spectral acceleration, S_a , spectral velocity, S_v , and spectral displacement, S_d , are constructed by plotting the maximum response quantity required for many SDOF systems with a range of spectral periods or frequencies (fig. 2.10). They therefore provide a convenient means of summarizing the peak response of all possible SDOF systems to a particular component of ground motion (e.g., Chopra, 1995)

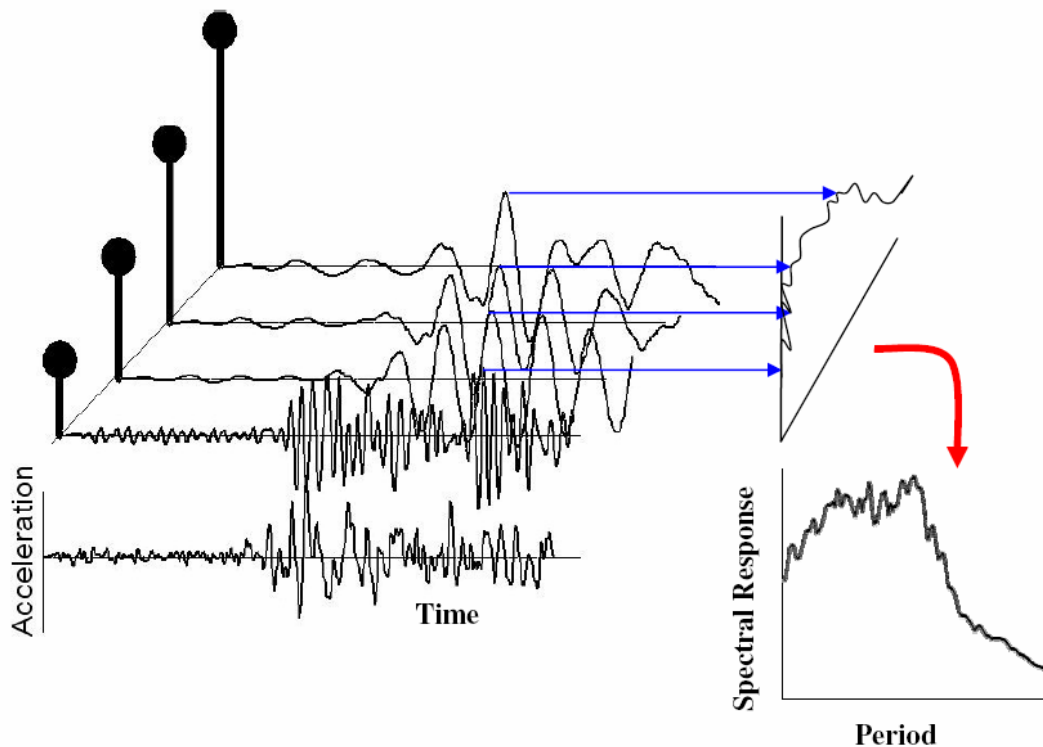


Figure 2.10. – Illustration of construction of response spectrum. Maximum response of each SDOF system is plotted against the period of the system

Approximate relationships exist between spectral acceleration, velocity and displacement. As these relationships are not exact the resulting values are called the pseudo spectral acceleration (PSA) and pseudo spectral velocity (PSV) respectively:

$$\text{PSA} = \left(\frac{2\pi}{T}\right)^2 S_d \quad (2.19)$$

$$\text{PSV} = \left(\frac{2\pi}{T}\right) S_d \quad (2.20)$$

A limitation of the response spectra is that they do not provide any information on the duration of ground shaking.

Spectrum intensity

Housner (1952) was one of the first authors proposing that the area under the velocity response spectra be used as a measure of the destructiveness. The Housner Spectrum Intensity (SI) is defined as:

$$SI = \int_{0.1}^{2.5} PSV(T, \xi) dT \quad (2.21)$$

where PSV is the pseudo-velocity spectrum curve and ξ is the damping coefficient.

Fourier amplitude spectrum

The Fourier transform decomposes a function into a spectrum of harmonic, sinusoidal components that, if summed, would make up the original function. Any harmonic signal is completely described if the amplitude and phase of the harmonic is known. Indeed, there are two types of Fourier spectra: Fourier amplitude spectra, which contain information on the amplitude of the harmonics, and Fourier phase spectra, which contain information on the phase. As it is the amplitude of the motions that are usually of most interest, only Fourier Amplitude Spectra are usually presented.

An example of Fourier Amplitude Spectrum from a natural recording is illustrated in [fig. 2.11](#).

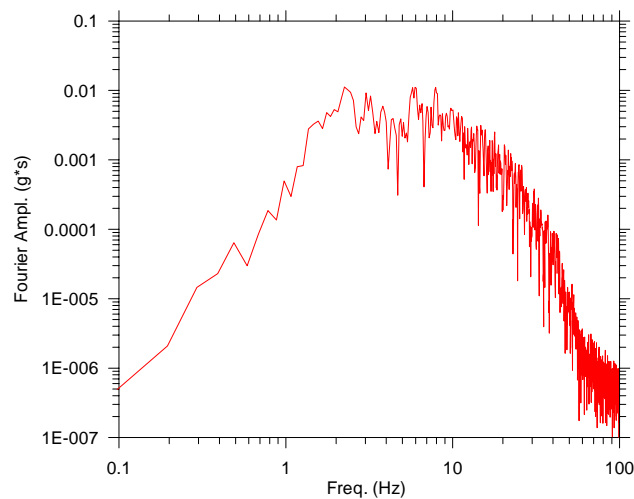


Figure 2.11. – Fourier Amplitude Spectrum from Genio Civile Station from 1972 Ancona earthquake (Italy)

2.5.3 Measures of energy

Arias Intensity

Many measures of energy have been proposed over the years, but the most widely used parameter is the Arias intensity (AI) ([Arias 1970](#)):

$$AI = \frac{\pi}{2g} \int_0^d a_g^2(t) dt \quad (2.22)$$

where g is the acceleration due to gravity, a_g is the ground acceleration and d is the total duration of the record. This intensity measure can be plotted as a function of time to form the Husid plot ([Husid 1969](#)) ([fig. 2.12](#)).

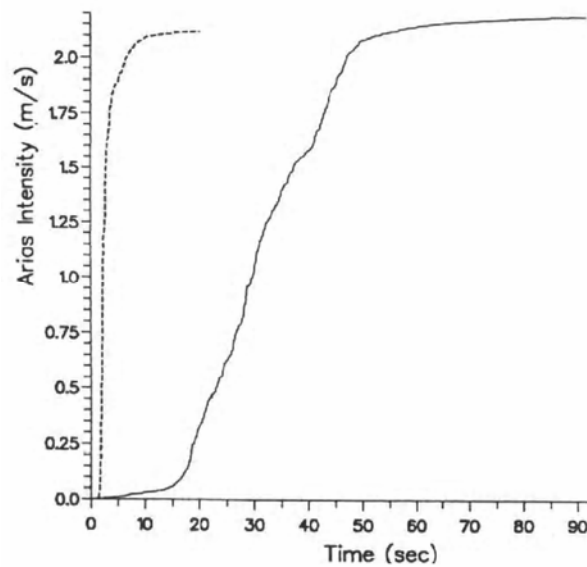


Figure 2.12. – Husid plot for combined horizontal components for two accelerograms recorded in San Salvador, with the same total energy but a different periods of time. Ms=7.3 for the offshore earthquake in 1982 (solid line) and Ms=5.4 for the local earthquake in 1986 (dashed line) (Bommer, 2001).

Damage potential

Araya and Saragoni (1980) and Saragoni (1985, 1990) proposed that the destructiveness of an earthquake is proportional to the energy contained in each pulse of motion. They use parameter, P_D , to measure the potential for damage as follows:

$$P_D = \frac{AI}{v_0^2} \quad (2.23)$$

where AI is Arias Intensity and v_0^2 is the intensity of zero crossings per second.

2.5.4 Definitions of Ground-Motion Duration

The duration of ground motion is related to the time required for rupture to develop across the fault surface, which is a function of the magnitude. There are a number of duration measures commonly used. This section briefly summarises the work of Bommer and Martínez-Pereira (1999) who conduct extensive reviews of the different definitions of duration.

Duration definitions can be divided into three groups: bracketed, uniform and significant durations. Each of these definitions is briefly described in the following sections.

Bracketed duration (D_B) measures are defined as the total time elapsed between the first and last excursions of a specified acceleration level, a_0 as illustrated in fig. 2.13. Usually it is assumed $a_0=0.05g$. The advantage of this definition is that it is conceptually simple. The disadvantage is that it considers only the

first and last excursions of the specified threshold and ignores the characteristics of the strong shaking phase. This can result in long durations being estimated for earthquakes with small sub-events occurring after the main shock.

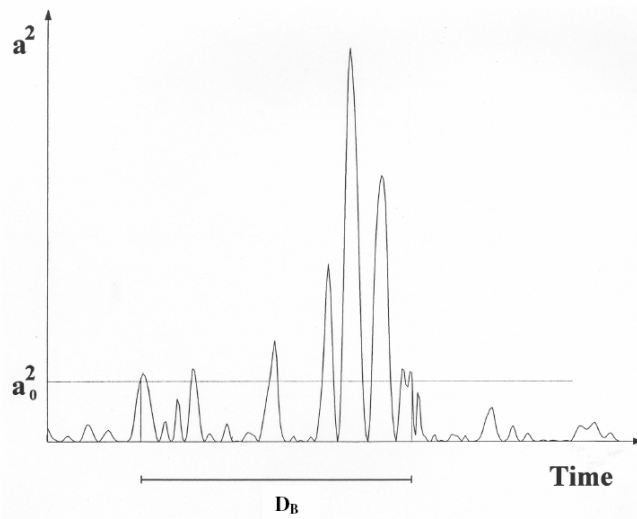


Figure 2.13. - Definition of Bracketed Duration (Bommer and Martínez-Pereira, 1999)

Uniform durations (D_U) are also defined by a threshold level of acceleration, a_0 , but rather than as the interval between the first and last excursions that exceed this level, the duration is defined as the sum of the time intervals during which the acceleration is greater than the threshold. The concept of uniform duration is illustrated in [fig. 2.14](#). This definition is less sensitive to the threshold level than the bracketed duration, but it has the disadvantage that it does not define a continuous time window of strong shaking.

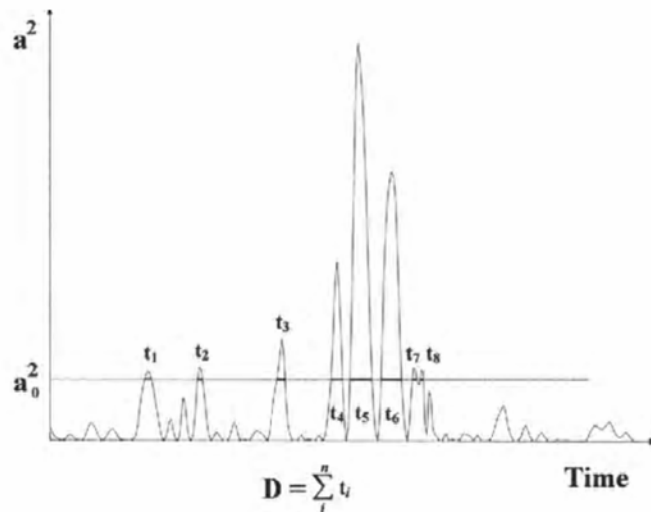


Figure 2.14. – Definition of Uniform Duration (Bommer and Martínez-Pereira, 1999)

Significant duration measures are based on the accumulation of energy in the accelerogram represented by the integral of the square of the ground acceleration, velocity or displacement. If the integral of the ground acceleration is employed then the quantity is related to the Arias intensity, AI. The significant duration is defined as the interval over which some proportion of the total integral is accumulated. This is illustrated for arbitrary limits on a plot of the build-up of Arias intensity, known as a Husid plot (Husid 1969), in [fig. 2.13](#). Significant duration measures have the advantage that they consider

the characteristics of the entire accelerogram and define a continuous time window in which the motion may be considered as strong. A common measure of significant duration is that defined by Trifunac and Brady (1975) related to the interval between 5% and 95% of AI.

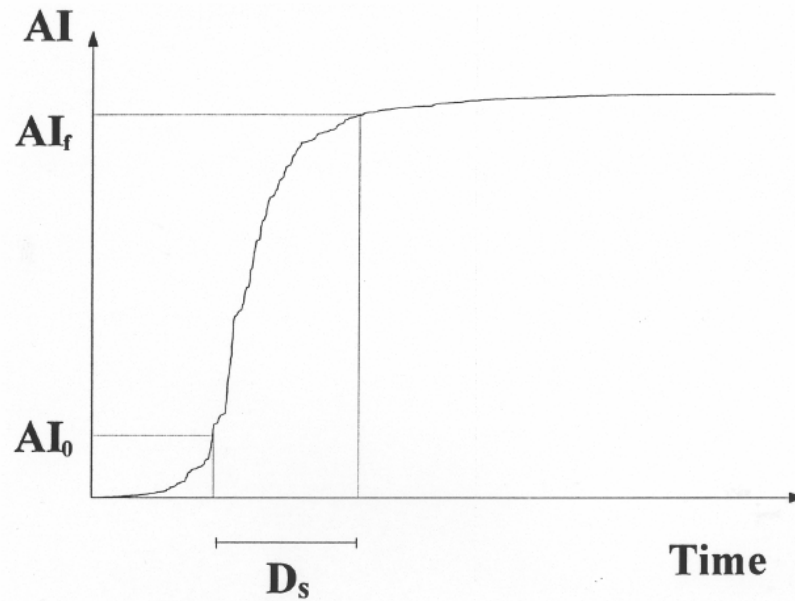


Figure 2.13. - Definition of Significant Duration (Bommer and Martínez-Pereira 1999)

All definitions of duration require a threshold level at which the ground motions are considered to be strong, and the duration measured. Depending on the duration measure employed this level can be defined as a fixed absolute value for all records, or can be a relative measure which is expressed as a fraction of the peak motion or the Arias Intensity of each record. This difference in definition is critical as it changes the behaviour of duration with site-to-source distance.

CHAPTER 3 THE ITALIAN ACCELEROMETRIC NETWORK

3.1 BRIEF NOTES ON THE HISTORICAL DEVELOPMENT OF THE ITALIAN ACCELEROMETRIC NETWORK

The national strong motion network in Italy consists of analogue and digital accelerographs permanently installed at selected sites distributed in the whole national territory with the exclusion of Sardinia.

The first large Italian accelerometer network was installed starting from the mid-1970s by ENEL (*Ente Nazionale Energia Elettrica*). The network was originally designed by ENEA (*Ente per le Nuove Tecnologie, l'Energia e l'Ambiente*) and then realized by ENEL between 1975 and 1976, within a joint project “ENEA-ENEL Commission for the study of seismic problems”, especially devoted to the seismic design of nuclear power plants. This early network recorded for over fifteen years several moderate to large earthquakes in Italy, some of them damaging (e.g., Irpinia earthquake in 1980).

In 1998 the array, which at that time included 237 analogue instruments, was acquired by the *Servizio Sismico Nazionale* (SSN) and was named *Rete Accelerometrica Nazionale* (RAN). Since 1998 a technical upgrading has been conducted by the SSN, which in 2001 merged into the *Dipartimento della Protezione Civile* (DPC), switching the oldest analogue instruments with new generation digital ones and increasing the number of measurements points adding new digital recording devices in areas considered at higher seismic hazard; in particular the location of each station was selected on the basis of a statistical analysis of the distribution of historical earthquakes with intensity greater than VI MCS (Marsan, 1998). As an example, 14 digital accelerometric stations were installed in Eastern Sicily, since is one of the most seismic areas in Italy, in selected locations taking into account the geological setting and signal to noise ratio. Over time, the RAN analogue instruments will be replaced with digital instruments, the final goal being a fully digital network of 400 recording instruments with a direct and real time connection to the acquisition center in Rome (RAN Data Center). More over, it is also planned a uniform spatial distribution of the accelerometers among the nation with a grid of 25-30 km at least in the most seismic zones (<http://www.protezionecivile.it/>).

The configuration at 2007 includes 298 accelerometers (fig. 3.1), 130 are analogue (i.e., Kinematics SMA-1 or RFT250) and 168 are relatively modern digital instruments (i.e., Kinematics Altus ETNA, Altus Everest), 159 of them optioned by a GSM/GPRS modem for data transmission (<http://www.protezionecivile.it/>).

Other than RAN, some local networks were also installed in the past years operated by public administrations or research institutions. For instance, ENEA owns permanent networks in particular area of interest such as Norcia and Cerreto di Spoleto in Umbria region, equipped with analogue and digital instruments respectively (<http://protprev.casaccia.enea.it/>).

Another main local network is owned by the *Università di Trieste, Dipartimento di Scienza della Terra*, which starting from 1993 developed the *Rete Accelerometrica Friuli Venezia Giulia* (RAF); over the years 30 recording stations were installed 9 of which subsequently dismissed (<http://www.dst.units.it/RAF06/RAF/index.html>). The RAF covers just the north-eastern part of the national territory, as illustrated in Fig. 3.2. Other local networks include those developed in Campania and Basilicata regions, operated the first by institute of *Analisi e Monitoraggio del Rischio Ambientale (AMRA)* and *Università di Napoli* and the second by the *Università della Basilicata*, and that in Northern Italy operated by *Istituto Nazionale di geofisica e Vulcanologia INGV* Milano; several accelerometer stations throughout Italy are also operated by Earthquake National Center of INGV.

Finally, it should be mentioned some temporary networks focused on the study of local effects, such as stations located in Umbria during the 1997-98 Umbria-Marche seismic events, as part of the so called “Rete di Pronto Intervento Accelerometrico del Servizio Sismico Nazionale (RAM)”.

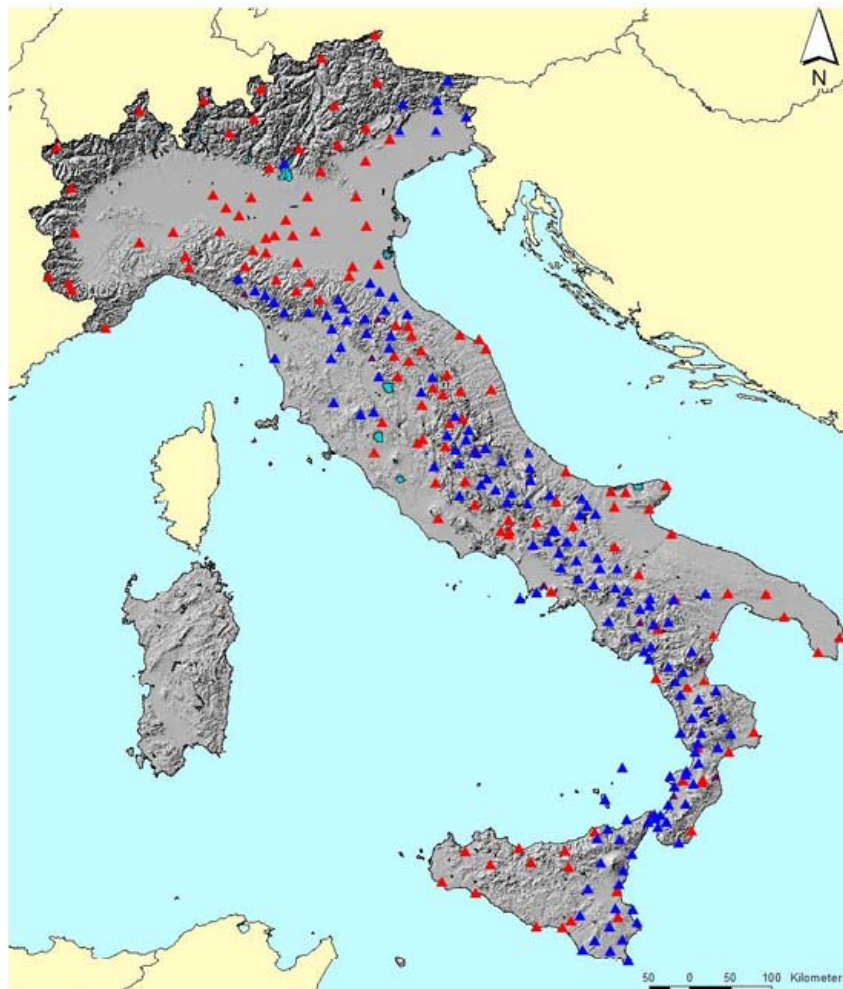


Figure 3.1. Distribution of RAN accelerometers (red=digitals, blue=analogue) (<http://www.protezionecivile.it/>)

3.2 TYPES OF ACCELEROGRAPHS

The first accelerographs were installed in the early 1930s to record earthquakes in California (United States). These early instruments are analogue and record the ground motion on paper or photographic film. One of the most popular analogue instruments is the SMA-1, which is triggered and starts recording when the ground motion exceeds a given threshold level. The ground motions are recorded by a weighted mirror rotating within the instrument displacement, changing the way light falls on the photographic film (fig. 3.2). The film is then processed and digitised. The digitisation process was initially completed manually on purpose built digitised machines, but more recently is conducted using automated processes and commercial scanners (Trifunac, 1999).

General characteristic of an SMA-1 accelerograph are summarized in Table 3.1 while fig. 3.3 reports an example of a recorded trace.

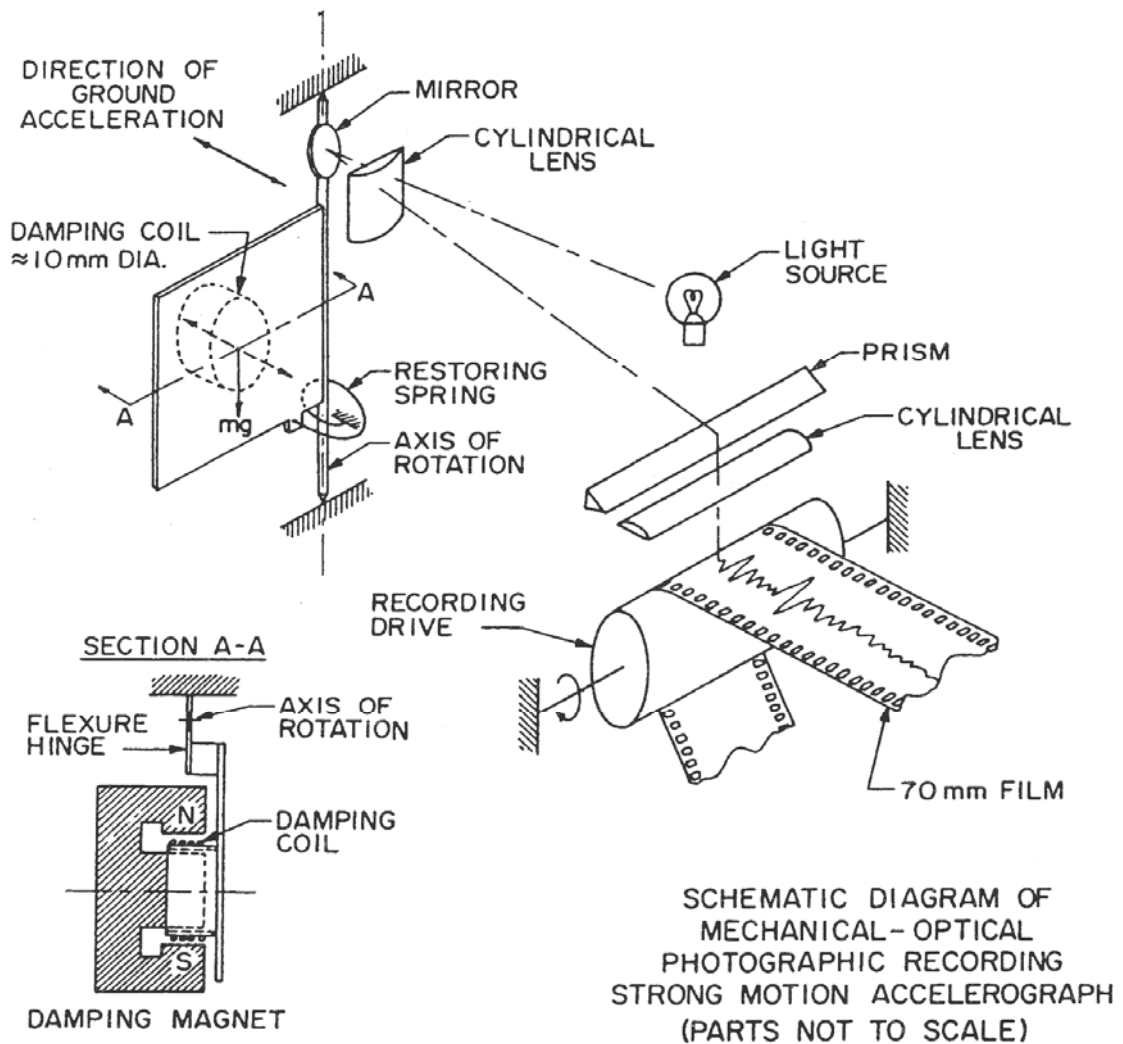


Figure 3.2. Schematic illustration of the recording mechanism of an SMA-1 accelerograph (Hudson, 1979).

Table 3.1: General characteristic of an analogue SMA-1 accelerograph (Faccioli and Paolucci, 2005)

Natural Frequency (Hz)	20-25
Damping (% of the critical value)	60
Sensitivity (cm/g)	1.9
Full Scale Amplitude (g)	1
Recording Support	70 mm Photographic Film
Total Recording Time Autonomy (min)	25
Dimensions (cm)	18x18x38
Weight (kg)	9

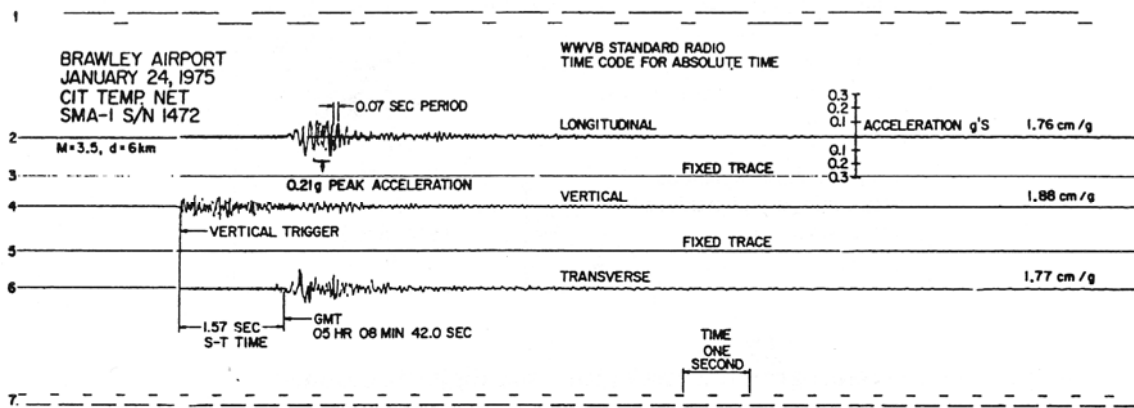


Figure 3.3. Typical record from an SMA-1 accelerograph (Hudson, 1979)

A second generation of digital accelerographs is gradually replacing the older analogue instruments. These operate using a force balance transducer and record digitally onto solid state or magnetic media. One such instrument is the K2 accelerograph (fig. 3.4). This instrument uses GPS to obtain timing accuracy to $\pm 0.5\text{ms}$ and can be connected to a network via radio, telephone or satellite communication links (www.kinematics.com).

The Etna Strong Motion Accelerograph (fig. 3.5) acquires and records acceleration data with 18 bits of resolution. The standard instrument comes equipped with 3 channels and includes an internal triaxial EpiSensor Force Balance Accelerometer. Data is stored in a removable PCMCIA memory card. Recorded events can be off-loaded automatically via modem, manually retrieved by PC, or by collecting the PCMCIA memory card. Time history data can then be evaluated for key parameters using Quicklook for Windows or converted to other file formats for further data analysis.

The advantages of a digital accelerograph compared to the analogue ones are:

- direct availability of a signal not affected by the noise due to the digitalization;
- higher sensibility leading to the possibility of recording also weak motions and minor aftershocks (fig. 3.6);

- availability of pre-event data, that is basically the acquisitions in a temporary memory section, of data preceding an event; this option solves the well known limitations of the analogue instruments related to the knowledge of the initial conditions and the consequent bias on integrations of the signal.



Figure 3.4. Kinematics K2 digital accelerograph (www.kinematics.com)



Figure 3.5. Kinematics Etna digital accelerograph (www.kinematics.com)

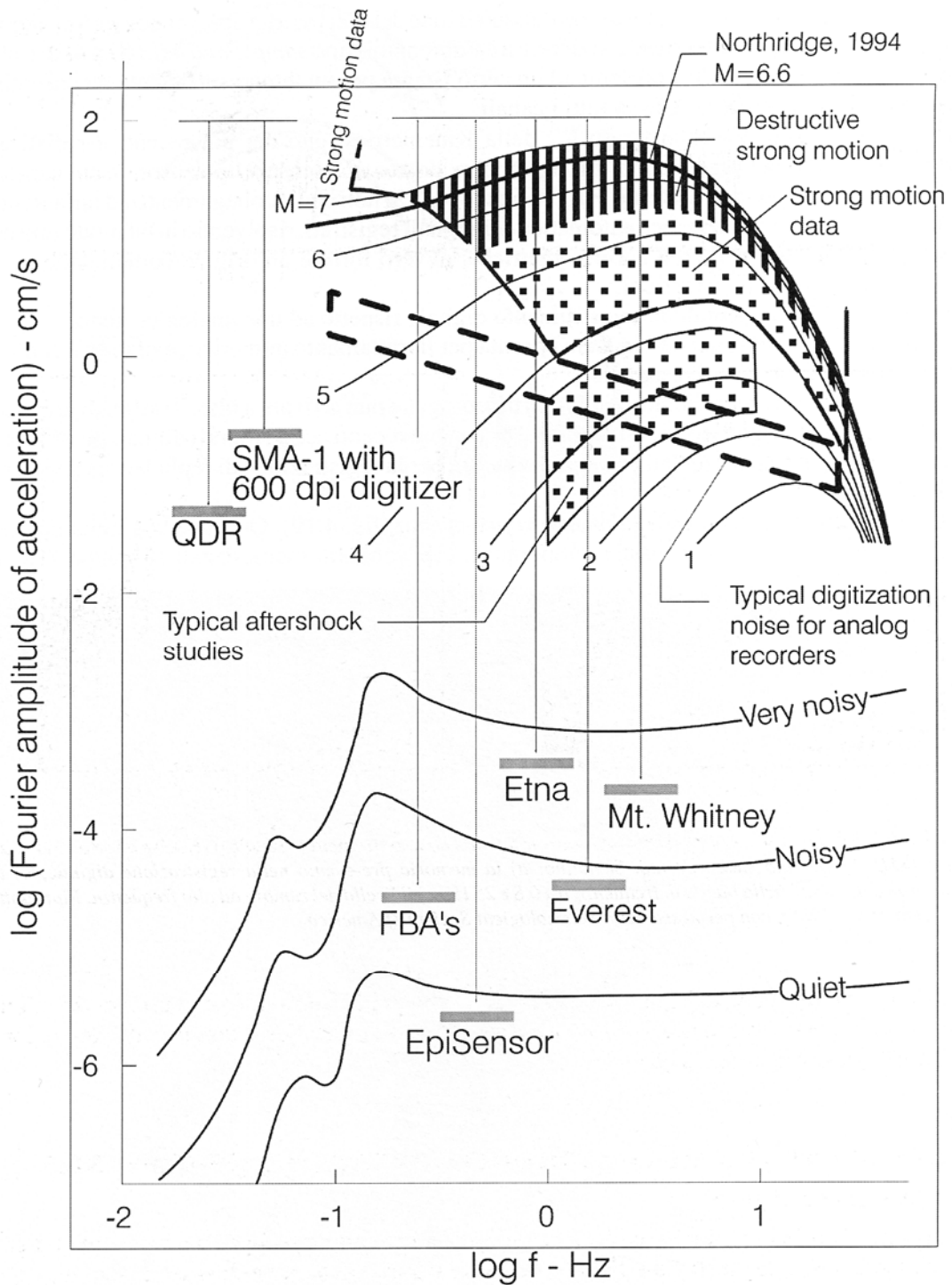


Figure 3.6. Fourier spectra of different earthquakes on sites affected by different noise levels, with overlapping of some analogue and digital instruments sensitivity (Trifunac and Todorovska, 2001).

A large amount of accelerograph are housed in ENEL electrical substations. Those cabins are masonry construction approximately 3–9 m square in plan view and 3–5 m tall; a typical example is shown in Figure 3.7.



Figure 3.7. ENEL electrical substation housing a recording instrument in Gubbio-Piana site (Umbria)

The instrument is mounted on a short pillar 20 cm in height above the floor slab and 60 cm in diameter (fig. 3.8). The pillar extends into the natural ground approximately 0.3-1.0 m and is isolated from the floor slab by a gap (Berardi et al., 1991).

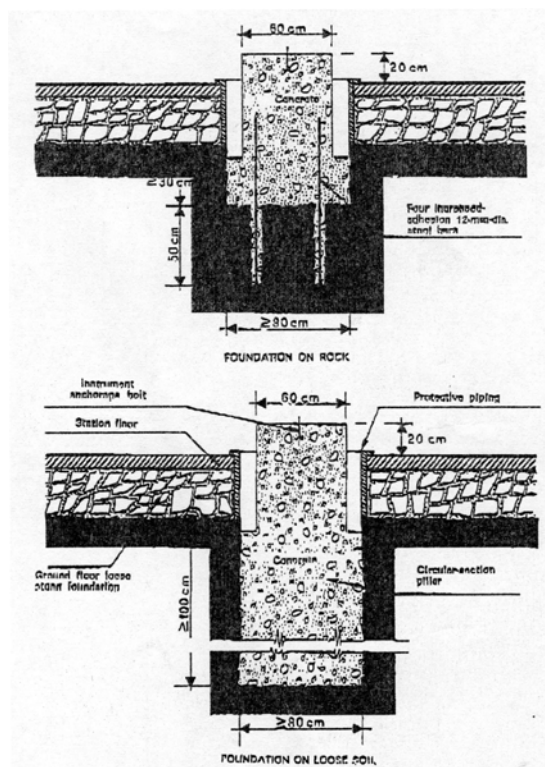


Figure 3.8. Foundation of the accelerograph anchorage pillar (Berardi et al., 1991).

Analysis by Berardi et al. (1991) indicates that this configuration would not be expected to introduce any significant modification to the recording from soil-foundation-structure interaction. Based on those analyses and empirical studies (e.g., Stewart, 2000), it is believed that recordings from structures of this type can be assumed to provide a reasonable approximation of free-field conditions.

3.3 GEOTECHNICAL AND GEOLOGICAL DATA AVAILABLE FOR RECORDING STATIONS

Although Italy has one of the richest database of seismic signals in the world, and notwithstanding the importance of local soil conditions on the seismic ground motion, the site characterization of Italian recording stations has not received much attention in the past.

Site characterization for Italian strong motion stations can be grouped into the following major categories: (1) site investigations at selected instruments that recorded the 1976 Friuli earthquake and 1980 Irpinia earthquake; (2) microzonation and other studies for local municipalities; and (3) individual site studies documented in the literature and from the files of consulting engineers and geologists with local experience.

The Friuli and Irpinia site investigations were generally performed at the recording sites and are the only ones coming from specific projects dedicated to detailed site characterization of the recording stations including field and laboratory testing. Those campaigns can then be considered the most useful because of number, quality and type of released data.

In the Friuli region a joint Commission ENEA-ENEL was established in 1975-1976 to characterize the subsoil of some accelerometric stations that were triggered by the Friuli earthquakes occurring in the period 1976-1980 (Fontanive et al., 1985). A list of the accelerometric stations subject to investigation is reported in Table 3.2. For each site, two boreholes were drilled to about 60 m depth and cross-hole measurements were made to evaluate shear wave velocity profiles. Additional on-site tests included seismic refraction measurements to estimate the p-wave profile.

Within the framework of the “Irpinia Project” a comprehensive in situ and laboratory investigation was carried out at the ENEL recording stations triggered by the 23 november, 1980, Irpinia earthquake. The results of the investigation, performed by ISMES between October 1989 and February 1991, are reported in three reports concerning respectively the in situ geotechnical investigation (ISMES, 1991a, 1991b, 1991c).

Table 3.2. List of the Friuli strong motion stations subject to geotechnical investigation

#	Accelerometric Station	Owner	SG	SR	DH	CH
1	Tolmezzo	ENEL	•	•		•
2	Somplago	ENEL		•		
3	Tarcento	ENEL	•			•
4	Maiano	ENEA/ENEL	•		•	•
5	Forgaria S. Rocco	ENEA	•		•	•
6	Forgaria Cornino	ENEA	•		•	•
7	Buia	ENEA	•		•	•

SG=boring log, SR = seismic refraction, DH = down-hole, CH = cross-hole

These information were subsequently analyzed and elaborated in the framework of a joint research project between ENEL and the *Dipartimento di Ingegneria Strutturale e Geotecnica*, Università di Roma “La Sapienza” (Palazzo, 1991a, 1991b). The Irpinia Project concerned 16 recording stations, 11 of these located close to the epicenter area and the remaining 5 at higher distance. A summary of the main activities and testing related to investigation campaign is illustrated in Table 3.3. In each site the following investigation were carried out:

- boring log drilled to a depth generally comprised between 80 and 100 m for the definition of the stratigraphic profile (labelled as SG in Table 3.3);
- destruction soil boring (labeled as FD in Table 3.3), drilled to the same depth as SG borehole, for the execution of cross hole tests, 5 m apart from the SG borehole;
- destruction soil boring drilled to a depth variable between about 10 and 100 m for installation of Casagrande and open standpipe piezometers (labeled as PZ in Table 3.3).

In some sites SPT as well as CPT (or CPTU) tests were also performed. A total number of 84 samples were retrieved, 54 of which were undisturbed. On these samples standard static and more advanced dynamic laboratory tests to determine the physical and mechanical soil properties were carried out (Table 3.4). The laboratory investigation included classification tests, elastic waves velocity measurements (BE), oedometer (ED), Consolidated Drained Triaxial (CID), Consolidated Undrained Triaxial (CIU), Unconsolidated Undrained Triaxial (UU), Resonant Column (RC) and Cyclic Triaxial (CTX) tests. As an example, fig. 3.10 illustrates the V_s and V_p profiles obtained from cross-hole test in Auletta strong motion station together with the stratigraphic conditions at the site.

Table 3.3. Main activities and testing related to the geotechnical investigation at the Irpinia stations

#	Station	SG	CH	Piezometer		SPT	CPT	Undisturbed Sampling
				Casagrande	Standpipe			
1	Bagnoli	•	•		•			
2	Calitri	•	•	•		•		•
3	Sannicandro	•	•		•	•		•
4	Tricarico	•	•		•			•
5	Vieste	•	•	•	•	•	•	•
6	Arienzo	•	•	•	•	•		•
7	Auletta	•	•		•			•
8	Bisaccia	•	•		•			
9	Bovino	•	•	•				•
10	Brienza	•	•	•	•	•		•
11	Rionero	•	•		•			•
12	San Severo	•	•	•		•	•	•
13	Sturno	•	•	•				•
14	Benevento	•	•	•		•		•
15	Garigliano	•	•			•	•	•
16	Mercato San Severino	•	•	•		•	•	•

Table 3.4. List of laboratory tests carried out at the Irpinia stations

#	Station	Laboratory tests							
		Classification	ED	BE	CID	CIU	UU	RC	CTX
1	Bagnoli	•							
2	Calitri	•						•	
3	Sannicandro	•	•	•			•	•	
4	Tricarico	•							
5	Vieste	•	•	•			•	•	
6	Arienzo	•	•					•	
7	Auletta	•		•			•		
8	Bisaccia	•	•						
9	Bovino	•	•						
10	Brienza	•		•		•		•	•
11	Rionero	•						•	•
12	San Severo	•		•	•	•	•	•	•
13	Sturno	•	•			•		•	
14	Benevento	•	•	•		•	•	•	•
15	Garigliano	•	•	•	•	•	•	•	•
16	Mercato San Severino	•	•	•		•	•	•	•

Microzonation and individual site studies carried out in proximity of the strong motion stations or on site of similar geologic conditions were also analyzed and are listed in Table 3.5. In particular microzonation studies available for Ancona (Working Group, 1981), Tarcento (Brambati et al., 1979) and Sant'Agapito (Isernia Administration, 1998) allowed to obtain information on geological/geotechnical site characteristics and, more importantly, V_s profiles from cross-hole or down-hole measurements. Other V_s profiles were obtained for Catania and Avezzano station from selected publications respectively by Maugeri and Frenna (1993) and AGI Working Group (1991), or from individual studies by geologists such as Naso station (Copat, 2007). Finally, estimated V_s profiles were extracted from Faccioli (1992) for Cairano and Conza stations.

Table 3.5. Recordings stations with V_s data from literature studies

#	Station	Agency	Type of test	V_s profile	Reference
1	Ancona Palombina	ENEA	CH	yes	Paciello et al. (1997)
2	Ancona Rocca	ENEA	CH	yes	Paciello et al. (1997)
3	Avezzano	DPC	CH	yes	AGI (.1991)
4	Cairano 1	DPC		no	Faccioli (1992)
5	Cairano 2	DPC		no	Faccioli (1992)
6	Cairano 3	DPC		no	Faccioli (1992)
7	Cairano 4	DPC		no	Faccioli (1992)
8	Catania Piana	DPC	CH	yes	Maugeri and Frenna (1993)
9	Conza base	DPC	Estimated	no	Faccioli (1992)
10	Conza vetta	DPC	Estimated	no	Faccioli (1992)
11	Naso	DPC	DH	yes	Copat (2007)
12	San Agapito	DPC	DH	yes	Isernia administration (1998)
13	Tarcento	DPC	CH	yes	Brambati et al. (1979)

As for the other recording sites, which are the majority, a monograph prepared by ENEL is generally available including geographical information, a picture of the recording station, a geological map (scale 1:50.000) and geological cross-sections (scale 1:50.000 and 1:2000). An example of such standardized form is illustrated in fig. 3.10 for Pellaro recording station. For stations lacking ENEL forms, geological information taken from the national map (scale 1:100.000) published by Servizio Geologico Nazionale are provided.

In summary, geotechnical site characterization of Italian recording stations is extremely poor. Only for about less than 10% of the whole number of stations a shear wave velocity is presently available (fig. 3.9). For the remaining stations only geological information, at different scale, is available. It is therefore

evident that a significant improvement is needed to increase the number of recording sites with reliable site characterization and measurement of shear wave velocity profile.

As a final remark, it should be mentioned that the problem of the geotechnical characterization of Italian recording stations has been recently investigated in the framework of the 2004-2006 DPC-INGV agreement, Project S6 and the results of the study were made available at the website <http://esse6.mi.ingv.it>. In parallel, the same topic is currently the subject of an on-going international project, i.e. the JRA4 activity of the European project NERIES (Network of Research Infrastructures for European Seismology, www.neries-eu.org).

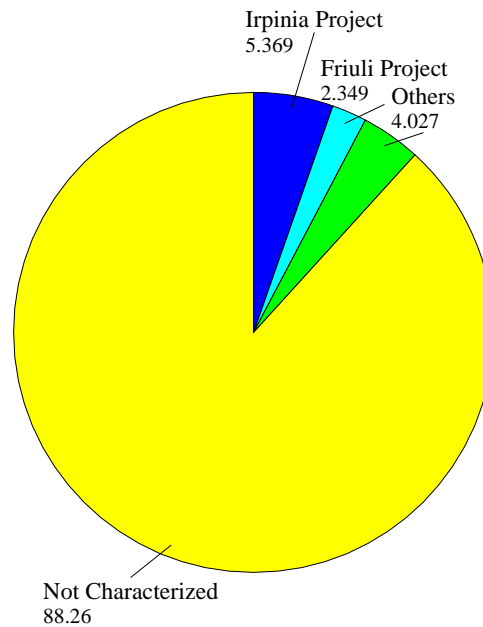


Figure 3.9. Distribution of geotechnical characterization (Vs profiles). Numbers indicate percentage.

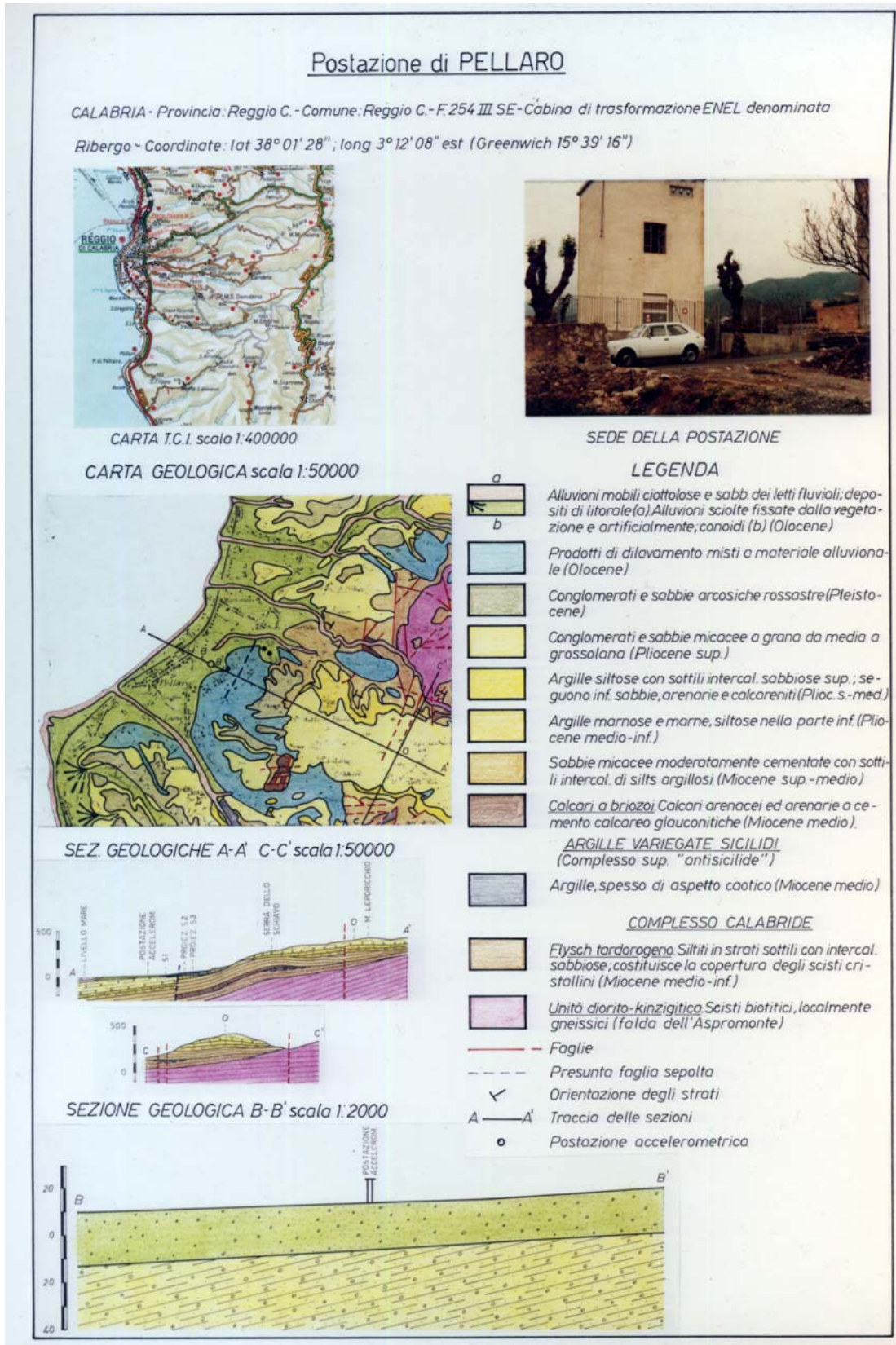


Figure 3.10. Standard forms prepared by ENEL for Pellaro (Calabria) recording station

CHAPTER 4 **GEOTECHNICAL CHARACTERIZATION OF SEVENTEEN UMBRIA-MARCHE RECORDING STATIONS BY THE SASW TECHNIQUE**

4.1 INTRODUCTION

As described in previous chapter 3, one of the critical aspects of the Italian accelerometric network is related to the characterization of subsoil of strong motion recording sites as most of the temporary and permanent stations sites have little or no quantitative information.

For that reason an investigation campaign was planned and realized to characterize some station's site in order to fill part of the big lack on geotechnical data available.

The spectral analysis of surface wave (SASW) method was used as in-situ technique because it is inexpensive and non-invasive (Stokoe and Nazarian, 1985). The choice of the sites was made with the goal of characterizing the highest number of recording stations on soil but also of increasing the percentage of characterized recordings themselves. It came out that the most productive way to operate was selecting stations that recorded Umbria-Marche 1997-98 events located in a limited area of Umbria region (just one in Marche region, right over the border). That allowed to consider sites with a short relative distance between each other and a satisfying number of recordings, with the benefit of short journeys from one site to the other leading to a number of 17 investigated stations in two weeks. The SASW site characterization work was essentially sponsored by Pacific Earthquake Engineering Research Center (PEER) and partially by the support of the Ministero dell'Università e della Ricerca (MIUR). The SASW test was conducted in collaboration with Dott. Robert Kayen from United States Geological Survey (USGS).

In this chapter, first a brief description of the Umbria-Marche earthquake sequence is presented and the location of the chosen sites is shown as well. Thereafter, the methodology used to carry out the SASW technique is illustrated together with the elaboration of experimental data for a representative site. The complete set of results is reported in Appendix A containing a form with data elaboration for each recording station. This work is also described in a USGS publication downloadable at the URL <http://pubs.usgs.gov/of/2008/1010/>.

4.2 THE 1997-98 UMBRIA-MARCHE, ITALY, EARTHQUAKE SEQUENCE AND SELECTED RECORDING STATIONS

The regions of Umbria and Marche were shaken by two events on September 26, 1997 near Colfiorito on the Umbria-Marche border. Temporary stations were deployed in the epicentral region and recorded two large shocks on October 3 and 6. Later on October 12, 14, and November 9, swarms of quakes occurred in the vicinity of the town of Sellano.

After almost five months of relative seismic quiescence, two strong motion event occurred in the northern part of Umbria (Gualdo Tadino area) on March 26th and April 3rd in 1998 (Decanini et al., 2002). The September events were the largest with magnitudes of M5.8 and M6.0, the two October quakes near Colfiorito were of M5.3 and the Sellano swarm had several major shocks that ranged from M4.5 – to – 5.7. Magnitude of 5.6 and 5.3 corresponded respectively to quakes of Gualdo Tadino occurred in 1998, The triaxial peak ground motions recorded for all of these events were, in Colfiorito, 0.38g and 0.44g horizontal and 0.33g vertical. In Nocera Umbra, motions reached 0.56g and 0.5g horizontal and 0.42g vertical (Trobiner et al., 1997).

The geologic setting of the rock in the mountainous Apennines region of the Umbria-Marche consists of folded and thrust-faulted Mesozoic and Cenozoic marl, marl clays, and limestone. Valley alluvium of Pleistocene and Holocene age fill the drainages and low-land areas. In general the region is dissected by a suite of NNW trending Cenozoic thrust faults, now undergoing extension. The setting of fault dissected marine units has been the source of over a score of shallow damaging earthquakes in the past 800 years.

The Umbria-Marche earthquake swarm severely damaged a hundreds of architecturally and culturally important structures, including the Basilica of St. Francesco in the town of Assisi, as well as palaces, towers, churches and historically important residences. In Foligno and Nocera Umbra, the towns medieval towers collapsed, and numerous city gates were damaged. Severe damage was almost exclusively found in the stone masonry constructed structures. Strong motion stations located within these towns, and temporary stations set up after the initial events in more rural settings were the object of SASW testing program.

A total of 17 strong motion instrument sites were considered. The list is reported in [Table 4.1](#) and their location is illustrated in [fig. 4.1](#).

Table 4.1. List of investigated sites

SITE	SITE NAME	STATE	LAT	LON
254BEV	BEVAGNA	UMBRIA	42.932	12.611
255 SMI	FOLIGNO - CHURCH ST MARIA	UMBRIA	42.954	12.699
256CSA	CASTELNUOVO ASSISI	UMBRIA	43.008	12.591
257CLF	COLFIORITO	UMBRIA	43.037	12.921
258CLC	COLFIORITO-CASERMETTE	UMBRIA	43.029	12.890
259NCR	NOCERA UMBRA	UMBRIA	43.111	12.785
260NCB	NOCERA UMBRA BISCONTINI	UMBRIA	43.104	12.805
261NCS	NOCERA UMBRA SALMATA	UMBRIA	43.148	12.791
262GBP	GUBBIO PIANA	UMBRIA	43.314	12.590
263GBB	GUBBIO - PARK COLLO	UMBRIA	43.358	12.595
264NCI	NORCIA - INDUSTRIAL PARK	UMBRIA	42.780	13.097
265NRC	NORCIA	UMBRIA	42.792	13.097
266NRA	NORCIA ALTAVILLA	UMBRIA	42.796	13.081
267CSC	CASCIA	UMBRIA	42.719	13.012
268CSP	CASCIA PETRUCCI APTMTS	UMBRIA	42.718	13.018
269SLW	SELLANO WEST	UMBRIA	42.886	12.922
270MTL	MATELICA	MARCHE	43.248	13.008

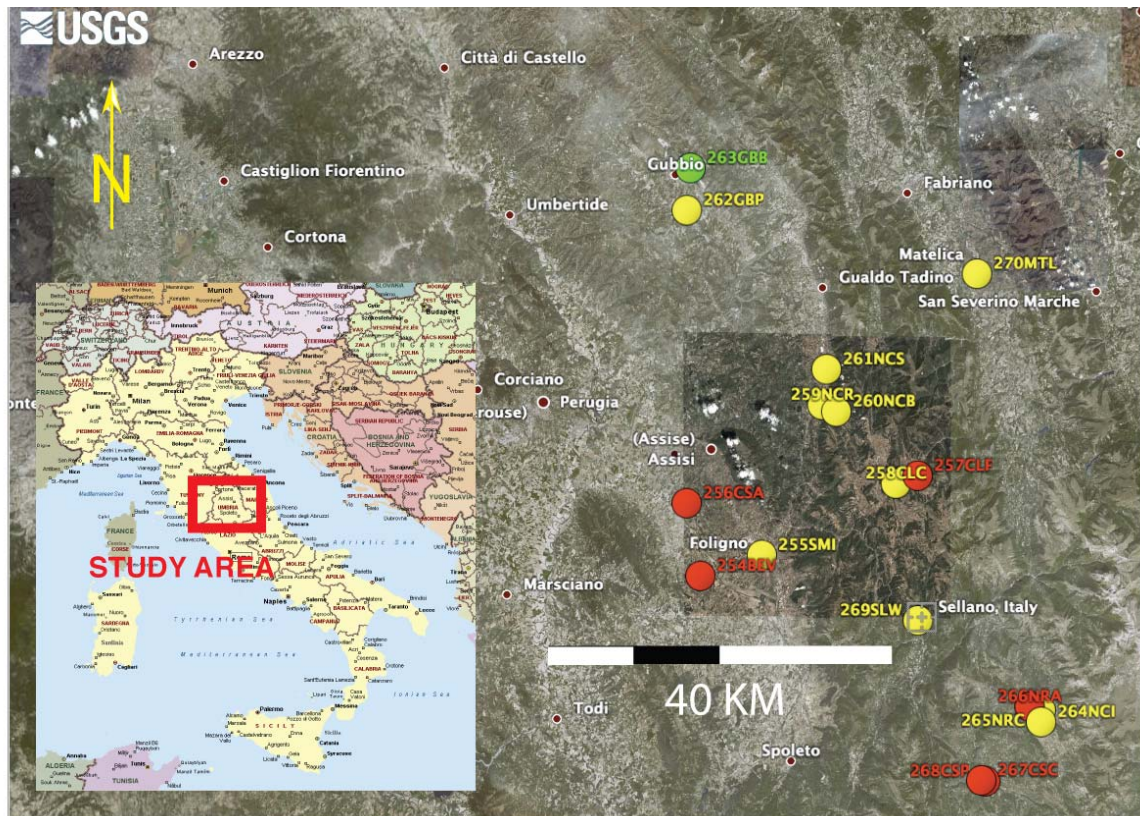


Figure 4.1. The seventeen Italian sites tested in this study are located in the states of Umbria and Marche. The color of the site marker indicates EC8 classification for C (Red), B (Yellow), and A (Green) (see paragraph 4.4)

4.3 THE SASW INSTRUMENTATION

As already stated in the introduction, the SASW method of testing is a portable, inexpensive, and efficient means of non-invasively estimating the stiffness properties of the upper 100 meters of the ground. Prior to the development of non-invasive surface wave methods, shear waves were measured in cased boreholes in rock or by penetration tests, both costly methods, using a conventional travel-time approach. For all of the sites studied in Umbria and Marche regions, the penetration method cannot sound to useful depths, and boreholes would be prohibitively expensive. The surface wave test apparatus is highly portable, allowing to measure in remote location where only small all-wheel drive vehicles can drive (e.g. Gubbio station in Park Collo Area).

The test apparatus consists of 1-Hz seismometers, a low frequency spectrum analyzer, two computer-controlled electro-mechanical harmonic-wave sources (shakers) and their amplifiers, cables and approximately 4.0kW of total electrical output from generators made available in each test region.

The 1-Hz Kinometrics1 receivers used (fig. 4.2) are designed for capturing vertical motions and cover the frequency range of interest in the active-source surface-wave test.



Figure 4.2. Particular of the 1-Hz Kinometrics1 receiver (picture shot from above).

For a source, the spectrum analyzer produces a sine wave signal that is split into a parallel circuit and by two separate power amplifiers to produce an in-phase continuous harmonic-wave. Two arrayed APS Dynamics Model 400 electro-mechanical shakers (fig. 4.3) receive the input waveform and oscillate in vertical motion to excite the ground.



Figure 4.3. Dual-shakers source system

The receivers record the waves and a fast Fourier transform (FFT) is performed on each of the two receiver signals, per directional array. In near-real time, the linear spectra, cross power spectra, and coherence are computed. The ability to perform near real-time frequency domain calculations and monitor the progress and quality of the test allows to adjust various aspects of the test to optimize the capture of the phase data. These aspects include the source-wave generation, frequency step-size between each sine-wave burst, number of cycles-per-frequency, total frequency range of all the steps, and receiver spacing. The dual shaker-sources are arrayed orthogonally to the SASW seismometer line.

The test steps through a suite of frequencies, and for each frequency phase computations are made. This method of swept-sine surface wave testing sweeps through a broad range of low frequencies in order to capture the surface wave-dispersion characteristics of the ground. This approach is a modification of the Continuous Sine Save Source Spectral Analysis of Surface Waves (CSS-SASW) test presented by Kayen and others (2004a, 2004b, 2005a, 2005b).

Spacing of the receivers stepped geometrically from 1 meter to 160 meters. The two seismometers are separated by a given distance, d , and the source is usually placed at a distance of d from the inner seismometer (fig. 4.4).



Figure 4.4. Configuration of the USGS surface wave testing system at site 262GBP Gubbio Soil Site Piana (43.314°N,12.59°E) composed of 1-Hz vertical motion sensors and two-100 kg electro-mechanical harmonic wave shakers. The shaker apparatus are arrayed in a parallel circuit and synchronized in phase for controlled swept-sine analysis.

Rayleigh wave wavelengths (λ) are computed by relating the seismometer spacing (d) and the phase angle (θ , in radians determined from the cross-power spectra) between the seismometers:

$$\lambda = 2\pi d/\theta \quad (4.1)$$

The Rayleigh wave surface wave velocity, V_r , is computed as the product of the frequency and its associated wavelength:

$$V_r = f\lambda \quad (4.2)$$

4.4 DISPERSION CURVE EVALUATION AND VELOCITY PROFILE

Computing the average dispersion curve for a site, requires a collection of a suite of individual data sets that relate Rayleigh wave phase velocities to their corresponding frequencies and wave-lengths. Regardless of the array dimensions, is routinely computed phase velocities for phase angles between 120 degrees and 1080 degrees, corresponding to wavelengths of $3d$ and $d/3$ respectively. If the data are noisy, the range is narrowed to 180 degrees and 720 degrees, or $2d$ and $d/2$. For example, if the array separation

was 3 meters, velocities are inverted for Rayleigh wavelengths of 1m-to-9 meters. Longer wavelengths sound more deeply into the ground and are needed to extend profiles depths. These long wavelength data are associated with low frequencies. Figure 4.5 presents a plot of a group of eight individual dispersion curves that together cover a range of wavelengths from 0.6 meters–to-400 meters. The averaged dispersion curve from these eight profiles is used to invert the velocity structure of the ground.

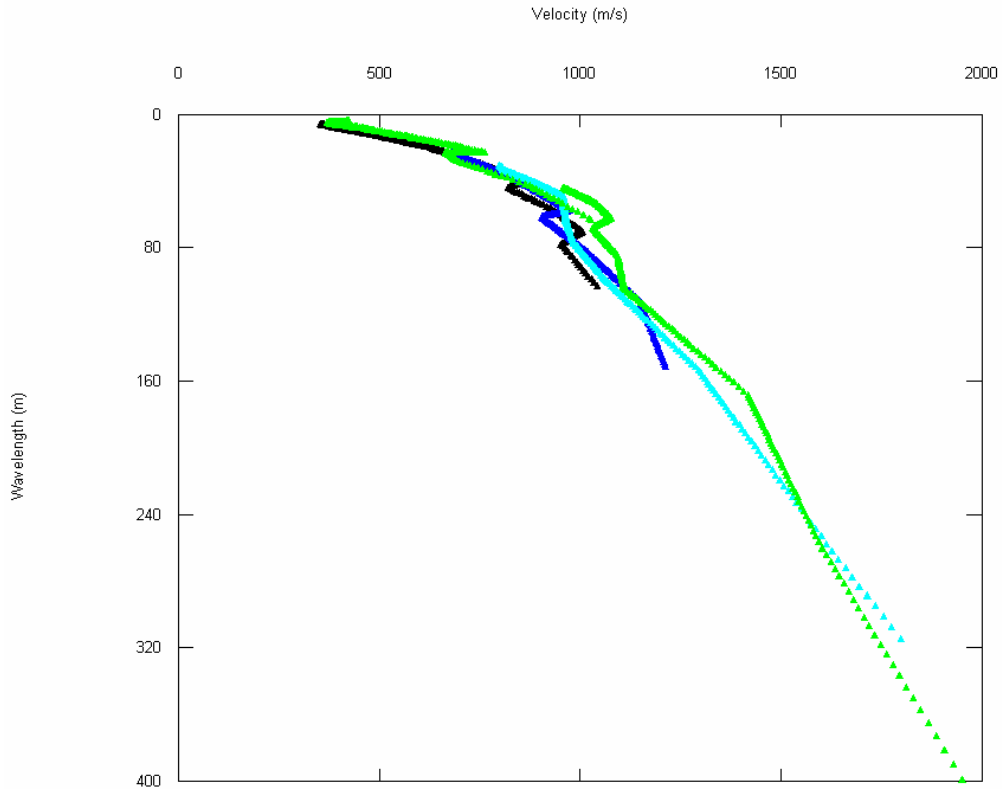


Figure 4.5. A group of eight dispersion curves covering a wavelength range of 1 meter to 400 meters (Cascia Station, Umbria)

The inversion process is used to estimate the soil stiffness model whose computed theoretical-dispersion curve is a best-fit with the experimental dispersion data collected in the field. That is, shear wave velocity profiles are inverted using an inversion code that hunts for the best-fit shear wave velocity profile whose theoretical dispersion curve is the closest match with the averaged field dispersion curve. The term “best-fit” refers to the minimum sum of the squares of residuals from the differences between the theoretical and experimental dispersion curves.

The inversion algorithm, WaveEq of OYO Corp. (Hayashi and Kayen, 2003) uses an automated-numerical approach that employs a constrained least-squares fit of the theoretical and experimental dispersion curves. For the Cascia, Umbria site, noted above in fig. 4.6, is inverted a shear wave velocity structure that rapidly climbs in stiffness from less than 300 m/s at the surface to in excess of 1900 m/s at 40 m. The averaged $V_{s,30}$ value for this site is 540 m/s.

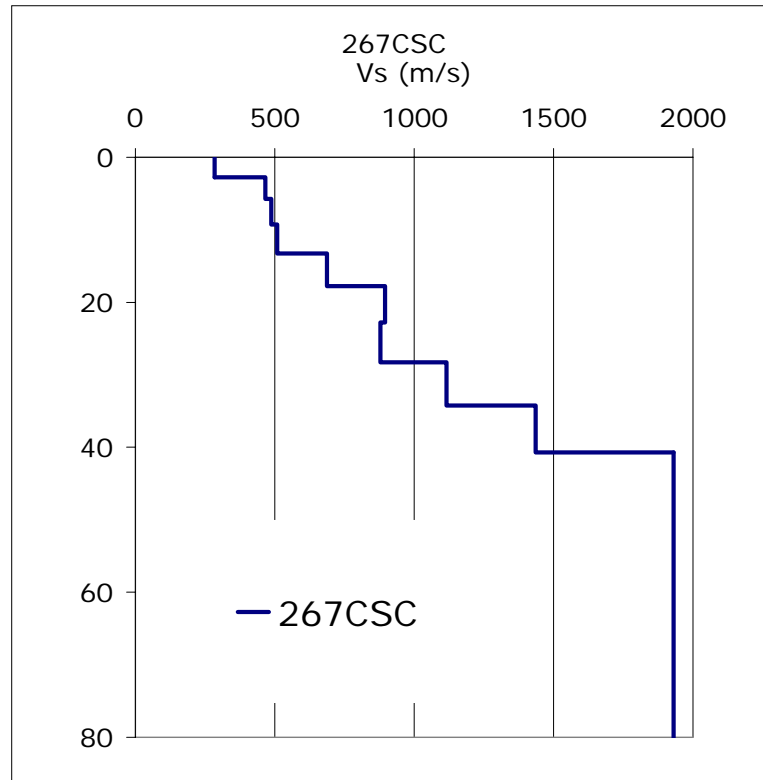


Figure 4.6. Shear wave velocity profile for Cascia, Umbria site.

The inversion of a theoretical velocity profile was performed using the inversion codes Wave-EQ. Typically, a ten to fifteen layer model was used for the inversion, with layer thicknesses geometrically expanding with depth. The increasing layer thicknesses correspond with decreasing dispersion information in the longer wavelength (deeper) portion of the dispersion curve. The profiles generally increase in stiffness with depth, though low velocity layers are present in several of the profiles.

The simplest way of characterizing the overall site condition is to use the average shear wave velocity in the uppermost 30 meters or 100 meters of the subsurface (V_{s30} ; V_{s100}). Equation reported above is used to compute this average velocity based on the unit layer thickness (d_i) and the corresponding interval-velocity (V_{Si}).

$$V_{S\text{-depth-averaged}} = \frac{\sum_{i=1}^n d_i}{\sum_{i=1}^n \frac{d_i}{V_{Si}}} \quad (4.3)$$

Following the described procedure the V_s profiles were obtained for entire set of Italian strong motion recording stations. These sites are listed in the order they were tested in Table 4.2 along with V_{s30} and V_{s100} values and EC8 site classification. The averaged velocities for the upper 30 meters ranged from 182 to 922 m/s. The velocities fall within EC8 categories “C”-through- “A”.

Table 4.2. Italian station locations and their corresponding computed 30 and 100 meter average shear wave velocities and site codes are presented as EC8,VS30, and VS100.

SITE NAME	REGION	LAT	LON	ECB	Vs_30 (m/s)	Vs_100 (m/s)
BEVAGNA	UMBRIA	42.932	12.611	C	182	278
FOLIGNO - CHURCH ST MARIA	UMBRIA	42.954	12.699	B	395	527
CASTELNUOVO ASSISI	UMBRIA	43.008	12.591	C	293	440
COLFIORITO	UMBRIA	43.037	12.921	C	317	719
COLFIORITO-CASERMETTE	UMBRIA	43.029	12.890	B	405	720
NOCERA UMBRA	UMBRIA	43.111	12.785	B	428	938
NOCERA UMBRA BISCONTINI	UMBRIA	43.104	12.805	B	442	823
NOCERA UMBRA SALMATA	UMBRIA	43.148	12.791	B	694	1170
GUBBIO PIANA	UMBRIA	43.314	12.590	B	492	864
GUBBIO - PARK COLLO	UMBRIA	43.358	12.595	A	922	1759
NORCIA - INDUSTRIAL PARK	UMBRIA	42.780	13.097	B	551	546
NORCIA	UMBRIA	42.792	13.097	B	677	1148
NORCIA ALTAVILLA	UMBRIA	42.796	13.081	C	218	264
CASCIA	UMBRIA	42.719	13.012	B	540	993
CASCIA PETRUCCI APTMTS	UMBRIA	42.718	13.018	C	339	488
SELLANO WEST	UMBRIA	42.886	12.922	B	509	713
MATELICA	MARCHE	43.248	13.008	B	437	767

CHAPTER 5 DATABASE OF ITALIAN STRONG MOTION ACCELEROGRAMS

5.1 INTRODUCTION

The characterization of earthquake ground motions for engineering applications generally involves the use of empirical models referred to as ground motion prediction equations (GMPEs) or attenuation relations. GMPEs describe the variation of particular intensity measures (such as peak acceleration, spectral acceleration, or duration) with magnitude, site-source distance, site condition, and other parameters. The most recent GMPEs for crustal earthquakes in active regions were developed as part of the Next Generation Attenuation (NGA) project (see chapter 7).

Because most GMPEs are empirical, they are dependent on the databases utilized in their development. The development of GMPEs requires a database of strong motion accelerograms and their intensity measures, a databank of site conditions for accelerometers, and a databank of earthquake source parameters. Most of the available GMPEs utilize inconsistent databases and databanks, in the sense that the data are derived from different sources of variable quality. One of the major thrusts of this project was to compile a consistent strong motion, site, and source Italian database in order to evaluate the applicability of the most recent Ground Motion Predictions Equations, developed in the Western United States (NGA 2008) for shallow crustal earthquakes in tectonically active regions, to Italian data.

The NGA GMPEs (Abrahamson and Silva, 2008; Boore and Atkinson, 2008; Campbell and Bozorgnia, 2008; Chiou and Youngs, 2008; Idriss, 2008) are intended to be applicable to geographically diverse regions – the only constraint being that the region is tectonically active and the earthquake hypocentral depth is relatively shallow. The databases involved are therefore large – the NGA database consists of 3551 recordings from 173 earthquakes. In some regions, there has been a preference towards the use of local GMPEs derived solely from data in that region. This practice has been particularly common in Europe (Bommer, 2006), with Italy and Greece being prominent examples. The current national hazard map for Italy (Working Group, 2004) was developed using GMPE modified from Sabetta and Pugliese (1996) and Ambraseys et al. (1996) (for style of faulting and different distance parameters, see Working Group, 2004 for details) along with even more localized GMPEs for particular regions within Italy (e.g., Malagnini and Montaldo, 2004). These local relations are based on relatively small databases – for example the Sabetta and Pugliese (1996) GMPE was derived from an Italian database of 95 recordings from 17 earthquakes. Local databases such as this are naturally smaller than world-wide databases, meaning that error in individual data points have greater influence on the GMPE.

A second major application of ground motion databases linked to site/source databanks is for dynamic analyses of structural and geotechnical systems. Recent research efforts have been directed towards providing guidance on ground motion selection and scaling (Goulet et al., 2007) – the ground motion database utilized in those studies is generally the NGA database. In Italy, dynamic analysis and design using accelerograms has been allowed for civil infrastructure since 2003 (OPCM 3274, 2003), although a recent seismic code (Norme Tecniche per le Costruzioni, 2008) specifically requires the use of natural recordings in lieu of synthetic motions for geotechnical applications. There is an urgent need for a database/databank to facilitate such ground motion selection in Italy.

In this chapter the data resources available for the Italian region are critically examined with respect to the above three attributes: ground motion, site, and source. A brief overview of the most important parameters is reported as well.

The results of recent work to enhance the breadth, quality, and consistency of the strong motion database and site and source databanks is also described. Those data resources are freely disseminated via the web on the site <http://www.sisma.dsg.uniroma1.it>, as described in chapter 6.

5.2 STRONG MOTION DATASET

Italian strong motion recordings can be found from a number of online sources and on compact disks. Perhaps the most widely recognized source is the European Strong Motion Database ESD (Ambraseys et al., 2004), which includes Italian data from ENEA, University of Trieste, and ENEL. Another unpublished source of data was developed by SSN and ENEA (Paciello et al., 1997) and contains ENEA and ENEL recordings. Since the formation of RAN, data from the most recent earthquakes in Italy (namely, 1997-1998 Umbria-Marche and 2002 Molise seismic sequences) are distributed by CDROMs published by SSN (2002) and DPC (2004). All of the available data (except stations owned by University of Trieste) has recently been assembled by INGV and DPC (Working Group S6, 2007), which also re-processed the data according to a procedure that included baseline correction, instrument correction (for analogue signals), and record-by-record filtering (see paragraph 5.2.1).

For this study, a total of 509 uncorrected (but digitized) 3-component recordings from 100 earthquakes with magnitude > 3.7 and 160 different recording stations were downloaded in March 2005. Those data are derived from the ESD database for events from 1972 to 1998 (479 three-component recordings) and from DPC (2004) for recordings of the 2002 Molise seismic sequence from the RAN array (30 three-component recordings). This database is comprised solely of data that was available from the aforementioned sources in March 2005.

The downloaded data were then processed in 2005 by the same seismologists responsible for the NGA data processing (Dr. Walter Silva and colleagues). This was done so that the Italian strong motion data set would be compatible with the NGA data in terms of data quality and in the definitions of usable bandwidth on a record-by-record basis.

As described next, before the processing phase, about 50% of downloaded raw recordings were excluded because of uncorrectable errors (e.g., s-triggering). Therefore the final database contains:

- 247 three-components recordings;
- 101 recording stations;
- 89 earthquakes.

The distribution of the recording stations across Italy is shown in [fig. 5.1](#). For this entire dataset were then obtained, acceleration, velocity and displacement uniformly corrected time-histories; pseudo-acceleration response spectral ordinates at 5% damping were also computed. A complete list of the 247 recordings with corresponding parameters and information is reported in the attached electronic support in a file named “Database Flatfile.xls”. The file includes also information on recorded earthquakes, station sites and recording instruments.



Figure 5.1. Spatial distribution of recording stations included in the database

5.2.1 Comparison between corrected data by ESD and PEER processing procedures

As already clarified, data processing reduced the size of the usable database to 247 recordings from 89 earthquakes and 101 different recording sites.

This significant reduction of the number of recordings (by 52%) relative to the uncorrected data results from delayed triggering of analogue instruments during shaking associated with shear waves (referred to as S-triggers). Figure 5.2 shows an example of an S-triggered record from the 1997 Umbria-Marche earthquake. As shown by Douglas (2003b), S-triggered records can have significantly biased response spectral accelerations, and hence it is suggested to avoid the use of such records for strong motion studies.

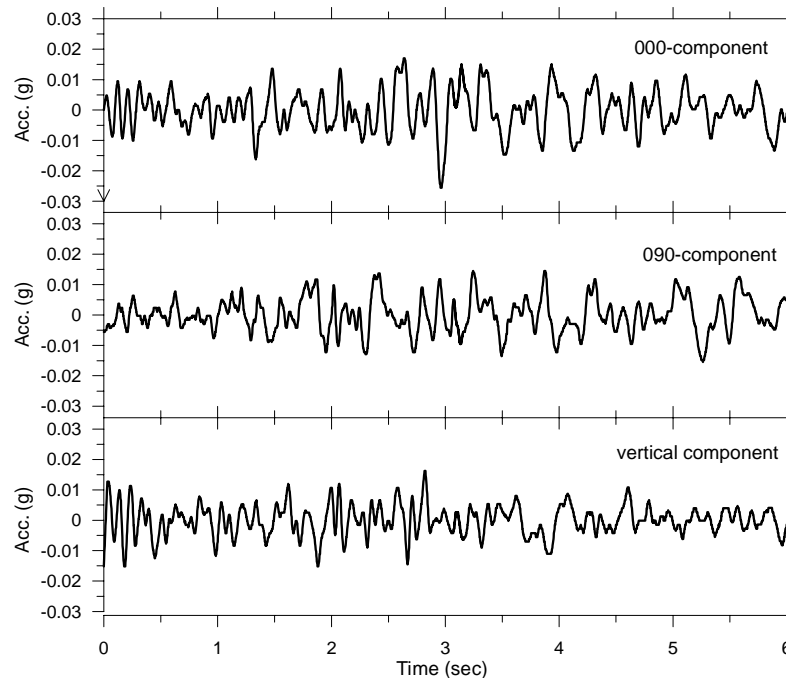


Figure 5.2. Example of S-triggered strong motion recording, Cascia station from 1997 Umbria-Marche earthquake

In figures 5.3 to 5.6 are compared several recordings processed as part of this study (labeled as “PEER”) to the processed records from the ESD database. Figure 5.3 shows an example of inadequate baseline correction of the processed ESD data as evidenced by excessive “wobble” of the displacement history. The differences in baseline correction do not significantly affect peak acceleration, but produce noticeable errors in peak velocity and displacement, which represent intensity measures sensitive to longer-period components of the waveform. Figure 5.4 shows Fourier amplitude spectra and 5%-damped pseudo acceleration response spectra for these same recordings. The Fourier spectra show similar amplitudes across the frequency range of 1-15 Hz. At higher frequencies, the PEER amplitudes generally exceed those from ESD due to a higher Nyquist frequency (100 Hz for PEER versus 25 Hz for ESD). However, these differences occur at relatively low values of Fourier amplitude ($< 10^{-4}$ g \times s), and do not significantly affect

intensity measures of typical engineering interest such as peak quantities (acceleration, velocity, displacement) or spectral accelerations. On the other hand, at lower frequencies, the PEER amplitudes are significantly smaller than ESD due to differences in baseline correction and high-pass filtering, and the effected Fourier amplitudes are relatively large (approximately 10-3 gxs). Those differences in the low frequency components of the waveform result in different values of peak velocity and displacement (fig. 5.3) and spectral acceleration for periods $T > 0.8$ sec. Because the ESD waveform is richer in low-frequency energy, the long-period spectral accelerations are higher for ESD than for PEER processing.

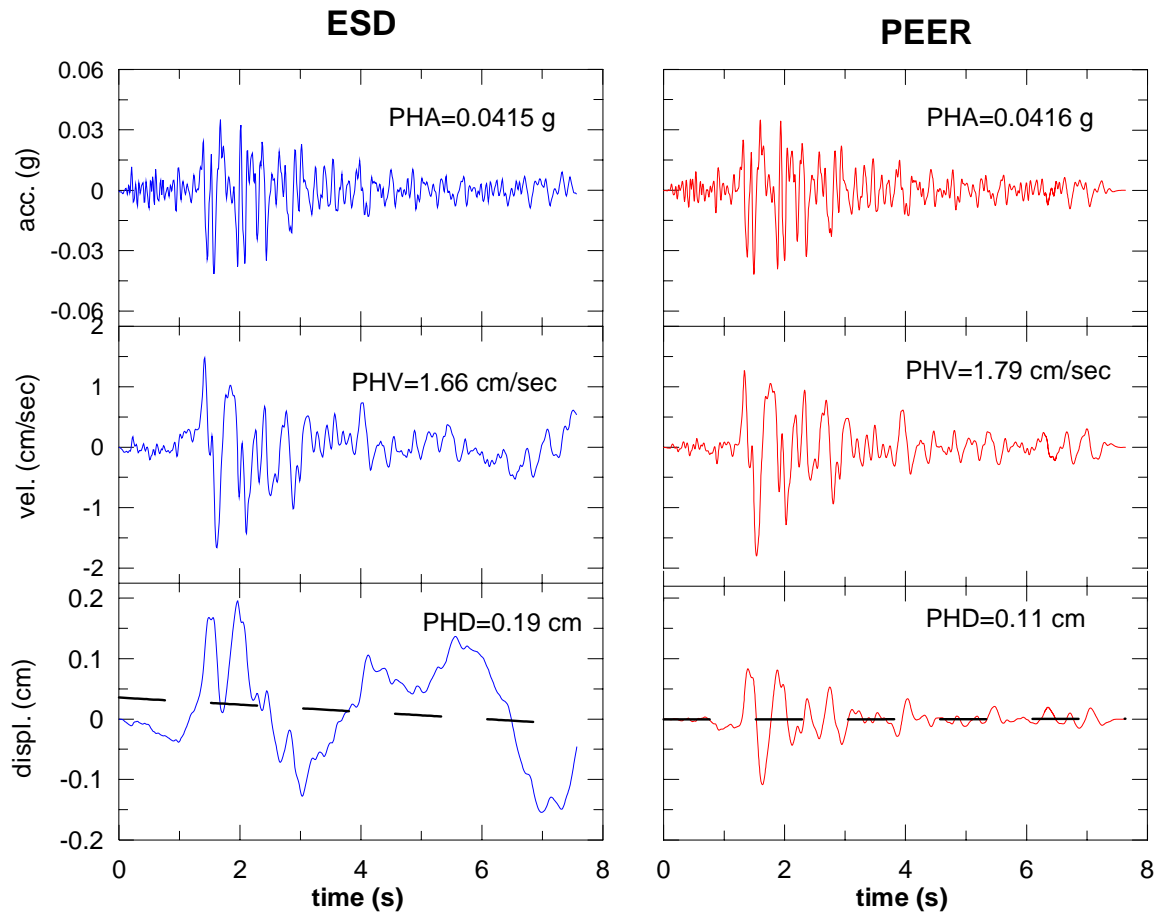


Figure 5.3. Comparison between ESD- and PEER-corrected waveforms using accelerometer recording at the Genio Civile station during the 1972 ML=4.7 Ancona earthquake

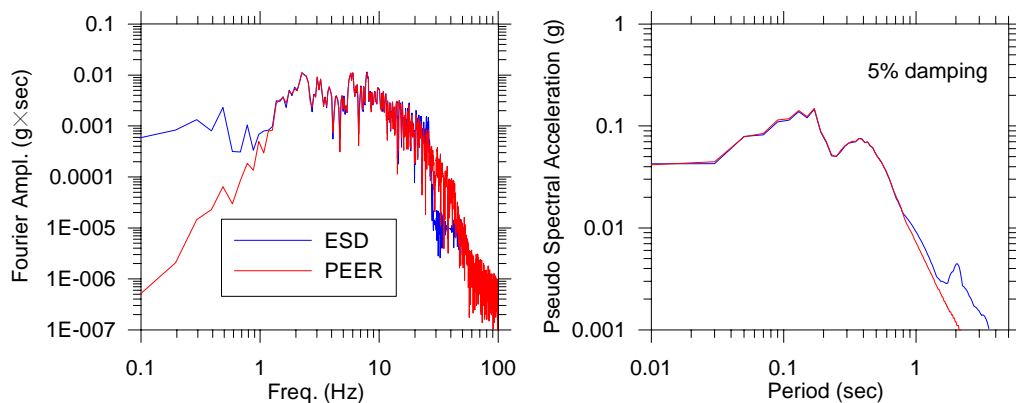


Figure 5.4. Comparison between Fourier and pseudo-acceleration response spectra calculated from ESD- and PEER-corrected accelerograms using data from the Genio Civile station during the 1972 ML=4.7 Ancona earthquake

Some of the uncorrected data contain multiple events within the acceleration histories. Waveforms from secondary events were generally removed in the PEER processing but were retained in ESD processing. This situation is evident in recordings of the Mw=6.9 1980 Irpinia Mainshock, as shown in [fig 5.5](#). It is not clear that the second event in the ESD data affected amplitude-related parameters (PHV, PHD, spectral acceleration) beyond the previously noted effects related to low-frequency energy content. However, the duration is clearly affected.

To evaluate potential for bias between the two datasets, we compare intensity measures calculated using the ESD and PEER databases in [figs. 5.6](#). Peak accelerations and velocities are generally comparable. The scatter in peak displacements is larger, with values from ESD mostly exceeding those from PEER.

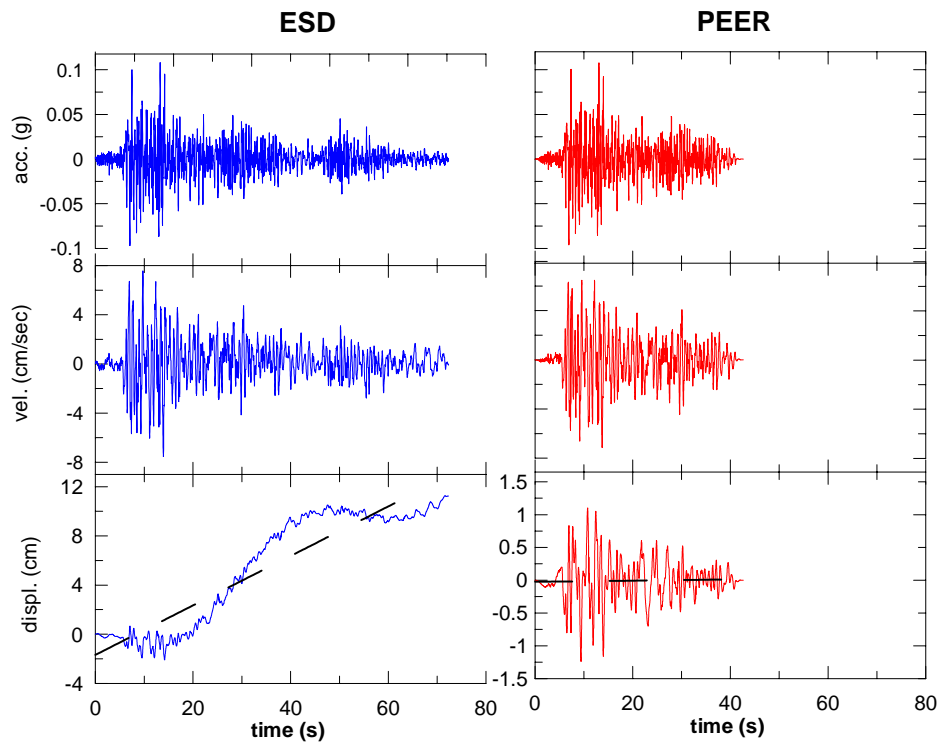


Figure 5.5. Comparison between ESD- and PEER-corrected waveforms using accelerometer recording at the Mercato San Severino station during the 1980 Mw=6.9 Irpinia earthquake. The uncorrected data and ESD processed data are interpreted to contain multiple triggering events.

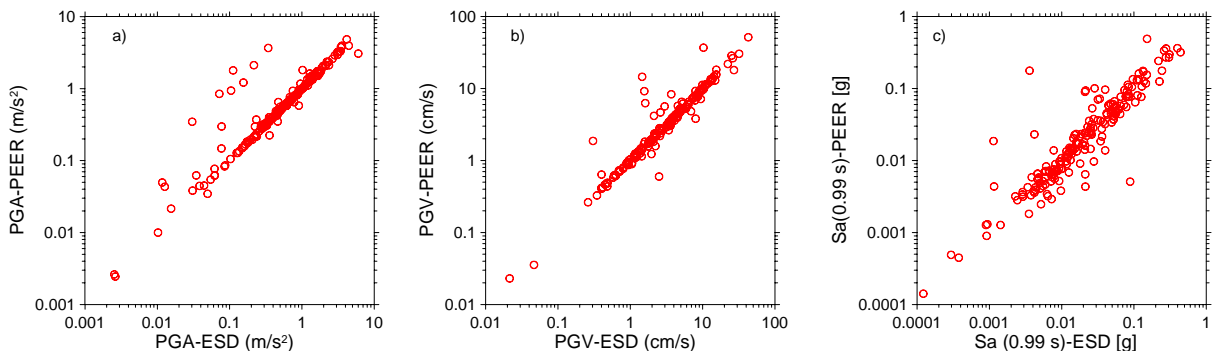


Figure 5.6. Comparison of ground motion intensity measures for corrected records in the ESD and PEER databases. The intensity measures that are compared are (a) peak acceleration, (b) peak velocity, and (c) spectral acceleration at 0.99 sec

5.3 SOURCE DATABANK

Attributes of the seismic source that are important for the development of GMPEs and ground motion selection for response history analysis include magnitude, source location and dimensions, and focal mechanism.

Point source information such as seismic moment and hypocenter location are extracted from a web site (INGV, 2007a) that reports the results of an INGV study termed “Project S6.” As described by Pondrelli et al. (2006), the Project S6 source parameters are available for most events between 1972 and 2004. Pondrelli et al. take CMT solutions from the Harvard moment tensor catalogue (e.g., Elkström et al., 2005) where available, which is for $M_w > 5.5$. For events since 1977,

Pondrelli et al. (2002, 2006) extend the Harvard dataset with the European-Mediterranean Regional CMT (RCMT) catalogue for $4.5 < M_w < 5.5$. Both Harvard CMT and RCMT solutions are based on model fits to medium and long period seismograms. Moment magnitudes are taken in Project S6 based on CMT and RCMT solutions. As explained by Pondrelli et al. (2006), additional magnitudes are obtained as follows: surface wave magnitude (M_s) is from the IRIS data management center (IRIS, 2007); body wave and local magnitude are taken from the USGS National Earthquake Information Center (<http://wwwneic.cr.usgs.gov/neis/epic/>) with some modifications by INGV. Generally just Local Magnitude (M_L) is available for all events.

For events not characterized by Project S6, hypocenter locations and magnitudes were taken, in order of preference, from the Parametric Catalogue of Italian Events (Working Group CPTI04, 2004) or from the ESD database (Ambraseys et al., 2004).

The finite fault parameters (strike, dip, rake, along-strike length, down-dip width, depth to top of rupture) have been compiled by INGV into the Database of Individual Seismogenic Sources (DISS) (INGV, 2007b; Basili et al., 2007). Those finite source parameters were compiled from the literature, and hence were developed using a variety of techniques (surface faulting, geologic investigations, magnitude-area scaling relationships, etc.). The 89 earthquakes included in the database are listed in Table 5.1, reported at the end of the chapter, with relative description parameters obtained as described so far.

Subsequently, hypocentral and epicentral distances were computed for all recordings while Joyner & Boore and rupture distances were evaluated just for stations that recorded well defined fault plane events. In fig. 5.7 the recording distribution with respect to rupture distance and local magnitude is plotted.

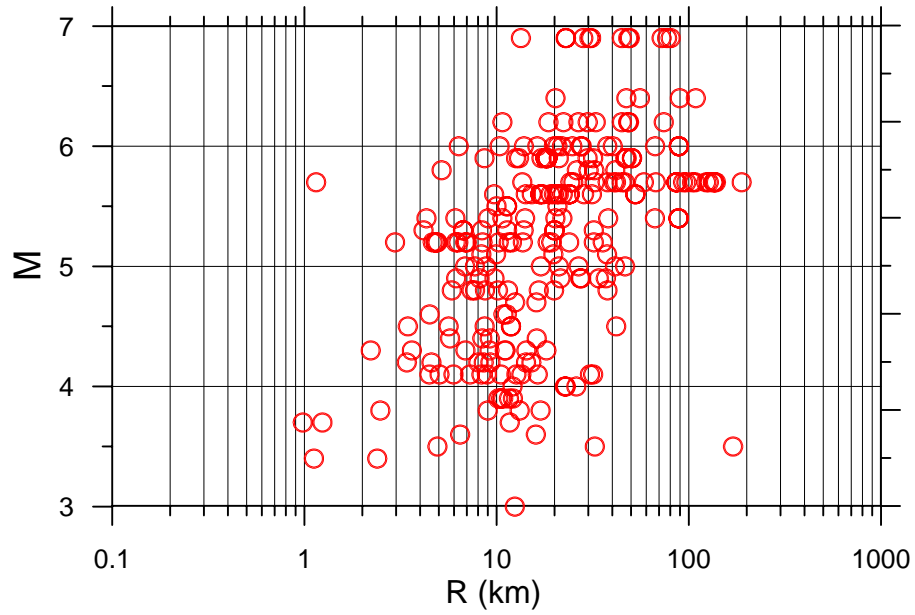


Figure 5.7. Data set distribution with respect to magnitude and rupture distance

As can be noted from [Table 5.1](#), most of the events listed in the database were generated by normal dip-slip fault movement. [Figure 5.8](#) summarizes the fault-mechanism distribution of the Italian earthquakes.

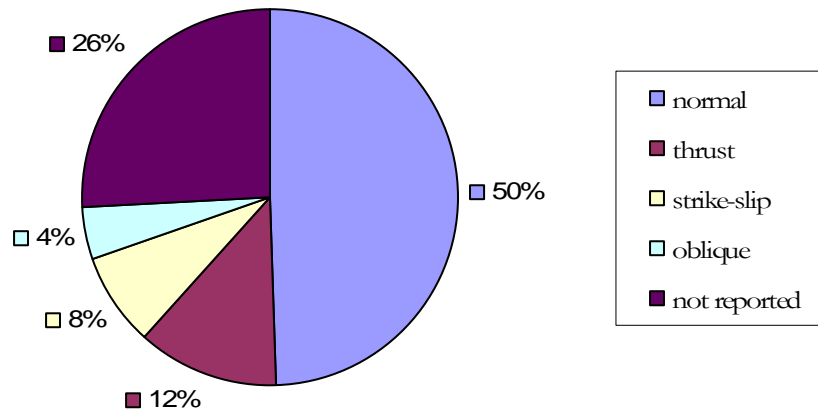


Figure 5.8. Earthquakes distribution based on fault-mechanism type

5.4 SITE DATABANK

Attributes of the recording sites that are important for the development of GMPEs and ground motion selection include the geotechnical site conditions and the instrument housing (see paragraph 5.5).

The site databank was compiled for 101 Italian strong motion stations that have produced the three-component 247 recordings referenced in the previous section.

5.4.1 General Considerations

As already stated in paragraph 2.4, wave propagation theory suggests that ground motion amplitude should depend on the density and shear wave velocity of near-surface media (e.g., Bullen, 1965; Aki and Richards, 1980). Density has relatively little variation with depth, and so shear wave velocity is the logical choice for representing site conditions. Two methods have been proposed for representing depth-dependent velocity profiles with a single representative value. The first takes the velocity over the depth range corresponding to one-quarter wavelength of the period of interest (Joyner et al., 1981), which produces frequency-dependent values. A practical problem with the quarter wavelength V_s parameter is that the associated depths are often deeper than can economically be reached with boreholes. A practical alternative is the average shear wave velocity in the upper 30 m of the site (V_{s30}), which has found widespread application.

Based on empirical studies by Borchardt and Glassmoyer (1994), Borchardt (1994) recommended V_{s30} as a means of classifying sites for building codes, and similar site categories were selected for the NEHRP seismic design provisions for new buildings (Dobry et al., 2000). GMPEs have since been developed that incorporate V_{s30} as the site parameter, including each of the NGA GMPEs except Idriss (2008). To develop those GMPEs, each site in the NGA database was assigned a V_{s30} value, with approximately 1/3 coming from on-site measurements and 2/3 coming from correlations with other, more readily available site information.

In the development of the NGA database, protocols were followed for estimating V_{s30} when on-site measurements (extending to a depth of at least 20 m) are not available. Those protocols are as follows (Borchardt, 2002):

- Velocity estimated based on nearby measurements on same geologic formation (site conditions verified based on site visit by geologist).
- Velocity estimated based on measurements on same geologic unit at site judged to have similar characteristics based on site visit by geologist.
- Velocity estimated based on average shear wave velocity for the local geologic unit; presence of the unit verified based on site visit by geologist.
- Velocity estimated based on average shear wave velocity for the geologic unit as evaluated from large-scale geologic map (1:24000 to 1:100000).

- Velocity estimated based on average shear wave velocity for the geologic unit as evaluated from small-scale geologic map (1:250000 to 1:750000).

Similar procedures for estimation of V_{s30} values at Italian strong motion stations were adopted with the results given in [Table 5.2](#) attached at the end of the chapter. Each site has been assigned V_{s30} value in the table along with an index pertaining to how the value was derived. Those indices are defined as:

- Category A: Velocity measured on-site using cross-hole, down-hole, or spectral analysis of surface wave methods;
- Category B: Velocity estimated based on nearby measurements on same geologic formation (site conditions verified based on site visit by geologist). This is similar to Categories (1)-(2) by Borchardt (2002).
- Category C: Velocity estimated based on measurements from the same geologic unit as that present at the site (based on local geologic map). This is similar to Categories (2)-(3) by Borchardt (2002).
- Category D: Velocity estimated based on general (non-local) correlation relationships between mean shear wave velocity and surface geology.

Next, method to assign V_{s30} values on the basis of surface geology for not investigated sites is described

5.4.2 Estimating Velocities for Sites without Measurements

For sites for which no local measurements of seismic velocities are available, V_{s30} values are estimated basing on correlations with surface geology. Correlations to estimate V_{s30} from surface geology are not available in the literature for geologic units in Italy. Accordingly, was tested the effectiveness in Italy of correlations developed for California and developed preliminary additional correlations for geologic units not represented in the California models.

The geology maps available for Italy include large-scale maps (1:100,000) by Servizio Geologico d'Italia that provide coverage of the entire country (and hence all recording stations) and local geologic maps/sections (typical scale 1:2000) by ENEL.

The local maps/sections are derived from a site visit by ENEL geologists and are available for 77 of 101 strong motion sites. Additional geologic information is available for a few sites from local microzonation reports or geologic reports for individual sites (references given in [Table 5.2](#)). The geologic classifications included in [Table 5.2](#) are based on the largest map scale that is available for the site.

The map scale from which the classification was taken is indicated in the table, with “local” referring to the aforementioned microzonation studies or geologic reports.

The best available correlations for California was judged to be those of [Wills and Clahan \(2006\)](#). A number of the Wills-Clahan geologic categories are descriptive of conditions encountered at Italian sites. Among these are Quaternary alluvium categories segregated by sediment depth and material texture

($Q_{al,thin}$; $Q_{al,deep}$; $Q_{al,coarse}$), older Quaternary alluvium (Q_{oa}), Quaternary to Tertiary alluvial deposits (Q_T), and Tertiary sandstone formations (T_{ss}). The relatively firm rock categories used by Wills-Clahan are generally not descriptive of Italian firm rock sites, which are often comprised of limestone, marls, and volcanic rocks.

Wills and Clahan (2006) provide mean and standard deviation values of V_{s30} for each geologic category based on California data. The applicability of those estimates to Italian sites is estimated by calculating V_{s30} residuals as:

$$R_i = (V_{s30})_{m,i} - (V_{s30})_{WC} \quad (5.1)$$

where $R_i = V_{s30}$ residual for site i , $(V_{s30})_{m,i}$ = value of V_{s30} from measurement at Italian site i , and $(V_{s30})_{WC}$ = mean value of V_{s30} from Table 1 of Wills and Clahan (2006). Due to the small number of sites falling in individual categories, sites are grouped into two general categories for analysis of residuals : Quaternary alluvium (combination of the thin, deep, and coarse sub-categories) and late Quaternary and Tertiary sediments (combination of Q_{oa} , Q_T and T_{ss}). Figure 5.9 shows histograms of residuals grouped in this manner. Also shown in fig. 5.9 is the range of velocities within \pm two standard deviations of zero using average values of standard deviation from Table 1 of Wills and Clahan (2006) for the grouped categories (taken as $\sigma_{WC}=85$ m/s for the Q_{al} categories and $\sigma_{WC}=170$ m/s for the $Q_{oa}/Q_T/T_{ss}$ categories).

The histogram for Q_{al} categories (fig. 5.9a) shows that the mean of residuals is nearly zero, but only 78% of the data fall within the $\pm 2\sigma_{WC}$ bands (approximately 95% should fall within this range if the Italian data shared the standard deviation of the California data). The histogram for the $Q_{oa}/Q_T/T_{ss}$ categories (fig. 5.9b) similarly shows a nearly zero mean, and 85% of the data fall within the $\pm 2\sigma_{WC}$ bands. Similar results are obtained if the grouped categories are broken down to smaller sub-categories (e.g., $Q_{al,deep}$ from Q_{al}). Hence, a preliminary conclusion is that the Wills-Clahan recommendations provide an unbiased estimate of V_{s30} for Italian alluvium sites of Quaternary to Tertiary age. However, the standard deviation of the Italian data is different, being larger for the Q_{al} categories are perhaps slightly smaller for the older alluvium and Tertiary categories.

As mentioned above, many of the rock sites listed in Table 5.2 have conditions geologically dissimilar to California such as limestone, marls, and volcanic rocks. Since it is unaware of existing correlations to V_{s30} for these types of materials, rock categories descriptive of Italian conditions that seem to generally have similar seismic velocities, were assembled. These categories are listed in Table 5.2 and are summarized as follows:

- Tm: This category consists of Tertiary Marl, often with surficial overconsolidated clays. It is common along the central-southern Apennines, and 13 sites in our database have this classification. A histogram of the Tm velocities is given in fig. 5.10a, showing a mean $V_{s30} = 670$ m/s and standard deviation = 190 m/s.
- Pc: This category consists of Pleistocene to Pliocene cemented conglomerate. Its occurrence is widespread in Sicily and the Apennines. Five sites in our database have this

classification, two of which have velocity measurements with $V_{s30} = 972$ and 1156 m/s. We use $V_{s30} = 1000$ m/s for sites without measurements.

- M_l , M_v , and M_g : This category comprises Mesozoic limestone (M_l), volcanic rocks (M_v), and gneiss (M_g). We group these three together for velocity characterization because the available data is inadequate to justify further discretization and the seismic velocities are generally high (> 1000 m/s). The M_l category includes 14 sites located in the Alps and Apennines. The M_v category applies to three sites located near the active volcanoes of Mt. Etna (Sicily) or Mt. Vesuvio (near Napoli). The M_g category is encountered only at the Messina and Milazzo Station in Sicily. A measured shear velocity of 1800 m/s is reported in Table 5.2 for Messina, but this measurement was made in a tunnel deep in the ground. Shallow velocities should be slower and hence the preferred V_{s30} value is given as 1000 m/s to be consistent with other the other Mesozoic categories.

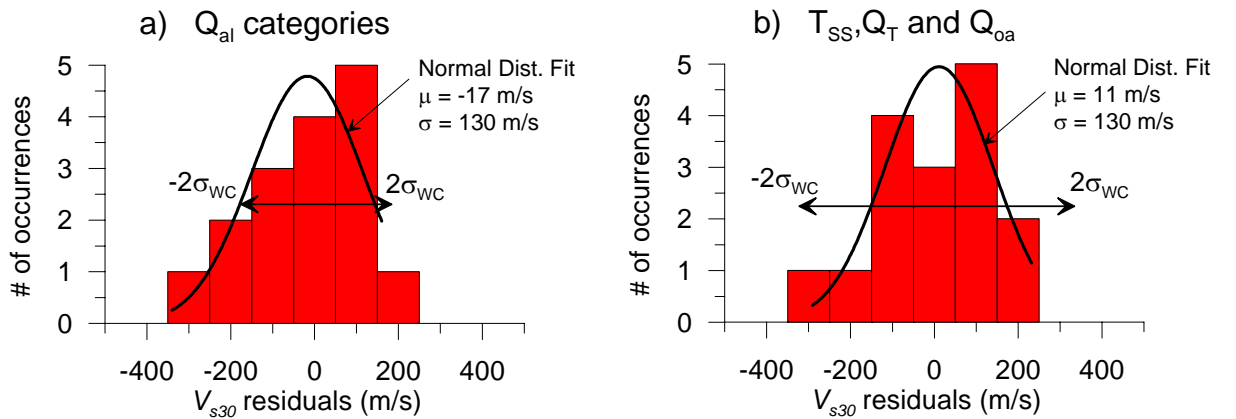


Figure 5.9. Histograms of V_{s30} residuals and normal distribution fits for (a) Quaternary alluvium categories and (b) older Quaternary, Quaternary-Tertiary, and Tertiary sandstone categories. The $\pm 2\sigma_{WC}$ limits indicate two standard deviations above and below zero from the Wills and Clahan (2006) correlation.

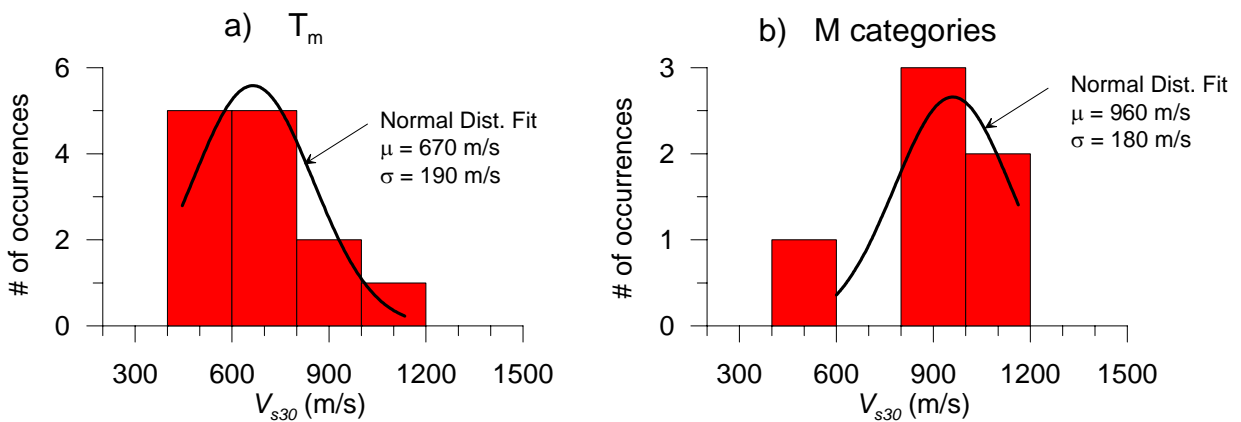


Figure 5.10. Histograms of V_{s30} values and normal distribution fit for (a) T_m category and (b) M categories

5.4.3 EC8 subsoil categories data distribution

The procedure described above and the data obtained from literature and site investigation as reported in previous sections, allowed to assign V_{s30} values to all recording stations listed in the database (see Table 5.2).

Based on those values, sites in object can also be classified following the Eurocode 8 (EC8) classification. Data distribution related to EC8 categories is summarized in fig. 5.11.

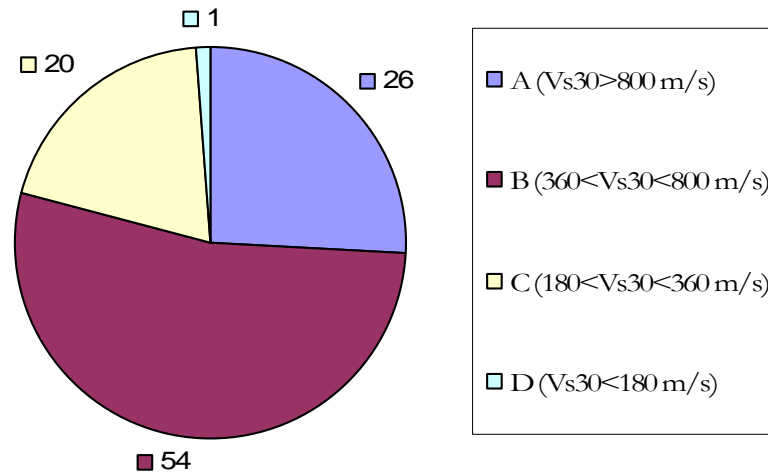


Figure 5.11. Recording stations' site distribution related to EC8 site classification

5.5 INSTRUMENT HOUSING

Housing information for the 101 strong motion stations is given in Table 5.2 attached at the end of the chapter. Most of the buildings (75) are in small cabins (CA) as described in chapter 3. Fifteen stations are at the foundation level of small buildings (typically single story buildings, 3-5 m in height, with footprint areas ranging from 10-30 m² (SB). Four instruments are on small slabs with no overlying structure, these are denoted as FF in Table 5.2. Remaining instruments have either unknown housing conditions or are located on dams (D) or in tunnels (T). Housing distribution is summarized in fig. 5.12.

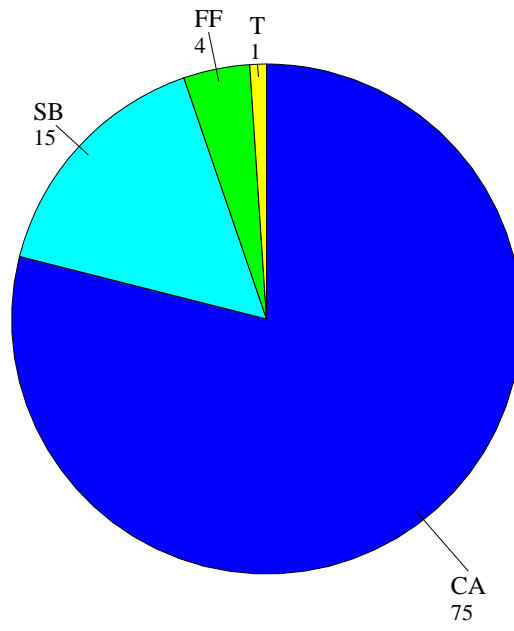


Figure 5.13. Recording stations distribution related to housing

Table 5.I. Source parameters for selected Italian earthquakes

#	Earthquake Name	Date	Time	Point Source Parameters									Finite Source Parameters											
		dd/mm/yyyy	(UTC)	Mw	Ms	ML	Mb	lat	long	Focal Mech.	Epicentral Intensity (MCS)	Focal Depth (km)	ref.	center lat	center long	strike	dip	L (km)	W (km)	z-top (ikm)	rake	slip	ref.	
1	Ancona	25/01/1972	23.22.17		4.0	4.0	4.8	43.70	13.41	normal		10	ESD											
2	Ancona	04/02/1972	2.42.18	5.2	4.8	4.6	4.5	43.633	13.550	oblique		8	CPT104											
3	Ancona	04/02/1972	9.18.30		4.3	4.4	4.3	43.730	13.380	oblique		8	ESD											
4	Ancona	04/02/1972	18.17.25		4.0	4.1	4.8	43.700	13.400	normal		10	ESD											
5	Ancona	05/02/1972	1.26.30		4.2	4.3	4.3	43.720	13.400	oblique		10	ESD											
6	Ancona	06/02/1972	1.34.19		4.1	4.3	4.6	43.700	13.430	oblique		5	ESD											
7	Ancona	06/02/1972	21.44.45				3.0	43.700	13.400	normal		2.5	S6_D5											
8	Ancona	08/02/1972	12.19.10			3.9		43.683	13.400	normal		2.5	S6_D5											
9	Ancona	14/06/1972	18.55.53	4.8	5.2	4.7	4.9	43.650	13.600	strike slip	8.5	3.0	S6_D5											
10	Ancona	14/06/1972	21.01.02			4.2		43.667	13.417	normal		21.0	S6_D5											
11	Ancona	21/06/1972	15.06.53			4.0		43.817	13.600	normal		4.0	S6_D5											
12	Friuli	06/05/1976	20.00.13	6.4	6.5	6.4	5.9	46.350	13.260	thrust	9.5	12.0	S6_D5	46.2507	13.1447	290	30	16	9	2	105	1.32	DISS-IS	
13	Friuli (aftershock)	07/05/1976	0.23.49	4.9		4.9		46.240	13.270	thrust		26.0	S6_D5											
14	Friuli (aftershock)	11/05/1976	22.44.01	5.0		5.3	4.9	46.290	12.990	thrust		13.0	S6_D5											
15	Friuli (aftershock)	18/05/1976	1.30.09	4.1		4.1		46.250	12.867	normal		5.0	S6_D5											
16	Friuli (aftershock)	09/06/1976	18.48.17	4.3		4.1		46.350	13.067	normal		16.0	S6_D5											
17	Friuli (aftershock)	11/06/1976	17.16.36	4.5		4.3		46.267	12.967	normal		18.0	S6_D5											
18	Friuli (aftershock)	17/06/1976	14.28.51	4.7		4.5		46.177	12.798	normal		15.0	S6_D5											
19	Friuli (aftershock)	07/09/1976	11.08.16	4.2		4.1		46.300	12.983	normal		5.0	S6_D5											
20	Friuli (aftershock)	11/09/1976	16.31.11	5.3	5.5	5.5	5.0	46.290	13.180	thrust	9	10.0	S6_D5											
21	Friuli (aftershock)	11/09/1976	16.35.03	5.6	5.4	5.8	5.3	46.300	13.317	thrust	9	9.0	S6_D5	46.2392	13.2634	277	30	6	4.5	2	90	0.45	DISS-IS	
22	Friuli (aftershock)	13/09/1976	18.54.47	4.6		4.3		46.283	13.200	normal		14.0	S6_D5											
23	Friuli (aftershock)	15/09/1976	3.15.19	5.9	6.0	6.1	5.7	46.300	13.190	thrust		2.0	S6_D5	46.2665	13.2151	274	35	8	5.5	2	90	0.83	DISS-IS	
24	Friuli (aftershock)	15/09/1976	4.38.53	4.9		4.8	4.8	46.267	13.167	normal		21.0	S6_D5											
25	Friuli (aftershock)	15/09/1976	9.21.18	5.9	5.9	6.0	5.4	46.300	13.183	thrust	8.5	21.0	S6_D5	46.2754	13.2009	276	35	10	6.4	6.5	110	0.75	DISS-IS	
26	Friuli (aftershock)	16/09/1977	23.48.07	5.3	5.1	5.3	5.1	46.280	12.980	thrust	7.5	21.0	S6_D5											
27	Calabria	11/03/1978	19.20.48	5.2	5.1	5.3		37.979	16.184	normal	8	5.0	S6_D5	38.01	15.98	86	45	6.4	4				DISS-MSw	
28	Basso Tirreno	15/04/1978	23.33.48	6.0	5.8	5.5	5.5	38.268	15.112	strike slip	9	22.0	S6_D5	38.2589	15.0500	147	83	12.1	8.6	1.5	180	0.6	DISS-IS	
29	Marche	21/05/1979	14.34.19			3.6		43.050	12.962	n.r.		33.0	S6_D5											
30	Colle	17/06/1979	4.49.38			3.8		43.153	12.881	n.r.		1.0	S6_D5											
31	Valnerina	19/09/1979	21.35.37	5.8	5.9	5.5	5.8	42.800	13.040	normal	8.5	6.0	S6_D5	42.71	13.07	156	45	9.7	5				DISS-MSw	
32	Umbria	21/09/1979	0.52.45			4.2		42.733	13.033	normal		1.0	S6_D5											
33	Umbria	28/09/1979	4.41.21			3.6		42.733	13.100	normal		6.0	S6_D5											
34	Norcia	08/11/1979	18.44.43			4.1		42.810	13.040	n.r.		4	ESD											
35	W of Cosenza	20/02/1980	2.34.01	4.4		4.2		39.286	16.152	normal		12.0	S6_D5											
36	Norcia	05/03/1980	6.23.37			3.4		42.785	13.085	n.r.		21.0	S6_D5											
37	Norcia	11/03/1980	5.20.08			3.4		42.812	13.090	n.r.		13.0	S6_D5											
38	Norcia	24/05/1980	20.16.05			4.3		42.815	13.126	n.r.		15.0	S6_D5											
39	Toscana	07/06/1980	18.35.01	4.6	4.1	4.3		44.050	10.600	normal		30.0	S6_D5											
40	Irpinia 1st	23/11/1980	18.34.52	6.9	6.8	6.5	6.0	40.760	15.309	normal		15.0	S6_D5	40.8021	15.2944	310	60	28	15	1	270	1.65	DISS-IS	
41	Irpinia 2nd	23/11/1980	18.35.13			6.2		40.846	15.332	normal		7.0	PEER	40.6842	15.4826	300	60	9	15	1	270	0.7	DISS-IS	
42	Irpinia (aftershock)	24/11/1980	0.24.02	5.0		4.9		40.811	15.268	normal		13.0	S6_D5											
43	Irpinia (aftershock)	24/11/1980	3.03.56	5.0		4.5		40.861	15.374	normal		9.0	S6_D5											
44	Irpinia (aftershock)	25/11/1980	21.53.37			3.8		40.986	15.222	n.r.		17.0	S6_D5											
45	Irpinia (aftershock)	26/11/1980	14.55.43			4.3		40.942	15.268	n.r.		15.0	S6_D5											

(continued on next page)

Table 5.I. Source parameters for selected Italian earthquakes (continued)

#	Earthquake Name	Date	Time	Point Source Parameters									Finite Source Parameters										
		dd/mm/yyyy	(UTC)	Mw	Ms	ML	Mb	lat	long	Focal Mech.	Epicentral Intensity (MCS)	Focal Depth (km)	ref.	center lat	center long	strike	dip	L (km)	W (km)	z-top (ikm)	rake	slip	ref.
46	Irpinia (aftershock)	26/11/1980	15.56.44					40.857	15.711	normal		n.r.	ESD										
47	Irpinia (aftershock)	30/11/1980	7.41.59			4.5		40.761	15.316	n.r.		18.0	S6_D5										
48	Irpinia (aftershock)	01/12/1980	19.04.31			4.6	4.3	40.885	15.308	n.r.		9.0	S6_D5										
49	Irpinia (aftershock)	16/01/1981	0.37.47	5.2	5.3	4.6	5.0	40.838	15.441	normal		10.5	S6_D5										
50	Irpinia (aftershock)	16/01/1981	4.36.51			3.9		40.782	15.352	n.r.		16.1	S6_D5										
51	Irpinia (aftershock)	16/01/1981	6.31.26			3.8		40.835	15.501	n.r.		12.9	S6_D5										
52	Irpinia (aftershock)	14/02/1981	17.27.46	4.9	4.8	4.7		41.061	14.794	thrust	7	10.1	S6_D5										
53	SW of Campobello di Mazara	07/06/1981	13.01.00	4.9		4.8		37.631	12.718	thrust		45.0	S6_D5										
54	Near coast of Scalea	21/03/1982	9.44.02			5.0		39.704	15.639	n.r.		18.9	S6_D5										
55	Arpiola	22/03/1984	0.16.25			3.5		44.270	9.910	n.r.		22.1	S6_D5										
56	Umbria	29/04/1984	5.02.59	5.6	5.2	5.2	5.1	43.208	12.568	normal	7	6.0	S6_D5	43.2251	12.5682	140	21	10	7	4	270	0.5	DISS-IS
57	Lazio Abruzzo	07/05/1984	17.49.42	5.9	5.8	5.9	5.4	41.701	13.863	normal	8	20.5	S6_D5	41.6964	13.9470	152	50	10	7.5	5	264	0.27	DISS-IS
58	Lazio Abruzzo (aftershock)	11/05/1984	10.41.50	5.5	5.2	5.7	5.2	41.708	13.890	normal		12.1	S6_D5										
59	Lazio Abruzzo (aftershock)	11/05/1984	13.14.56	4.8		4.6		41.754	13.919	normal		12.2	S6_D5										
60	Lazio Abruzzo (aftershock)	11/05/1984	16.39.18			4.4		41.685	13.880	n.r.		11.8	S6_D5										
61	N of Reggio di Calabria	14/05/1985	5.44.36			3.8		38.231	15.668	n.r.		11.8	S6_D5										
62	Casamaina	20/05/1985	10.00.28			4.2		42.266	13.372	n.r.		11.5	S6_D5										
63	Off coast of Numana	22/06/1986	14.07.51			3.7		43.569	13.745	n.r.		5.3	S6_D5										
64	Potenza	05/05/1990	7.21.17	5.8	5.6	5.2	5.2	40.640	15.860	strike slip	7	22.5	S6_D5	40.6780	15.8520	95	88	7.9	6.2	14.8	175	0.26	DISS-IS
65	Sicilia-Orientale	13/12/1990	0.24.26	5.6	5.2	5.4	5.3	37.270	15.322	strike slip	7	7.0	S6_D5										
66	Umbria Marche	26/09/1997	0.33.16	5.7	5.6	5.6	5.5	43.023	12.891	normal		3.5	S6_D5	42.9990	12.9267	148	40	9	6	4	277	0.38	DISS-IS
67	Umbria Marche	26/09/1997	9.40.30	6.0	6.1	5.8	5.7	43.015	12.854	normal	8.5	9.9	S6_D5	43.0874	12.8358	152	40	12	7.5	4	280	0.37	DISS-IS
68	Umbria Marche (aftershock)	03/10/1997	8.55.22	5.2		5.0		43.043	12.825	normal		12.1	S6_D5										
69	Umbria Marche (aftershock)	04/10/1997	16.13.33	4.7		4.5		42.916	12.906	normal		6.2	S6_D5										
70	Umbria Marche (aftershock)	06/10/1997	23.24.00	5.4		5.4		43.028	12.847	normal		3.9	S6_D5										
71	Umbria Marche (aftershock)	07/10/1997	1.24.34	4.2		4.1		43.037	12.846	normal		4.9	S6_D5										
72	Umbria Marche (aftershock)	07/10/1997	5.09.57	4.5		4.3		43.036	12.859	normal		1.7	S6_D5										
73	Umbria Marche (aftershock)	11/10/1997	3.20.56			3.7		43.105	12.790	n.r.		3.5	S6_D5										
74	Umbria Marche (aftershock)	12/10/1997	11.08.36	5.2		5.1		42.906	12.920	normal		0.1	S6_D5										
75	Umbria Marche (aftershock)	12/10/1997	20.15.29			4.0		n.r.	n.r.	normal		10	ESD										
76	Umbria Marche (aftershock)	13/10/1997	13.09.21	4.4		4.1		42.862	12.940	normal		0.7	S6_D5										
77	Umbria Marche (aftershock)	14/10/1997	15.23.00	5.6	5.6	5.5	5.3	42.898	12.899	normal		7.3	S6_D5	42.9133	12.9342	144	40	6	6	2.5	260	0.28	DISS-IS
78	Umbria Marche (aftershock)	14/10/1997	23.23.28			4.1		42.956	12.872	n.r.		4.1	S6_D5										
79	Umbria Marche (aftershock)	16/10/1997	12.00.31	4.3		4.5		43.044	12.884	strike slip		2.4	S6_D5										
80	Umbria Marche (aftershock)	08/11/1997	15.31.54			4.1		42.863	12.974	n.r.		0.3	S6_D5										
81	Umbria Marche (aftershock)	09/11/1997	19.07.33	4.9		4.5		42.846	12.988	normal		1.5	S6_D5										
82	Umbria Marche (aftershock)	01/12/1997	22.37.05			3.5		42.858	12.978	n.r.		1.8	S6_D5										
83	Umbria Marche (aftershock)	21/03/1998	16.45.10	5.0		4.4		42.949	12.914	normal		1.1	S6_D5										
84	Umbria Marche (aftershock)	26/03/1998	16.26.18	5.3	4.8			43.146	12.809	n.r.	6	44.8	S6_D5										
85	Umbria Marche (aftershock)	03/04/1998	7.26.00	5.1		5.3		43.185	12.757	normal		1.9	S6_D5										
86	Umbria Marche (aftershock)	05/04/1998	15.52.20	4.8		4.5		43.190	12.767	normal		4.4	S6_D5										
87	Trasaghis-Friuli	28/05/1998	9.39.19			4.1		46.295	13.049	n.r.		11.0	ESD										
88	Molise	31/10/2002	7.40.48	5.7	5.6	5.4	5.2	41.717	14.893	strike slip	7.5	25.2	S6_D5	41.6876	14.9391	267	82	10.5	8	12	203		DISS-IS
89	Molise	01/11/2002	1.55.12	5.7	5.6	5.3	5.5	41.742	14.843	strike slip		21.4	S6_D5	41.6959	14.8141	261	86	9.4	8	12	195		DISS-IS

Table 5.II. Recording stations information

#	Station				Geology					V _{s30} (m/sec)						Housing (2)	
	Name	Agency	Latitude	Longitude	Age	Description	Scale (plan/section)	Wills-Clahan class.	Our class.	Source (1)	Type	Measured	Estimated	Preferred	EC8 class.		Reference
1	Ancona-Palombina	ENEA	43.602	13.474	Pleistocene	clay with silt and sand	1:50000 / 1:2000	QT		A	CH	256	455	256	C	Working group (1981)	SB
2	Ancona-Rocca	ENEA	43.621	13.513	Miocene	marls	1:50000 / 1:2000		Tm	A	CH	549	600	549	B	Working group (1981)	SB
3	Aquilpark-Citta	DPC	42.346	13.401	Pleistocene	coarse alluvium	local	QT		C			455	455	B		FF
4	Aquilpark-Galleria	DPC	42.346	13.401	Pleistocene	coarse alluvium	local	QT		C			455	455	B		T
5	Aquilpark-Parcheggio	DPC	42.346	13.401	Pleistocene	coarse alluvium	local	QT		C			455	455	B		SB
6	Arienzo	DPC	41.027	14.469	Pleistocene	cinerities, piroclastic and conid material (5m), campanian ignimbrite, overlying limestones of campano-lucana platform	1:50000 / 1:2000		Mv	A	CH	905	1000	905	A	Palazzo (1991)	CA
7	Assergi	DPC	42.42	13.52	Terziario	sandy clay and marls	1:50000 / 1:2000		Tm	C			600	600	B		CA
8	Assisi-Stallone	DPC	43.075	12.607	Cretacico	limestone and marls	1:50000 / 1:2000		MI	C			1000	1000	A		SB
9	Atina	ENEA	41.620	13.801	Giurassico	dolomitic limestone	1:50000 / 1:2000		MI	C			1000	1000	A		CA
10	Atina-Pretura Piano Terra	ENEA	41.645	13.783	Miocene	clay and clay with marls with layers of gray and yellow sandstone	1:50000 / 1:2000		Tm	C			600	600	B		SB
11	Atina-Pretura Terrazza	ENEA	41.645	13.783	Miocene	clay and clay with marls with layers of gray and yellow sandstone	1:50000 / 1:2000		Tm	C			600	600	B		SB
12	Auletta	DPC	40.556	15.395	Pliocene	lacustrine and deltaic polygenic conglomerate with sandy-clay cement	1:50000 / 1:2000		Pc	A	CH	1156	1000	1156	A	Palazzo (1991)	CA
13	Avezzano	DPC	42.03	13.43	Quaternario	Alluvium	1:100000	Qal,deep		B	CH	120	280	120	D	A.G.I. (1991)	CA
14	Bagnoli-Irpino	DPC	40.831	15.068	Cretacico	limestone	1:50000 / 1:2000		MI	A	CH	1163	1000	1163	A	Palazzo (1991)	CA
15	Barcis	DPC	46.187	12.554	Olocene	debris on marls	1:50000 / 1:2000	Qal,coarse		D			354	354	C		CA
16	Barga	DPC	44.068	10.461	Pleistocene	coarse non cemented alluvium deposit on gravel and conglomerate	1:50000 / 1:2000	Qoa		D			387	387	B		CA
17	Bevagna	DPC	42.932	12.611	Olocene	clay, clay/sand and sand deposit on "bisciaro"	1:50000 / 1:2000	Qal,deep		A	SASW	182	280	182	C	This study	CA
18	Bisaccia	DPC	41.010	15.376	Pliocene	cemented conglomerate with sandy thin layers	1:50000 / 1:2000		Pc	A	CH	972	1000	972	A	Palazzo (1991)	CA
19	Borgo-Cerreto Torre	ENEA	42.814	12.915	Terziario	limestone	1:50000 / 1:2000		MI	C			1000	1000	A		SB
20	Bovino	DPC	41.249	15.342	Pliocene	sand and sandstone with conglomerate and sandy clay	1:50000 / 1:2000	QT		A	CH	356	455	356	C	Palazzo (1991)	CA
21	Brienza	DPC	40.472	15.634	Olocene	recent alluvium on red flysch	1:50000 / 1:2000	Qal,coarse		A	CH	516	354	516	B	Palazzo (1991)	CA
22	Buia	ENEA	46.222	13.090	Olocene	alternance of gravels and pebbels, mix of gravely sand and silty sand	1:50000 / 1:2000	Qal,coarse		A	CH	254	354	254	C	Fontanive et al. (1985)	CA
23	Cairano 1	DPC	40.890	15.296	Pliocene	marls	1:50000 / 1:2000		Tm	C			625	600	B	Faccioli (1992)	CA
24	Cairano 2	DPC	40.887	15.312	Pliocene	marls	1:50000 / 1:2000		Tm	C			625	600	B	Faccioli (1992)	CA
25	Cairano 3	DPC	40.887	15.334	Pliocene	marls	1:50000 / 1:2000		Tm	C			625	600	B	Faccioli (1992)	CA
26	Cairano 4	DPC	40.886	15.348	Pliocene	marls	1:50000 / 1:2000		Tm	C			625	600	B	Faccioli (1992)	CA
27	Caltri	DPC	40.898	15.439	Pliocene	sandstone, sand with levels of marls	1:50000 / 1:2000	Tss		A	CH	518	515	518	B	Palazzo (1991)	CA
28	Cascia	DPC	42.719	13.013	Oligocene	marls	1:50000 / 1:2000		Tm	A	SASW	540	600	540	B	This study	SB
29	Cascia-Cabina Petrucci	DPC	42.755	13.004	Pleistocene	sandy and gravely deposit	1:100000	Qoa		A	SASW	339	387	339	A	This study	SB
30	Cassinio-Sant' Elia	ENEA	41.523	13.864	Miocene	clay and clay with marls with layers of gray and yellow sandstone	1:50000 / 1:2000		Tm	C			600	600	B		CA
31	Castelnuovo-Assisi	DPC	43.007	12.591	Olocene	recent alluvium of clayey layers on sands an silt	1:50000 / 1:2000	Qal,deep		A	SASW	293	280	293	C	This study	CA
32	Castiglione Messer Marino	DPC	41.868	14.449	Miocene	marls	1:100000		Tm	C			600	600	B		CA
33	Catania-Piana	DPC	37.447	15.047	Olocene	alluvium clayey and sandy deposit on Pleistocene clay	1:50000 / 1:2000	Qal,deep		A	CH	261	280	261	C	Frenna & Maugeri (1993)	CA

(continued on next page)

Table 5.II. Recording stations information (continued)

#	Station				Geology					V _{s30} (m/sec)						Housing (2)	
	Name	Agency	Latitude	Longitude	Age	Description	Scale (plan/section)	Wills-Clahan class.	Our class.	Source (1)	Type	Measured	Estimated	Preferred	EC8 class.		Reference
34	Chieti	DPC	42.36	14.14	Quaternario	gray clay and marls	1:100000	Qoa		D			387	387	B		CA
35	Codroipo	DPC	45.959	12.984	Quaternario	coarse grevly alluvium	1:50000 / 1:2000	Qoa		D			387	387	B		CA
36	Coflorito	DPC	43.037	12.921	Pleistocene	lacustrium deposit	1:50000 / 1:2000	Qoa		A	SASW	317	387	317	C	This study	CA
37	Coflorito-Casermette	DPC	43.028	12.900	Olocene	lacustrium and fluviolacustrum sandy-clayey sediments	1:100000	Qal.coarse		A	SASW	405	354	405	B	This study	SB
38	Conegliano Veneto	DPC	45.883	12.288	Quaternario	gravely alluvium	1:50000 / 1:2000	Qoa		D			387	387	B		CA
39	Contrada Fiumicella-Teora	ENEA	40.881	15.255	Pleistocene	alluvium	1:100000	Qoa		D			387	387	B		FF
40	Conza-Base	DPC	40.875	15.327	Pliocene	marls and clay	1:50000 / 1:2000		Tm	C		625	600	625	B	Faccioli (1992)	CA
41	Conza-Vetta	DPC	40.872	15.329	Pliocene	gravely and sandy conglomerate on Pliocene clay	1:50000 / 1:2000	QT		D		406	455	406	B	Faccioli (1992)	CA
42	Cosenza	DPC	39.304	16.247	Pleistocene	gray clays	1:50000 / 1:2000	QT		D			455	455	B		CA
43	Feltre	DPC	46.019	11.912	Olocene	recent sandy-silty alluvium on Quaternary deposit	1:50000 / 1:2000	Qal.coarse		D			354	354	C		CA
44	Ferruzzano	DPC	38.051	16.132	Miocene	varicoloured clay	1:100000		Tm	C			600	600	B		CA
45	Foligno Santa Maria Infraportas-Base	ENEA	42.955	12.704	Olocene	recent alluvium	1:50000 / 1:2000	Qal.deep		A	SASW	395	280	395	B	This study	SB
46	Forgaria-Cornino	ENEA	46.221	12.997	Pleistocene	Pleistocene alluvium deposit (50 m) on Miocene marls and sandstone	1:50000 / 1:2000	Qoa		A	CH	454	387	454	B	Fontanive et al. (1985)	CA
47	Garigliano-Centrale Nuc. 1	DPC	41.258	13.833	Olocene	alluvium deposit	1:50000 / 1:2000	Qal.deep		A	CH	187	280	187	C	Palazzo (1991)	CA
48	Garigliano-Centrale Nuc. 2	DPC	41.258	13.833	Olocene	alluvium deposit	1:50000 / 1:2000	Qal.deep		A	CH	187	280	187	C	Palazzo (1991)	CA
49	Gemona-Li Furnie	trieste univ	46.267	13.115	Oligocene	gravel, sand and silt	1:50000 / 1:2000	Qal.coarse		D			354	354	C		n.r.
50	Gemona-Scugelars	trieste univ	46.283	13.142	Oligocene	gravel, sand and silt	1:100000	Qal.coarse		D			354	354	C		n.r.
51	Genio-Civile	DPC	43.623	13.516	Miocene	marls	local		Tm	B		549	600	549	B	Working group (1981)	SB
52	Gubbio	DPC	43.357	12.602	Miocene	marls with levels of sandstone	1:50000 / 1:2000		Tm	A	SASW	922	600	922	A	This study	CA
53	Gubbio-Piana	DPC	43.313	12.589	Pleistocene	alluvium	1:50000 / 1:2000	Qoa		A	SASW	492	387	492	B	This study	CA
54	Lab.Gran Sasso	DPC	42.436	13.554	Eocene	limestone	1:100000		MI	C		1000	1000	A		SB	
55	Lauria-Galdo	DPC	40.021	15.89	Giurassico	limestone	1:50000 / 1:2000		MI	C		1000	1000	A		CA	
56	Maiano-Piano Terra	DPC	46.187	13.069	Olocene	gravely alluvium with sand and silt	1:50000 / 1:2000	Qal.coarse		A	CH	344	354	344	C	Palazzo (1991)	SB
57	Maiano-Prato	DPC	46.187	13.069	Olocene	gravely alluvium with sand and silt	1:100000	Qal.coarse		A	CH	344	354	344	C	Palazzo (1991)	FF
58	Matelica	DPC	43.249	13.007	Pleistocene	gravely and sandy alluvium	1:50000 / 1:2000	Qoa		A	SASW	437	387	437	B	This study	CA
59	Mazara del Vallo	DPC	37.653	12.611	Pleistocene	cemented deposit	1:100000		Pc	C		1000	1000	A		CA	
60	Mercato San Severino	DPC	40.789	14.763	Olocene	recent alluvium (20m) on volcanic rock(20m) on recent alluvium (20m) on limestone	1:50000 / 1:2000	Qal.thin		A	CH	451	349	451	B	Palazzo (1991)	CA
61	Messina 1	DPC	38.207	15.516	Pretriassico	volcanic and metamorphic rock	1:100000		Mg	B	CH	1800	1000	1000	A	Baldovini et al.(1993)	CA
62	Milazzo	DPC	38.232	15.244	Pretriassico	metamorphic rock	1:50000 / 1:2000		Mg	B	CH	1800	1000	1000	A	Baldovini et al. (1993)	CA
63	Moggio	trieste univ	46.406	13.189	Triassico	limestone	1:100000		MI	C		1000	1000	A		CA	
64	Naso	DPC	38.119	14.786	Pliocene	clayey sand and conglomerate	1:100000	QT		B	DH	223	455	223	C	Dott.Copat. Personal com.	CA
65	Nocera Umbra	DPC	43.113	12.785	Miocene	sandstone on marls	1:100000	Tss		A	SASW	428	515	428	B	This study	CA
66	Nocera Umbra 2	DPC	43.113	12.785	Miocene	sandstone on marls	1:100000	Tss		A	SASW	428	515	428	B	This study	CA

(continued on next page)

Table 5.II. Recording stations information (continued)

#	Station				Geology					V _{s30} (m/sec)						Housing (2)	
	Name	Agency	Latitude	Longitude	Age	Description	Scale (plan/section)	Wills-Clahan class.	Our class.	Source (1)	Type	Measured	Estimated	Preferred	EC8 class.		Reference
67	Nocera Umbra-Biscontini	DPC	43.103	12.805	Miocene	sandstone on marls	local	Tss		A	SASW	442	515	442	B	This study	n.r.
68	Nocera Umbra-Salmata	DPC	43.149	12.797	Olocene	detritus	1:50000 / 1:2000	Qal,coarse		A	SASW	694	354	694	B	This study	CA
69	Norcia	DPC	42.791	13.096	Pleistocene	sandy and gravely alluvium and detritus	1:50000 / 1:2000	Qoa		A	SASW	678	387	678	B	This study	CA
70	Norcia-Altavilla	ENEA	42.796	13.089	Quaternario	recent alluvium, palustrine and lacustrine deposit	1:50000 / 1:2000	Qal,thin		A	SASW	218	349	218	C	This study	SB
71	Norcia-Zona Industriale	ENEA	42.775	13.097	Quaternario	lacustrine and fluvio-lacustrine deposit	1:50000 / 1:2000	Qal,thin		A	SASW	551	349	551	B	This study	CA
72	Ortucchio	DPC	41.953	13.642	Olocene	sandy-clayey recent alluvium, locally gravely	1:50000 / 1:2000	Qal,coarse		D			354	354	C		CA
73	Patti-Cabina Prima	DPC	38.134	14.976	Miocene	sandy limestone	1:50000 / 1:2000		Tm	C		600	600	600	B		CA
74	Pellaro	DPC	38.024	15.654	Olocene	weak alluvium fixed by vegetation on marls	1:100000	Qal,thin		D		349	349	349	C		CA
75	Poggio-Picenze	DPC	42.322	13.54	Pleistocene	alternation of silt and breccia	1:50000 / 1:2000	QT		D		455	455	455	B		CA
76	Ponte Corvo	DPC	41.499	13.683	Pleistocene	limestone and sandstone	1:50000 / 1:2000		MI	C		1000	1000	1000	B		CA
77	Pradis	trieste univ	46.248	12.888	Cretacico	limestone	1:50000 / 1:2000		MI	C		1000	1000	1000	B		CA
78	Procisa Nuova	ENEA	40.87	15.19	Pleistocene	recent alluvium	1:100000	Qoa		D		387	387	387	B		CA
79	Rieti	DPC	42.430	12.821	Olocene	alluvium deposit	1:100000	Qal,deep		D		280	280	280	C		CA
80	Rionero in Vulture	DPC	40.927	15.669	Pleistocene	vulcanic silt and gravel	1:50000 / 1:2000	Qoa		A	CH	539	387	539	B	Palazzo (1991)	CA
81	Roccamonfina	DPC	41.287	13.980	Olocene	weakly cemented detritus (10m) on volcanic rock	1:100000	Qal,coarse		D		354	354	354	C		CA
82	Roggiano-Gravina	DPC	39.619	16.171	Pliocene	sand and conglomerate weakly cemented	1:100000	QT		D		455	455	455	B		A
83	San Agapito	DPC	41.567	14.233	Pleistocene	alluvium deposit	local	QT		B	DH	553	455	553	B	Isernia Adm: Microzonation	CA
84	San Francesco	trieste univ	46.309	12.935	Triassico	limestone	1:100000		MI	C		1000	1000	1000	A		CA
85	San Marco dei Cavoti	DPC	41.306	14.88	Miocene	yellow sand and sandstone	1:100000	Tss		D		515	515	515	B		CA
86	San Rocco	ENEA	46.221	12.997	Cretacico	limestone	1:50000 / 1:2000		MI	C		600	1000	600	B	Fontanive et al. (1985)	FF
87	Sannicandro	DPC	41.833	15.572	Pleistocene	silty clay	local		Tm	A	CH	865	600	865	A	Palazzo (1991)	CA
88	Sellano Ovest	DPC	42.87	12.92	Miocene	marls	local		Tm	A	SASW	509	600	509	B	This study	CA
89	Sirolo	DPC	43.517	13.619	Miocene	marls with weak level on top	1:50000 / 1:2000		Tm	C		600	600	600	B		CA
90	Sortino	DPC	37.163	15.030	Miocene sup	vulcanic rock (15m) on limestone	1:50000 / 1:2000		Mv	C		1000	1000	1000	A		CA
91	Spoleto	DPC	42.736	12.737	Pleistocene	cemented conglomerate	borehole		Pc	C		1000	1000	1000	A		CA
92	Sturno	DPC	41.021	15.115	Oligocene	clay and marls	1:50000 / 1:2000		Tm	A	CH	1134	600	1134	A	Palazzo (1991)	CA
93	Tarcento	DPC	46.226	13.210	Olocene	sandy deposit (10m) on marls and sandstone	1:50000 / 1:2000	Qal,coarse		A	CH	843	354	843	A	Brambati et al (1979)	CA
94	Tolmezzo-Diga Ambiesta	DPC	46.382	12.982	Cretacico	limestone	1:50000 / 1:2000		MI	A	CH	1092	1000	1092	A	Fontanive et al. (1985)	D
95	Torre del Greco	DPC	40.797	14.383	Olocene	weak volcanic rock (high voids presence)	1:50000 / 1:2000		Mv	C		1000	1000	1000	A		CA
96	Tregnago	DPC	45.525	11.134	Cretacico	limestone	1:50000 / 1:2000		MI	C		1000	1000	1000	A		CA
97	Tricarico	DPC	40.619	16.156	Miocene	fractured limestone and marls	1:50000 / 1:2000		Tm	A	CH	446	600	446	B	Palazzo (1991)	CA
98	Valle	trieste univ	46.158	13.393	Eocene	marls and sandstone in alternation with limestone breccia	1:100000		Tm	C		600	600	600	B		CA
99	Vasto	DPC	42.111	14.71	Pleistocene	yellow sand in alternation with sandy clay	1:100000	Qoa		D		387	387	387	B		CA
100	Villa San Giovanni	DPC	38.216	15.647	Pleistocene	conglomerate	1:50000 / 1:2000		Pc	C		1000	1000	1000	A		CA
101	Villetta Barrea	DPC	41.759	13.989	Cretacico	limestone	1:50000 / 1:2000		MI	C		1000	1000	1000	A		D

CHAPTER 6 SISMA (SITE OF ITALIAN STRONG MOTION ACCELEROGRAMS): A WEB-DATABASE OF GROUND MOTION RECORDINGS FOR ENGINEERING APPLICATIONS

6.1 INTRODUCTION

In the last two decades the number of strong motion databases that can now be accessed via Internet has significantly increased. Two of the most important web sites for accessing strong motion data are COSMOS and PEER. The COSMOS web site (<http://db.cosmos-eq.org>) contains more than 4,000 records from around the world, essentially from western US, Japan and New Zealand. The PEER databank (<http://peer.berkeley.edu/smcat>) includes 1557 records from 143 shallow crustal earthquakes in active tectonic regions. However, very few accelerograms from Europe are currently available in the PEER and COSMOS sites. The most important source of European records is the ESD (European Strong Motion Database) website (<http://www.isesd.cv.ic.ac.uk>) which includes more than 3,000 strong motions accelerograms recorded in Europe and Middle East and associated earthquake-, station- and waveform-parameters. Those records have not been uniformly processed and generally lack the source and site metadata that is typical of records in the PEER database.

In Italy only the past few years have witnessed a renewed interest of researchers and practicing engineers in the development of national databases of strong motion accelerograms. One of the main motivation is due to the fact that recent seismic codes in Italy allow the use of natural accelerograms for the design of structural and geotechnical systems.

In this context, very recently a research project, developed in the framework of the 2004-2006 DPC-INGV agreement, project S6, produced the ITACA (Italian Accelerometric Archive) website (<http://itaca.mi.ingv.it>). ITACA contains 2182 waveforms from 1004 earthquakes with magnitude ranging from very low values up to 6.9.

In this chapter the website created to disseminate the strong motion database and the source and site databank is described. That website is called SISMA, i.e. Site of Italian Strong Motion Accelerograms (<http://sisma.dsg.uniroma1.it>). It is expected that the same data will subsequently be archived at the PEER web site. Unlike ITACA, the database developed in this study does not include a large number of weak records of limited engineering interest ($M < 4$).

The principal objective of the SISMA website is to provide high quality Italian strong motion records whose associated parameters are consistent and reliable and can be used for most engineering

applications. This paper mainly focuses on the principal search criteria being developed within SISMA for the selection of time-histories records involving seismological, ground motion and site parameters.

6.2 DATABASE SUMMARY

The database is composed of 247 Italian three-component corrected accelerograms from 101 recording sites and 89 earthquakes that occurred in the period 1972-2002. Appropriate source parameters (magnitude, hypocenter location, fault mechanism, etc.) associated with the seismic events were included. All distances were re-calculated as already described and accelerometric data were uniformly processed. Time-histories of acceleration and pseudo-acceleration response spectra (5% structural damping) were then computed.

The magnitude of the events is always available as local magnitude M_L . Moment magnitudes M_W are available for 60% of the earthquakes from moment tensor solutions. Surface wave magnitudes (M_S) are also available for 36% of the events.

Re-calculated epicentral and hypocentral distances are available for all recordings while Joyner and Boore distances (r_{jb}) and closest distance from the rupture (r_{rup}) have been re-calculated only when fault solutions are available, corresponding to about 45% of the recordings. About 85% of the records have been obtained at distances of less than 50 km from the source while the remaining 15% data are essentially concentrated at distances between 50 and 100 km.

Fault rupture classification has been obtained for slightly less than 70% of the earthquakes in the databank, in which records from normal rupture mechanism dominate with about 40 earthquakes belonging to this category; remaining events are related to strike-slip (7), oblique (4) and thrust (10) ruptures.

Site classification was based on the equivalent value for the shear-wave velocity over the uppermost 30 m, according to EC8 classification system. It has been possible to classify slightly less than 50% of stations from measured shear wave velocity profile, inferred from literature data or measured in-situ by ad hoc SASW investigations (see chapter 4) whereas for the remaining stations V_{s30} parameter has been estimated based on correlations with surface geology (see section.5.4).

6.3 SEARCHING, DISPLAYING AND DOWNLOADING DATA

The design of SISMA allows records to be located in several ways, depending upon a user's interest. Three different search criteria can be employed, i.e. "Search Eqk", "Search Station" and "Search Recording" by using the respective buttons on the SISMA front page.

6.3.1 Earthquake Searching

Clicking on the button "Search Eqk", will display the page shown in [fig. 6.1](#) which currently includes 6 search options: earthquake name, year of occurrence, region, fault mechanism, local magnitude and focal depth. Local magnitude has been preferred to other magnitude definitions as search criterion because it is available for all the earthquakes included in the database. Anyway, other magnitude values (M_w , M_s , m_b) are also provided, where available, in a detailed information page for a given earthquake.

Figure 6.1. SISMA: "Search earthquake" screenshot

Once chosen values are inserted in the *Search Eqk Tab* window, the list related to that selection will appear by clicking on the Search button on the left-downer corner of the page ([fig. 6.2](#)).

SISMA
SITE OF ITALIAN STRONG MOTION ACCELEROGRAMS

Home | Search Eqk | Search Station | Search Recording

Search Eqk Result Tab

89 Records found, listed from 1 to 20.
[First/Previous] 1 | 2 | 3 | 4 | 5 [Next/Last]

NAME	DATE	TIME	LAT.	LONG.	FAULT MECH.	FOCAL DEPTH	MI	
Ancona	25/01/1972	23:22:17	43.700	13.410	Normal	10.0	4.00	More Info
Ancona	04/02/1972	02:42:18	43.633	13.550	Oblique	8.0	4.60	More Info
Ancona	04/02/1972	09:18:30	43.730	13.380	Oblique	8.0	4.40	More Info
Ancona	04/02/1972	18:17:25	43.700	13.400	Normal	10.0	4.10	More Info
Ancona	05/02/1972	01:26:30	43.720	13.400	Oblique	10.0	4.30	More Info
Ancona	06/02/1972	01:34:19	43.700	13.430	Oblique	5.0	4.30	More Info
Ancona	06/02/1972	21:44:45	43.700	13.400	Normal	2.5	3.00	More Info
Ancona	08/02/1972	12:19:10	43.683	13.400	Normal	2.5	3.90	More Info
Ancona	14/06/1972	18:55:53	43.650	13.600	Strike - Slip	3.0	4.70	More Info
Ancona	14/06/1972	21:01:02	43.667	13.417	Normal	21.0	4.20	More Info
Ancona	21/06/1972	15:06:53	43.817	13.600	Normal	4.0	4.00	More Info
Friuli	06/05/1976	20:00:13	46.350	13.260	Thrust	12.0	6.40	More Info
Friuli (aftershock)	07/05/1976	00:23:49	46.240	13.270	Thrust	26.0	4.90	More Info
Friuli (aftershock)	11/05/1976	22:44:01	46.290	12.990	Thrust	13.0	5.30	More Info
Friuli (aftershock)	18/05/1976	01:30:09	46.250	12.867	Normal	5.0	4.10	More Info
Friuli (aftershock)	09/06/1976	18:48:17	46.350	13.067	Normal	16.0	4.10	More Info
Friuli (aftershock)	11/06/1976	17:16:36	46.267	12.967	Normal	18.0	4.30	More Info
Friuli (aftershock)	17/06/1976	14:28:51	46.177	12.798	Normal	15.0	4.50	More Info
Friuli (aftershock)	07/09/1976	11:08:16	46.300	12.983	Normal	5.0	4.10	More Info
Friuli (aftershock)	11/09/1976	16:31:11	46.290	13.180	Thrust	10.0	5.50	More Info

Export: [CSV](#) | [Excel](#) | [XML](#) | [PDF](#) | [RTF](#)

For a new search click [here](#).

SAPIENZA UNIVERSITÀ DI ROMA
DISG Dipartimento di Ingegneria Strutturale e Geotecnica
AGI Associazione Geotecnica Italiana

Figure 6.2. SISMA: “Search earthquake Result Tab” screenshot

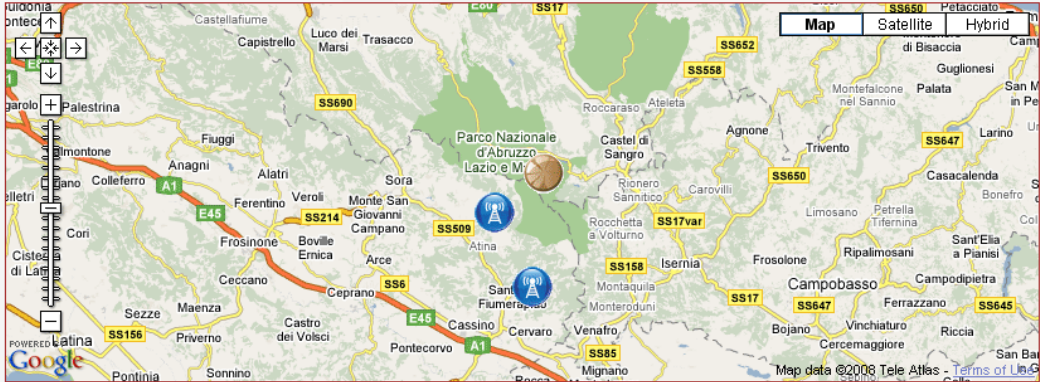
The table can be exported by the user in various formats as indicated at the bottom of the list in the same page. Moreover, each event is detailed in single dedicated pages consultable by clicking the “More Info” button on the right-end of the requested earthquake row in the list.

The called form, saveable as a pdf format, (fig.6.3) contains all the information related to the chosen event, including its graphical location (📍) with related recording stations (📡) activated by the earthquake in object. This feature makes use of the GoogleMap web service (<http://www.google.com/apis/maps>). Mentioned recordings are also listed in the end of the form with their identification code.

sisMa
SITE OF ITALIAN STRONG MOTION ACCELEROGRAMS

PDF | Close

Eqk Details - code Lazi_70



Legend: This Earthquake Triggered Stations

GENERAL DATA

Eqk Name	Lazio-Abruzzo (aftershock)	Latitude	41.708	Longitude	13.89
Eqk Date	11/05/1984	Fault Mechanism	Normal	Mw	5.5
Eqk Time	10.41.50	Focal Depth	12.1	Ms	5.2
Region	Lazio	Epicentral Intensity	Unknown	MI	5.7
				Mb	5.2

FAULT SOLUTION

Center Latitude	0.0	Length [km]	0.0
Center Longitude	0.0	Width [km]	0.0
Strike	0	Min Depth [km]	0.0
Dip	0	Max Depth [km]	0.0
Rake	0	Slip	0.0

REFERENCES

Working group S6 (2007) Data base of the Italian strong-motion data (1972-2004) <http://itaca.mi.ingv.it>

EQK RELATED STATIONS

Name	Latitude	Longitude	Region	Agency	Inst.Type	Inst.Housing	Site class.(EC8)	Vs 30 [m/s]
Atina-Pretura Basement	41.645	13.783	Lazio	Enea	Analogic	SB	B	600
Atina-Pretura Roof	41.645	13.783	Lazio	Enea	Analogic	SR	B	600
Cassino-Sant' Elia	41.523	13.864	Lazio	Enea	Analogic	CA	B	600

PDF Close

SAPIENZA UNIVERSITÀ DI ROMA
DiSG Dipartimento di Ingegneria Strutturale e Geotecnica
AGI Associazione Geotecnica Italiana

Figure 6.3. SISMA: “Earthquake details” screenshot

One more useful option is the chance of switching to station or recording searching pages, described below, just by clicking on symbols or codes in the form.

6.3.2 Station Searching

Station information can be searched same way. By clicking on the button “Search Station”, the window shown in [fig. 6.4](#) is displayed. In this case the searchable station parameters are station name and region, instrument type and housing, agency, and site classification according to EC8 or V_{s30} .

Figure 6.4. SISMA: “Search Station” screenshot

As an example, in [fig. 6.5](#) the search result after writing Ancona in the *Station Name* tab is displayed, with basic information available on the stations; the table can be exported in several formats as well.

STATION NAME	LATITUDE	LONGITUDE	REGION	AGENCY	INST.TYPE	INST.HOUSING	SITE (EC8)	Vs 30	
Ancona-Palombina	43.602	13.474	Marche	Enea	Analogic	SB	C	256	More Info
Ancona-Rocca	43.621	13.513	Marche	Enea	Analogic	SB	B	549	More Info

Figure 6.5. SISMA: “Search station results table” screenshot


Also in this case, for a given station, by clicking on the button “more info” at the right side of the table, a pop-up window appears containing more detailed information about the station, the instrument

and the main geological and geotechnical data; further, a list of all recordings made at the station is available along with a link to the recordings' details.

Another feature allows users to view a map of all the epicenters of the earthquakes recorded by the selected station, as shown in [fig. 6.6](#) for the Ancona Palombina station.



Figure 6.6. Map showing location of the earthquakes recorded by Ancona Palombina station

As for earthquake searching options, the detailed form of the recording stations, appearing after clicking the “More Info” button, can be saved as a pdf, but in this case it is also possible to display and/or save the V_s profile, if available, by clicking the  button located in the center left of the page ([fig. 6.7](#)).

[Figure 6.7](#) also shows the possibility to query the database on Station, Recorded Earthquakes and Recordings data, directly by clicking on the pop-up windows corresponding to each symbol.

For each station a form was compiled reporting all the information available. A sample of this form is reported in Appendix B for Auletta station.

SISMA
SITE OF ITALIAN STRONG MOTION ACCELEROGRAMS

[Vs Profile](#) | [PDF](#) | [Close](#)

Station Details - code Anco_72

[Anco_20](#) | [Info](#) | **Recording** | [Map](#) | [Satellite](#) | [Hybrid](#)

Recording by Station: **Anco_72**

PGA: 0.039
Ep. Distance: 12
[Link to Recording Details](#)

Legend: ● This Station ● Recorded Earthquakes

Map data ©2008 Tele Atlas - [Terms of Use](#)

GENERAL DATA

Name	Ancona-Palombina	Agency	Enea
Latitude	43.602	Instrument housing	SB
Longitude	13.474	Site classification (EC8)	C
Region	Marche	Morphology	Unknown

INSTRUMENT DATA

Instrumental Type	Analogic		Model	SMA-1
	X	Y		
Sensitivity [cm/g]	4.0	3.6		
Natural Frequency [Hz]	18.5	18.9		
Damping	0.6	0.6		
Full Scale Amplitude [g]	0.0	0.0		
Sample Period [s]	999.999	Working Status	No	
Installation Date	13/06/1979	Removing Date	17/12/1981	

GEOLOGIC AND GEOTECHNICAL INFO

Age	Pleistocene	Vs Source	A
Unit		Vs Profile Depth	60
Description	Clay with silt and sand	Vs 30 [m/s]	256
Borehole	Unknown	Site classification (EC8)	C
Borehole Depth	0	InSitu Test	CH
		Lab Test	

[Vs Profile](#)

REFERENCES

1) Ambraseys, N., Smit, P., Sigbjornsson, R., Suhadolc, P. and Margaris, B. (2002). Internet-Site for European Strong-Motion Data, European Commission, Research-Directorate General, Environment and Climate Programme. - 2) Working group (1981). Elementi di Microzonazione sismica dell'area Anconetana. Consiglio Nazionale delle Ricerche-Progetto Finalizzato Geodinamica, pub. n.430

ASSOCIATED RECORDINGS

Code	Eqk Name	Eqk Date	Eqk Time	Mw	Ep. Distance [km]	PGA [g]
207226	Ancona	06/02/1972	21:44:45	0.0	12.0	0.039
217227	Ancona	08/02/1972	12:19:10	0.0	10.0	0.107
227228	Ancona	14/06/1972	18:55:53	4.8	11.0	0.139
237229	Ancona	14/06/1972	21:01:02	0.0	8.0	0.217
247230	Ancona	21/06/1972	15:06:53	0.0	25.0	0.291

[PDF](#) | [Close](#)

SAPIENZA UNIVERSITÀ DI ROMA | **DISG** Dipartimento di Ingegneria Strutturale e Geotecnica | **AGI** Associazione Geotecnica Italiana

Figure 6.7. SISMA: “Station details” screenshot

6.3.3 Recording Searching

In the “Search recording” window, the search parameters can be a combination of earthquake, fault mechanism, distance, site classification and ground motion parameters, as displayed in [fig. 6.8](#).

Figure 6.8. SISMA: “Search recording” screenshot

SISMA offers a large number of searchable strong motion parameters such as peak ground acceleration (PGA), peak ground velocity (PGV), peak ground displacement (PGD), significant duration, Arias intensity (I_a), mean period (T_m), predominant periods (T_p), spectral acceleration at $T=1$ s and Housner Intensity (SI).

An example search result is shown in [fig 6.9](#), the search criteria being all the records having $PGA=0.1-0.3g$ on type C soil according to EC8.

This figure lists all the currently selected records grouped by earthquake in ascending magnitude order along with some basic information.

SISMA
SITE OF ITALIAN STRONG MOTION ACCELEROGRAMS

Home | Search Eqk | Search Station | Search Recording

Search Recording Result Tab

57 Records found, listed from 1 to 20.
[First/Previous] 1 | 2 | 3 | Next/Last]


EQK	MI	FAULT MECH.	STATION	INSTR. TYPE	EP. DIST.	SITE (EC8)	PGA mean	PGA UP	
Anco_21	3.90	Normal	Ancona-Palombina	Analogic	10.81	C	0.107	0.028	More Info
Anco_22	4.70	Strike - Slip	Ancona-Palombina	Analogic	11.47	C	0.139	0.066	More Info
Anco_23	4.20	Normal	Ancona-Palombina	Analogic	8.57	C	0.217	0.119	More Info
Anco_24	4.00	Normal	Ancona-Palombina	Analogic	25.98	C	0.291	0.129	More Info
Anco_24	4.00	Normal	Ancona-Rocca	Analogic	22.91	B	0.121	0.113	More Info
Umbr_79	5.80	Normal	Assisi-Stallone	Digital	19.86	A	0.177	0.078	More Info
Umbr_78	5.60	Normal	Assisi-Stallone	Digital	25.05	A	0.132	0.041	More Info
Umbr_82	5.40	Normal	Assisi-Stallone	Digital	20.20	A	0.139	0.053	More Info
Lazi_69	5.90	Normal	Atina	Analogic	13.07	A	0.107	0.063	More Info
Lazi_70	5.70	Normal	Atina-Pretura Roof	Analogic	11.32	B	0.112	0.036	More Info
Irpi_53	6.50	Normal	Bagnoli-Irpino	Analogic	22.84	A	0.157	0.107	More Info
Umbr_78	5.60	Normal	Borgo-Cerreto Torre	Unknown	24.19	A	0.185	0.111	More Info
Umbr_86	5.10	Normal	Borgo-Cerreto Torre	Unknown	10.25	A	0.166	0.083	More Info
Irpi_53	6.50	Normal	Brienza	Analogic	44.82	B	0.200	0.203	More Info
Friu_46	5.80	Thrust	Buia	Analogic	19.50	C	0.157	0.089	More Info
Friu_47	6.10	Thrust	Buia	Analogic	17.12	C	0.102	0.078	More Info
Irpi_61	4.60	Normal	Cairano 1	Analogic	4.65	B	0.152	0.036	More Info
Irpi_61	4.60	Normal	Cairano 2	Unknown	4.92	B	0.143	0.042	More Info
Irpi_61	4.60	Normal	Cairano 3	Analogic	6.13	B	0.130	0.049	More Info
Irpi_53	6.50	Normal	Calitri	Analogic	13.36	A	0.131	0.170	More Info

Export: [CSV](#) | [Excel](#) | [XML](#) | [PDF](#) | [RTF](#)

For a new search click [here](#).

SAPIENZA UNIVERSITA DI ROMA
DiSG Dipartimento di Ingegneria Strutturale e Geotecnica
AGI Associazione Geotecnica Italiana

Figure 6.9. Table listing records having $PGA=0.1-0.3g$ on type C soil according to EC8

For a given recording, by clicking on the button “more info” a pop-up window appears as shown in [fig. 6.10](#) with the details concerning the earthquake, station, and strong motion parameters. Acceleration, displacement, and velocity histories can be plotted along with Fourier and pseudo-acceleration response spectra (5% damping) by clicking on the button  located at the lower right of the window. This information is also downloadable as a two-page pdf file including recording details and plots ([fig. 6.11](#)).


Finally, acceleration time-histories and pseudo-acceleration response spectra for the three components are available for download as an ASCII format in a zip file ( button at the lower right in the window).



Figure 6.10. Recording details for one of the Ancona Palombina station records

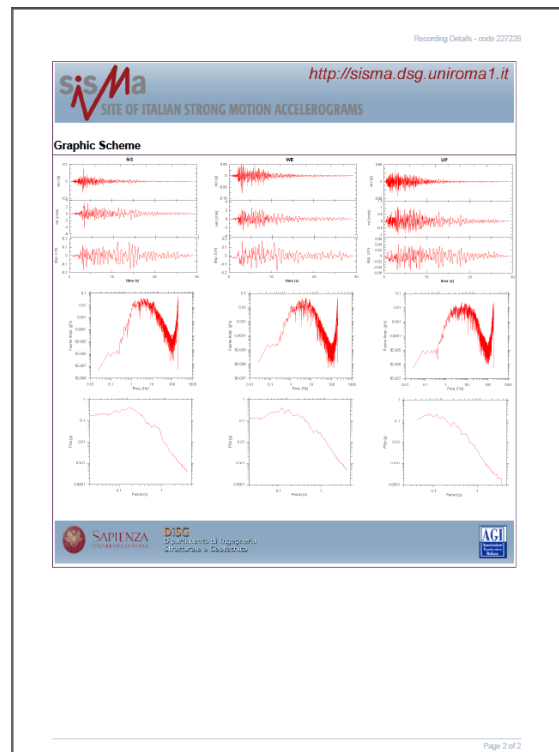
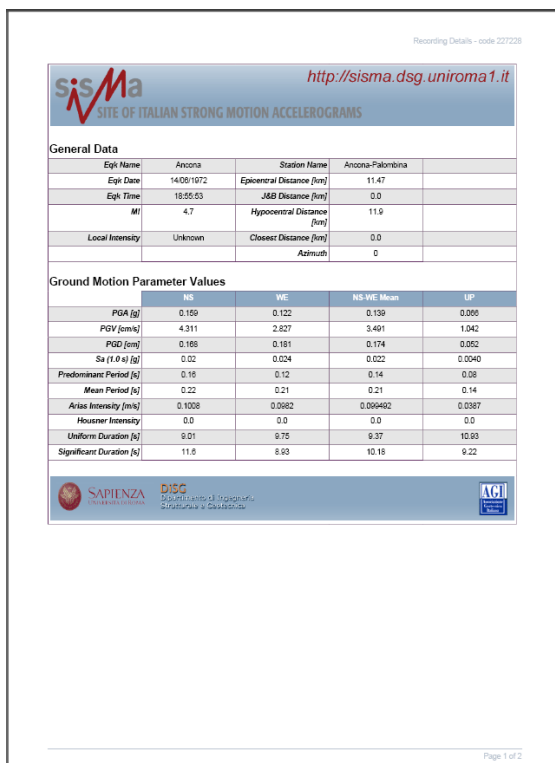


Figure 6.11. Recording Details PDF screenshot

CHAPTER 7 **GROUND MOTION PREDICTION EQUATIONS (GMPEs) FOR ITALY, EUROPE AND WESTERN U.S.**

7.1 INTRODUCTION

The quantitative estimation of ground-shaking hazard at a specific site is provided by Seismic Hazard Analyses (SHA).

In order to estimate the level of shaking for a particular site, different strong motion parameters, also referred as Intensity Measures (IMs), include PGA, PGV, PGD, duration and spectral ordinates that must be consistent with seismic hazard. The prediction of IMs can be carried out by means of empirical equations known as attenuation relations or Ground Motion Prediction Equations (GMPEs). They are obtained from statistical regressions of ground-motion datasets.

Seismic hazard may be analyzed deterministically (DSHA), as when particular earthquake scenario is assumed, or probabilistically (PSHA), in which uncertainties in earthquake size, location, and time of occurrence are explicitly considered.

As an example, in the following, PSHA procedure is described through its main steps. For a given sites it is needed to perform:

1. source and location identification: this includes the characterization of all earthquake sources capable of producing significant ground motion at the site and all potential ruptures within the source;
2. site-to-source distances (r) evaluation: it is the calculation of distances between the source and the given site; the current procedure considers, beside the well known epicentral and hypocentral distances, Joyner & Boore and rupture distances (see Ch.3). The probability approach requests the evaluation of the probability density function of the latter values $f(r)$;
3. estimation of the level of magnitude (m) related to each source: for each source, identified as in point 1., it's important to define the earthquake-size potentially released by the considered fault. Even in this step, for PSHA, the probability density function $f(m)$ is requested;
4. estimation of the Intensity Measures (IMs) distribution conditioned on m and r : this step is the one related to the development of Ground Motion Prediction Equation better defined in the next paragraph and main object of this chapter.

Considering multiple sources and an assigned time interval Δt , it is possible to calculate the *average exceedance rate* $\nu(\text{IM})$ as:

$$\nu(\text{IM}) = \sum_{i=1}^{N_{fi}} \nu_i \times \iint_{m,r} f(m)f(r)P(\text{IM} > z|m,r)dmdr \quad (7.1)$$

where ν_i is the *annual rate of occurrence* of earthquake with magnitude m for the fault i and N_{fi} is the total number of identified faults.

The procedure described above allows to develop Seismic Hazard Curves for individual source zones and combined to express the aggregate hazard at a particular site. Specifically, the probability of exceeding a particular value of ground motion parameter, is calculated for one possible earthquake at one possible source location and then multiplied by the probability that particular magnitude earthquake would occur at that particular location. The process is then repeated for all possible magnitudes and locations with the probabilities of each summed (Kramer,1996).

Figure 7.1 reports an example of Seismic Hazard Curve that represents the probability (Probability of Exceedance PE) to have a value of the Intensity Measure (e.g: PGA) greater then a design value (z), at least once in Δt years.

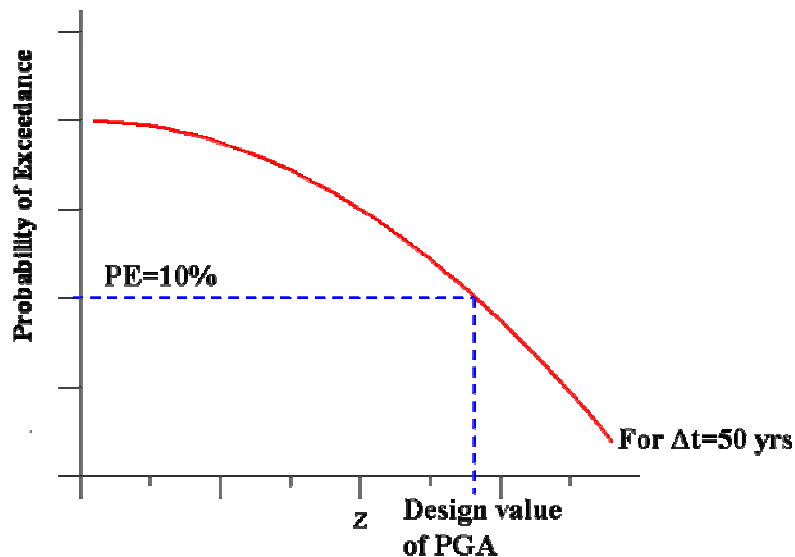


Figure 7.1. Example of a Sesimic Hazard Curve for PGA and $\Delta t=50$ years

An acceptable value of the probability diffused by worldwide codes is $PE=10\%$ in $\Delta t= 50$ years; the relative design IM can then be graphically obtained as reported in the figure (Design value of PGA).

Extending the latter practice to multiple sites, it is finally possible to define Hazard Risk Maps representing the zonation of expected IM values in a given time interval. The example in [figure 7.2](#) is the Hazard Map of Italy developed by INGV related to the expected PGA (statistically intended) in a time interval of 475 years.

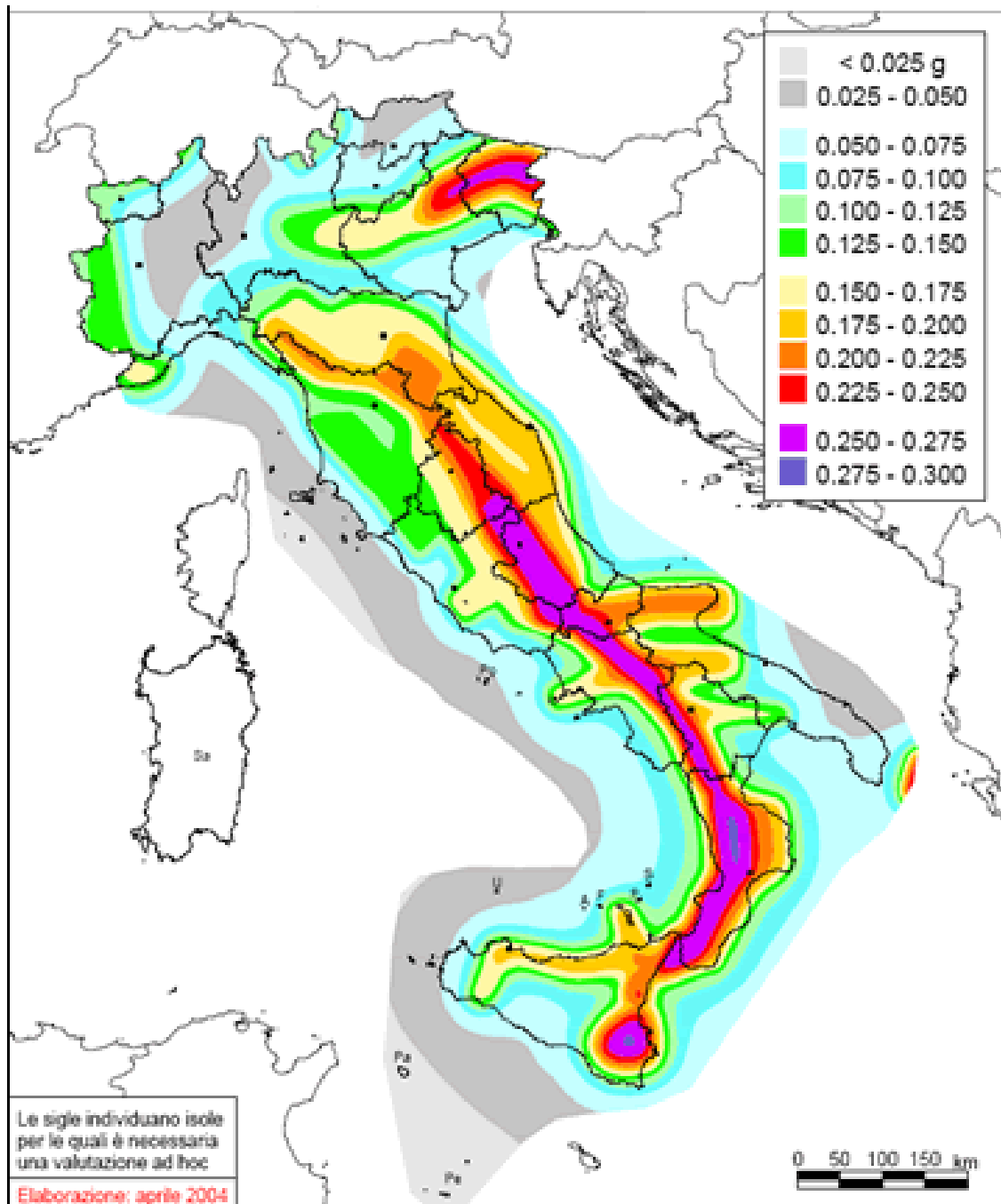


Figure 7.2. Seismic Hazard Map for Italy for PGA (PE=10% in 475 years, INGV 2004)

The probability approach previously described includes systematic consideration of uncertainty in the values of parameters of a particular seismic hazard model. Referring to step 4 of previous section, in some cases it is not simple to make the best choice of the most adequate GMPE model to use in the analyses. A convenient framework for the explicit treatment of model uncertainty is provided by the *logic trees* (Power et al., 1981; Kulkarni et al., 1984; Coppersmith and Youngs, 1986) approach, that allows to use alternative models, each of which is assigned a weighting factor that is interpreted as the relative likelihood of that model being correct (Kramer, 1996).

7.2 GROUND MOTION PREDICTION EQUATIONS

As already stated the evaluation of seismic hazard requires the use of probabilistic distributions of intensity measures (IMs) conditioned on the occurrence of an earthquake with a particular magnitude (m) at a given site-source distance (r). The probability density function (PDF) for a single IM is written as $f(\text{IM}|m,r)$, and is usually log-normal. Attenuation relationships define the statistical moments of these PDFs (e.g.: medians, standard error terms) in terms of parameters such as m and r .

The most commonly used ground motion intensity measure is spectral acceleration at a specified damping level (usually 5%). Attenuation relationships are also available for other intensity measures, including peak horizontal velocity, vertical spectral acceleration, Arias intensity, duration-related parameters, and mean period (Stewart et al. 2001).

7.2.1 General formulation and effect of magnitude/distance

Attenuation functions for median spectral acceleration generally have a form similar to the following:

$$\ln(\text{IM}) = f_1(F_T) + f_2(M) + f_3(r) + f_4(S_T) + \varepsilon_\sigma \quad (7.2)$$

where F_T is a factor related to the rupture mechanism; S_T is a site factor containing more variables (stratigraphic amplification, basin effects, non linearity, etc.); $f(M)$ is the source term depending on magnitude; $f(r)$ is the path scaling term where r represents site-source distance, and is measured differently by different investigators; the ε_σ term, finally, represents the variability of the residuals, which are

difference between the observed and the predicted values of parameters; it is usually the number of standard deviation below or above the median value.

The typical mathematic GMPE expression is:

$$\ln(\text{IM}) = c_1 + c_2M - c_3 \ln r - c_4r + c_5F_T + c_6S_T + \varepsilon_\sigma \quad (7.3)$$

In more complex forms, coefficients c_3, c_6 and c_7 are defined in terms of M and r . Many of these coefficients also have been found to be dependent on the tectonic environment of the regions in which the earthquake occurred.

The terms related to distance r includes the geometric attenuation and anelastic attenuation, respectively expressed by $c_3 \ln r$ and c_4r terms. Some attenuation relations assume $c_3=1$ which is the theoretical value for spherical spreading of the wave front from a point source in a homogeneous whole space. If unconstrained, c_3 typically is greater than 1; sometimes c_3 is varied as a function of distance to accommodate differences in the geometric attenuation of different wave types, such as direct waves or surface waves, and to account for the critical reflection off the base of the crust or other strong crustal.

Considering distance definitions reported in chapter 2, r_{epi} and r_{hypo} are basically used to for characterizing distances for small earthquakes that can be represented by a point source, hence they poorly measure distances of events related to large rupture planes. Experience has shown that attenuation relations that use point-source measures should not be used to estimate ground motion close to large earthquakes unless there is absolutely no other alternative available (Campbell, 2003). Therefore, at least for earthquakes occurring on large fault planes, r_{rup} and r_{jb} should be used.

Most earthquakes in active tectonic regions have one of four focal mechanisms: strike-slip, reverse, oblique, and normal. The strike-slip mechanism is generally taken as a “reference” mechanism, and no correction is necessary (i.e., $f(F_T) = 0$). Significant differences are observed between reverse earthquake motions and strike-slip. No corrections are generally made for normal-slip earthquakes, although a separate set of attenuation relations is necessary for extensional tectonic regimes. little data are available for oblique-slip earthquakes, and the $f(F_T)$ correction for oblique-slip is often taken as half of $f(F_T)$ for reverse earthquakes (Stewart et al., 2001).

The local site conditions term take allow to take in account on the GMPE of the effect on the wave propagation due to the material lying directly beneath the considered site, from the surface to the basement rock. The parameters that define the dynamic response of the material are shear wave velocity (V_s) and depth of the sediments beneath the site.

Traditionally, some attenuation models used a simple rock/soil classification of ground conditions, setting $S_T=1$ for soil and $S_T=0$ for rock, while in the common practice more sophisticated expressions were developed, mostly related to the V_{s30} value, corresponding to the average value of V_s in the top 30 m of a site profile, given by the formula:

$$V_{s30} = \frac{\sum_{i=1}^n d_i}{\sum_{i=1}^n \frac{d_i}{V_{si}}} \quad (7.4)$$

where d_i is the thickness and V_{si} the shear wave velocity of soil layer i .

Recent GMPEs, specifically the ones developed in NGA project, assume a more complex site effect including terms related to the *basin effect* and non-linear response (see section 7.3.3).

7.3 OVERVIEW OF MOST USED GMPEs

Development of GMPEs is strongly increased in the last years all over the world (Douglas, 2004c). Differences between those relations are basically related to the functional forms and the dataset on which regression analyses were performed. Beside the complexity of the analytic relations, GMPEs can be segregated on the base of used datasets as worldwide, European or national relationships. It is common practice in Italy to develop also relations on regional dataset limited to restricted areas within national boundaries. A brief summary of the most representative GMPEs are described below, focusing on most recent or used in practice.

7.3.1 GMPEs in Italy

The most common GMPEs developed on a national database are the ones proposed by Sabetta and Pugliese (1987, 1996). The Authors developed in 1987 an attenuation relation for peak ground acceleration (PGA) prediction while in 1996 proposed a similar form for pseudo-velocity response spectrum for 5% damping (Douglas, 2001b, 2004c). Despite the small amount of data and the limits related to the simplified functional form and regression procedure, as detailed below, the latter relation is

still used for seismic hazard analyses in Italy (Montaldo et al. 2005). Next the two GMPEs are reported with their main characteristics.

Sabetta & Pugliese (1987)

Functional form

$$\log(\text{PGA}) = a + b M - \log(r^2 + h^2)^{1/2} + e S \quad (7.5)$$

where

- PGA is in g
- $M = M_S$ if M_S and $M_L \geq 5,5$; $M = M_L$ otherwise;
- r = epicentral distance;
- $S=0$ for stiff and deep soil ($V_s > 800$ m/s or $H > 20$ m); $S=1$ for shallow soil $5 \leq H \leq 20$ m;

The relation is obtained from a *Simple Least Square* regression analyses run on 95 recording data, coming from 17 earthquakes, with a selection criterion of at least 2 recordings for earthquake with $M > 4.5$. Maximum horizontal component of PGA is used. The site effect is modelled by a very simple functions (eS) non linear or basin effect terms are not considered.

Sabetta & Pugliese (1996)

Functional form

$$\log(Y) = a + b M - \log(r^2 + h^2)^{1/2} + e_1 S_1 + e_2 S_2 \quad (7.6)$$

where

- Y is the pseudo-velocity for 5% damping;
- data used are the same of Sabetta & Pugliese, 1987;
- $M = M_S$ if M_S and $M_L \geq 5,5$; $M = M_L$ otherwise;
- r = epicentral distance;
- three site categories used: $S_1=1, S_2=0$ for shallow soil ($H \leq 20$ alluvium $400 \leq V_s \leq 800$ m/s); $S_1=0, S_2=1$ for deep soil ($H > 20$ alluvium $400 \leq V_s \leq 800$ m/s); $S_1=0, S_2=0$ for stiff soil ($V_s > 800$ m/s).

As already pointed, some attenuation relations were developed referring to restricted sub-dataset. It comes out that many GMPEs were proposed for local areas within national boundaries; some of more interests are listed below with the corresponding area of applicability:

- [De Natale \(1988\)](#) – Campi Flegrei (volcanic area near Naples);
- [Malagnini & Hermann \(2000\)](#) – Umbria Marche;
- [Malagnini et al. \(2002\)](#) – NE Italy;

- Morasca et al. (2002) – Western Alps.

7.3.2 GMPEs in Europe

The most significant GMPEs based on European data are:

- Ambraseys et al. (1996);
- Spudich et al. (1997/1999);
- Berge-Thierry et al. (2003);
- Ambraseys et al (2005);
- Akkar and Bommer (2007).

In the following only the more recent are described in detail.

Berge-Thierry et al. (2003)

The functional form is:

$$\log_{10} \text{PSA}(f) = a(f)M_S + b(f)r_{\text{hyp}} - \log_{10} r + c_{1,2}(f) \quad (7.7)$$

authors referred to:

- 965 horizontal and 485 vertical components of 83% European earthquakes (50% Italian events) and 17% American $M > 6$ events;
- Focal depth < 30 km (shallow crustal);
- $4 < M_S < 7.9$ and $4 < d_{\text{hyp}} < 330$ km;
- Signal time lengths at least 10 s;
- Free field site condition (no basement housed);
- Soil term: rock ($V_S > 800$ m/s) and alluvium ($300 < V_S < 800$ m/s);
- Fault mechanism, hanging wall or directivity effect were not considered.

Ambraseys et al. (2005)

This relation is an upgrade of the previous Ambraseys et al. (1996). The used functional form is

$$\log y = a_1 + a_2 M_w + (a_3 + a_4 M_w) \log(d_2 + a_5^2)^{0.5} + a_6 S_S + a_7 S_A + a_8 F_N + a_9 F_T + a_{10} F_O \quad (7.8)$$

where

- Joyner and Boore distance is used;

- Site term: $S_S = 1$ for soft soil sites and 0 otherwise; $S_A = 1$ for stiff soil sites and 0 otherwise;
- Fault mechanism term: $F_N = 1$ for normal faulting earthquakes and 0 otherwise; $F_T = 1$ for thrust faulting earthquakes and 0 otherwise; $F_O = 1$ for odd faulting earthquakes and 0 otherwise;
- Dataset: 595 recordings from 338 recording stations triggered by European and Middle Eastern earthquakes with $M_w \geq 5$.

Authors observed that recordings relative to $M > 6$ present PGA and SA values very close to ones from Ambraseys et al. (1996), while for small M and short distances previous equation (worse constrained in that range) predict higher values.

Akkar and Bommer (2007)

Authors provided empirical prediction for PGV derived from strong-motion records from Europe and Middle East. The functional form used is:

$$\log(\text{PGV}) = b_1 + b_2 M + b_3 M^2 + (b_4 + b_5 M) \log(r_{jb}^2 + b_6^2)^{0.5} + b_7 S_S + b_8 S_A + b_9 F_N + b_{10} F_R \quad (7.9)$$

in this relation:

- The database is essentially that used by Ambraseys et al. 2005, but the records were systematically re-filtered (Akkar and Bommer, 2006);
- M_w and r_{jb} are considered and the validity range can be assumed as $5 < M < 7.6$ and $5 < d < 100$ km;
- Site term: $S_S = 1$ if stiff soil, 0 otherwise; $S_A = 1$ if soft soil, 0 otherwise;
- Fault mechanism term: $F_N = 1$ if normal rupture, 0 otherwise; $F_R = 1$ if reverse rupture, 0 otherwise;
- Geometric mean and max value were both considered;
- Equations have been derived using 1-stage max-Likelihood regression method (Joyner & Boore, 1993);

In their work authors point that comparisons with Ambraseys et al. (2005) confirm the significant influence of cut-off frequency in filtering data. Beside that, important conclusions reached in this work are:

1. Analyses of residuals seem to show an influence of non-linearity soil response;
2. Comparison with NGA GMPEs (see next section) confirms that no significant difference can be noted, so European and American data could be used together for a more consistent study;
3. no evidence exists on regional variations.

7.3.3 The Next Generation of Ground Motion Attenuation Models (NGA)

NGA project is a multidisciplinary research program coordinated by the Pacific Engineering Research Center-Lifelines Program (PEER-LL), in partnership with the U.S. Geological Survey and the Southern California Earthquake Center (SCEC).

The objective of the project is to develop new ground-motion prediction relationships for shallow crustal earthquakes in the western United States and similar active tectonic regions, through a comprehensive and highly interactive research program (Power et al., 2008).

Five sets of ground motion relationships were developed by teams working independently but interacting with one another throughout the development process. Teams, listed below, are the same that developed models after the previous project of 1997 :

- N. Abrahamson and W. Silva;
- D. Boore and G. Atkinson;
- K. Campbell and Y. Bozorgnia;
- B. Chiou and R. Youngs;
- I.M. Idriss.

The common database of recorded ground motion for developers is the expanded NGA worldwide dataset nowadays including 172 earthquakes, 1400 recording stations and about 3500 multicomponent recordings. Each developer team was required to use subset of the database developed during the NGA project and to use supporting information (e.g., source parameters, source-to-site distance, local site conditions of the station, etc.), selecting or excluding data at the discretion of each team (Power et al., 2008).

To meet the needs of earthquake engineering community, all NGA models were required to be applicable to:

- PGA, PGV and 5% Sa in the period range of 0 to 10 seconds;
- Average horizontal ground motion, as well as ground motion in the fault-strike-normal and fault-strike-parallel directions;
- M_w range of 5 to 8.5 (strike-slip earthquakes) and 5 to 8 (reverse and normal earthquakes);
- Distance range of 0 to 200 km;
- Commonly used site classification schemes.

Next, functional forms and main peculiarities of NGA GMPEs are reported, reminding that reports documenting NGA relationships are available electronically from PEER web site (http://peer.berkeley.edu/products/rep_nga_models.html).

Abrahamson & Silva (2008)

Functional form for the median ground motion is:

$$\ln Sa(g) = f_1(M, R_{rup}) + a_{12}F_{RV} + a_{13}F_{NM} + a_{15}F_{AS} + F_{HW}f_4(R_{jb}, R_{rup}, R_x, W, \delta, Z_{TOR}, M) + f_5(\hat{PGA}_{1100}, V_{s30}) + f_6(Z_{TOR}) + f_8(R_{rup}, M) + f_9(R_{rup}) + f_{10}(Z_{1.0}, V_{s30}) \quad (7.10)$$

where the meaning of the parameters is listed [table 7.1](#). simplified from the table of the original paper.

Table 7.1. Definition of parameters used in the regression analyses

Parameter	Definition	Notes
M	Moment magnitude	
R_{rup}	Rupture distance (km)	
R_{jb}	Joyner&Boore distance (km)	
R_x	Horizontal distance (km) from top edge of rapture	Measured perpendicular to the fault strike
Z_{TOR}	Depth-to top of rapture (km)	
F_{RV}	Flag for reverse faulting earthquakes	1 for reverse and reverse/oblique 0 otherwise
F_{NM}	Flag for normal faulting earthquakes	1 for normal 0 otherwise
F_{AS}	Flag for aftershocks	1 for aftershocks 0 for mainshocks, foreshocks and swarms
F_{HW}	Flag for hanging wall sites	1 for sites on hanging wall side of sites 0 otherwise
δ	Fault dip in degrees	
$Z_{1.0}$	Depth to $V_s=1.0$ km/s at the site (m)	
\hat{PGA}_{1100}	Median peak acceleration (g) for $V_{s30}=1100$ m/s	
W	Down-dip rapture width (km)	

Functional forms of single terms are given below.

Base model for Magnitude and distance dependence:

$$f_1(M, R_{rup}) = \begin{cases} a_1 + a_4(M - c_1) + a_8(8.5 - M)^2 + [a_2 + a_3(M - c_1)]\ln(R) & \text{for } M \leq c_1 \\ a_1 + a_5(M - c_1) + a_8(8.5 - M)^2 + [a_2 + a_3(M - c_1)]\ln(R) & \text{for } M > c_1 \end{cases} \quad (7.11)$$

where

$$R = \sqrt{R_{rup}^2 + c_4^2} \quad (7.12)$$

Hanging wall model:

$$f_4(R_{jb}, R_{rup}, R_x, W, \delta, Z_{TOR}, M) = a_{14}T_1(R_{jb})T_2(R_x, W, \delta)T_3(R_x, Z_{TOR})T_4(M)T_5(\delta) \quad (7.13)$$

Where

$$T_1(R_{jb}) = \begin{cases} 0 & \text{for } R_{jb} \geq 30 \text{ km} \\ 1 - \frac{30}{R_{jb}} & \text{for } R_{jb} < 30 \text{ km} \end{cases} \quad (7.14)$$

$$T_2(R_x, W, \delta) = \begin{cases} 0.5 + \frac{R_x}{2W \cos(\delta)} & \text{for } R_x \leq W \cos(\delta) \\ 1 & \text{for } R_x > W \cos(\delta) \text{ or } \delta = 90 \end{cases} \quad (7.15)$$

$$T_3(R_x, Z_{TOR}) = \begin{cases} 1 & \text{for } R_x \geq Z_{TOR} \\ \frac{R_x}{Z_{TOR}} & \text{for } R_x < Z_{TOR} \end{cases} \quad (7.16)$$

$$T_4(M) = \begin{cases} 0 & \text{for } M \leq 6 \\ M - 6 & \text{for } 6 < M < 7 \\ 1 & \text{for } M \geq 7 \end{cases} \quad (7.17)$$

$$T_5(\delta) = \begin{cases} 1 - \frac{\delta - 70}{20} & \text{for } \delta \geq 70 \\ 1 & \text{for } \delta < 70 \end{cases} \quad (7.18)$$

Site response model:

$$f_5(\hat{P}\hat{G}A_{1100}, V_{s30}^*) = \begin{cases} a_{10} \ln\left(\frac{V_{s30}^*}{V_{LIN}}\right) - b \ln(\hat{P}\hat{G}A_{1100} + c) + b \ln\left(\hat{P}\hat{G}A_{1100} + c \left(\frac{V_{s30}^*}{V_{LIN}}\right)\right) & \text{for } V_{s30} < V_{LIN} \\ (a_{10} + bn) \ln\left(\frac{V_{s30}^*}{V_{LIN}}\right) & \text{for } V_{s30} \geq V_{LIN} \end{cases} \quad (7.19)$$

$$V_{s30}^* = \begin{cases} V_{s30} & \text{for } V_{s30} < V_1 \\ V_1 & \text{for } V_{s30} \geq V_1 \end{cases} \quad (7.20)$$

$$V_1 = \begin{cases} 1500 \text{ m/s} & \text{for } T \leq 0.5\text{s} \\ \exp\left[8.0 - 0.795 \ln\left(\frac{T}{0.21}\right)\right] & \text{for } 0.5\text{s} < T \leq 1.0\text{s} \\ \exp\left[6.76 - 0.297 \ln(T)\right] & \text{for } 1.0\text{s} < T < 2.0\text{s} \\ 700 \text{ m/s} & \text{for } T \geq 2.0\text{s} \\ 862 \text{ m/s} & \text{for PGV} \end{cases} \quad (7.21)$$

Depth-to-Top of rupture model:

$$f_6(Z_{TOR}) = \begin{cases} \frac{a_{16} Z_{TOR}}{10} & \text{for } Z_{TOR} < 10 \text{ km} \\ a_{16} & \text{for } Z_{TOR} \geq 10 \text{ km} \end{cases} \quad (7.22)$$

Large distance model:

$$f_8(R_{rup}, M) = \begin{cases} 0 & \text{for } R_{rup} < 100 \text{ km} \\ a_{18}(R_{rup} - 100)T_6(M) & \text{for } R_{rup} \geq 100 \text{ km} \end{cases} \quad (7.23)$$

$$T_6(M) = \begin{cases} 1 & \text{for } M < 5.5 \\ 6.5 - M & \text{for } 5.5 \leq M \leq 6.5 \\ 0 & \text{for } M > 6.5 \end{cases} \quad (7.24)$$

Soil depth model:

$$f_{10}(Z_{1.0}, V_{s30}) = a_{21} \ln\left(\frac{Z_{1.0} + c_2}{\hat{Z}_{1.0}(V_{s30}) + c_2}\right) + \begin{cases} a_{22} \ln\left(\frac{Z_{1.0}}{200}\right) & \text{for } Z_{1.0} \geq 200 \text{ km} \\ 0 & \text{for } Z_{1.0} < 200 \text{ km} \end{cases} \quad (7.26)$$

$$\ln(\hat{Z}_{1.0}(V_{s30})) = \begin{cases} 6.745 & \text{for } V_{s30} < 180 \text{ m/s} \\ 6.745 - 1.35 \ln\left(\frac{V_{s30}}{180}\right) & \text{for } 180 \leq V_{s30} \leq 500 \text{ m/s} \\ 5.394 - 4.48 \ln\left(\frac{V_{s30}}{180}\right) & \text{for } V_{s30} > 500 \text{ m/s} \end{cases} \quad (7.27)$$

$$a_{21} = \begin{cases} 0 & \text{for } V_{s30} \geq 1000 \text{ m/s} \\ \frac{-(a_{10} + bn) \ln\left(\frac{V_{s30}^*}{\min(V_1, 1000)}\right)}{\ln\left(\frac{Z_{1.0} + c_2}{\hat{Z}_{1.0}(V_{s30}) + c_2}\right)} & \text{for } (a_{10} + bn) \ln\left(\frac{V_{s30}^*}{\min(V_1, 1000)}\right) + e_2 \ln\left(\frac{Z_{1.0} + c_2}{\hat{Z}_{1.0}(V_{s30}) + c_2}\right) < 0 \\ e_2 & \text{otherwise} \end{cases} \quad (7.28)$$

$$e_2 = \begin{cases} 0 & \text{for } T < 0.35 \text{ s or } V_{s30} > 1000 \text{ m/s} \\ -0.25 \ln\left(\frac{V_{s30}}{1000}\right) \ln\left(\frac{T}{0.35}\right) & \text{for } 0.35 \leq T < 2.0 \text{ s} \\ -0.25 \ln\left(\frac{V_{s30}}{1000}\right) \ln\left(\frac{2}{0.35}\right) & \text{for } T > 2.0 \text{ s} \end{cases} \quad (7.29)$$

$$a_{22} = \begin{cases} 0 & \text{for } T < 2.0 \text{ s} \\ 0.0625(T - 2) & \text{for } T \geq 2.0 \text{ s} \end{cases} \quad (7.30)$$

Boore & Atkinson (2008)

The model is:

$$\ln Y = F_M(M) + F_D(R_{jb}, M) + F_S(V_{s30}, R_{jb}, M) + \epsilon\sigma_T \quad (7.31)$$

with single terms explained below.

Magnitude function:

$$F_M(M) = e_1U + e_2SS + e_3NS + e_4RS + \begin{cases} e_5(M - M_h) + e_6(M - M_h)^2 & \text{for } M \leq M_h \\ e_7(M - M_h) & \text{for } M > M_h \end{cases} \quad (7.32)$$

where U, SS, NS and RS are dummy variables to denote unspecified, strike-slip, normal-slip and reverse-slip fault type, and the “hinge magnitude” M_h for the shape of the magnitude scaling, is a coefficient to be set during the analyses so as e_i coefficients.

Distance function:

$$F_D(R_{jb}, M) = [c_1 + c_2(M - M_{ref})] \ln\left(\frac{R}{R_{ref}}\right) + c_3(R - R_{ref}) \quad (7.33)$$

where

$$R = \sqrt{R_{jb}^2 + h^2}$$

with c_1, c_2, c_3, M_{ref} and R_{ref} determined in the analyses.

Site amplification function:

it consists of a non linear and a linear term:

$$F_S = F_{LIN} + F_{NL} \quad (7.34)$$

with the linear term is expressed by the expression

$$F_{LIN} = b_{lin} \ln\left(\frac{V_{s30}}{V_{ref}}\right) \quad (7.35)$$

while the non linear term varies depending on the value of the initial predicted (pga4nl) for $V_{s30}=V_{ref}=760$ m/s referred to assigned threshold values. Specifically:

$$F_{NL} = \begin{cases} b_{nl} \ln(\text{pga_low} / 0.1) & \text{for } \text{pga4nl} \leq a_1 \\ b_{nl} \ln(\text{pga_low} / 0.1) + c[\ln(\text{pga4nl} / a_1)]^3 & \text{for } a_1 < \text{pga4nl} \leq a_2 \\ b_{nl} \ln\left(\frac{\text{pga4nl}}{0.1}\right) & \text{for } a_2 < \text{pga4nl} \end{cases} \quad (7.36)$$

in which

$$c = (3\Delta y - b_{nl}\Delta x) / \Delta x^2 \quad (7.37)$$

$$d = -(2\Delta y - b_{nl}\Delta x) / \Delta x^3 \quad (7.38)$$

with

$$\Delta x = \ln\left(\frac{a_2}{a_1}\right) \quad (7.39)$$

$$\Delta y = b_{nl} \ln(a_2 / \text{pga_low}) \quad (7.40)$$

The non linear slope b_{nl} is also a function of both period and V_{s30} .

Campbell & Bozorgnia (2008)

Authors adopted for the median of intensity measure prediction, the model

$$\ln(\text{IM}) = f_{\text{mag}} + f_{\text{dis}} + f_{\text{flt}} + f_{\text{hng}} + f_{\text{site}} + f_{\text{sed}} \quad (7.41)$$

with the following description of each term:

Magnitude term

$$f_{\text{mag}} = \begin{cases} c_0 + c_1 M & M \leq 5.5 \\ c_0 + c_1 M + c_2 (M - 5.5) & 5.5 < M \leq 6.5 \\ c_0 + c_1 M + c_2 (M - 5.5) + c_3 (M - 6.5) & M > 6.5 \end{cases} \quad (7.42)$$

Distance term

$$f_{\text{dis}} = (c_4 + c_5 M) \ln\left(\sqrt{R_{\text{rup}}^2 + c_6^2}\right) \quad (7.43)$$

Fault mechanism term

$$f_{\text{flt}} = c_7 F_{\text{RV}} f_{\text{flt},Z} + c_8 F_{\text{NM}} \quad (7.44)$$

with

$$f_{\text{flt},Z} = \begin{cases} Z_{\text{TOR}} & Z_{\text{TOR}} < 1 \\ 1 & Z_{\text{TOR}} \geq 1 \end{cases} \quad (7.45)$$

Hanging-wall term

$$f_{\text{hng}} = c_9 f_{\text{hng},R} f_{\text{hng},M} f_{\text{hng},Z} f_{\text{hng},\delta} \quad (7.46)$$

with

$$f_{\text{hng},R} = \begin{cases} 1 & R_{\text{jb}} = 0 \\ \frac{[\max(R_{\text{rup}}, \sqrt{R_{\text{jb}}^2 + 1}) - R_{\text{jb}}]}{\max(R_{\text{rup}}, \sqrt{R_{\text{jb}}^2 + 1})} & R_{\text{jb}} > 0, Z_{\text{TOR}} < 1 \\ \frac{(R_{\text{rup}} - R_{\text{jb}})}{R_{\text{rup}}} & R_{\text{jb}} > 0, Z_{\text{TOR}} \geq 1 \end{cases} \quad (7.47)$$

$$f_{\text{hng},M} = \begin{cases} 0 & M \leq 6.0 \\ 2(M - 6.0) & 6.0 < M < 6.5 \\ 1 & M \geq 6.5 \end{cases} \quad (7.48)$$

$$f_{\text{hng},Z} = \begin{cases} 0 & Z_{\text{TOR}} \geq 20 \\ (20 - Z_{\text{TOR}})/20 & 0 \leq Z_{\text{TOR}} < 20 \end{cases} \quad (7.49)$$

$$f_{\text{hng},\delta} = \begin{cases} 1 & \delta \leq 70 \\ (90 - \delta)/20 & \delta > 70 \end{cases} \quad (7.50)$$

Site response term

$$f_{\text{site}} = \begin{cases} \left\{ c_{10} \ln\left(\frac{V_{s30}}{k_1}\right) + k_2 \left\{ \ln\left[A_{1100} + c \left(\frac{V_{s30}}{k_1}\right)^n \right] - \ln[A_{1100} + c] \right\} \right\} & V_{s30} < k_1 \\ (c_{10} + k_2 n) \ln\left(\frac{V_{s30}}{k_1}\right) & k_1 \leq V_{s30} < 1100 \\ (c_{10} + k_2 n) \ln\left(\frac{1100}{k_1}\right) & V_{s30} \geq 1100 \end{cases} \quad (7.51)$$

Basin effect term

$$f_{\text{sed}} = \begin{cases} c_{11}(Z_{2.5} - 1) & Z_{2.5} < 1 \\ 0 & 1 \leq Z_{2.5} \leq 3 \\ c_{12}k_3 e^{-0.75} [1 - e^{-0.25(Z_{2.5}-3)}] & Z_{2.5} > 3 \end{cases} \quad (7.52)$$

where $Z_{2.5}$ is the depth to the 2.5 km/s shear-wave velocity horizon.

Chiou & Youngs (2008)

The model used by Chiou and Youngs is

$$\ln(y_{\text{site}}) = \ln(y_{\text{ref}}) + f_{\text{site}}(V_{s30}, y_{\text{ref}}) \quad (7.53)$$

where y_{ref} is the ground motion on the reference site condition whose V_{s30} values is assumed to be 1130 m/s because it is expected that there will not be significant nonlinear site response at this velocity. the prediction of y_{ref} related to the earthquake i and site j is given by the following combined model formulation, in which every row represent respectively style-of-faulting term, magnitude term, distance term (short and large distance scaling), anelastic attenuation (γ) term and source site geometric effects term.

$$\begin{aligned} \ln(y_{\text{ref}_i}) = & c_1 + [c_{1a}FR_{Vi} + c_{1b}F_{NMi} + c_7(Z_{\text{TOR}_i} - 4)](1 - AS_i) + [c_{10} + c_{7a}(Z_{\text{TOR}_i} - 4)]AS_i + \\ & + c_2(M_i - 6) + \frac{c_2 - c_3}{c_n} \ln(1 - e^{c_n(c_M - M_i)}) + \\ & + c_4 \ln[R_{\text{rup}_{ij}} + c_5 \cosh\{c_6 \max(M_i - c_{\text{HM}}, 0)\}] + (c_{4a} - c_4) \ln(\sqrt{R_{\text{rup}_{ij}}^2 + c_{\text{RB}}^2}) + \\ & + \left\{ c_{\gamma 1} + \frac{c_{\gamma 2}}{\cosh[\max(M_i - c_{\gamma 3}, 0)]} \right\} R_{\text{rup}_{ij}} + \\ & + c_9 F_{\text{HW}_{ij}} \tanh\left(\frac{R_{\text{X}_{ij}} \cos^2 \delta_i}{c_{9a}}\right) \left\{ 1 - \frac{\sqrt{R_{\text{JB}_{ij}}^2 + Z_{\text{TOR}_{ij}}^2}}{R_{\text{rup}_{ij}} + 0.001} \right\} + \eta_i \end{aligned} \quad (7.54)$$

while site term, divided in surface site effect and sediment thickness effect (shallow and deep), is:

$$\begin{aligned}
f_{\text{site}}(V_{s30}, y_{\text{ref}}) &= \Phi_1 \cdot \min\left(\ln\left(\frac{V_{s30ij}}{1130}\right), 0\right) + \\
&+ \Phi_2 \left\{ e^{\Phi_3(\min(V_{s30ij}, 1130) - 360)} - e^{\Phi_3(1130 - 360)} \right\} \ln\left(\frac{y_{\text{refij}} + \Phi_4}{\Phi_4}\right) + \\
&+ \Phi_5 \left(1 - \frac{1}{\cosh[\Phi_6 \cdot \max(0, Z_{1,0} - \Phi_7)]} \right)
\end{aligned} \tag{7.55}$$

Idriss (2008)

This GMPE represents the most simple relation within the project, where the pseudo-absolute acceleration for period T (PSA(T)) is predicted through the simple functional form

$$\ln[\text{PSA}(T)] = \alpha_1(T) + \alpha_2(T)M - [\beta_1(T) + \beta_2(T)M] \ln(R_{\text{rup}} + 10) + \gamma(T)R_{\text{rup}} + \varphi(T)F \tag{7.56}$$

where, $\gamma(T)$ is a “distance “adjustment factor (partially accounts for anelastic attenuation) and $\varphi(T)$ is a source mechanism factor; F=0 for “strike slip” events and 1 for “reverse”.

CHAPTER 8 **ADEQUACY OF EMPIRICAL GROUND MOTION MODELS FOR WORLD-WIDE SHALLOW CRUSTAL EARTHQUAKES RELATIVE TO ITALIAN DATA**

8.1 **INTRODUCTION**

An important issue for many practical applications is whether ground motions or GMPEs for one region can be applied to another. For example, this issue prompted considerable study for the SSHAC Level 4 PSHA (Budnitz et al., 1997) performed for the PEGASOS project in Switzerland (Abrahamson et al., 2002). The region of the PEGASOS project site has relatively few ground motion recordings, and hence GMPEs are borrowed from other areas for use in PSHA. Cotton et al. (2006) describe how source characteristics, path effects related to geometric spreading and anelastic attenuation, and site effects can vary from region-to-region. Those underlying physics ideally should be manifest in how a GMPE represents the scaling of a particular ground motion intensity measure (IM) with respect to magnitude, distance, and site condition.

The database used to develop the NGA models is large (3551 recordings from 173 earthquakes) relative to those used for relatively local regions, as is common in Europe. As mentioned previously, the NGA database is international, with most recordings derived from Taiwan, California, and Europe/Turkey (Chiou et al., 2008). As noted by Stafford et al. (2008), because of the large size and high quality of the NGA database, certain effects are well resolved in some of the NGA GMPEs that could not be evaluated using the European (or Italian) data. Examples include the effects of depth to top of rupture and nonlinear site response. The NGA data also provides the opportunity to constrain relatively complex functional forms for magnitude and distance scaling as compared to models typically used in Europe, as described further subsequently in the chapter.

Because the NGA models represent a major advancement in GMPEs for PSHA due to the quality and size of the database coupled with the relative sophistication of some of the functional forms, it is naturally of interest to determine if the NGA models can be applied in specific geographic regions such as Italy. This issue has been examined in a number of previous studies, the results of which are summarized in the next section. The objective in this chapter is to examine this issue by specifically testing the ability of the NGA models to capture the magnitude-scaling, distance-scaling, and site effects represented in the Italian dataset. This testing is of interest for two principal reasons (1) possible application of NGA

GMPEs for PSHA in Italy and (2) testing the NGA models against a dataset principally populated by extensional (normal fault) earthquakes, which are poorly represented in the NGA database.

As shown in the following section, previous studies have not specifically tested the ability of NGA models to capture the magnitude-, distance-, and site-scaling represented by the European data (at least in a statistically robust way). In the subsequent section, analysis of residuals are performed to investigate the magnitude-scaling, distance-scaling and site effects issues. Components of the NGA models that are compatible or inadequate relative to the Italian data are identified. Components of the NGA models judged to be inadequate are then modified, retaining the other features. The chapter ends with an interpretation of the results and conclusions.

The focus on Italian data is a matter of convenience and does not reflect an opinion on the part of the authors that ground motions should be examined on the basis of political boundaries. It is predicated on the re-evaluation of the Italian dataset according to standards similar to those utilized for the NGA database, as presented chapter 5. As improvements in the European dataset are made elsewhere, work of this type should be undertaken for broader regions without regard to political boundaries. In that vein, the work here presented should be viewed as a progress report on the broader question of application of world-wide shallow crustal GMPEs in Europe.

8.2 RECENT STUDIES COMPARING EUROPEAN AND CALIFORNIA STRONG GROUND MOTIONS

There are three general approaches that have been used to compare ground motions or GMPEs between regions: (1) direct comparison of median predictions of particular IMs from GMPEs for different regions (Campbell and Bozorgnia, 2006; Stafford et al., 2008); (2) analysis of variance (Douglas, 2004a,b); and (3) calculation of normalized residuals using a regional dataset and target model that are interpreted with a likelihood approach to evaluate the consistency of the data distribution with respect to the model (Scherbaum et al., 2004; Stafford et al., 2008).

8.2.1 Comparison of Medians from GMPEs

Figure 8.1 shows an example of the first approach. Estimates of peak horizontal acceleration (PHA) and 5%-damped pseudo spectral acceleration from the Akkar and Bommer (2007a) and Ambrasseys et al. (2005) models are compared to those from the NGA2008 models of Abrahamson and Silva (AS), Boore and Atkinson (BA), Campbell and Bozorgnia (CB), and Chiou and Young (CY). As shown by Campbell and Bozorgnia (2006) and Stafford et al. (2008), the European and NGA predicted medians generally compare well over the range of distances and magnitudes well constrained by the data. The bands of results for the three magnitudes generally show reasonably consistent vertical offsets from

model-to-model (e.g., the difference between M7 and M5 PGA at $R_{jb} = 30$ km for each model is reasonably consistent with estimates from the other models). This suggests generally consistent levels of magnitude scaling. The slopes of the medians for a given magnitude are generally steeper for the European relations than the NGA relations, suggesting faster distance attenuation. This potential difference in the distance attenuation was not noted by Campbell and Bozorgnia (2006) or Stafford et al. (2008).

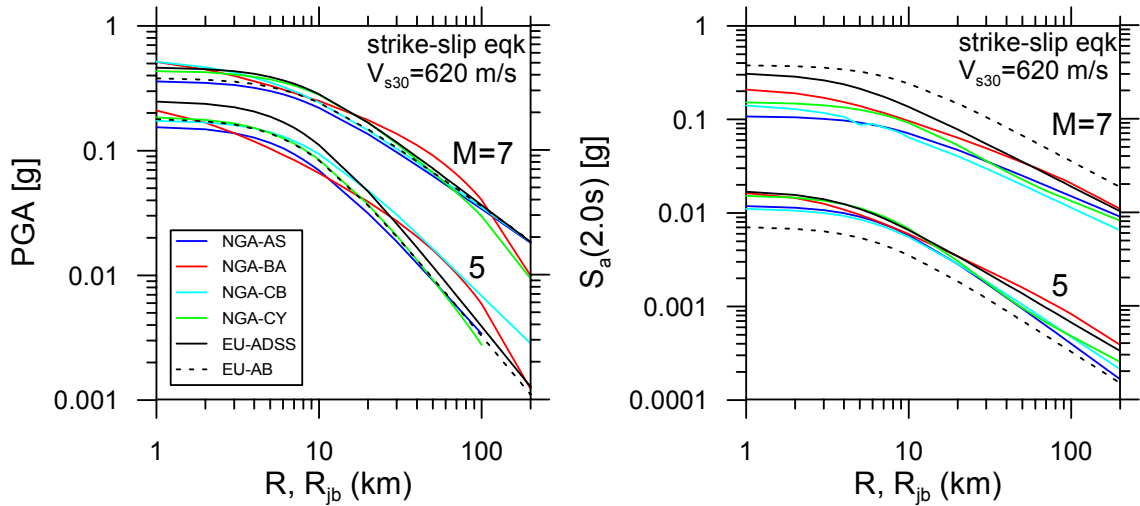


Figure 8.1. Comparison of median predictions of PGA and 2.0 s pseudo spectral acceleration for strike slip earthquakes and soft rock site conditions from NGA and European GMPEs.

8.2.2 Analysis of Variance

The approach termed “analysis of variance” was applied by Douglas (2004a) to compare ground motions for five local regions within Europe and Douglas (2004b) to compare ground motions from Europe, New Zealand, and California. The procedure involves calculating the mean (μ) and variance (σ^2) of the log of the data inside of particular magnitude and distance bins (M-R bins) for two different regions (e.g., Europe and California) and combinations of regions. Individual data points are adjusted for a linear site factor from Ambrasseys et al. (1996) before the calculation of mean and variance. These results are then used in two ways. First, for a given M-R bin and pair of regions, the variance across regions [termed (σ^2)inter-region] is compared to the within-region variance [termed (σ^2)intra-region] using statistical tests that evaluate whether the data sets are significantly distinct. If (σ^2)inter-region > (σ^2)intra-region in a statistically significant way, there is likely to be significantly different medians between regions. The second use of the binned results is to plot medians for each M-R bin together for pairs of regions.

Using the above approach, Douglas (2004a) found similar variances for the various regions in Europe, indicating a lack of regional variations. Accordingly, Douglas (2004b) combined all of the European data into a single category for comparison to New Zealand and California data. The Europe-California comparisons indicate that approximately half of the M-R bins demonstrate significantly different inter- and intra-region variances. The distinction was towards larger ground motions in California

(Douglas, 2004b). Careful analysis of Figure 1 of Douglas (2004b) indicates that the California and European means for most M-R bins have similar amplitudes in short distance bins (< 20 km), whereas California amplitudes are larger at larger distances (> 30 km). Thus, Douglas' (2004b) finding of larger California ground motions could be alternatively expressed as more rapid distance attenuation in Europe. Offsets between California and European means within a given well-populated distance category (e.g., 10-15 km) do not vary significantly across magnitude bins, suggesting similar levels of magnitude scaling.

8.2.3 Overall Goodness-of-Fit of Model to Data

This approach, developed by Scherbaum et al. (2004), provides an overall evaluation of goodness-of-fit of a GMPE to a dataset. A normalized residual is calculated for recording j from event i in a dataset as:

$$Z_{T,ij} = \frac{\ln(IM_{obs,ij}) - \ln(IM_{mod,ij})}{\sigma_T} \quad (8.1)$$

where $\ln(IM_{obs,ij})$ represents the IM of the data, $\ln(IM_{mod,ij})$ represents the median model prediction, and σ_T represents the total standard deviation of the model (combination of inter- and intra-event standard deviations). If the data is unbiased with respect to the model, the normalized residuals (Z_T) should have zero mean and standard deviation of one – i.e., the properties of the standard normal variate. Accordingly, in simple terms, the procedure of Scherbaum et al. (2004) consists of comparing the actual Z_T distribution to that of the standard normal variate. Note that this procedure tests both misfit of the median and standard deviation.

Stafford et al. (2008) extended this method to consider both inter- and intra-event variability. They compared European data to the NGA relation of Boore and Atkinson (2008) and the European models of Ambrasseys et al. (2005) and Akkar and Bommer (2007a,b). The Boore and Atkinson (2008) relation was shown to match the median of the European data nearly as well as European GMPEs. The Boore and Atkinson standard deviation is lower than European values, which was attributed to the magnitude-dependence of the European GMPE standard deviation models whereas the Boore and Atkinson standard deviation is homoskedastic.

8.2.4 Interpretation

It should be emphasized that the Scherbaum et al. (2004) approach assesses model performance in an overall sense – i.e., all aspects of the model (magnitude-scaling, distance-scaling, site effects) are evaluated in a lumped manner. If one of these model components was in error, that effect could be obscured through compensating errors in the analysis of normalized residuals. Accordingly, while the results of Stafford et al. (2008) are certainly promising with respect to the application of NGA relations in Europe, they do not specifically address whether individual components of the NGA models are adequate

with respect to European data. Because there is some evidence of faster distance attenuation of European data relative to California data (Douglas, 2004b) and active regions generally (Figure 8.1), a formal analysis of the adequacy of the NGA relations with respect to magnitude-scaling, distance-scaling, and site effects is needed. These issues are addressed in the remainder of this chapter.

8.3 ATTRIBUTES OF NGA AND EUROPEAN GROUND MOTION PREDICTION EQUATIONS

Ground motion prediction equations are formulated with varying degrees of complexity in their functional form as a result of author preference and the size and completeness of the database used in the analysis. The NGA models include two relatively simplified models (BA and I) and three more complex models (AS, CB, and CY). Attributes of the NGA models and several European relations with respect to magnitude-, distance, and Vs30-scaling are summarized below. The European models are Ambraseys et al. (2005) and Akkar and Bommer (2007a), which are referred to subsequently as ADSS and AB, respectively.

Table 8.1 summarizes the principal attributes of the magnitude-scaling in the GMPEs considered here. Magnitude scaling varies from linear (I, ADSS) to nonlinear functions expressed as 2nd order polynomials (AS, BA, AB), piecewise linear relations (CB), and more complex forms (CY).

Table 8.1. Magnitude scaling attributes of NGA and recent European GMPEs

GMPE	M-scaling ¹	Notes ²	Parameters ³
NGA AS2008	2nd-order polynomial	Separate style of faulting term	M_w ; F
NGA BA 2008	$M \leq M_h$: 2nd-order polynomial $M > M_h$: Linear	Coefficients depend on focal mech; M_h set by regression	M_w ; F
NGA CB 2008	Multiple connected line segments, slope depending on M_w	Separate style of faulting term	M_w ; F
NGA CY2008	sum of linear term & $c' \times \ln(1 - \exp\{c'' - c''M\})$	Separate style of faulting term, main shocks only	M_w ; F
NGA I 2008	Linear	Separate style of faulting term	M_w ; F
Eur. AB 2007	2nd-order polynomial	Separate style of faulting term	M_w ; F
Eur. ADSS 2005	Linear	Separate style of faulting term	M_w ; F

¹ c' , c'' , etc. indicate coefficients or combinations of coefficients determined by regression

² In each case, magnitude also affects distance scaling

³ M_w =Moment magnitude; F=focal mechanism

Figure 8.2 shows the variation with magnitude of PGA and T=2 sec spectral acceleration for a strike-slip, surface rupture earthquake at $R=R_{jb}=30$ km and rock site conditions. Similar period dependence of the slope of the scaling relationships is observed in each model. Note also the flattening of the scaling at large magnitude for all GMPEs except I and ADSS.

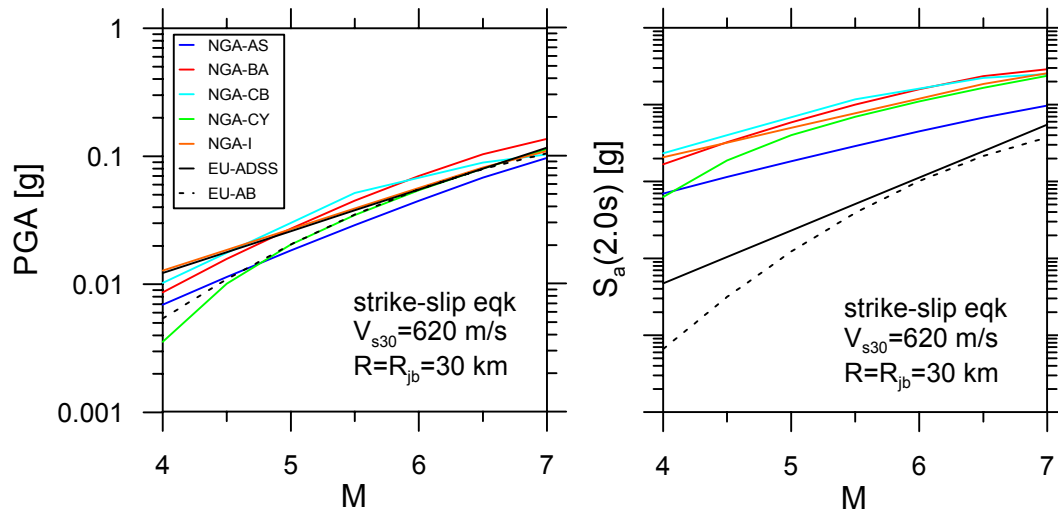


Figure 8.2. Comparison of magnitude scaling of PGA and 2.0 s S_a for strike slip earthquakes and soft rock site conditions from NGA and European GMPEs.

Table 8.2 shows the forms of the distance attenuation functions in the GMPEs used here. Many of the models (AS, CB, AB, ADSS) utilize a relatively simple form consisting of the product of a linear function of magnitude and the natural log of the SRSS (square root of sum of squares) of distance and an additive distance term (denoted h in Table 8.II). The linear term accounts for the decrease of attenuation with increasing magnitude (the intercept is negative and the coefficient for the change of slope with magnitude is positive). The BA and CY models account for the variation of distance attenuation with distance to capture the dominant effects of body waves at distances $< 40\text{--}70$ km and surface waves at larger distances. Additional anelastic attenuation terms (represented by $\gamma(M)$) are included by CY and I. Figure 8.1 compares the distance attenuation of NGA and European models. As noted previously, the European slopes are slightly greater. Among the NGA models, the steepening of the slope of the median curve with for $> \sim 70$ km is apparent in Figure 8.1 from the BA and CY models whereas the AS and CB slopes are constant. Also noteworthy is the relative values of slopes in the approximate distance range of 10–70 km, where much of the data lies. In this range, the steepest slope is CY, the flattest is BA, and AS and CB are intermediate. These differences have significant implications with respect to the Italian data, as discussed further below.

The models by AS, CB, and CY include hanging wall terms, which account for the larger ground motions observed on the hanging wall of dipping faults. As shown in Table 8.2, a distance parameter used to help define this effect for the AS and CY models is R_x , which is defined in Figure 8.3. Additional terms used to define hanging wall effects include depth to top of rupture (Z_{tor}), dip angle (δ), and down-dip fault width (W).

Table 8.2. Distance scaling functions used in NGA and recent European GMPEs

GMPE	R-scaling ¹	Notes	Parameters ²
NGA AS2008	$[a_2 + a_3(M - M_r)] \times \ln(\sqrt{R^2 + h^2})$	Additional hanging wall, depth to top of rupture, and large distance scaling terms	$R, R_{jb}, R_x, Z_{tor}, W, \delta$
NGA BA 2008	$[c_1 + c_2(M - M_r)] \times \ln\left(\frac{\sqrt{R_{jb}^2 + h^2}}{R_{ref}}\right) + c_3(\sqrt{R_{jb}^2 + h^2} - R_{ref})$	none	R_{jb}
NGA CB 2008	$[c_4 + c_5M] \times \ln(\sqrt{R^2 + h^2})$	Additional hanging wall term with functional dependence on δ and Z_{tor}	$R, R_{jb}, Z_{tor}, \delta$
NGA CY 2008	$c_4 \ln[R + c_5 \cosh\{c_6 \max(M - M_r, 0)\}] + (c_{4a} - c_4) \ln(\sqrt{R^2 + h^2}) + \gamma(M) \times R$	Additional hanging wall terms with functional dependence on δ and Z_{tor}	$R, R_{jb}, R_x, Z_{tor}, \delta$
NGA I 2008	$-\beta_1 + \beta_2 M \times \ln(R + 10) + \gamma(T)R$	None	R
Eur. AB 2007	$[b_4 + b_5M] \times \ln(\sqrt{R_{jb}^2 + h^2})$	None	R_{jb}
Eur. ADSS 2005	$[a_3 + a_4M] \times \ln(\sqrt{R_{jb}^2 + h^2})$	Separate style of faulting term	R_{jb}

¹ a, c, and β terms format retained from original model; h and M_r variables used here to show compatibility across models, these terms do not necessarily match those in the source publications. R_{ref} is specific to BA (2008)

² R=rupture distance; R_{jb} =closest distance to horizontal projection of rupture plane; R_x defined in Figure 3; Z_{tor} =depth to top of rupture; W=fault width; δ =dip angle

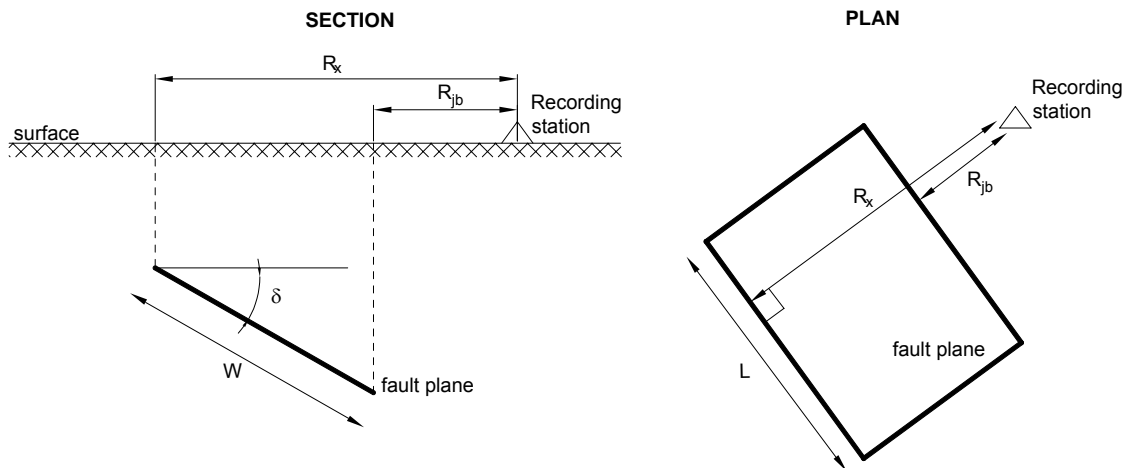


Figure 8.3. Schematic illustration of dipping fault and measurement of R_x parameter used in hanging wall terms for the AS and CY GMPEs.

The site terms utilized in the GMPEs vary significantly in complexity. All NGA models except Idriss (2008) utilize V_{s30} as a site term. As shown in Figure 8.4, the level of amplification for weak input motions (corresponding to nearly elastic conditions) increases with decreasing V_{s30} . In the AS, BA, CB,

and CY GMPEs, the reference rock parameter used with the nonlinear components of the site terms is \widehat{PGA}_{1100} , which is the median peak acceleration on rock with $V_{s30}=1100$ m/s. As shown in Figure 8.4, the absolute value of the slope of the amplification function relative to \widehat{PGA}_{1100} decreases with increasing V_{s30} .

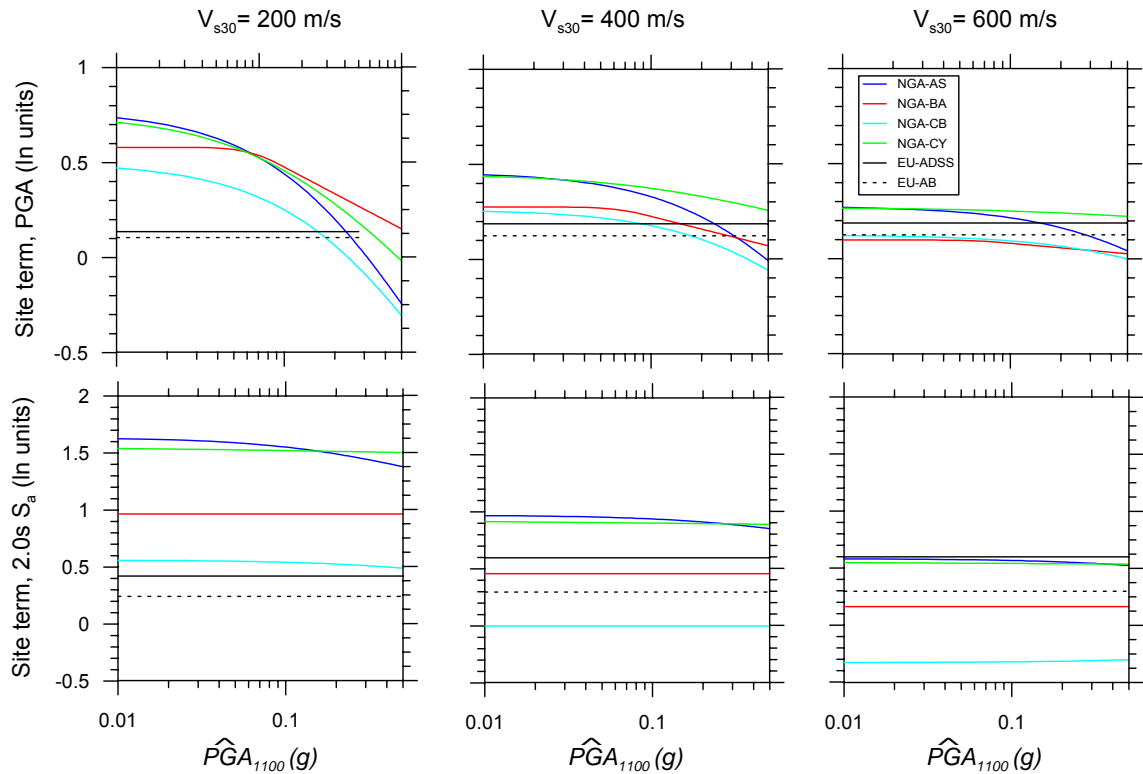


Figure 8.4. Comparison of site terms for PGA and 2.0 s pseudo spectral acceleration from NGA and European GMPEs

While the NGA site terms were developed using different procedures (simulation-based, empirical, etc.), Figure 8.4 shows that the resulting models from AS, BA, CB, and CY are generally similar. The Idriss (2008) model does not have a site term. The ADSS and AB site terms are linear and constant for qualitative site descriptors (soft soil, stiff soil, rock). In addition to V_{s30} , the AS, CB, and CY site models include a basin depth term, which is taken as the depth to a particular shear wave velocity isosurface. AS and CY take this depth as $Z_{1.0}$ (depth to $V_s=1.0$ km/s) whereas CB take this depth as $Z_{2.5}$ (depth to $V_s=2.5$ km/s).

For the analyses here conducted, each of the GMPEs listed in Tables 8.1 and 8.2 are considered except Idriss (2008). That model is excluded due its lack of a site term. A significant fraction of the Italian data are on soil site conditions and hence require the use of a site term.

8.4 DATASET

The database used in this study is the one presented in chapter 5. As already explained, the strong motion data were corrected and uniformly processed by the same seismologists (Walter Silva and Robert Darragh) who prepared the data for NGA. During this process, about 50% of the Italian motions were screened out because of s-triggers and other problems. Figure 8.5 shows the number of available recordings as a function of the maximum usable period, taken as the inverse of $1.25 \times f_{HP}$, where f_{HP} is the high-pass corner frequency used in the data processing, which varies from record-to-record according to signal characteristics.

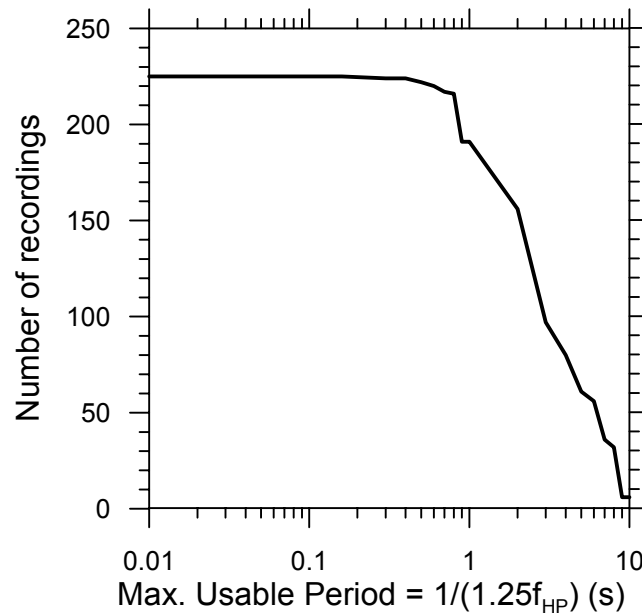


Figure 8.5. Variation of number of available recordings ($M \geq 4$ eqks) in Italian database with the maximum usable period, which is taken as the inverse of $1.25 \times f_{HP}$ (f_{HP} = high pass corner frequency used in data processing)

Note that there is a significant drop off in the data for periods $> 2-3$ sec and results obtained from the data should not be considered useful at those long periods.

Closest distance (R) and Joyner&Boore distance (R_{jb}) are taken to the fault rupture plane where available. For small magnitude earthquakes without a finite fault model, R is taken as the hypocentral distance and R_{jb} is taken as the epicentral distance. Since the only events without finite fault models are small in magnitude and hence have small fault dimensions, this approximation was considered to be reasonable. For events with unknown hypocentral depth and focal mechanism, those parameters were estimated based on available data from the local region.

The hanging wall index compiled by Chiou indicates whether a site is located in the hanging wall, footwall, or in a neutral (side) position relative to a dipping fault. For hanging wall sites, parameter R_x is estimated as:

$$R_x \approx R_{jb} + W \cos(\delta) \quad (8.2)$$

where W = fault width and δ = dip angle. Parameters W and δ are compiled for earthquakes with finite source models (see Ch.5). For other events where these parameters were needed, they were estimated using empirical models for W (Wells and Coppersmith, 1994) and dip angles for nearby fault (for δ). Distance R_x is not needed for footwall or neutral sites. The approximation in Eq. 2 is because R_x is strictly measured normal to the fault strike, as shown in Figure 8.3. Since the hanging wall region can extend slightly beyond the ends of the fault, there will be some sites for which the use of Eq. 2 is approximate. As indicated in Table 8.2, another parameter needed for some of the NGA hanging wall terms is depth to top of rupture (Z_{top}). As with dip angle, this is taken from the finite fault database where available and otherwise is calculated assuming the hypocenter is at mid-width as follows:

$$Z_{top} \approx Z_{hyp} - \frac{W}{2} \sin(\delta) \quad (8.3)$$

where Z_{hyp} =hypocentral depth. Additional adjustments are made on a case-by-case basis as needed (i.e., $Z_{top} < 0$, etc.).

Figure 8.6 shows the magnitude-distance distribution relative to that in the NGA database described by Chiou et al. (2008).

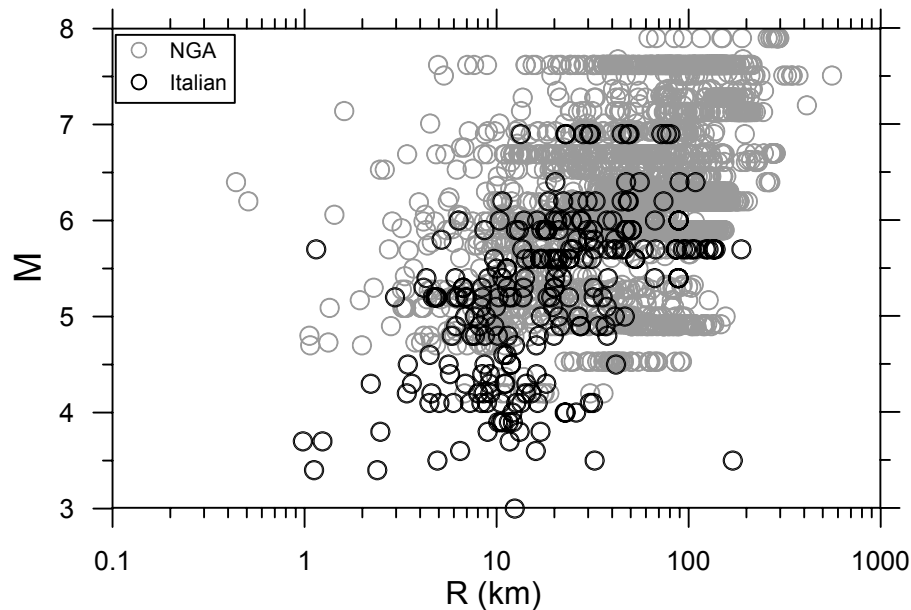


Figure 8.6. Distribution of NGA and Italian data with respect to magnitude and rupture distance

Relative to the NGA data, the Italian data is generally sparse for $R < 10$ km and $M > 6.5$. There is a reasonable degree of overlap in the datasets for $R=10-70$ km and $M=4.5-6$. The Italian data is richer than NGA for $M < 4.5$. An important distinction between the NGA and Italian databases concerns the preponderance of normal fault earthquake in the Italian data (44 of 89 events). In contrast, the PEER database has only 13 normal fault earthquakes with 87 recordings. Accordingly, comparison of the PEER NGA relations to Italian data provides the opportunity to test their applicability for a predominantly extensional region, which is of considerable practical importance in other regions as well (e.g., basin and range in United States).

The database presented in chapter 5 includes V_{s30} parameters for all Italian sites, which are used here to formulate the site terms. Basin depth terms $Z_{1.0}$ is taken from velocity profiles where available. Otherwise $Z_{1.0}$ is estimated from V_{s30} using the following function proposed by CY from the NGA database:

$$\ln(Z_{1.0}) = 28.5 - \frac{3.82}{8} \ln(V_{s30}^8 + 387.7^8) \quad (8.4)$$

where $Z_{1.0}$ is in km and V_{s30} is in m/s. Depth term $Z_{2.5}$ is evaluated from $Z_{1.0}$ using the following relation similarly derived from the NGA data by Campbell and Bozorgnia (2007):

$$Z_{2.5} = 0.519 + 3.595Z_{1.0} \quad (8.5)$$

where both depths are in km. These empirical depth estimates may not apply to Italy, but, by using medians that are dependent on V_{s30} for the vast majority of sites, the average basin effect in the NGA GMPEs are essentially used. Some resultant bias, especially at long periods, would not be surprising.

8.5 NOTE ON “MIXED RANDOM EFFECTC” MODEL FOR REGRESSIONS ANALYSIS

The *Mixed Random Effect Model*, compared to the classical simple least square approach, has the peculiarity of considering each event (intended as earthquake in the specific case) as random within a group of possible events.

For that model, the error term is partitioned into two parts: inter-event and intra-event terms. For a typical functional form:

$$\ln y_{ij} = f(M, r) + \eta_i + \varepsilon_{ij} \quad (8.6)$$

where is η_i the random effect for the i th event. The η_i represent inter-event variations and the ε_{ij} represent intra-event variations (fig.8.7). The η_i and ε_{ij} are assumed to be independent normally distributed variates with variances τ^2 and σ^2 respectively, while the total error is obtained as follows

$$\sigma_{TOT} = \sqrt{\sigma^2 + \tau^2} \quad (8.7)$$

The random effect term relative to the inter-event variations represent the difference between the general prediction model and every single event; for a given model with standard deviations τ and σ the event term is calculated as

$$\eta_i = \frac{\tau^2 \sum_{j=1}^{n_i} (y_{ij} - \mu_{ij})}{n_i \tau^2 + \sigma^2} \quad (8.8)$$

where n_i is the number of recordings for the i -th event, y_{ij} is the j -th recording of the i -th event and μ_{ij} is the value estimated by the assumed model.

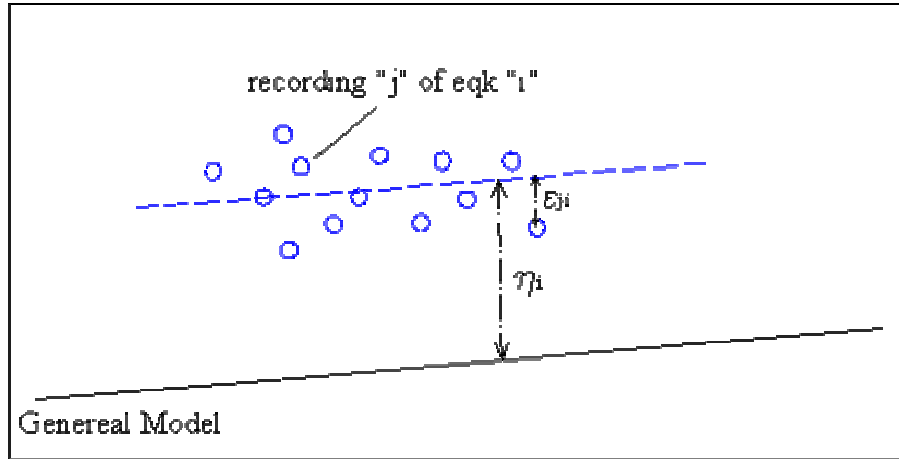


Figure 8.7. Schematic representation of inter-event (η_i) and intra-event (ϵ_{ij}) error

The practical meaning of the Mixed Random Effect Method is strictly related to the assumption on the data in the analysis, in this case intended as their statistic weight.

Specifically, the simple least squares would consider same weights of each recordings, while the choice of Random Effect allows to focus on single events instead of single recordings.

Therefore, the latter method consents to take in account the implicit variables, otherwise not considered, that represent differences between single events.

An example to clarify how reported so far can be easily represented by the case of two earthquakes of same magnitude, one of them well recorded (high number of related recordings) and the other recorded by a few stations. Simple least squares method would consider in such case all the recordings together as statistical population, with no differentiation between the two diverse earthquakes. The two events present, instead, different peculiarities between each other, usually not explicitly included in assumed functional forms, except if Random Effect is used. The latter would imply, in this example, an analysis running on two statistical population instead of one, attributing different statistic weight to different events.

Referring to previous paragraph, the following steps summarizes the analyses procedure of Random Effect methodology:

1. calculation of inter-event η_i (representing a sort of average error between single event and general prediction);
2. correction of every single data by inter-event term η_i ;
3. least square regression analysis on data corrected as above.

8.6 DATA ANALYSIS

8.6.1 Overall GMPE Mean and Standard Deviation Terms

To evaluate the magnitude-, distance-, and site-scaling issues described above, residuals between the data and a particular GMPE referred to with index k ($k=1\dots 6$ for the six models from Tables 8.1 and 8.2 that are utilized) are evaluated. The residuals are calculated as:

$$\left(R_{i,j}\right)_k = \ln\left(IM_{i,j}\right)_{data} - \ln\left(IM_{i,j}\right)_k \quad (8.9)$$

In Eq. 8.9, index i refers to the earthquake event and index j refers to the recording within event i .

Hence, $\left(R_{i,j}\right)_k$ is the residual of data from recording j in event i as calculated using GMPE k . Term $\ln\left(IM_{i,j}\right)_{data}$ represents the geometric mean of the two horizontal components of the data in natural log units while term $\ln\left(IM_{i,j}\right)_k$ represents the median calculated using GMPE k in natural log units.

Residuals are calculated using Eq. 8.9 for six GMPEs – AS, BA, CB, CY, AB, and ADSS. The analysis of residuals with respect to magnitude-, distance-, and site-scaling requires that event-to-event variations be separated from variations of residuals within events. This is accomplished by performing a mixed effects regression (Abrahamson and Youngs, 1992) of residuals according to the following function:

$$\left(R_{i,j}\right)_k = c_k + \left(\eta_i\right)_k + \left(\varepsilon_{i,j}\right)_k \quad (8.10)$$

where c_k represents a mean offset of the data relative to GMPE k , η_i represents the event term for event i (explained below), and $\varepsilon_{i,j}$ represents the intra-event residual for recording j in event i . Event term η_i represents approximately the mean offset of the data for a given event from the predictions provided by the GMPE median (after adjusting for mean offset c_k). Event terms provide a convenient mechanism for testing the ability of a GMPE to track the magnitude scaling of recordings in a dataset, as shown below. Event terms are assumed to be log-normally distributed, and generally have nearly zero mean and standard deviation (in natural log units) denoted as τ . Intra-event error ε is also assumed to be log-normally distributed with nearly zero mean and standard deviation $=\sigma$.

Figure 8.8 shows the distribution of event terms from the Italian data as a function of the number of recordings per event.

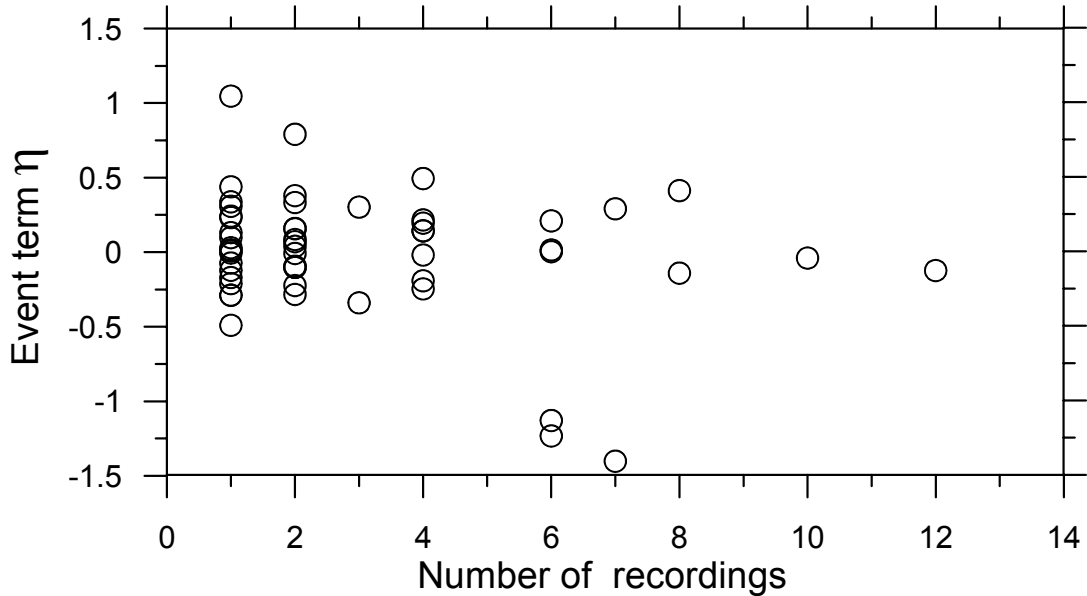


Figure 8.8. Variation of event terms with number of recordings, showing decrease of scatter for events with more recordings. Data from 1- and 2-recording events are not used in this study due to large scatter of event terms.

The scatter of event terms is large for sparsely recorded events (1-2 recordings) but is relatively stable for events with three or more recordings. Accordingly, for subsequent analysis data events with only one or two recordings were removed from the data set.

Using the dataset for earthquakes with three or more recordings, mixed effects regressions were performed using Eq. 8.9 for the aforementioned six GMPEs for five different ground motion intensity measures (IMs): peak acceleration and 5%-damped pseudo spectral acceleration (S_a) at periods of 0.2, 0.5, 1.0 and 2.0 seconds. The results are summarized in Table 8.3, which shows for each GMPE and IM values of c , τ , and σ .

Table 8.3. Summary of regression results for NGA GMPEs residuals relative to Italian data

GMPE	Period (s)	c	σ	τ	M-scaling		R-scaling	
					b_M	1-p	b_R	1-p
NGA AS	PGA	-0.15 ± 0.32	0.71	0.76	-0.16 ± 0.37	0.60	-0.19 ± 0.13	0.99
	0.2	-0.14 ± 0.31	0.80	0.71	0.02 ± 0.36	0.08	-0.16 ± 0.15	0.96
	0.5	-0.23 ± 0.32	0.86	0.57	0.20 ± 0.38	0.68	-0.07 ± 0.14	0.70
	1.0	-0.11 ± 0.30	0.75	0.69	0.31 ± 0.34	0.92	-0.04 ± 0.14	0.46
	2.0	-0.04 ± 0.31	0.86	0.68	0.24 ± 0.32	0.85	0.07 ± 0.16	0.58
NGA BA	PGA	0.09 ± 0.32	0.73	0.72	-0.36 ± 0.36	0.94	-0.31 ± 0.14	1.00
	0.2	0.10 ± 0.31	0.83	0.68	-0.24 ± 0.34	0.83	-0.34 ± 0.16	1.00
	0.5	-0.08 ± 0.29	0.86	0.64	0.07 ± 0.32	0.32	-0.21 ± 0.14	0.99
	1.0	-0.03 ± 0.28	0.74	0.64	0.21 ± 0.32	0.81	-0.13 ± 0.14	0.93
	2.0	-0.06 ± 0.29	0.86	0.61	0.06 ± 0.30	0.30	-0.05 ± 0.16	0.42
NGA CB	PGA	-0.17 ± 0.31	0.73	0.70	0.24 ± 0.32	0.85	-0.24 ± 0.14	1.00
	0.2	-0.25 ± 0.28	0.81	0.61	-0.08 ± 0.30	0.38	-0.22 ± 0.16	1.00
	0.5	-0.37 ± 0.28	0.88	0.78	0.19 ± 0.30	0.77	-0.10 ± 0.15	0.81
	1.0	-0.28 ± 0.26	0.75	0.58	0.26 ± 0.28	0.93	-0.06 ± 0.14	0.62
	2.0	-0.26 ± 0.25	0.88	0.50	0.14 ± 0.22	0.77	0.03 ± 0.18	0.24
NGA CY	PGA	0.08 ± 0.30	0.64	0.69	-0.29 ± 0.35	0.89	-0.08 ± 0.12	0.79
	0.2	0.16 ± 0.28	0.74	0.61	-0.14 ± 0.30	0.65	-0.08 ± 0.14	0.72
	0.5	0.00 ± 0.27	0.91	0.57	0.05 ± 0.28	0.30	-0.04 ± 0.15	0.44
	1.0	-0.02 ± 0.25	0.77	0.52	0.15 ± 0.24	0.78	-0.02 ± 0.14	0.19
	2.0	-0.12 ± 0.27	0.91	0.53	0.06 ± 0.24	0.36	0.12 ± 0.17	0.84
EU AB	PGA	0.04 ± 0.30	0.68	0.69	-0.29 ± 0.34	0.90	-0.11 ± 0.12	0.90
	0.2	0.04 ± 0.28	0.80	0.58	-0.10 ± 0.28	0.51	-0.14 ± 0.14	0.95
	0.5	-1.02 ± 0.31	0.80	0.69	-0.22 ± 0.34	0.78	-0.24 ± 0.14	0.99
	1.0	0.06 ± 0.25	0.75	0.53	0.06 ± 0.26	0.36	0.02 ± 0.14	0.22
	2.0	0.02 ± 0.25	0.87	0.49	-0.11 ± 0.22	0.67	0.06 ± 0.16	0.54
EU ADSS	PGA	-0.17 ± 0.28	0.68	0.65	-0.04 ± 0.34	0.21	-0.07 ± 0.13	0.70
	0.2	-0.29 ± 0.28	0.80	0.60	0.10 ± 0.30	0.49	-0.08 ± 0.15	0.72
	0.5	-0.42 ± 0.32	0.76	0.71	0.31 ± 0.34	0.92	0.03 ± 0.14	0.36
	1.0	-0.37 ± 0.29	0.76	0.65	0.39 ± 0.30	0.98	0.05 ± 0.14	0.53
	2.0	-0.55 ± 0.28	0.87	0.57	0.25 ± 0.26	0.94	0.11 ± 0.08	0.80

Figure 8.9a plots the average misfit of Italian data to the GMPEs as expressed by parameter c , along with $\pm 95\%$ confidence intervals on the estimate of c . Parameter c is not generally significantly offset from zero, nor does it have a significant trend with period. An exception is CB, for which c is consistently and significantly negative for $T > \sim 0.2$ s. Negative values of c indicate an average over-prediction of the Italian data by the CB GMPE. Figures 8.9b-c plot the inter- and intra-event standard deviations (τ and σ , respectively) versus period as evaluated from the regressions performed using Eq. 7. Results are shown for the NGA GMPEs only. Also shown in Figures 8b-c are the ranges of τ and σ provided by a representative NGA GMPE (CY) and a European GMPE (AB) for $M=5-7$. The standard deviation terms from the Italian data are significantly larger than those provided by CY and the other NGA relations. Intra-event standard deviation σ is similar to values obtained previously by AB for Europe, but our τ terms are much larger. This is caused by three events with large negative event terms (Molise 31-10-2002

and 01-11-2002, Trasaghis-Friuli 28-5-1998), as shown in Figure 8.8. If those events were omitted from the calculation, τ would reduce to values comparable to those from previous studies. Accordingly, difference in Figure 8.9b can be considered as a result of the poorly sampled database and corresponding large impact of these outliers. Consideration of the larger intra-event standard deviation of European data in PSHA is advisable. Additional discussion on appropriate standard deviation terms for practical application is given in the Interpretation and Conclusions section.

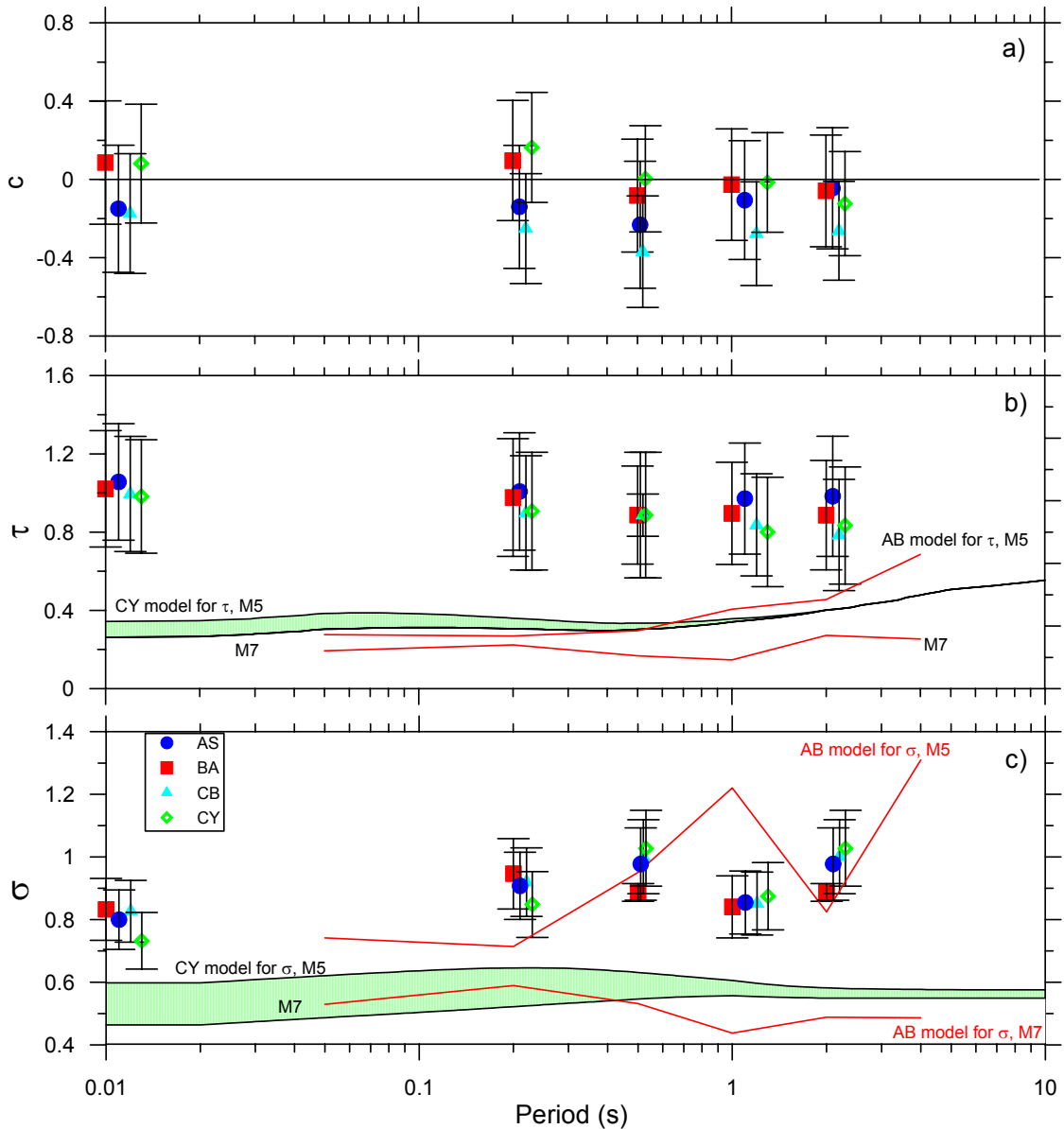


Figure 8.9. Variation with period of mean bias parameter ($\hat{\mu}$), inter-event dispersion ($\hat{\tau}$), and intra-event dispersion ($\hat{\sigma}$) evaluated from regression of NGA residuals relative to Italian data with Eq. 8.9.

8.6.2 Magnitude Scaling

Next question is how well the selected GMPEs capture the magnitude scaling of the Italian dataset. The event terms are plotted against magnitude in Figure 8.10 for the IMs of PGA, 0.2 s Sa, and 1.0 s Sa.

To help illustrate trends, a fit line and its $\pm 95\%$ confidence intervals is also plotted, the fit being made according to:

$$\eta_i = a_M + b_M M_i + (\kappa_M)_i \quad (8.11)$$

In Eq. 8.11, subscript k has been dropped, but the regressions are performed separately for each GMPE. Parameters a_M and b_M represent the regression coefficients and $(\kappa_M)_i$ is the residual of the fit for event i . Slope b_M is of particular interest because if non-zero and significant, it suggests the magnitude scaling in the model does not match the data. The columns under the heading ‘M-scaling’ in Table 8.3 indicate values of b_M , its $\pm 95\%$ confidence intervals, and the outcome of hypothesis testing described below.

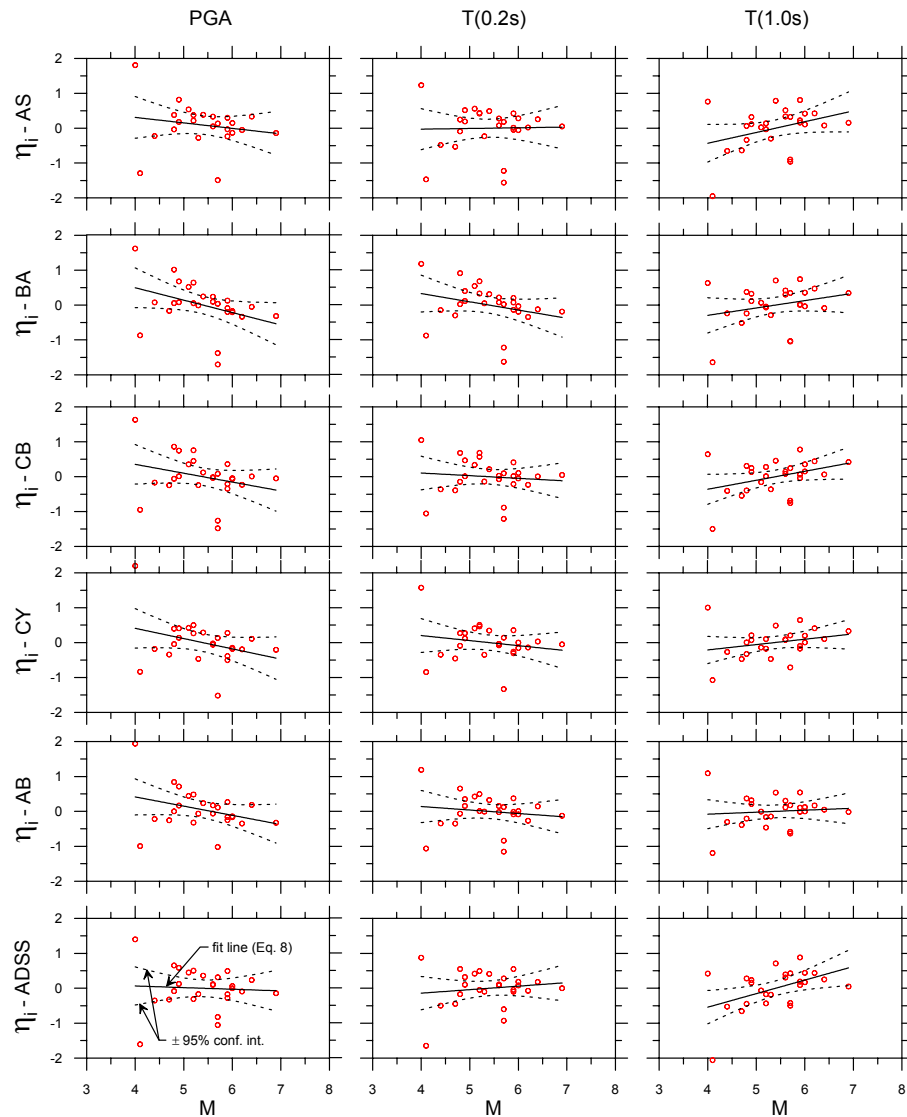


Figure 8.10. Variation of event terms for Italian data with magnitude for PGA, $0.2 s S_w$ and $1.0 s S_w$.

The statistical significance of the magnitude-dependence of event terms is assessed two ways. The first significance test consists of comparing the absolute value of b_M to its estimation error (taken as the

$\pm 95\%$ confidence intervals shown in Table 8.3). When $|b_M|$ exceeds the estimation error, the nonlinearity is considered significant. Secondly, sample ‘t’ statistics are compiled to test the null hypothesis that $b_M=0$. This statistical testing provides a significance level = p that the null hypothesis cannot be rejected. For clarity of expression, values of $1-p$, which we refer to as a “rejection confidence for a zero slope model”, are tabulated in Table 8.3. As shown, the rejection confidence levels are consistently small (i.e., $< 95\%$). Therefore, while the slope of the trend lines (b_M) in Figure 8.10 are non-zero, they are not statistically significant. This, in turn, suggests that the magnitude-dependence of the event terms is not significant. On the basis of this result, a first conclusion is that the selected GMPEs adequately capture the magnitude scaling of the Italian dataset.

8.6.3 Distance Scaling

Distance scaling is tested by examining trends of intra-event residuals $\varepsilon_{i,j}$ as a function of distance. Recall that per Eq. 10, $\varepsilon_{i,j}$ is the remaining residual after mean error (c) and event term (η_i) are subtracted from the total residual. Figure 8.11 shows $\varepsilon_{i,j}$ for IMs of PGA, 0.2 s Sa, and 1.0 s Sa. To help illustrate trends, a fit line and its $\pm 95\%$ confidence intervals is also plotted, the fit being made according to:

$$\varepsilon_{i,j} = a_R + b_R R_{i,j} + (\kappa_R)_{i,j} \quad (8.12)$$

Parameters a_R and b_R are regression parameters and κ_R is the residual of the fit for recording j from event i . Subscript k has been dropped in Eq. 8.12, which strictly holds for GMPEs using rupture distance. For BA, AB, and ADSS, $R_{j,b}$ replaces R as the distance parameter in Eq. 8.12. The slope parameter (b_R in this case) represents approximately the misfit of the distance scaling in the Italian dataset and the selected GMPEs. The columns under the heading ‘R-scaling’ in Table 8.3 indicate values of b_R , its $\pm 95\%$ confidence intervals, and the rejection confidence for a $b_R=0$ model ($1-p$) from hypothesis testing.

The results in Figure 8.11 and Table 8.3 indicate mixed findings with respect to misfits between the NGA distance scaling and the Italian data. The CY GMPE demonstrates no significant misfit across all tested periods, as evidenced by values of b_R that are smaller than their confidence intervals and low rejection confidence for the zero slope null hypothesis ($< \sim 80\%$). On the other hand, the AS, BA, and CB models produce statistically significant values of b_R ranging from approximately -0.2 to -0.3 at short periods (PGA and 0.2 s Sa). None of the NGA models show bias in the distance attenuation for long period ($T \geq 1.0$ s). These negative values of b_R at short periods indicate faster distance attenuation of the Italian data relative to these GMPEs. Note that the lack of significant b_R in the CY model is consistent with the relatively fast distance attenuation of this model in the 10-70 km range relative to the other NGA GMPEs, as shown in Figure 8.1. Moreover, the largest b_R values are observed for the BA model, which has the slowest distance attenuation, with AS and CB being intermediate cases.

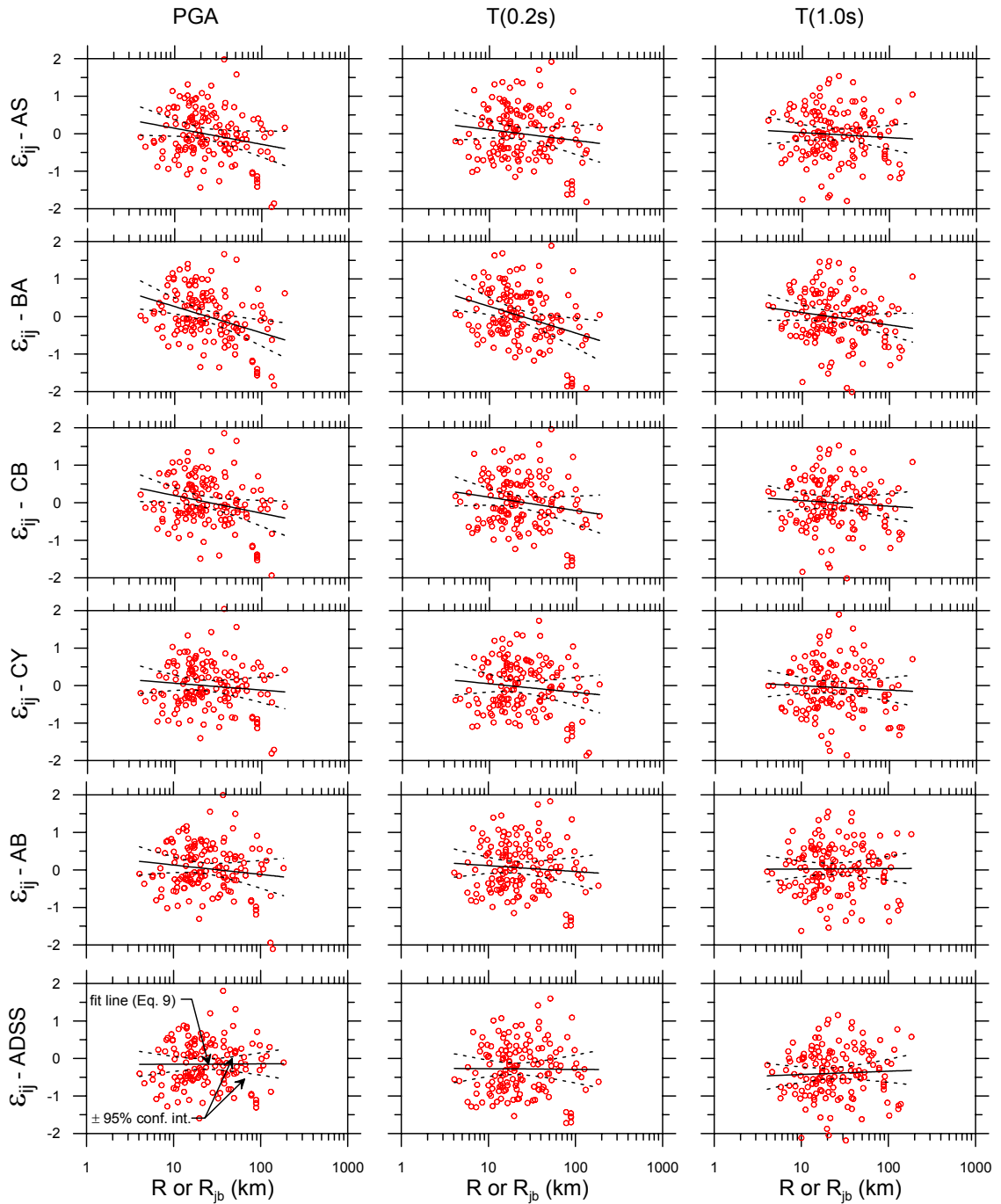


Figure 8.11. Variation of intra-event residuals for Italian data with distance for PGA, $0.2 s S_w$, and $1.0 s S_w$.

To further examine the distance attenuation misfit, Italian data are regressed against the AS, BA, and CB functional forms to re-evaluate selected distance parameters. In these regressions, all model parameters in the GMPE functions are fixed at the published values except for one or two parameters in the distance function that require modification to remove the aforementioned bias. These regressions are not performed for CY because of the lack of trends in the residuals described above. Recalling the distance attenuation functions given in Table 8.2, the parameters that are re-evaluated as part of this analysis are as follows:

AS: Parameter a_2 is modified along with constant term a_1 . Parameters a_3 , M_r , and h are not modified, nor is the large distance attenuation function modified.

BA: Parameter c_1 is modified along with the constant term, which BA take as a function of focal mechanism (e_1 to e_4 for unknown, strike slip, normal slip, and reverse slip, respectively). Values of e_1 to e_4 from BA are fixed to preserve the variations between focal mechanism in the original model, but evaluate a new additive term that is applied with e_1 to e_4 and which is independent of focal mechanism. Terms c_2 , c_3 , M_r , h , and R_{ref} are not modified.

CB: Parameter c_4 is modified along with constant term c_0 and additive distance term c_6 (similar to h in Table 8.2). Parameter c_5 is not modified.

Note that in each case the term that is modified scales nearly directly the distance term and represents effects of geometric spreading and anelastic attenuation.

The modification of the above parameters was performed using mixed effects procedures with the following equations:

$$\text{AS: } \ln(IM)_{i,j} = a'_1 + f'_R + f_{Source} + f_{Site} + \eta'_i + \varepsilon'_{i,j} \quad (8.13)$$

$$\text{BA: } \ln(IM)_{i,j} = F'_R + F'_M + F_S + \eta'_i + \varepsilon'_{i,j} \quad (8.14)$$

$$\text{CB: } \ln(IM)_{i,j} = f'_{mag} + f'_{dis} + f_{flt} + f_{hmg} + f_{site} + f_{sed} + \eta'_i + \varepsilon'_{i,j} \quad (8.15)$$

where the prime (') indicates the function is modified and the lack of prime means the functions are used exactly as given in the published relations. For all models, η'_i and $\varepsilon'_{i,j}$ represent newly determined inter- and intra-event error terms. For AS, a'_1 is a newly regressed constant term; f'_R is the distance term in Table 8.2 with newly regressed coefficient a_2 (referred to as a'_2); f_{Source} indicates the magnitude function in f_1 , the focal mechanism flag terms, hanging wall term (f_4), top-of-rupture term (f_6), and large distance model (f_8); f_{Source} indicates the V_{s30} term (f_5) and basin depth term (f_{10}); For BA, F'_R is the distance term in Table 8.2 with c_1 replaced with newly regressed c'_1 ; F'_M is identical to the BA magnitude term except for the new additive constant term noted above, which we will refer to as e'_0 ; F_S is the V_{s30} -dependent site term. For CB, f'_{mag} is identical the CB magnitude term except for a new constant term c'_0 , f'_{dis} is the distance term in Table 8.2 with c_4 and c_6 replaced with newly regressed c'_4 and c'_6 , and the remaining terms are fault type, hanging wall, site, and depth terms that are not modified.

Analyses begin with a straightforward mixed effects regression as described above. The prediction of the modified GMPE at short distance where then checked to evaluate compatibility with the original GMPE. As shown in Figure 8.7, the Italian data is sparse at close distance and so cannot constrain short-distance ground motions. Hence, compatibility of short-distance ground motions between the modified and original GMPE is enforced. This compatibility occurred “naturally” (i.e., as a direct outcome of the

regression) for the AS model (all periods) and BA (all periods except PGA). For BA (PGA) and CB (all periods), additional adjustments were necessary to establish this compatibility. For BA (PGA), an appropriate value of e'_0 was selected and c'_1 then regressed through an iterative process. A similar process was used for CB, although the additive distance term (denoted h in Table 8.2 but taken as c_6 in the CB model) is also regressed and constant term c'_0 is manually adjusted to achieve compatibility of short-distance IMs.

Table 8.4 shows for each of the NGA GMPEs the original values of the regressed parameters (without primes) and the modified values (with primes, '). Figure 8.12 shows the distance attenuation of the original and modified GMPEs for PGA, 0.2 s S_a , and 1.0 s S_a for a soft rock site conditions ($V_{s30}=620$ m/s) and magnitudes of $M=5$ and 7.

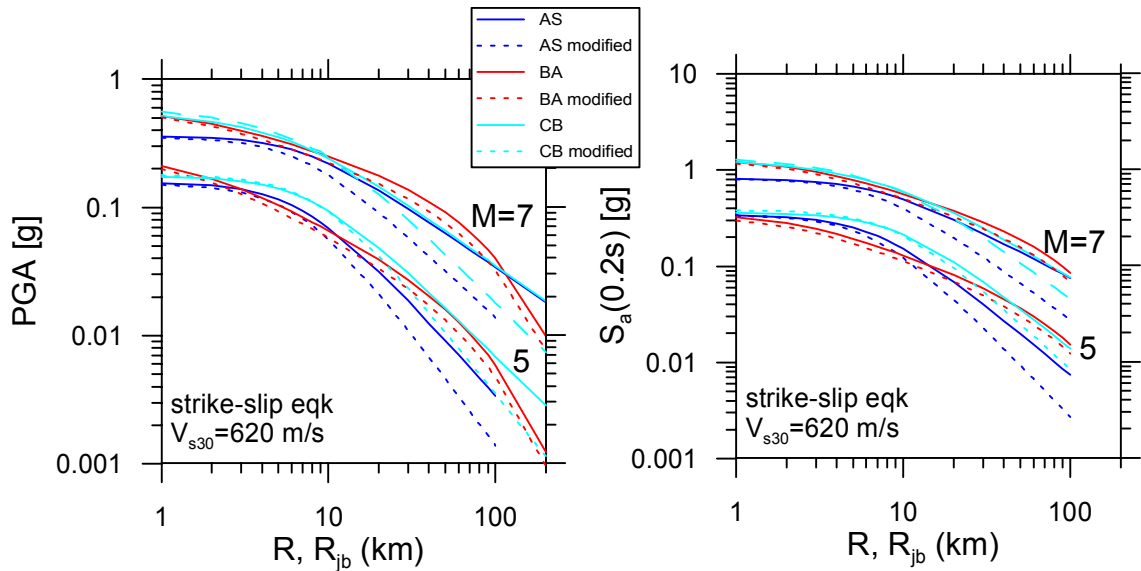


Figure 8.12. Variation of median ground motions with distance and magnitude from NGA and modified NGA relations developed in this study.

In Table 8.4, values established through regressions are shown with $\pm 95\%$ confidence intervals whereas values that are fixed manually have no confidence intervals. The absolute value of the modified distance-attenuation terms (a'_2 for AS, c'_1 for BA, c'_4 for CB) are consistently larger than the original values, consistent with the faster distance attenuation in the Italian data.

Table 8.4. Summary of modified GMPE parameters for constant and distance scaling terms and effect on trends of intra-event residuals with distance

GMPE	Period (s)	GMPE Regression Parameters						R-scaling (mod GMPE)	
		a_2	a_1	a_2'	a_1'	τ'	σ'	b_R'	1-p
NGA AS	PGA 0.2	-0.97	0.80	-1.30 ± 0.18	1.72 ± 0.68	0.78	0.67	0.01 ± 0.12	0.12
		-0.97	1.69	-1.34 ± 0.21	2.81 ± 0.74	0.71	0.77	0.01 ± 0.14	0.11
NGA BA	PGA 0.2 0.5	c_1	c_1'	e_0'	τ'	σ'	0.00 ± 0.12	0.00	
		-0.66	-0.76 ± 0.16	0.07 ± 0.60	0.70	0.82			
		-0.58	-0.63 ± 0.10	0	0.77	0.87			
		-0.69	-0.75 ± 0.08	0	0.63	0.80	-0.01 ± 0.12	0.12	
NGA CB	PGA ¹ 0.2 ²	c_4	c_6	c_4'	c_6'	τ'	σ'	-0.07 ± 0.12	0.73
		-2.12	5.60	-2.48 ± 0.80	7.14 ± 3.40	0.78	0.67		
		-2.22	7.60	-2.46 ± 0.90	7.60	0.72	0.78		

¹ constant term was fixed to $c_0 = -0.18$

² constant term was fixed to $c_0 = 0.11$

After adjusting the constant and distance terms as described above, the magnitude-dependence of event terms (η'_i) and the distance dependence of intra-event residuals ($\varepsilon'_{i,j}$) are checked. As shown in Figure 8.13, the magnitude-scaling of the modified GMPEs remains appropriate (results are similar to those shown in Figure 8.10).

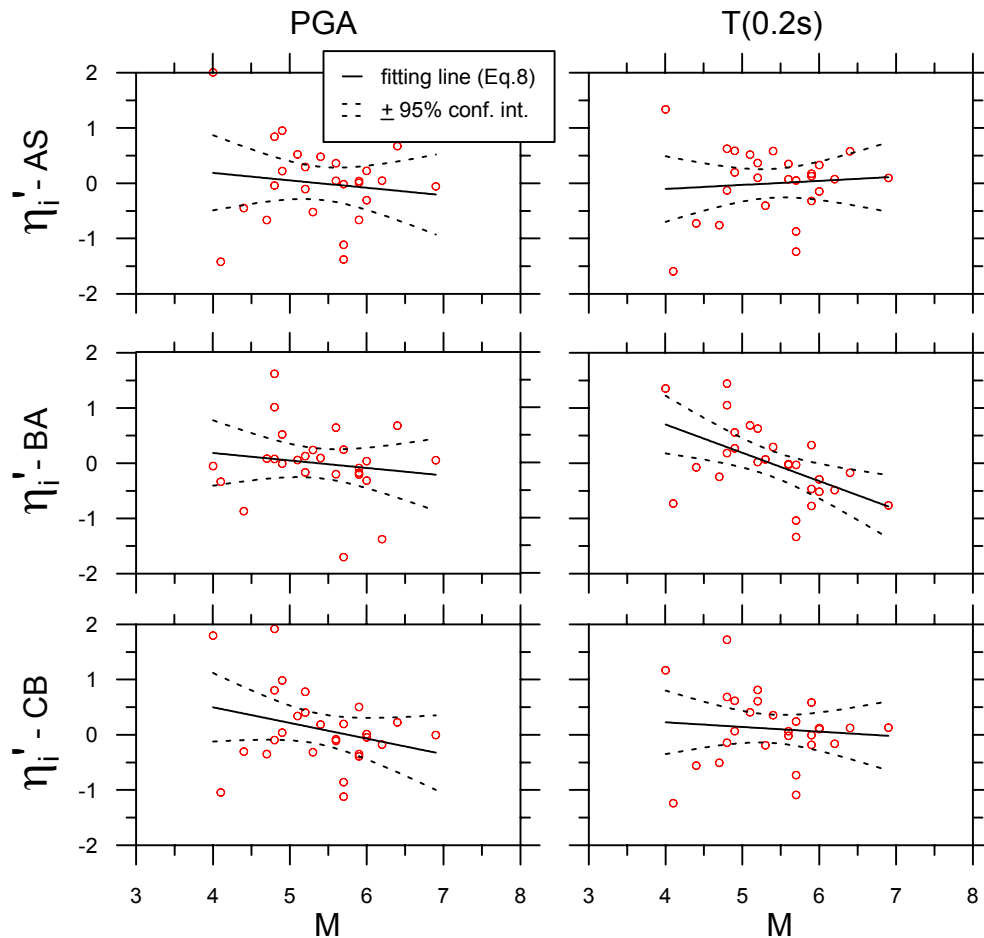


Figure 8.13. Variation of event terms for modified AS, BA, and CB GMPEs with magnitude for PGA and 0.2 s S_d . Magnitude dependence of event terms are similar to the original models presented in Figure 9.

Figure 8.14 shows that the trends in the distance-scaling observed in Figure 8.11 are removed with the revised coefficients. This is also confirmed by the hypothesis test results in Table 8.4, which show a low confidence (1-p) in rejecting the null hypothesis of zero slope.

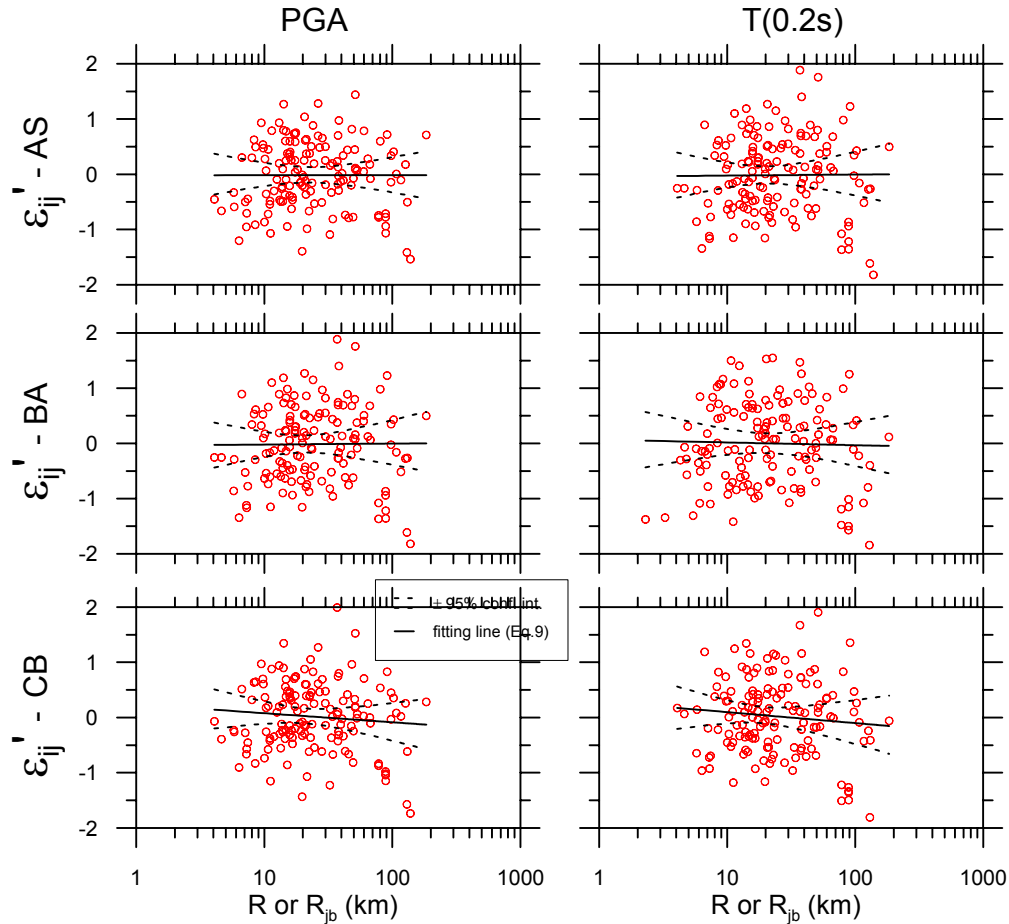


Figure 8.14. Variation of intra-event residuals for modified AS, BA, and CB GMPEs with distance for PGA and 0.2 s S_a . The statistically significant distance-dependence of residuals from the original models presented in Figure 10 are removed.

8.6.4 Site Effects

Scaling of ground motions with V_{s30} in the NGA GMPEs is evaluated using versions of the models without distance bias (original CY, modified versions of AS, BA, CB). This is done so that distance-bias is not mapped into the analysis of V_{s30} . We begin by examining in Figure 8.15 trends of intra-event residuals ($\varepsilon_{i,j}$ or $\varepsilon'_{i,j}$) as a function of V_{s30} for the IMs of PGA, 0.2 s S_a , and 1.0 s S_a . Trends are illustrated with a fit line:

$$\varepsilon_{i,j} = a_V + b_V (V_{s30})_{i,j} + (\kappa_V)_{i,j} \quad (8.16)$$

Parameters a_V and b_V are regression parameters and κ_V is the residual of the fit for recording j from event i . Eq. 8.16 strictly holds for the CY GMPE; for AS, BA, and CB, $\varepsilon'_{i,j}$ replaces ε_{ij} in Eq. 8.16. Slope parameter b_V represents approximately the misfit of the distance scaling in the Italian dataset and the selected GMPEs. Table 8.5 shows values of b_V , their $\pm 95\%$ confidence intervals, and the rejection confidence for a $b_V=0$ model (1-p) from hypothesis testing. The results in figure 8.15 and Table 8.5 indicate no statistically significant trends with V_{s30} . This suggests that the V_{s30} -based site terms in the NGA GMPEs may be compatible with the Italian data.

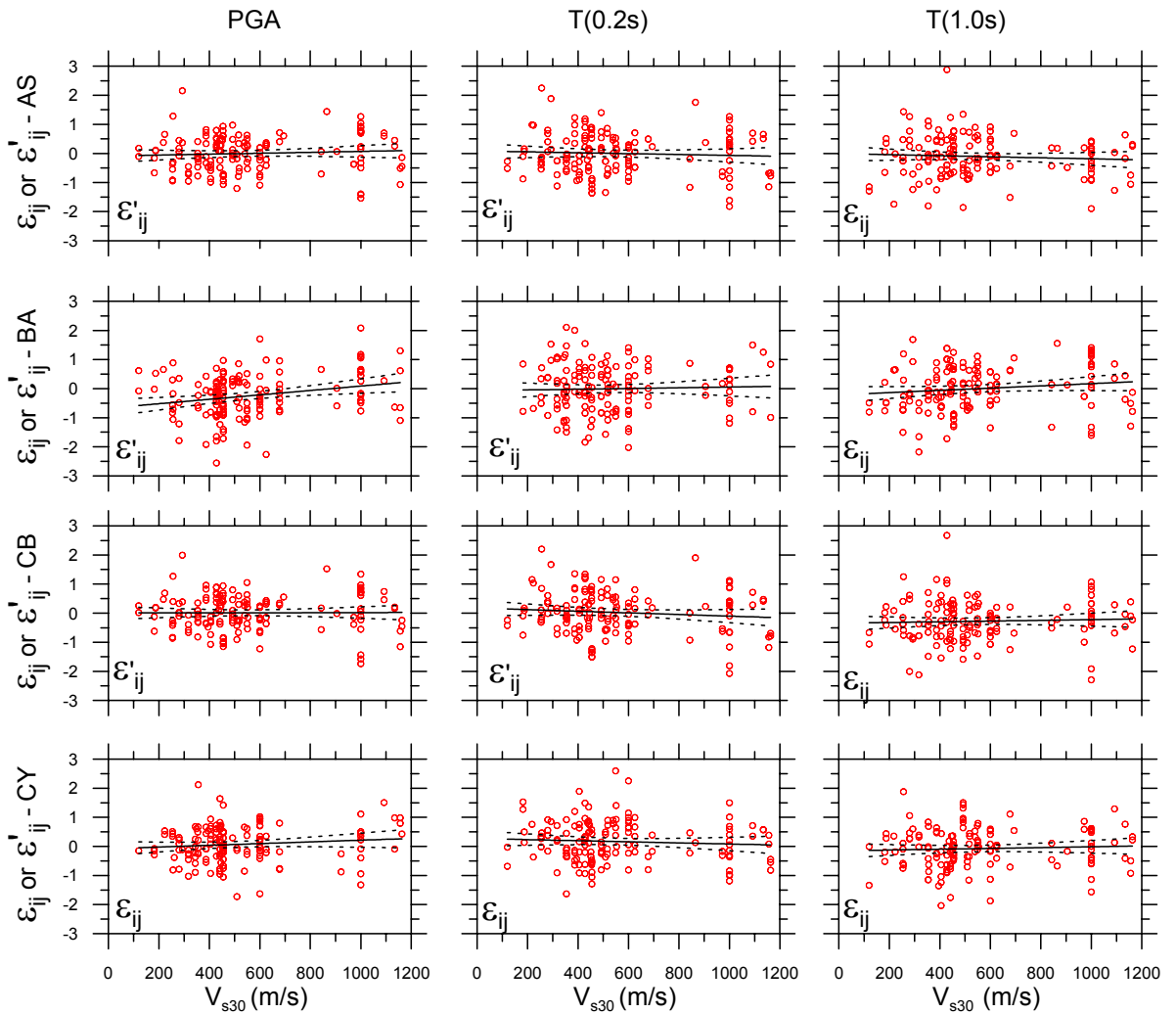


Figure 8.15. Variation of intra-event residuals with average shear wave velocity in upper 30 m (V_{s30}). Residuals shown are for original GMPE when shown without prime (ε_{ij}) and for modified GMPE when shown with prime (ε'_{ij}).

Table 8.5. Summary of modified GMPE parameters for constant and distance scaling terms and effect on trends of intra-event residuals with distance

GMPE	Period (s)	V_{s30} -scaling (mod GMPE)		Rock ($V_{s30} = 800-1100$ m/s)			Soil ($V_{s30} = 180-300$ m/s)		
		bv.	1-p	a_{PGA}	b_{PGA}	(1-p) _b	a_{PGA}	b_{PGA}	(1-p) _b
NGA AS	PGA	0.0002 ± 0.0004	0.58	-0.27	-0.14	0.61	-0.68	-0.34	0.94
	0.2	-0.0002 ± 0.0004	0.50	-0.45	-0.24	0.84	-1.34	-0.75	1.00
	1	-0.0003 ± 0.0004	0.81	-1.16	-0.14	0.58	-1.25	-0.43	0.96
NGA BA	PGA	0.0004 ± 0.0004	0.89	0.77	0.11	0.62	-0.24	-0.23	0.77
	0.2	0.0000 ± 0.0005	0.04	-0.02	-0.10	0.56	-1.18	-0.70	1.00
	1	0.0000 ± 0.0004	0.09	0.11	0.06	0.45	-0.56	-0.36	0.95
NGA CB	PGA	0.0000 ± 0.0004	0.06	-0.17	-0.15	0.71	-0.82	-0.40	0.99
	0.2	-0.0003 ± 0.0004	0.78	-0.57	-0.19	0.80	-1.41	-0.75	1.00
	1	0.0004 ± 0.0005	0.91	-0.24	-0.04	0.26	-0.91	-0.45	0.99
NGA CY	PGA	0.0000 ± 0.0004	0.06	-0.55	-0.34	0.97	-1.11	-0.54	1.00
	0.2	0.0003 ± 0.0004	0.80	-0.35	-0.40	0.99	-1.12	-0.75	1.00
	1	0.0003 ± 0.0004	0.76	-0.59	-0.23	0.91	-0.33	-0.38	0.93

Because of the well established practice of using linear site terms in European GMPEs, this study seeks to more deeply explore the nonlinearity of site effects implied by the Italian data. This analysis begins by re-evaluating residuals for recordings in the dataset relative to the NGA GMPEs with V_{s30} fixed at the reference value of 1100 m/s, basin depth $Z_{1,0}$ set to zero and $Z_{2,5}$ set to 0.52 km (per Eq. 5). Residuals evaluated in this manner are written as $\varepsilon_{i,j}^{1100}$ and are calculated as:

$$\left(\varepsilon_{i,j}^{1100}\right)_k = \ln\left(IM_{i,j}\right)_{data} - \left[\ln\left(IM_{i,j}^{1100}\right)_k + \eta_i\right] \quad (8.17)$$

where $\left(IM_{i,j}^{1100}\right)_k$ indicates the prediction of GMPE k for the reference rock conditions described above (using modified GMPEs where appropriate) and η_i is the event term evaluated from Eq. 7 for CY (which is replaced with η'_i for AS, BA, and CB, per Eq. 13-15). Those residuals are then grouped into two categories, one corresponding to recordings made on firm rock site conditions ($V_{s30} = 800$ to 1100 m/s) and the other to soft to medium soil conditions ($V_{s30} = 180$ to 300 m/s). Figure 8.16 shows those residuals plotted as a function of \widehat{PGA}_{1100} , which is the median peak acceleration from the respective GMPEs for the magnitude, distance, and other parameters associated with the recordings. We illustrate trends in the results with fit lines regressed according to the following equation for data in each category:

$$\varepsilon_{i,j}^{1100} = a_{PGA} + b_{PGA} \widehat{PGA}_{i,j}^{1100} + (\kappa_{PGA})_{i,j} \quad (8.18)$$

where a_{PGA} and b_{PGA} are the regression parameters and $(\kappa_{PGA})_{i,j}$ is the misfit of the line to the residual for recording j from event i. Those coefficients are given in Table 8.5.

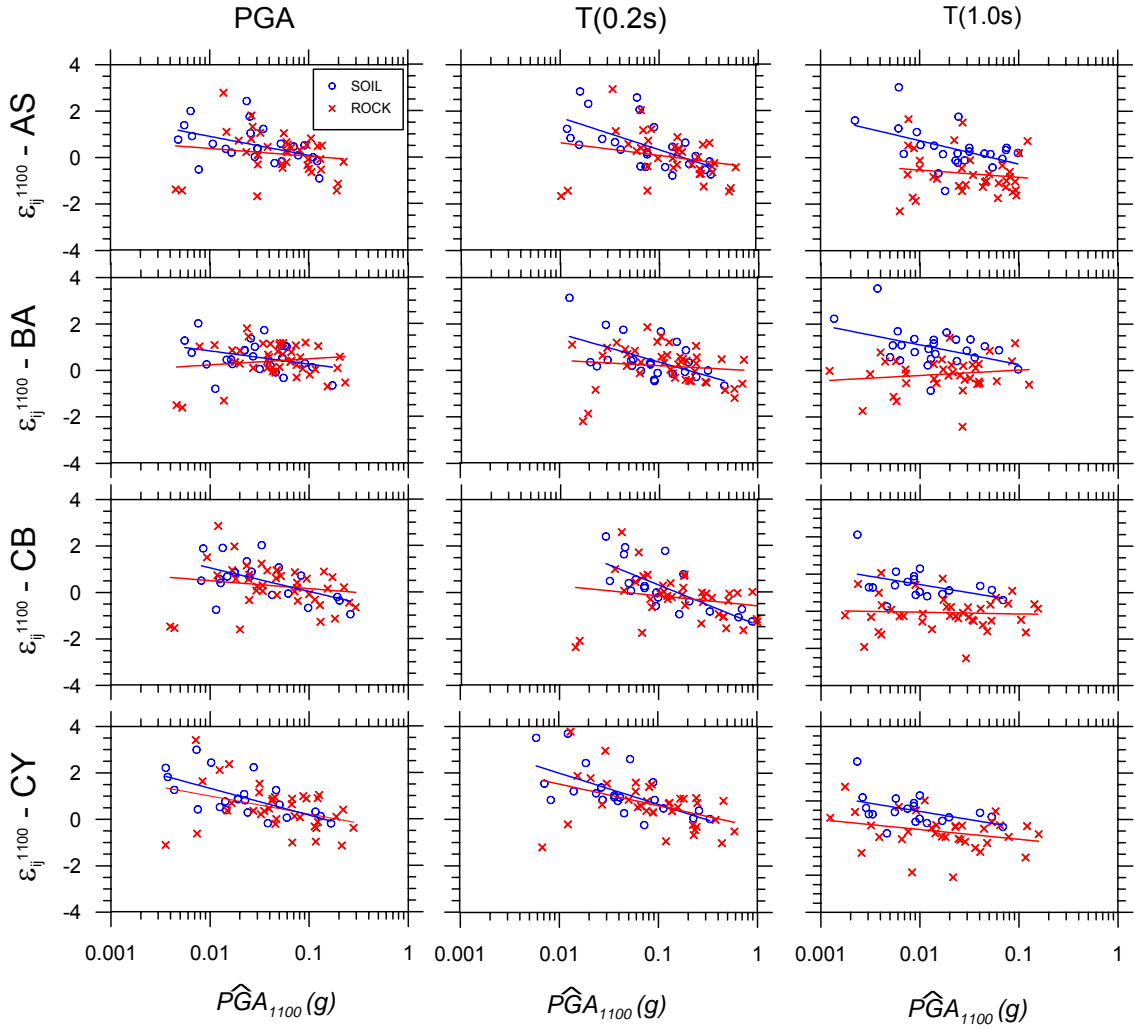


Figure 8.16. Variation of reference-site intra-event residuals (defined using Eq. 14) with median anticipated reference site peak acceleration, \widehat{PGA}_{1100} . Residuals shown are for original GMPE when shown without prime (ϵ_{ij}) and for modified GMPE when shown with prime (ϵ'_{ij}).

For each of the GMPEs considered, the results show (1) for low values of \widehat{PGA}_{1100} , larger residuals occur for the soil category than the rock category and (2) the slope of the $\epsilon'_{i,j} - \widehat{PGA}_{1100}$ relationship (b_{PGA}) is significantly negative, as established by hypothesis test results, for the soil category but is generally not significantly different from zero for the rock category (CY is an exception). These results demonstrate a nonlinear site effect for the IMs of PGA and Sa for $T \leq 1.0$ s. Moreover, the difference between the $\epsilon'_{i,j} - \widehat{PGA}_{1100}$ fit for soil and rock represents an implied site effect inherent to the Italian data relative to the $V_{s30}=1100$ m/s site condition adopted as a reference in Eq. 14. That implied site effect is compared to the V_{s30} -based site term in the AS, BA, CB, and CY GMPEs in figure 8.17. Although the absolute position of the site term varies somewhat relative the GMPE site term, the general slopes are generally similar. In the few cases where the slopes appear dis-similar (e.g., BA and CB at $T=1.0$ sec), the slopes of the implied site term is not significant, as indicated by the wide confidence intervals. This

suggests that the NGA site terms are providing approximately the correct level of nonlinearity for these Italian soil sites.

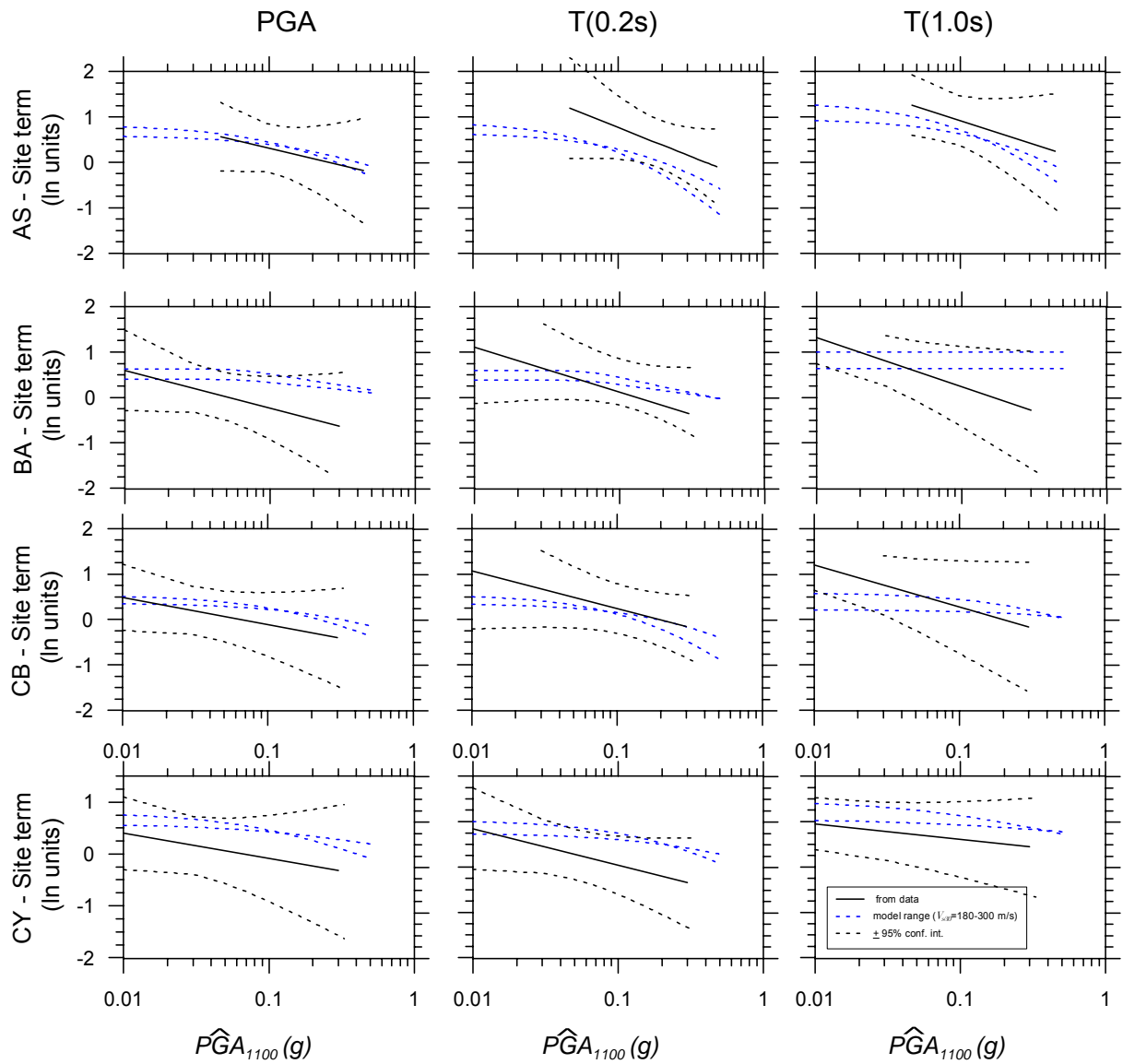


Figure 8.17. Comparison of range of GMPE site terms for $V_{s30}=180-300$ m/s sites to approximate site effect inferred from Italian data relative to $V_{s30}=1100$ m/s reference condition.

8.7 INTERPRETATION AND CONCLUSIONS

In this chapter, it is investigated the compatibility of strong motion data in Italy with Ground Motion Prediction Equations (GMPEs) established by the Next Generation Attenuation (NGA) project for shallow crustal earthquakes in active regions. Using a mixed effects procedure, event terms (inter-event

residuals) and intra-event residuals of the Italian data relative to the NGA GMPEs are evaluated. The event terms do not show a statistically significant trend with magnitude, indicating that the magnitude-scaling in the NGA GMPEs is compatible with the Italian data. Two recent European relations are also shown to be compatible with magnitude scaling implied by the Italian data, which is not surprising given that a large fraction of the European dataset was recorded in Italy.

Distance scaling is investigated by examining trends of intra-event residuals with distance. For three of four NGA relations (AS, BA, CB), the residuals demonstrate a statistically significant trend with distance for short periods ($T \leq 0.2\text{-}0.5$ s) that is suggestive of faster attenuation of Italian data. For the fourth NGA GMPE (CY) and the European GMPEs, the residuals do not demonstrate a trend with distance that we consider to be significant. Parameters in the NGA GMPEs that account for distance attenuation are adjusted through regression, which de-trends the residuals. The observed faster attenuation of Italian data relative to many of the NGA GMPEs is consistent with previous work that has shown faster distance attenuation of European data relative to California data (Douglas, 2004b). Moreover, as shown in figure 8.18, the finding of faster attenuation of Italian data is consistent with higher crustal damping as represented by lower frequency-dependent Q values from the Umbria/Apennines region of Italy (which contributes about 2/3 of the Italian recordings) relative to values for central and southern California (which contributes much of the NGA data).

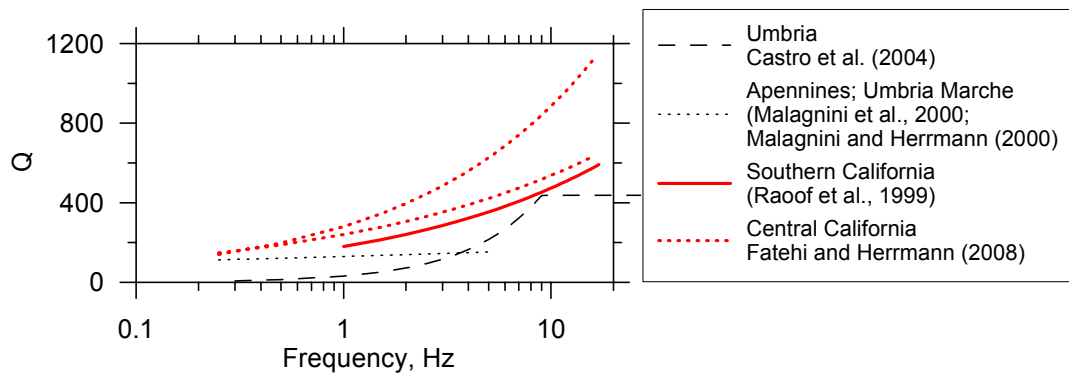


Figure 8.18. Comparison of relatively large Q values from California with smaller values from Apennines region of Italy, indicating higher crustal damping in the Italian region producing most of the recordings in the present database.

Scaling with respect to site condition is investigated by plotting intra-event residuals versus average shear wave velocity in the upper 30 m (V_{s30}). Those residuals are calculated relative to modified NGA GMPEs for those with modified distance parameters (AS, BA, CB). The results indicate no trend with V_{s30} , suggesting that the NGA site terms are compatible with Italian data. Since the NGA site terms are nonlinear, which is inconsistent with past European practice of using linear site terms, it is also specifically investigated whether the Italian data support of the use of a nonlinear site term. This is done by examining residuals of Italian data relative to the NGA GMPEs evaluated for a reference firm rock condition. A group of data on firm rock show no trend of residuals with \widehat{PGA}_{100} , which represents the median amplitude of shaking expected on firm rock. However, a group of data from soil sites show a statistically

significant trend with \widehat{PGA}_{100} . The differences between these trends for firm rock and soil imply a nonlinear site term having a slope relative to \widehat{PGA}_{100} that is generally consistent with the NGA site terms. Accordingly, conclusion is that nonlinear site response should be incorporated into site terms for GMPEs for Europe.

Whereas many aspects of the NGA GMPEs are compatible with the Italian data, the scatter of the Italian data significantly exceeds that implied by the NGA standard deviation models. In particular, event-to-event variability as expressed by the standard deviation of event terms (τ) exceeds values from NGA by amounts ranging from 0.4 to 0.7 in natural log units. Intra-event standard deviation (σ) is also larger in Italian data than NGA, but by amounts on the order of 0.2 to 0.4. The large τ terms it is interpreted to be a by-product of the poorly sampled dataset, whereas the larger σ terms is considered to be more reliable.

In summary, it is recommended that NGA GMPEs for median ground motions be utilized for hazard analysis in Italy. The CY median NGA relation can be used in its current form. The AS, BA, and CB NGA relations can also be used, but with modification of (generally) two parameters in the evaluation of median ground motions – one being a constant term and the second representing attenuation from geometric spreading and anelastic attenuation. The associated functional forms for distance attenuation are given in Table 8.2. With respect to standard deviation terms, it is suggested the use of the τ terms (representing inter-event variability) in the original NGA equations. It is recommended σ (representing intra-event variability) be taken as the sum of the NGA values and the $\Delta\sigma$ given values. For critical projects, perhaps both options should be considered in a logic tree framework to account for epistemic uncertainty (Bommer et al., 2005).

Finally, while this work has focused on Italy, it is believed that ground motions know nothing of political boundaries and that the results presented here are likely applicable elsewhere in Europe.

CHAPTER 9 SUMMARY AND CONCLUSIONS

This thesis focuses on the development of a strong motion database as well as site and source databanks for strong motion studies utilizing Italian data. The intent was to assemble and disseminate Italian data in a format that is similar to that used in the Next Generation Attenuation project, which applies to world-wide active tectonic regions (but which only sparsely sampled Italian data). The principal users of these data resources are expected to be researchers performing empirical ground motion studies and engineers selecting ground motions for dynamic analyses of structural and geotechnical systems in Italy.

The ground motion database developed here includes only about half of the available recordings due to various issues such as s-triggers that can bias ground motion intensity measures evaluated from the data. We document these biases, which affect principally longperiod measures of ground motion as well as duration-related parameters.

The database is composed of 247 Italian three-component corrected accelerograms from 101 recording sites and 89 earthquakes that occurred in the period 1972-2002. A source databank is compiled: appropriate source parameters (magnitude, hypocenter location, fault mechanism, etc.) associated with the seismic events were taken from the results of the recent projects from INGV while fault solutions were taken from DISS (Database of Individual Seismogenic Sources) website. Moment tensor solutions derived from instrumental recordings are available for most events, providing estimates of source location, seismic moment, and moment magnitude. For earthquakes with $M_w \geq 5.5$, finite source parameters include fault strike, dip, rake, along-strike rupture length, downdip width, and depth to top of rupture. Based on these data, all distances were re-calculated. The accelerometric data were processed by Dr. Walter Silva and colleagues, i.e. the same team of seismologists responsible for the PEER data processing. Time-histories of acceleration and pseudo-acceleration response spectra (5% structural damping) were then computed.

The magnitude of the events is always available as local magnitude M_L . Moment magnitudes M_W are available for 60% of the earthquakes from moment tensor solutions. Surface wave magnitudes are also available for 36% of the events.

Re-calculated epicentral and hypocentral distances are available for all recordings. Joyner and Boore distances (r_b), i.e. closest distance from the surface projection of the fault rupture, and closest distance from the rupture (r_n) have been re-calculated only when fault solutions are available corresponding to about 45% of the recordings. About 85% of the records have been obtained at distances of less than 50 km from the source while the remaining 15% data are essentially concentrated at distances between 50 and 100 km.

Fault rupture classification has been obtained for slightly less than 70% of the earthquakes in the databank. Records from normal rupture mechanism dominate, about 40 earthquakes belonging to this category; remaining events are related to strike-slip (7), oblique (4) and thrust (10) ruptures.

One of the major effort of the study concerns the improvement of site characterization of recording stations.

A databank of site conditions at Italian ground motion recording stations is compiled that includes geologic characteristics and seismic velocities at 101 sites with strong motion recordings. Geologic characterization is derived principally from local geologic investigations by ENEL that include detailed mapping and cross sections. For sites lacking such detailed study, geologic characterization is from 1:100,000 scale maps by Servizio Geologico d'Italia. Seismic velocities are extracted from the literature for 22 sites with on-site measurements and 14 additional sites with local measurements on similar geology. Data sources utilized include post earthquake site investigations (Friuli and Irpinia events), microzonation studies, and miscellaneous investigations performed by researchers or consulting engineers/geologists. Additional seismic velocities are measured using a spectral analysis of surface wave (SASW) technique for 17 sites that recorded the 1997-1998 Umbria-Marche earthquake sequence. The compiled velocity measurements provide data for 53 of the 104 sites. For the remaining sites, average seismic velocities in the upper 30 m (V_{s30}) was estimated using a hybrid approach as follows (1) for sites on Quaternary alluvium and Quaternary-Tertiary sediments, V_{s30} -values based on regional correlations for California are assigned, once validated against the available Italian data; and (2) for sites on Tertiary Limestone, conglomerate, and Mesozoic-age rocks, V_{s30} -values based on average velocities from similar units elsewhere in Italy are assumed.

Derived from this database is the national website SISMA (Site of Italian Strong Motion Accelerograms) which was designed to be a user-friendly system intended to provide freely downloadable strong motion data and metadata for engineering application. The design of SISMA allows searches to be conducted based on event parameters, station metrics, and record characteristics. Event parameters include location, magnitude, and fault mechanism. Site parameters include EC8 category and V_{s30} . More advanced searches can be performed using combinations of earthquake, station, and strong motion parameters (e.g., PGA, PGV, PGD, Ia, IH, etc.). An additional feature of SISMA is the capability of displaying interactive maps of epicenter locations of seismic events recorded by a selected station which makes use of the GoogleMap web service.

Based on the database available, the compatibility of strong motion data in Italy with Ground Motion Prediction Equations (GMPEs) established by the Next Generation Attenuation project for shallow crustal earthquakes in active regions was investigated. Using a mixed effects procedure, event terms (inter-event residuals) and intra-event residuals of the Italian data were evaluated. The event terms

do not show a statistically significant trend with magnitude, indicating that the magnitude-scaling in the NGA GMPEs is compatible with the Italian data. Two recent European relations are also shown to be compatible with magnitude scaling implied by the Italian data, which is not surprising given that a large fraction of the European dataset was recorded in Italy.

Distance scaling was investigated by examining trends of intra-event residuals with distance. For three of four relations (Abrahamson & Silva, Boore and Atkinson, Campbell and Bozorgnia), the residuals demonstrate a statistically significant trend with distance for short periods ($T \leq 0.2-0.5$ s) that is suggestive of faster attenuation of Italian data. For the fourth NGA GMPE (Chiou and Youngs) and the European GMPEs, the residuals do not demonstrate a significant trend with distance. Parameters in the GMPEs that account for geometric spreading are adjusted through regression, which de-trends the residuals. The observed faster attenuation of Italian data relative to many of the NGA GMPEs is consistent with previous work that has shown faster distance attenuation of European data relative to California data (Douglas, 2004b).

Scaling with respect to site condition is investigated by plotting intra-event residuals versus average shear wave velocity in the upper 30 m (V_{s30}). Those residuals are calculated relative to modified NGA GMPEs for those with modified distance parameters (Abrahamson & Silva, Boore and Atkinson, Campbell and Bozorgnia). The results indicate no trend with V_{s30} , suggesting that the NGA site terms are compatible with Italian data. Since the NGA site terms are nonlinear, which is inconsistent with past European practice of using linear site terms, we also specifically investigate whether the Italian data support of the use of a nonlinear site term. This is done by examining residuals of Italian data relative to the NGA GMPEs evaluated for a reference firm rock condition. A group of data on firm rock show no trend of residuals with PGA_{1100} , which represents the median amplitude of shaking expected on firm rock. However, a group of data from soil sites show a statistically significant trend with PGA_{1100} . The differences between these trends for firm rock and soil imply a nonlinear site term having a slope relative to PGA_{1100} that is generally consistent with the NGA site terms. Accordingly, it is concluded that nonlinear site response should be incorporated into site terms for GMPEs for Europe.

Whereas many aspects of the NGA GMPEs are compatible with the Italian data, the scatter of the Italian data significantly exceeds that implied by the NGA standard deviation models. In particular, event-to-event variability as expressed by the standard deviation of event terms exceeds values from NGA by amounts ranging from 0.4 to 0.7 in natural log units. Intra-event standard deviation is also larger in Italian data than NGA, but by amounts on the order of 0.2 to 0.4. These are substantial differences.

In summary, it is recommended that NGA GMPEs for median ground motions be utilized for hazard analysis in Italy. The Chiou and Youngs NGA relation can be used in its current form. The Abrahamson & Silva, Boore and Atkinson, Campbell and Bozorgnia NGA relations can also be used, but it is recommended modification of two parameters in the evaluation of median ground motions – one being a constant term and the second representing attenuation from geometric spreading. Standard deviation terms from the NGA models may require modification for use in Italy with the additive $\Delta\tau$ and

$\Delta\sigma$ terms, but it is not certain that the high standard deviations are not an artefact of the relatively poorly sampled dataset. Judgment should be exercised with respect to the use of NGA standard deviations terms versus the much larger values provided by the additive terms. Perhaps both options could be considered in a logic tree framework to account for epistemic uncertainty (Bommer et al., 2005).

Two main issues emerged from the current study that can be addressed through research:

1) a significant improvement and update of the site databank is needed to complete the catalogue of available geological/geotechnical information about recording stations and to increase the number of stations with a reliable site characterization and a quantitative description of the shear wave velocity profile. This can be accomplished by means of low-cost geophysical investigations such as SASW technique, such it has been carried out in the Umbria-Marche regions.

2) Finally, while this work has focused on Italy, it is believed that ground motions know nothing of political boundaries and that the results presented here are likely applicable elsewhere in Europe. We anticipate that future work will formally evaluate data from other regions in a manner similar to what is described here.

REFERENCES

- Abrahamson, N.A. and Sommerville, P.G. (1996). "Effects of hanging-wall and foot-wall on ground motions recorded during the Northridge earthquake. *Bull Seism Soc Am*, 86(1b), S93-S99.
- Abrahamson, N.A., and Shedlock, K.M. (1997). "Overview (of modern attenuation relationships)," *Seism. Res. Letters*, 68(1), 9-23.
- Abrahamson, N.A. and Silva, W.J. (2008). "Summary of the Abrahamson and Silva NGA ground motion relations," *Earthquake Spectra*, 24 (S1). accepted for publication.
- Abrahamson, N.A., Birkhauser, P., Koller, M., Mayer-Rosa, D., Smit, P.M., Sprecher, C., Tinic, S. and Graf, R. (2002). "PEGASOS- A comprehensive probabilistic seismic hazard assessment for nuclear power plants in Switzerland," *Proceedings of the Twelfth European Conference on Earthquake Engineering*, Paper no 633, London.
- A.G.I.: Associazione Geotecnica Italiana (1986). "Caratteristiche geotecniche dell'argilla del Fucino". *Rivista Italiana di Geotecnica*
- Aki, K. and Richards, P.G. (1980). *Quantitative seismology: Theory and methods*. Vol. 1, W.H. Freeman, San Francisco, CA.
- Akkar, S. and Bommer, J.J. (2007a). "Prediction of elastic displacement response spectra in Europe and the Middle East," *Earthq Eng Struct Dyn*, 36, 1275-1301.
- Akkar, S. and Bommer, J.J. (2007b). "Empirical prediction equations for peak ground velocity derived from strong motion records from Europe and the Middle East," *Bull Seism Soc Am*, 97(2), 511-530.
- Ambraseys, N.N., Simpson K.A. and Bommer J.J. (1996). "Prediction of horizontal response spectra in Europe." *Earthquake Engineering and Structural Dynamics*, 25(4), 371-400.
- Ambraseys, N.N., Douglas, J., Sigbjörnsson, R., Berge-Thierry, C., Suhadolc, P., Costa, G., and Smit, P.M. (2004). "Dissemination of European strong-motion data, Volume 2," *Proc. 13th World Conference on Earthquake Engineering*, Vancouver, B.C., Canada, Paper 32 (electronic file).
- Ambraseys, N.N., Douglas, J., Smit, P. and Sarma, S.K. (2005). "Equations for the estimation of strong ground motions from shallow crustal earthquakes using data from Europe and the Middle East: Horizontal peak ground acceleration and spectral acceleration," *Bull. Earthquake Eng.*, 3(1), 1-53.
- Araia, R. and Saragoni, G.R. (1980). "Capacity of the Strong Ground-Motion to cause structural damage." *Proceedings of the 7th WCEE*, Istanbul, pp. 483-490.
- Arias, A. (1970). "A measure of earthquake intensity". In R.J. Hansen, ed. *Seismic Design for Nuclear Power Plants*. MIT Press. Cambridge, Massachusetts, pp.438-483.
- Baldovini, G., Lavorato, A., Prati, G. (1993). "La galleria ferroviaria dei Peloritani: problemi di progetto." *AGI - XVIII Convegno Nazionale di Geotecnica*, Rimini 11-13 Maggio.
- Basili, R., Valensise, G., Vannoli, P., Burrato, P., Fracassi, U., Mariano, S., and Tiberti, M. M. (2007). "The database of individual seismogenic sources (DISS), version 3: summarizing 20 years of research on Italy's earthquake geology," *Tectonophysics*, in press.

- Bard P.-Y., Riepl-Thomas, J. (1999). "Wave propagation in complex geological structures and their effects on strong ground motion." In *Wave motion in Earthquake Engineering*, Kausel and Manolis eds., WIT Press, chapter 2: 37-95.
- Berardi, R., Longhi, G., Rinaldis, D. (1991). "Qualification of the European strong-motion databank: influence of the accelerometric station response and pre-processing techniques." *European Earthquake Engineering*, 2, 38-49.
- Berge-Thierry, C., Cotton, F., Scotti, O., Griot-Pommer, D.-A., & Fukushima, Y. (2003). "New empirical response spectral attenuation laws for moderate European earthquakes". *Journal of Earthquake Engineering*, 7(2), 193–222.
- Bolt, B.A. (1989). "The nature of earthquake ground motion, in F.Naeim, ed.". *The Seismic Design Handbook*. Van Nostrand Reinhold. New York.
- Bommer, J.J. (1991). "The design and engineering application of an earthquake strong-motion database". PhD thesis, Imperial College, University of London.
- Bommer, J.J. (2006). "Empirical estimation of ground motion: advances and issues," *Proc. 3rd Int. Sym. on the Effects of Surface Geology on Seismic Motion*, Grenoble, France, Paper No. KN8 (electronic file).
- Bommer, J.J. and Martinez-Pereira, A.. (1999). "The effective duration of earthquake strong motion." *Journal of Earthquake Engineering*. 3, 127-172.
- Bommer, J.J., Scherbaum, F., Bungum, H., Cotton, F., Sabetta, F., and Abrahamson, N.A. (2005) "On the use of logic trees for ground-motion prediction equations in seismic hazard analysis," *Bull. Seism. Soc. Am.*, 95(2), 377-389
- Boore, D.M. and Bommer, J.J. (2005). "Processing of strong motion accelerograms: needs, options, and consequences," *Soil Dynamics and Earthquake Engng.*, 25, 93-115.
- Boore, D.M. and Atkinson, G.M. (2008). "Ground motion prediction equations for the average horizontal component of PGA, PGV, and 5%-damped PSA at spectral periods between 0.01 and 10.0 s," *Earthquake Spectra*, 24 (S1). accepted for publication.
- Borcherdt, R.D. (1994). "Estimates of site-dependent response spectra for design (methodology and justification)," *Earthquake Spectra*, 10(4), 617-653.
- Borcherdt, R.D. 2002. Empirical evidence for site coefficients in building code provisions. *Earthquake Spectra*, 18(2): 189–217.
- Borcherdt, R. D. and Glassmoyer, G. (1994). "Influences of local geology on strong and weak ground motions recorded in the San Francisco Bay region and their implications for site-specific building-code provisions" *The Loma Prieta, California Earthquake of October 17, 1989--Strong Ground Motion*, U. S. Geological Survey Professional Paper 1551-A, A77-A108.
- Brambati, A., Faccioli E., Carulli G.B., Cucchi F., Onori R., Stefanini S., Ulcigrai F. (1979). "Studio di Microzonizzazione delle'area di Tarcento," Regione autonoma Friuli-Venezia Giulia – Università degli studi di Trieste.
- Budnitz, R.J., Apostolakis, G., Boore, D.M., Cluff, L.S., Coppersmith, K.J., Cornell, C.A. and Morris, P.A. (1997). Recommendations for probabilistic seismic hazard analysis: guidance on uncertainty and use of experts. Nuclear Regulatory Commission, NUREG/CR–6372.
- Bullen, K.E. (1965). *An introduction to the theory of seismology*, Cambridge Univ. Press, Cambridge, U.K.

- Consiglio Nazionale delle Ricerche, CNR (1981). "Microzonazione sismica dell'area Anconetana". CNR. Progetto Finalizzato Geodinamica, pubbl. n.ro 430.
- Campbell, K. W., and Bozorgnia, Y. (2007). "Campbell-Bozorgnia NGA ground motion relations for the geometric mean horizontal component of peak and spectral ground motion parameters," PEER Report No. 2007/02, Pacific Earthquake Engineering Research Center, University of California, Berkeley, 238 pp.
- Campbell, K.W. and Bozorgnia, Y. (2008). "NGA ground motion model for the geometric mean horizontal component of PGA, PGV, PGD, and 5%-damped linear elastic response spectra for periods ranging from 0.01 to 10 s," *Earthquake Spectra*, 24 (S1). accepted for publication.
- Castro, R.R., F. Pacor, D. Bindi, G. Franceschina, and L. Luzi (2004). "Site response of strong motion stations in the umbria, central Italy, region," *Bull. Seism. Soc. Am.*, 94 (2), 576–590.
- Chiou, B.S.-J. and Youngs, R.R. (2008). "Chiou and Youngs PEER-NGA empirical ground motion model for the average horizontal component of peak acceleration and pseudo-spectral acceleration for spectral periods of 0.01 to 10 seconds," *Earthquake Spectra*, 24 (S1). accepted for publication.
- Chiou, B.S.-J., Darragh, R., Gregor, D., and Silva, W.J. (2008). "NGA project strong-motion database," *Earthquake Spectra*, 24 (S1). accepted for publication.
- Chopra, A. K. (1995). "Dynamics of Structures—Theory and Application to Earthquake Engineering". Prentice Hall International, Inc.
- Coppersmith, K.J. and Youngs, R.R. (1986). "Capturing uncertainty in probabilistic seismic hazard assessments with intraplate tectonic environments" *Proceedings, 3rd U.S.National Conference on Earthquake Engineering*. Charleston, South Carolina, Vol.1, pp.301-312.
- Cornell, C.A. (1968). "Engineering seismic risk analysis". *Bull. Seism. Soc. Am.* 58, 1583–1606.
- Cotton, F., Scherbaum, F., Bommer, J.J., and Bungum, H. (2006). "Criteria for selecting and adjusting ground-motion models for specific target regions: Application to central Europe and rock sites," *Journal of Seismology*, 10, 137-156.
- Darragh, R., Silva, W.J., and Gregor, N. (2004). "Strong motion record processing for the PEER center," *Proceedings of Workshop on Strong Motion Record Processing*, Richmond, CA, May 26-27, 2004 (<http://www.cosmos-eq.org/recordProcessingPapers.html>).
- Decanini, L., Mollaioli, F., Oliveto, G. (2002) *Structural and seismological implications of the 1997 seismic sequence in Umbria and Marche, Italy. Innovative approach to Earthquake engineering*. WIT Press, 229-323.
- De Natale, G., Faccioli, E. and Zollo, A., 1988, Scaling of peakground-motions from digital recordings of small earthquakes at Campi Flegrei, Southern Italy, *Pure Appl. Geophys.* 126, 37–53.
- Dipartimento della Protezione Civile, DPC (2004) - Ufficio Servizio Sismico Nazionale - Servizio Sistemi di Monitoraggio, DPC-USSN (2004). "The Strong Motion Records of Molise Sequence (October 2002 - December 2003)" CD-ROM, Rome.
- Dobry, R., Borcherdt, R.D., Crouse, C.B., Idriss, I.M., Joyner, W.B., Martin, G.R., Power, M.S., Rinne, E.E., and Seed, R.B. (2000). "New site coefficients and site classification system used in recent building seismic code provisions," *Earthquake Spectra*, 16 (1), 41-67.

- Douglas, J. (2001a). "A critical reappraisal of some problems in engineering seismology". Thesis submitted to University of London for the degree of PhD and for the Diploma of the Imperial College of Department of Civile and Environmental Engineering- Imperial College of Science, Technology and Medicine, London.
- Douglas, J. (2001b). "A comprehensive worldwide summary of strong-motion attenuation relationships for peak ground acceleration and spectral ordinates (1969-2000)", Engineering Seismology and Earthquake Engineering, Report no. 01-1, January 2001.
- Douglas, J. (2003a). "Earthquake ground motion estimation using strong-motion records: a review of equations for the estimation of peak ground acceleration and response spectra ordinates," Earth Science Review, 61, 43-104.
- Douglas, J. (2003b). "What is a poor quality strong-motion record?" Bull. Earthquake Engineering, 1, 141-156.
- Douglas, J. (2004a). "An investigation of analysis of variance as a tool for exploring regional differences in strong ground motions," Journal of Seismology, 8, 485-496.
- Douglas, J. (2004b). "Use of analysis of variance for the investigation of regional dependence of strong ground motion," Proc. 13th World Conf. Eq. Engrg., Vancouver, Canada, Paper 29 (electronic file).
- Douglas, J. (2004c). "Ground motion estimation equations 1964-2003," Research Report No. 04-001-SM, Imperial College, London.
- Douglas, J. (2006). "Errata of and additions to 'Ground motion estimation equations 1964-2003'," Intermediary Report BRGM/RP-54603-FR, Bureau de recherches géologiques et minières.
- Ekström, G., Dziewonski, A.M., Maternovskaya, N.N., Nettles, M. (2005). "Global seismicity of 2003: centroid-moment tensor solutions for 1087 earthquakes." Physics of the Earth and Planetary Interiors, 148, 327-351.
- Faccioli, E. (1992). "Selected aspects of the characterization of seismic site effects, including some recent European contributions," Proc. International Symposium on The Effects of Surface Geology on Seismic Motion (ESG1992), Odaware, Japan, Vol. 1, 65-96.
- Faccioli, E. and Paolucci, R. (2005). "Elementi di sismologia applicati all'ingegneria." Pitagora Editrice Bologna.
- Fatehi, A. and R.B. Herrmann (2008). "High-frequency ground-motion scaling in the Pacific northwest and in northern and central California," Bull. Seism. Soc. Am., 98 (2), 709-721.
- Frenna, S.M. and Maugeri M. (1993). "Fenomeni di amplificazione sismica sulla piana di Catania durante il terremoto del 13\12\1990". Atti del VI convegno nazionale L'ingegneria sismica in Italia. 13-15 ott. 1993. Perugia, Italy.
- Fontanive, A., Gorelli, V., Zonetti, L. (1985). "Raccolta di informazioni sulle postazioni accelerometriche del Friuli," Commissione ENEA-ENEL per lo studio dei problemi sismici connessi con la realizzazione di impianti nucleari, Rome, Italy.
- Goulet, C.A., Watson-Lamprey, J., Baker, J., Luco, N., and Yang, T.Y. (2007). "Assessment of ground motion selection and modification (GMSM) methods for non-linear dynamic analyses of structures," in Geotechnical Earthquake Engineering and Soil Dynamics-IV, ASCE Geotechnical Special Publication No. xx, D. Zheng, M. Manzari, and D. Hiltunen (eds.), Paper No. xxx (submitted).

- Gutenberg, B. (1945). "Magnitude determination for deep-focus earthquakes". *Bull. Seism. Soc. Am.*, 35, 117-130.
- Gutenberg, B. and Richter, F.C. (1936). "On seismic waves (third paper)". *Gerlands Beitrage zur Geophysik*. Vol. 47, pp.73-131.
- Hanks, T.C. and Kanamori, H. (1979). "A moment magnitude scale". *Journal of Geophysical Research*. Vol.84, pp. 2348-2350.
- Hayashi, K. and Kayen, R. (2003). "Comparative test of three surface wave methods at Williams Street Park in San Jose, USA" . 2003 Joint Meeting of Japan Earth and Planetary Science , University of Tokyo, Tokyo, Japan. May 26-29, 2003. Paper S051-009.
- Hudson, D.E. (1979). "Reading and interpreting strong motion accelerograms." *Earthquake Engineering Research Institute, Berkeley*, 112 pp.
- Husid, R. (1969). "The effect of gravity on the collapse of yielding structures with earthquake excitation." *Proceedings of Fourth World Conference of Earthquake Engineering*, vol. II, pp. A-4 31-43.
- Housner, G.W. (1952). "Spectrum intensity of strong motion earthquakes." *Proceedings of Symposium on Earthquake and blast effects on structures*. pp. 20-36.
- ISMES (1991a). "Progetto Irpinia. Indagini Geotecniche in sito." *Prog. DTA 4929; DOC. RTF-DTA 1121*.
- ISMES (1991b). "Progetto Irpinia. Indagini Geofisiche." *Prog. DGF 4929; DOC. RTF-DGF 448*.
- ISMES (1991c). "Progetto Irpinia. Prove di Laboratorio." *Prog. DTA 4929; DOC. RTF-DTA 071*
- Istituto Nazionale di Geofisica e Vulcanologia, INGV (2007a). Project S6: Database of Italian accelerometric data from 1972 to 2004, web site url: <http://esse6.mi.ingv.it> , last accessed November 2007.
- Istituto Nazionale di Geofisica e Vulcanologia, INGV (2007b). Database of Individual Seismogenic Sources, web site url: <http://legacy.ingv.it/DISS>, last accessed November 2007.
- Idriss I.M. (1985). Evaluating seismic risk in engineering practice. *Proc. of the 11th Int. Conf. on Soil Mechanics and Foundations Eng. , san Francisco, Volume 1, 255-320*
- Idriss, I.M. (2008). "An NGA empirical model for estimating the horizontal spectral values generated by shallow crustal earthquakes," *Earthquake Spectra*, 24 (S1). accepted for publication.
- Incorporated Research Institutions for Seismology, IRIS (2007). IRIS Data Management Center, <http://www.iris.edu/about/DMC/>, last accessed November 2007.
- Isernia Administration (1998). "Indagini geognostiche prospezioni geofisiche e prove di laboratorio finalizzate all'adozione della variante generale del piano regolatore comunale".
- Joyner, W.B., Warrick, R.E., and Fumal, T.E. (1981). "The effect of Quaternary alluvium on strong ground motion in the Coyote Lake, California earthquake of 1979," *Bull. Seism. Soc. Am.*, 71, 1333-1349.
- Kanamori, H. (1977). "The energy release in great earthquakes". *Journal of Geophysical Research*. Vol.82, pp. 2981-1987.

- Kanamori, H. and Anderson, D.L. (1975). "Theoretical basis of some empirical relations in seismology" *Bull. Seism. Soc. Am.* 65 (5), 1073–1095.
- Kayen, R. (2005). "The spectral analysis of surface waves measured at William Street Park, San Jose, California, using swept-sine harmonic waves. In Asten and Boore, eds., *Blind comparisons of shear-wave velocities at closely-spaced sites in San Jose, California.*" US Geological Survey Open File Report 2005.
- Kayen, R., D. Minasian, R.E.S. Moss, B.D. Collins, N. Sitar, D. Dreger and C. Carver (2004a). "Geotechnical reconnaissance of the 2002 Denali Fault, Alaska," *Earthquake Spectra*, 20 (3), 639-667.
- Kayen, R., Seed, R. B., Moss, R.E., Cetin, O., Tanaka, Y., and Tokimatsu, K. (2004b) *Global Shear Wave Velocity Database for Probabilistic Assessment of the Initiation of Seismic-Soil Liquefaction. Proceedings of the 11th Int'l. Conf. On Soil Dynamics and Earthquake Engineering, January 7-9, 2004, Berkeley, CA, p. 506-512.*
- Kayen, R., Thompson, E., Minasian, D., Moss, R.E.S., Collins, B.D., Sitar, N., Dreger, D., Carver, G. (2004c) *Geotechnical Reconnaissance of the November 3, 2002 M7.9 Denali Fault Earthquake, Earthquake Spectra*, 20(3) p. 639-667.
- Kayen, R., Carkin, B., Minasian, D., and Tinsley, J. (2005a). "Shear wave velocity of the ground near southern California TRINET sites using the spectral analysis of surface waves method (SASW) and parallel-arrayed harmonic-wave sources". Open-File Report 2005-1169, U.S. Geological Survey, <http://pubs.usgs.gov/of/2005/1365/2005>.
- Kayen, R., Carkin, B., Minasian, D., and Tinsley, J. (2005b). "Shear Wave Velocity of the Ground Near Southern California TRINET Sites Using the Spectral Analysis of Surface Waves Method (SASW) and Parallel-Arrayed Harmonic-Wave Sources". Open-File Report 2005-1169, <http://pubs.usgs.gov/of/2005/1365/2005>
- Kayen R., Scasserra G., Stewart J.P., and Lanzo G. (2008) *Shear Wave Structure of Umbria and Marche, Italy, Strong Motion Seismometer Sites Affected by the 1997 Umbria-Marche, Italy, earthquake sequence* : U.S. Geological Survey, Open File Report 2008- 1010, 46 pg; [available on the World Wide Web at URL <http://pubs.usgs.gov/of/2008/1010/>].
- Kramer, S.L. (1996). "Geotechnical Earthquake Engineering". Prentice-Hall, Inc.
- Kulkarni, R.B., Youngs, R.R. and Coppersmith, K.J. (1984). "Assessment of confidence intervals for results of seismic hazard analysis". *Proceedings of 8th World Conference on Earthquake Engineering, San Francisco. Vol.1, pp. 263-270.*
- Lanzo, G. and Silvestri F. (1999). "Risposta sismica locale – Teoria ed esperienze". Hevelius edizioni.
- Malagnini, L. and R. B. Herrmann (2000). "Ground-motion scaling in the region of the 1997 Umbria–Marche earthquake (Italy)," *Bull. Seism. Soc. Am.* 90 (4), 1041–1051.
- Malagnini, L. and Montaldo, V. (2004) "Relazioni di attenuazione del moto del suolo App.3 al Rapporto Conclusivo", *Redazione della mappa di pericolosità sismica (Ordinanza PCM 20.03.03, n.3274)*, Istituto Nazionale di Geofisica e Vulcanologia.
- Malagnini, L., R. B. Herrmann, and M. Di Bona (2000). "Ground motion scaling in the Apennines (Italy)," *Bull. Seism. Soc. Am.* 90 (4), 1062–1081.
- Malagnini, L., Akinci, A., Herrmann, R.B., Pino, N.A. and Scognamiglio, L., (2002). "Characteristics of the ground-motion in Northeastern Italy". *Bull. Seism. Soc. Am.* 92, 2186–2204.

- Marsan, P. (1998). "Moto sismico, parametri di interesse ingegneristico, reti sismiche ed accelerometriche." *Problemi di ingegneria geotecnica nelle aree sismiche*, CISM, Udine 27-29 ottobre.
- McGuire, R.K. (1976). "FORTRAN computer program for seismic risk analysis". US Geological Survey, Open-File Report 76-0067, 68 pp.
- Montaldo, V., Faccioli, E., Zonno, G., Akinci, A. and Malagnini, L. (2005). "Treatment of round-motion predictive relationships for the reference seismic hazard map Italy". *Journal of Seismology* (2005)9: 295-216
- Morasca, P., Malagnini, L., Akinci, A. and Spallarossa, D., 2002, Ground-motion scaling in the Western Alps, *Seism. Res. Lett.* 73, 251.
- Nazarian, S. and Stokoe, K. (1984). "In situ shear wave velocities from spectral analysis of surface waves, Proc. Eighth World Conference on Earthquake Engineering, San Francisco, California, Vol. III, pp. 31-39.
- Norme Tecniche per le Costruzioni, DM 14 gennaio 2008, Gazzetta Ufficiale della Repubblica Italiana del 04/02/2008, n. 29, Suppl. Ordinario n. 30 (<http://www.infrastrutture.gov.it/consuplp>)
- Oglesby, D. D., Archuleta, R. J., and Nielsen, S. B. (1996). "Earthquakes on dipping faults: The effects of broken symmetry". *Science*, 280, 1055-1059.
- Ordinanza del Presidente del Consiglio dei Ministri, OPCM "Primi elementi in materia di criteri generali per la classificazione sismica del territorio nazionale e di normative tecniche per le costruzioni in zona sismica." 20 marzo 2003, Ordinance No. 3274.
- Paciello, A., Properzi, C., Rindaldis, D., Stedile, L. (1997). "Database delle registrazioni accelerometriche". ENEA Dipartimento Ambiente-Servizio Sismico Nazionale.
- Palazzo, S. (1991a). "Progetto Irpinia - Elaborazione dei risultati delle indagini geotecniche in sito ed in laboratorio eseguite nelle postazioni accelerometriche di Bagnoli Irpino, Calitri, Auletta, Bisaccia, Bovino, Brienza, Rionero in Vulture, Sturmo, Benevento e Mercato S. Severino," Ente Nazionale Energia Elettrica (ENEL), Direzione delle Costruzioni, Rome, Italy.
- Palazzo, S. (1991b). "Progetto Irpinia - Elaborazione dei risultati delle indagini geotecniche in sito ed in laboratorio eseguite nelle postazioni accelerometriche di Sannicandro, Tricarico, Vieste, Areinzo, S. Severo e Garigliano," Ente Nazionale Energia Elettrica (ENEL), Direzione delle Costruzioni, Rome, Italy.
- Pitilakis, K. (2004). "Chapter 5: Site Effects. In: Recent advances in Earthquake Geotechnical Engineering and Microzonation." Atilla Ansal ed., Kluwer Academic Publishers, pp. 139-198.
- Pondrelli, S., Morelli, A., Ekström, G., Mazza, S., Boschi, E., Dziewonski, A.M. (2002). "European-Mediterranean regional centroid-moment tensors: 1997-2000," *Physics of the Earth and Planetary Interiors*, 130, 71-101.
- Pondrelli, S., Salimbeni, S., Ekström, G., Morelli, A., Gasperini, P., and Vannucci, G. (2006). "The Italian CMT dataset from 1977 to the present," *Physics of the Earth and Planetary Interiors*, 159, 286-303.
- Power, M.S., Coppersmith, K.J., Youngs, R.R., Schwartz, D.P. and Swan, R.H. (1981). "Seismic exposure analyses for the WNP-2 and WNP-1/4 site: Appendix 2.5K to Amendment no.18 Final safety analysis report for WNP-2. Woodward-Clyde consultants, San Francisco. 63 pp.

- Power, M., Chiou, B., Abrahamson, N., Bozorgnia, Y., Shantz, T., and Roblee, C., (2008). "An Overview of the NGA Project." Earthquake Spectra Special Issue on the Next Generation of Ground Motion Attenuation (NGA) Project. Earthquake Engineering Research Institute, March.
- Raof, M., R. B. Herrmann, and L. Malagnini (1999). "Attenuation and excitation of three-component ground motion in Southern California," *Bull. Seism. Soc. Am.* 89 (4), 888–902.
- Richter, F.C. (1935). "An instrumental earthquake scale". *Bull. Seism. Soc. Am.* Vol.25, pp.1-32.
- Riepl, J. (1997). "Effets de site: evaluation experimentale et modelisations multidimensionelle. Application au site-test EUROSEISTEST (Grece)." These de Doctorat de l'Université Joseph Fourier, Grenoble, 1, pp.227.
- Rinaldis, D. (2004). "Acquisition and processing of analogue and digital accelerometric records: ENEA methodology and experience from Italian earthquake". Proc. Workshop on strong-motion record processing. Consortium of Organizations of Strong-Motion Observation Systems (COSMOS), Richmond, CA.
- Sabetta, F. and Pugliese, A. (1987). "Attenuation of peak horizontal attenuation and velocity from Italian strong motion records" *Bull. Seism. Soc. Am.*, 77(5), 1491-1513.
- Sabetta, F. and Pugliese, A. (1996). "Estimation of response spectra and simulation of nonstationary earthquake ground motion," *Bull. Seism. Soc. Am.*, 86(2), 337-352.
- Saragoni, G.R. (1990). "Response Spectra and Earthquake destructiveness." Proceedings of the 4th U.S.National Conference on earthquake Engineering. Palm Springs, California, (2) 35-43.
- Scasserra, G., Stewart, J.P., Kayen, R.E., and Lanzo, G. (2008: in review). "Database for earthquake strong motion studies in Italy," *Journal of Earthquake Engineering*, Imperial College Press.
- Scherbaum, F., Cotton, F., and Smit, P. (2004). "On the use of response spectral reference data for the selection and ranking of ground motion models for seismic hazard analysis in regions of moderate seismicity: the case of rock motion," *Bull. Seism. Soc. Am.*, 94 (6), 2164-2185.
- Shin, T. C., K. W. Kuo, W. H. K. Lee, T. L. Teng, and Y. B. Tsai (2000). "A preliminary report on the 1999 Chi-Chi (Taiwan) earthquake". *Seism. Res. Lett.* 71, 24–30.
- Spudich, P., Fletcher, J. B., Hellweg, M., Boatwright, J., Sullivan, C., Joyner, W. B., Hanks, T. C., Boore, D. M., McGarr, A., Baker, L. M., & Lindh, A. G. (1997). "SEA96 — A new predictive relation for earthquake ground motions in extensional tectonic regimes". *Seismological Research Letters*, 68(1), 190–198.
- Spudich, P., Joyner, W. B., Lindh, A. G., Boore, D. M., Margaris, B. M., & Fletcher, J. B. (1999). "SEA99: A revised ground motion prediction relation for use in extensional tectonic regimes". *Bulletin of the Seismological Society of America*, 89(5), 1156–1170.
- SSN-Monitoring System Group (2002) - The Strong Motion Records of Umbria-Marche Sequence, (September 1997 - June 1998). CD-ROM, 2002
- Stafford, P.J., Strasser, F.O., and Bommer, J.J. (2008: in press). "An evaluation of the applicability of the NGA models to ground motion prediction in the Euro-Mediterranean region," *Bulletin of Earthquake Engineering*, 6.
- Stewart, J.P. (2000). "Variations between foundation-level and free-field earthquake ground motions," *Earthquake Spectra*, 16 (2), 511-532.

- Stewart, J.P., Chiou, S.J., Bray J.D., Sommerville, P.G., Graves, R.W. and Abrahamson, N.A. (2001). "Ground Motion Evaluation Procedures for Performance-Based Design". Pacific Earthquake Engineering Research Center-Report. September 2001.
- Stokoe, K. and Nazarian, S. (1985) Use of Raleigh Waves in liquefaction Studies, in, R.D. Woods, ed., Measurement and use of Shear Wave Velocity for Evaluating Dynamic Soil Properties. ASCE, N.Y., 1-17.
- Tento, A., Franceschina, L., Marcellini, A. (1992). "Expected round motion evaluation for Italian sites." Proceedings of Tenth World Conference on Earthquake Engineering, vol.1, 489-494.
- Trifunac, M.D. and Todorovska M.I. (2001). "Evolution of accelerographs, data processing, strong motion arrays and amplitude and spatial resolution in recording strong earthquake motion." Soil Dynamic and Earthquake Engineerine., 21, 537-555.
- Trobiner, S. et al. (1997) Reconnaissance Report on the Umbria-Marche, Italy, Earthquakes of 1997, EERI Special Earthquake Report – December 1997, 12 p.
- Wells, D. L., and Coppersmith, K. J. (1994). "New empirical relationships among magnitude, rupture length, rupture width, rupture area, and surface displacement," Bull. Seism. Soc. Am., 84, 974-1002.
- Wills, C.J. and Clahan, K.B. (2006). "Developing a map of geologically defined site-condition categories for California," Bull. Seism. Soc. Am., 96(4a), 1483-1501.
- Working Group CPTI (2004). "Catalogo Parametrico dei Terremoti Italiani, versione 2004 (CPTI04)" Istituto Nazionale di Geofisica e Vulcanologia (INGV), Bologna.
- Working Group (2004). "Redazione della mappa di pericolosità sismica (Ordinanza PCM 20.03.03, n.3274) All.to 1 Rapporto Conclusivo" Istituto Nazionale di Geofisica e Vulcanologia.
- Working Group S6 (2007). Data base of the Italian strong-motion data (1972-2004), <http://itaca.mi.ingv.it>

APPENDIX A

Results of the SASW testing in Umbria and Marche regions

UMBRIA-MARCHE, ITALY SMR Stations

Site ID 254BEV
NEHRP CLASS: D
Vs30 182 (m/s)
SUB-CLASS D-
Vs100 278 (m/s)
Location

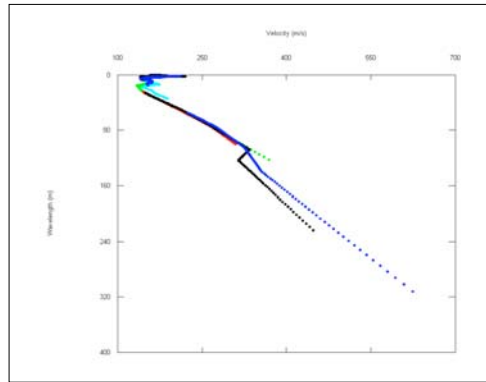
SMR Station SMI
State UMBRIA
Description
POSITION BEVAGNA
LAT (N) 42.9324
LON (E) 12.6111

Data Type SWEPT-SINE SASW
Investigators KAYEN, SCASSERRA
Date collected 11-Nov-2006

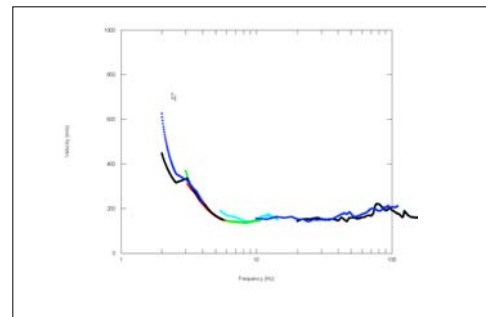
TEST METHODS PARALLEL-ARRAY SOURCES;
 CONTINUOUS HARMONIC
 WAVE-SASW; 3D AMBIENT
 MICROTREMOR ANALYSIS

PROJECT NAME UMBRIA-MARCHE
 SMR CHARACTERIZATION
SPONSOR PEER, UNIV OF ROME

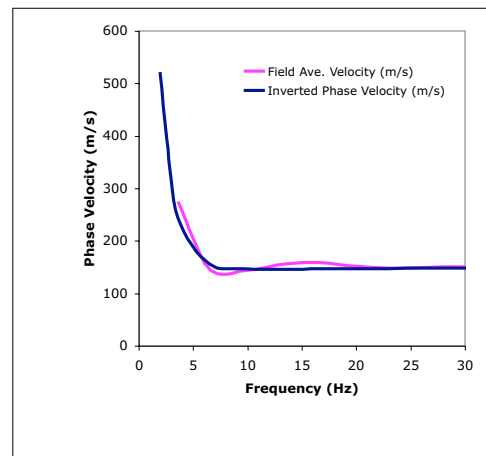
SITE SUB CLASS: Vs30 (m/s)
 A >1500 m/s
 B+ 1080 < Vs30 ≤ 1500 m/s
 B- 720 < Vs30 ≤ 1080 m/s
 C+ 540 < Vs30 ≤ 720 m/s
 C- 360 < Vs30 ≤ 540 m/s
 D+ 270 < Vs30 ≤ 360 m/s
 D- 180 < Vs30 ≤ 270 m/s
 E <180 m/s
 F Special Soil Conditions: Liquefiable soils; quick and high sensitivity clays; collapsible cemented soils; peats>3m; high (>75) PI soils thicker than 8m; soft/medium stiff clays thicker than 36m.



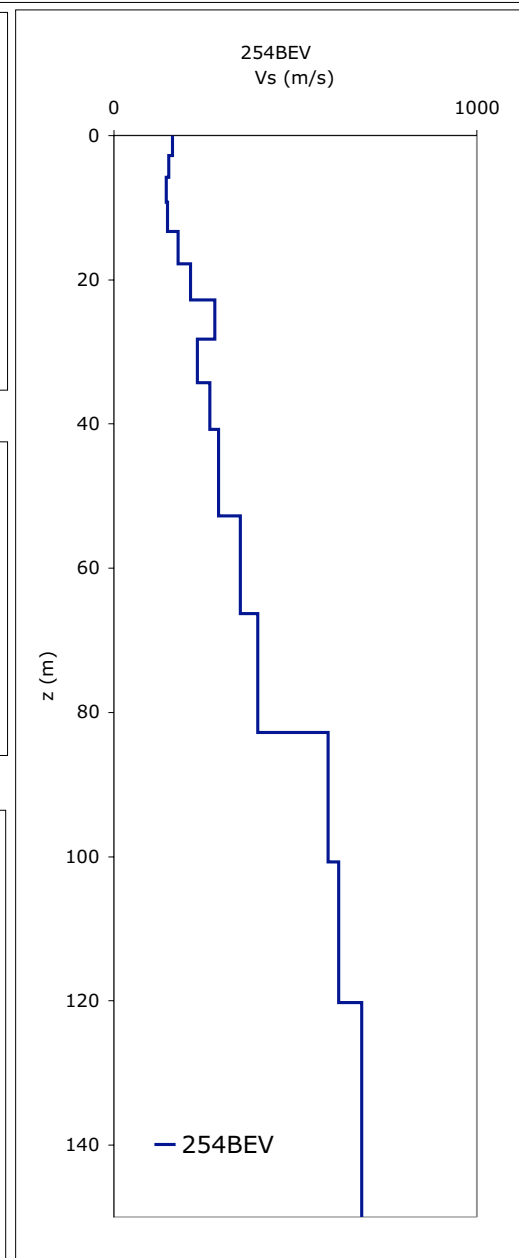
(A) Merged Field-LAMBDA Dispersion Curves



(B) Merged Field-Frequency Dispersion Curves



(C) Inversion-theoretical dispersion curve versus averaged field dispersion curve,



(D) Shear Wave Velocity SASW

254BEV	DISPERSION DATA			INVERSION PROFILE	
Site Disp. Vr (m/s)	Theoretical Disp. Vr (m/s)	Frequency (Hz)		Inversion Vs (m/s)	Depth (m)
				160.8	0.0
540.0	522.9	1.9		160.8	2.8
375.0	393.4	2.5		151.6	2.8
275.9	244.3	3.6		151.6	5.8
148.5	157.1	6.4		144.2	5.8
144.7	148.5	9.7		144.2	9.3
157.5	147.5	13.6		147.9	9.3
159.8	147.7	16.5		147.9	13.3
152.5	148.2	19.9		175.8	13.3
149.0	148.5	23.0		175.8	17.8
150.7	148.8	26.3		210.7	17.8
151.7	148.9	29.5		210.7	22.8
149.4	148.9	32.6		277.3	22.8
152.1	148.6	35.8		277.3	28.3
153.8	148.4	38.8		230.2	28.3
155.7	148.0	42.4		230.2	34.3
145.8	147.8	45.5		264.8	34.3
155.3	147.5	48.7		264.8	40.8
160.2	147.3	52.3		288.6	40.8
158.6	147.2	54.9		288.6	52.8
157.3	147.0	58.5		347.6	52.8
				347.6	66.3
				396.4	66.3
				396.4	82.8
				589.2	82.8
				589.2	100.8
				619.4	100.8
				619.4	120.3
				683.5	120.3
				683.5	150.3
				683.5	150.3
				Vs30	181.8

UMBRIA-MARCHE, ITALY SMR Stations

Site ID 255 SMI
NEHRP CLASS: C
Vs30 395 (m/s)
SUB-CLASS C-
Vs100 527 (m/s)
Location

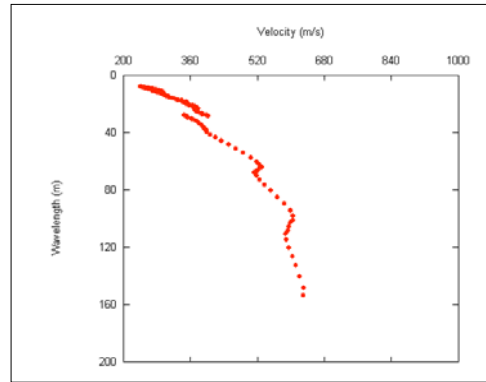
SMR Station SMI
State UMBRIA
Description CHURCH ST MARIA
POSITION FOLIGNO
LAT (N) 42.95417
LON (E) 12.69892

Data Type SWEPT-SINE SASW
Investigators KAYEN, SCASSERRA
Date collected 12-Nov-2006

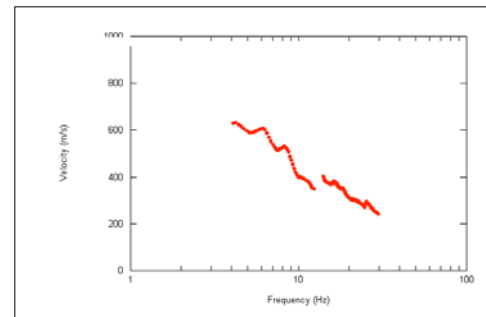
TEST METHODS PARALLEL-ARRAY SOURCES;
 CONTINUOUS HARMONIC
 WAVE-SASW; 3D AMBIENT
 MICROTREMOR ANALYSIS

PROJECT NAME UMBRIA-MARCHE
 SMR CHARACTERIZATION
SPONSOR PEER, UNIV OF ROME

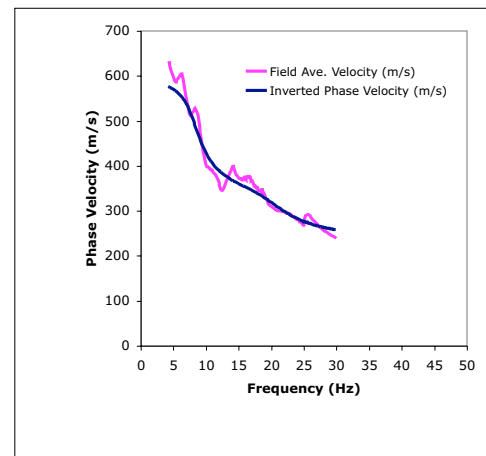
SITE SUB CLASS: Vs30 (m/s)
 A >1500 m/s
 B+ 1080 < Vs30 ≤ 1500 m/s
 B- 720 < Vs30 ≤ 1080 m/s
 C+ 540 < Vs30 ≤ 720 m/s
 C- 360 < Vs30 ≤ 540 m/s
 D+ 270 < Vs30 ≤ 360 m/s
 D- 180 < Vs30 ≤ 270 m/s
 E <180 m/s
 F Special Soil Conditions: Liquefiable soils; quick and high sensitivity clays; collapsible cemented soils; peats>3m; high (>75) PI soils thicker than 8m; soft/medium stiff clays thicker than 36m.



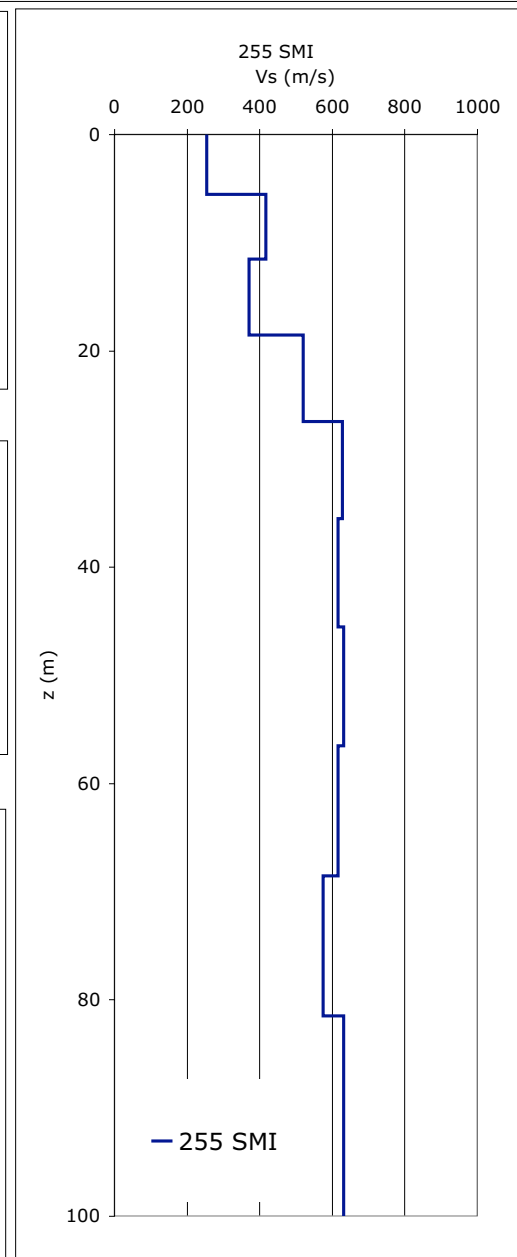
(A) Merged Field-LAMBDA Dispersion Curves



(B) Merged Field-Frequency Dispersion Curves



(C) Inversion-theoretical dispersion curve versus averaged field dispersion curve,



(D) Shear Wave Velocity SASW

255 SMI	DISPERSION DATA			INVERSION PROFILE	
Site Disp. Vr (m/s)	Theoretical Disp. Vr (m/s)	Frequency (Hz)		Inversion Vs (m/s)	Depth (m)
				254.3	0.0
629.4	578.0	4.1		254.3	5.5
631.3	576.8	4.3		416.8	5.5
621.5	575.4	4.4		416.8	11.5
611.7	573.9	4.6		370.0	11.5
604.0	572.4	4.8		370.0	18.5
596.1	570.8	4.9		519.8	18.5
589.6	569.1	5.1		519.8	26.5
587.9	567.2	5.3		628.1	26.5
593.5	565.3	5.5		628.1	35.5
596.2	563.1	5.6		615.1	35.5
600.2	560.7	5.8		615.1	45.5
605.2	558.1	6.0		631.3	45.5
605.8	555.3	6.2		631.3	56.5
600.2	552.0	6.3		615.2	56.5
585.0	548.5	6.5		615.2	68.5
567.8	544.6	6.7		575.4	68.5
552.0	540.1	6.9		575.4	81.5
537.7	535.1	7.0		631.3	81.5
526.0	529.9	7.2		631.3	100.0
518.0	524.1	7.4			
513.4	518.0	7.6			
518.7	511.7	7.7			
521.6	504.9	7.9			
525.3	497.6	8.1			
530.3	490.1	8.2			
524.7	483.1	8.4			
519.2	475.9	8.6			
504.9	468.9	8.8			
486.1	462.2	8.9			
469.2	455.9	9.1			
451.7	449.6	9.3			
434.4	443.7	9.5			
				Vs30	395.2

UMBRIA-MARCHE, ITALY SMR Stations

Site ID 256CSA
NEHRP CLASS: D
Vs30 293 (m/s)
SUB-CLASS D+
Vs100 440 (m/s)
Location

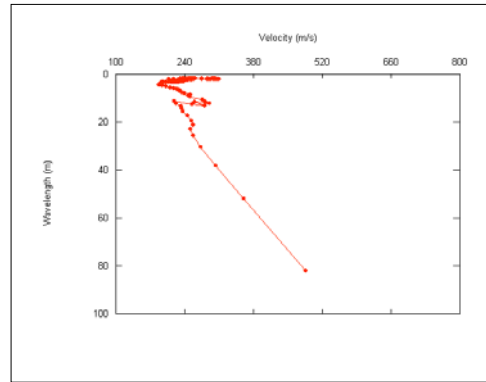
SMR Station CSAD
State UMBRIA
Description CASTEL NUOVO ASSISI
POSITION ASSISI
LAT (N) 43.0081
LON (E) 12.5905

Data Type SWEPT-SINE SASW
Investigators KAYEN, SCASSERRA
Date collected 12-Nov-2006

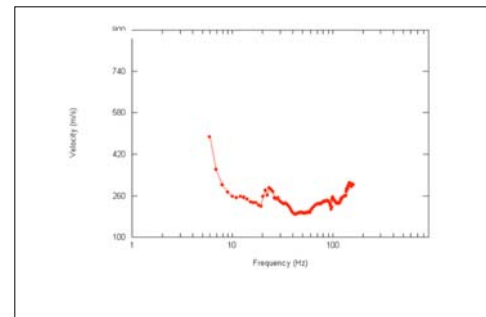
TEST METHODS PARALLEL-ARRAY SOURCES;
 CONTINUOUS HARMONIC
 WAVE-SASW; 3D AMBIENT
 MICROTREMOR ANALYSIS

PROJECT NAME UMBRIA-MARCHE
 SMR CHARACTERIZATION
SPONSOR PEER, UNIV OF ROME

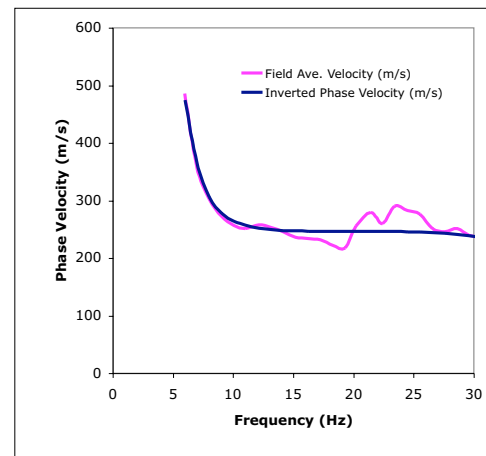
SITE SUB CLASS: Vs30 (m/s)
 A >1500 m/s
 B+ 1080 < Vs30 ≤ 1500 m/s
 B- 720 < Vs30 ≤ 1080 m/s
 C+ 540 < Vs30 ≤ 720 m/s
 C- 360 < Vs30 ≤ 540 m/s
 D+ 270 < Vs30 ≤ 360 m/s
 D- 180 < Vs30 ≤ 270 m/s
 E <180 m/s
 F Special Soil Conditions: Liquefiable soils; quick and high sensitivity clays; collapsible cemented soils; peats>3m; high (>75) PI soils thicker than 8m; soft/medium stiff clays thicker than 36m.



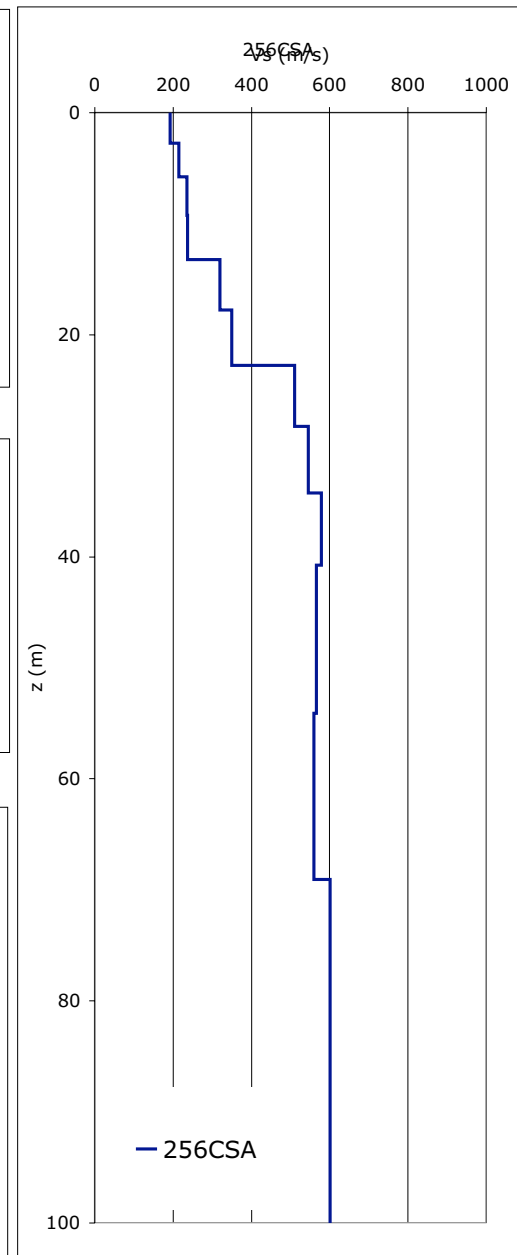
(A) Merged Field-LAMBDA Dispersion Curves



(B) Merged Field-Frequency Dispersion Curves



(C) Inversion-theoretical dispersion curve versus averaged field dispersion curve,



(D) Shear Wave Velocity SASW

256CSA	DISPERSION DATA			INVERSION PROFILE	
Site Disp. Vr (m/s)	Theoretical Disp. Vr (m/s)	Frequency (Hz)		Inversion Vs (m/s)	Depth (m)
				192.7	0.0
486.1	475.3	5.9		192.7	2.8
360.5	367.6	6.9		215.4	2.8
303.5	306.9	8.0		215.4	5.8
273.0	279.2	9.0		236.1	5.8
257.8	265.3	10.0		236.1	9.3
252.1	258.2	10.9		236.6	9.3
257.8	253.1	12.1		236.6	13.3
253.7	250.5	13.1		319.3	13.3
246.1	249.0	14.1		319.3	17.8
246.1	248.1	15.2		349.3	17.8
246.1	247.7	16.2		349.3	22.8
246.1	247.5	17.2		510.1	22.8
246.1	247.5	18.3		510.1	28.3
232.7	247.5	19.3		545.3	28.3
255.7	247.5	20.2		545.3	34.3
251.4	247.5	21.4		578.2	34.3
251.4	247.5	22.4		578.2	40.8
251.4	247.3	23.4		565.8	40.8
251.4	246.9	24.4		565.8	54.1
251.4	246.2	25.5		559.2	54.1
251.4	245.3	26.6		559.2	69.1
246.9	243.9	27.6		600.2	69.1
252.1	242.1	28.6		600.2	100.0
240.1	239.6	29.6			
235.4	236.5	30.6			
231.1	232.9	31.6			
229.5	228.9	32.6			
231.8	224.7	33.7			
228.4	220.6	34.8			
224.0	217.0	35.8			
218.1	213.7	36.8			
211.3	210.5	37.8			
				Vs30	293.2

UMBRIA-MARCHE, ITALY SMR Stations

Site ID 257CLF
NEHRP CLASS: D
Vs30 317 (m/s)
SUB-CLASS D+
Vs100 719 (m/s)
Location

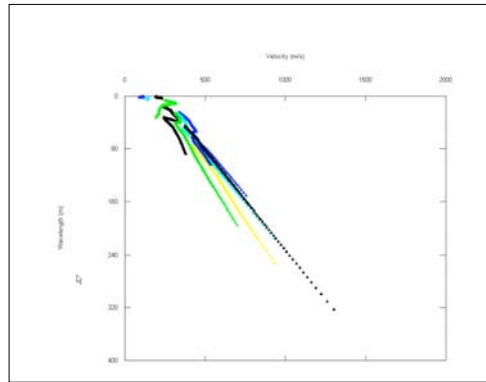
SMR Station CLF
State UMBRIA
Description COLFIORITO-NR.MARCHE BRDR
POSITION COLFIORITO
LAT (N) 43.03737
LON (E) 12.92118

Data Type SWEPT-SINE SASW
Investigators KAYEN, SCASSERRA
Date collected 11/13/200

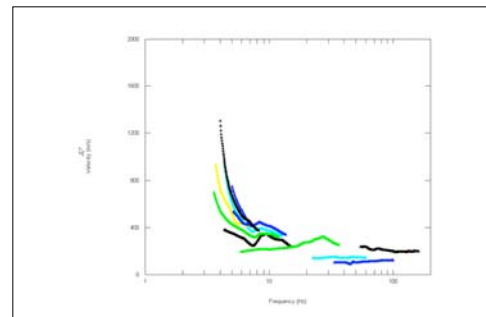
TEST METHODS PARALLEL-ARRAY SOURCES;
 CONTINUOUS HARMONIC
 WAVE-SASW; 3D AMBIENT
 MICROTREMOR ANALYSIS

PROJECT NAME UMBRIA-MARCHE
 SMR CHARACTERIZATION
SPONSOR PEER, UNIV OF ROME

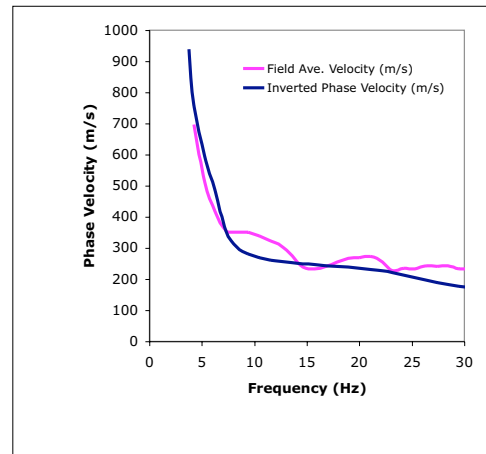
SITE SUB CLASS: Vs30 (m/s)
 A >1500 m/s
 B+ 1080 < Vs30 ≤ 1500 m/s
 B- 720 < Vs30 ≤ 1080 m/s
 C+ 540 < Vs30 ≤ 720 m/s
 C- 360 < Vs30 ≤ 540 m/s
 D+ 270 < Vs30 ≤ 360 m/s
 D- 180 < Vs30 ≤ 270 m/s
 E <180 m/s
 F **Special Soil Conditions:** Liquefiable soils; quick and high sensitivity clays; collapsible cemented soils; peats>3m; high (>75) PI soils thicker than 8m; soft/medium stiff clays thicker than 36m.



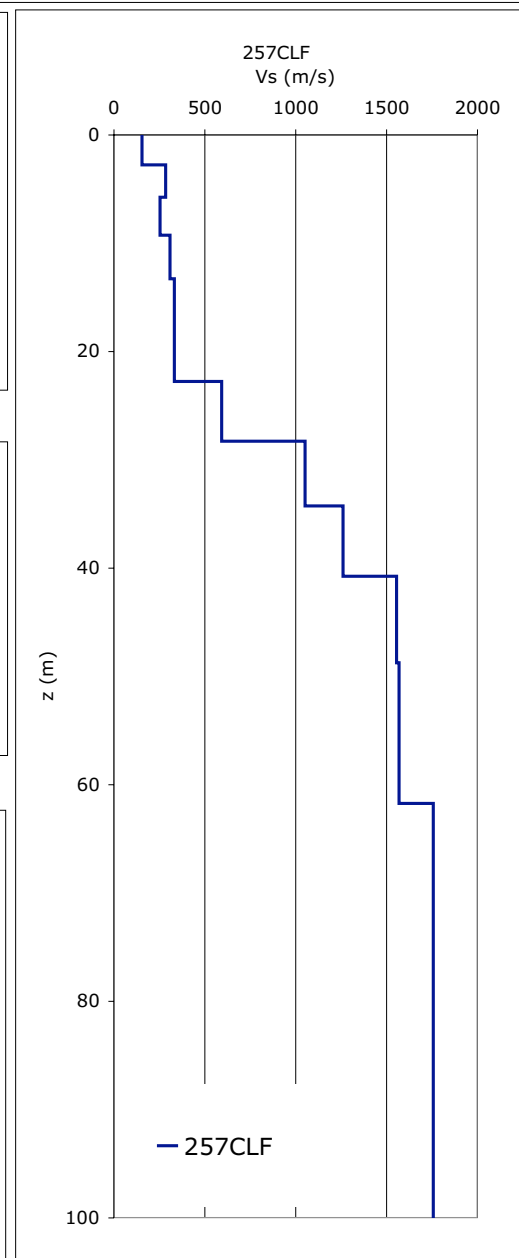
(A) Merged Field-LAMBDA Dispersion Curves



(B) Merged Field-Frequency Dispersion Curves



(C) Inversion-theoretical dispersion curve versus averaged field dispersion curve,



(D) Shear Wave Velocity SASW

UMBRIA-MARCHE, ITALY SMR Stations

Site ID 257CLF
NEHRP CLASS: D
Vs30 317 (m/s)
SUB-CLASS D+
Vs100 719 (m/s)
Location

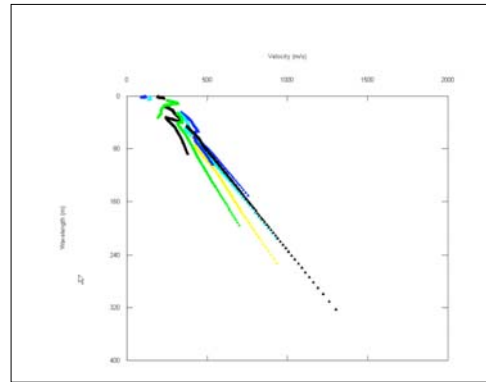
SMR Station CLF
State UMBRIA
Description COLFIORITO-NR.MARCHE BRDR
POSITION COLFIORITO
LAT (N) 43.03737
LON (E) 12.92118

Data Type SWEPT-SINE SASW
Investigators KAYEN, SCASSERRA
Date collected 11/13/200

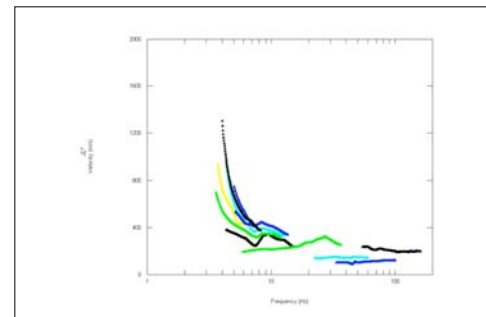
TEST METHODS PARALLEL-ARRAY SOURCES;
 CONTINUOUS HARMONIC
 WAVE-SASW; 3D AMBIENT
 MICROTREMOR ANALYSIS

PROJECT NAME UMBRIA-MARCHE
 SMR CHARACTERIZATION
SPONSOR PEER, UNIV OF ROME

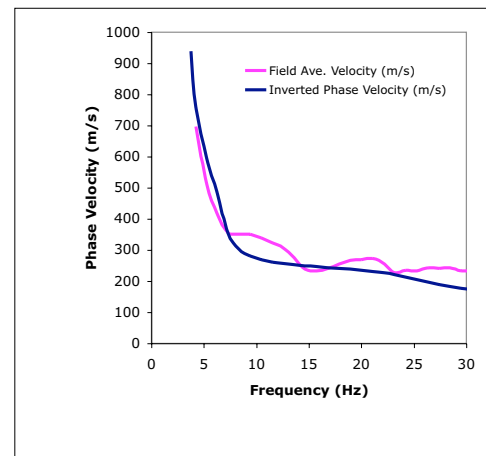
SITE SUB CLASS: Vs30 (m/s)
 A >1500 m/s
 B+ 1080 < Vs30 ≤ 1500 m/s
 B- 720 < Vs30 ≤ 1080 m/s
 C+ 540 < Vs30 ≤ 720 m/s
 C- 360 < Vs30 ≤ 540 m/s
 D+ 270 < Vs30 ≤ 360 m/s
 D- 180 < Vs30 ≤ 270 m/s
 E <180 m/s
 F **Special Soil Conditions:** Liquefiable soils; quick and high sensitivity clays; collapsible cemented soils; peats>3m; high (>75) PI soils thicker than 8m; soft/medium stiff clays thicker than 36m.



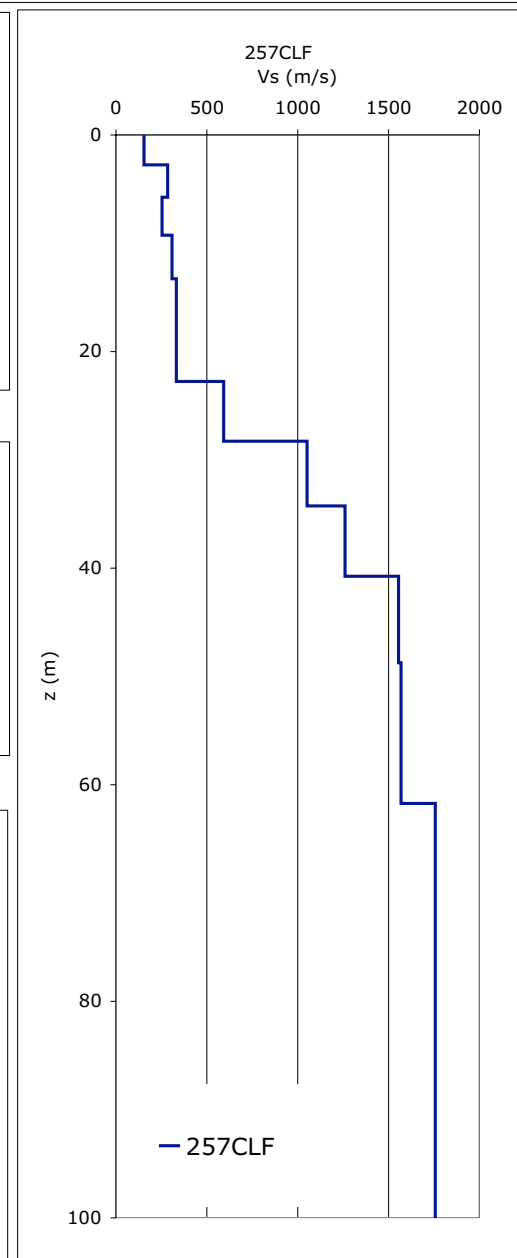
(A) Merged Field-LAMBDA Dispersion Curves



(B) Merged Field-Frequency Dispersion Curves



(C) Inversion-theoretical dispersion curve versus averaged field dispersion curve,



(D) Shear Wave Velocity SASW

UMBRIA-MARCHE, ITALY SMR Stations

Site ID 258CLC
NEHRP CLASS: C
Vs30 405 (m/s)
SUB-CLASS C-
Vs 80 720 (m/s)
Location

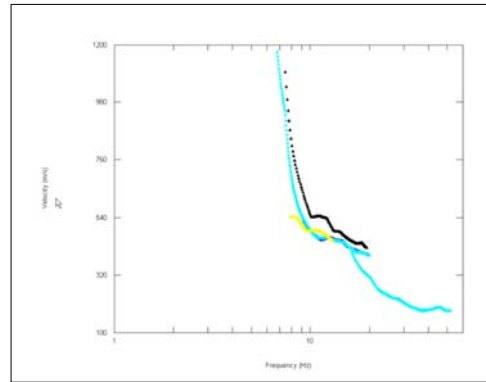
SMR Station CLF
State UMBRIA
Description COLFIORITO-CASERMETTE
POSITION COLFIORITO
LAT (N) 43.02865
LON (E) 12.89037

Data Type SWEPT-SINE SASW
Investigators KAYEN, SCASSERRA
Date collected 11/13/200

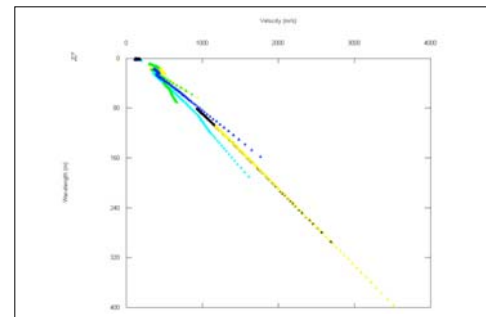
TEST METHODS PARALLEL-ARRAY SOURCES;
 CONTINUOUS HARMONIC
 WAVE-SASW; 3D AMBIENT
 MICROTREMOR ANALYSIS

PROJECT NAME UMBRIA-MARCHE
 SMR CHARACTERIZATION
SPONSOR PEER, UNIV OF ROME

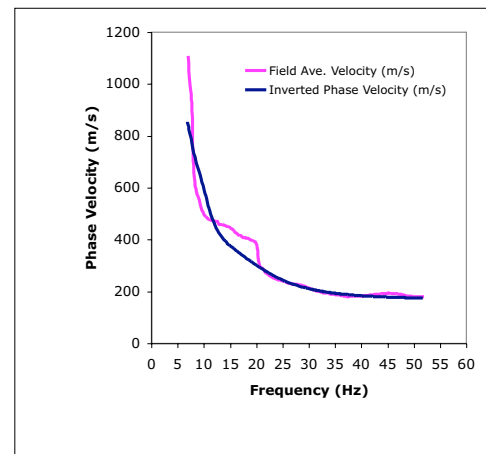
SITE SUB CLASS: Vs30 (m/s)
 A >1500 m/s
 B+ 1080 < Vs30 ≤ 1500 m/s
 B- 720 < Vs30 ≤ 1080 m/s
 C+ 540 < Vs30 ≤ 720 m/s
 C- 360 < Vs30 ≤ 540 m/s
 D+ 270 < Vs30 ≤ 360 m/s
 D- 180 < Vs30 ≤ 270 m/s
 E <180 m/s
 F Special Soil Conditions: Liquefiable soils; quick and high sensitivity clays; collapsible cemented soils; peats>3m; high (>75) PI soils thicker than 8m; soft/medium stiff clays thicker than 36m.



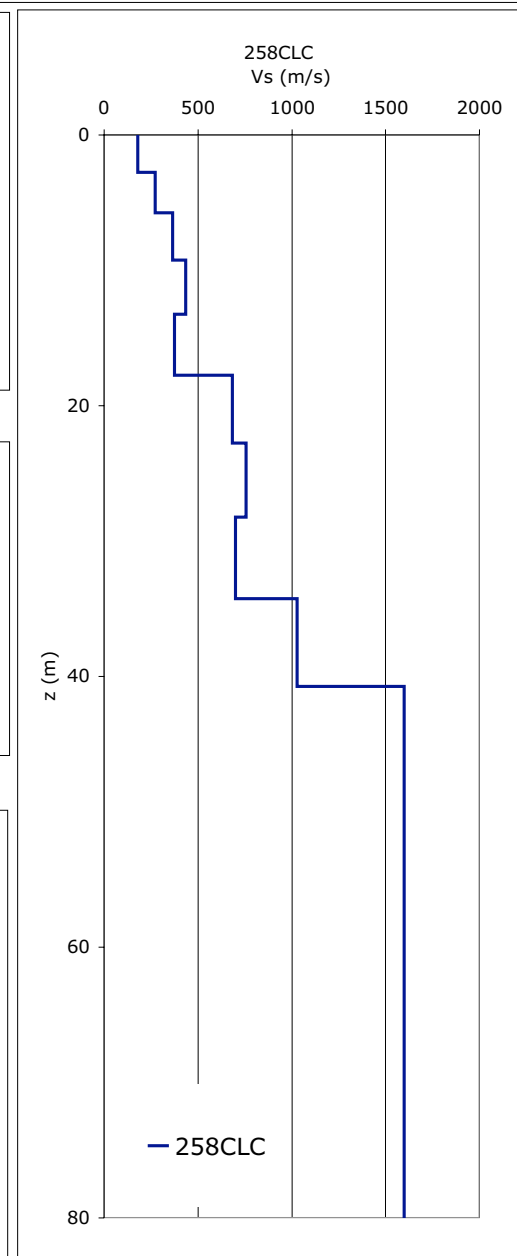
(A) Merged Field-LAMBDA Dispersion Curves



(B) Merged Field-Frequency Dispersion Curves



(C) Inversion-theoretical dispersion curve versus averaged field dispersion curve,



(D) Shear Wave Velocity SASW

258CLC	DISPERSION DATA			INVERSION PROFILE	
Site Disp. Vr (m/s)	Theoretical Disp. Vr (m/s)	Frequency (Hz)		Inversion Vs (m/s)	Depth (m)
				180.5	0.0
1171.0	858.0	6.8		180.5	2.8
1110.7	844.3	6.9		273.0	2.8
997.7	808.2	7.2		273.0	5.8
916.4	776.4	7.5		366.0	5.8
721.5	746.8	7.9		366.0	9.3
624.3	723.3	8.1		435.0	9.3
588.7	699.2	8.5		435.0	13.3
569.1	676.5	8.8		373.5	13.3
541.9	654.9	9.1		373.5	17.8
526.4	635.1	9.4		683.1	17.8
508.6	613.0	9.7		683.1	22.8
496.3	590.4	10.0		755.1	22.8
491.4	567.8	10.3		755.1	28.3
484.9	544.7	10.6		700.3	28.3
482.3	521.8	10.9		700.3	34.3
478.3	501.2	11.2		1029.2	34.3
476.7	482.9	11.5		1029.2	40.8
476.3	466.5	11.8		1597.3	40.8
473.2	452.4	12.1		1597.3	80.0
471.7	440.3	12.4			
464.0	429.7	12.7			
461.8	420.7	13.0			
459.9	411.4	13.4			
457.4	404.0	13.6			
457.0	397.3	13.9			
454.3	390.7	14.3			
453.3	384.7	14.6			
449.5	379.1	14.9			
442.9	374.0	15.2			
437.3	368.8	15.5			
431.1	364.1	15.8			
428.3	359.5	16.1			
				Vs30	404.7

UMBRIA-MARCHE, ITALY SMR Stations

Site ID 259NCR
NEHRP CLASS: C
Vs30 428 (m/s)
SUB-CLASS C-
Vs100 938 (m/s)
Location

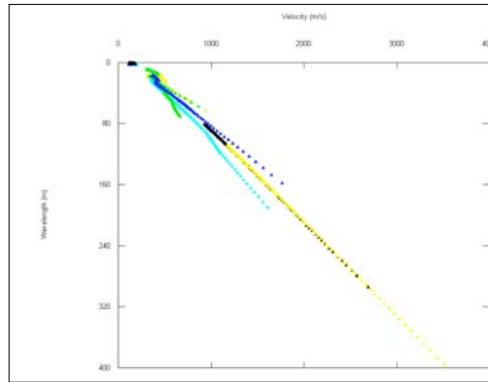
SMR Station NCR
State UMBRIA
Description NOCERA
POSITION NOCERA
LAT (N) 43.11134
LON (E) 12.78467

Data Type SWEPT-SINE SASW
Investigators KAYEN, SCASSERRA
Date collected 14-Nov-2006

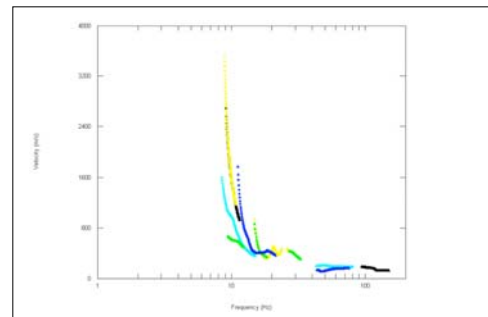
TEST METHODS PARALLEL-ARRAY SOURCES;
 CONTINUOUS HARMONIC
 WAVE-SASW; 3D AMBIENT
 MICROTREMOR ANALYSIS

PROJECT NAME UMBRIA-MARCHE
 SMR CHARACTERIZATION
SPONSOR PEER, UNIV OF ROME

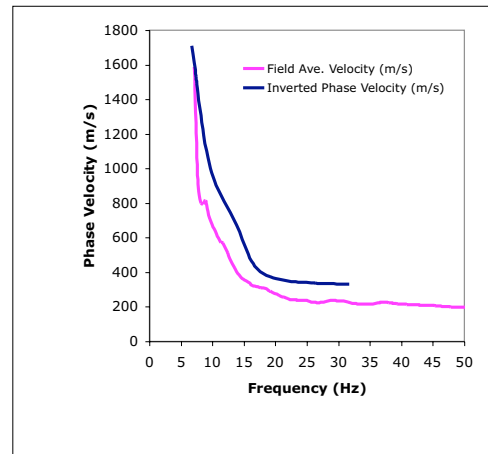
SITE SUB CLASS: Vs30 (m/s)
 A >1500 m/s
 B+ 1080 < Vs30 ≤ 1500 m/s
 B- 720 < Vs30 ≤ 1080 m/s
 C+ 540 < Vs30 ≤ 720 m/s
 C- 360 < Vs30 ≤ 540 m/s
 D+ 270 < Vs30 ≤ 360 m/s
 D- 180 < Vs30 ≤ 270 m/s
 E <180 m/s
 F Special Soil Conditions: Liquefiable soils; quick and high sensitivity clays; collapsible cemented soils; peats>3m; high (>75) PI soils thicker than 8m; soft/medium stiff clays thicker than 36m.



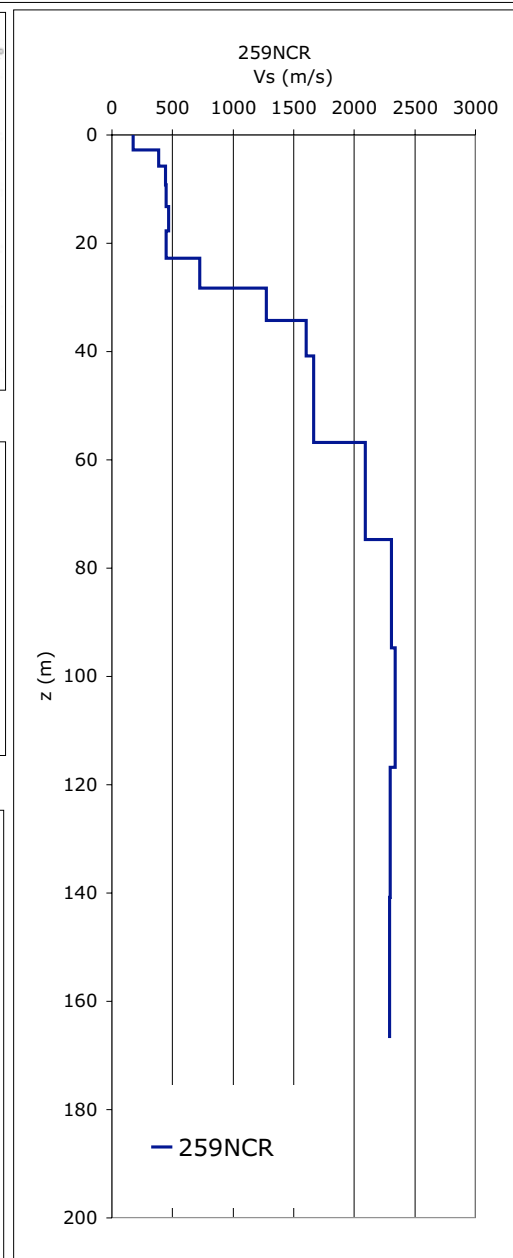
(A) Merged Field-LAMBDA Dispersion Curves



(B) Merged Field-Frequency Dispersion Curves



(C) Inversion-theoretical dispersion curve versus averaged field dispersion curve,



(D) Shear Wave Velocity SASW

259NCR	DISPERSION DATA			INVERSION PROFILE	
Site Disp. Vr (m/s)	Theoretical Disp. Vr (m/s)	Frequency (Hz)		Inversion Vs (m/s)	Depth (m)
				175.5	0.0
2000.0	1713.5	6.7		175.5	2.8
1600.0	1538.5	7.3		386.7	2.8
1559.8	1494.7	7.4		386.7	5.8
1403.4	1199.7	8.5		443.7	5.8
1318.9	1037.8	9.4		443.7	9.3
1218.6	927.9	10.3		446.6	9.3
885.3	848.4	11.3		446.6	13.3
646.4	781.9	12.2		466.1	13.3
537.8	714.3	13.2		466.1	17.8
525.6	638.7	14.2		446.5	17.8
517.3	549.6	15.1		446.5	22.8
434.0	466.2	16.1		721.9	22.8
393.3	421.1	17.1		721.9	28.3
380.2	395.5	18.0		1275.9	28.3
404.3	378.6	19.0		1275.9	34.3
403.2	367.5	20.0		1601.2	34.3
409.8	359.9	20.9		1601.2	40.8
408.7	353.8	22.0		1666.2	40.8
398.9	349.5	22.9		1666.2	56.8
406.3	347.3	23.5		2090.6	56.8
402.7	340.4	26.2		2090.6	74.8
407.0	339.4	26.8		2307.8	74.8
402.3	338.0	27.7		2307.8	94.8
403.3	336.8	28.7		2337.3	94.8
386.2	335.8	29.6		2337.3	116.8
357.2	335.0	30.6		2298.2	116.8
333.0	335.0	31.6		2298.2	140.8
0.0	0.0	0.0		2289.1	140.8
0.0	0.0	0.0		2289.1	166.8
0.0	0.0	0.0		2289.1	166.8
0.0	0.0	0.0			
0.0	0.0	0.0		Vs30	427.9

UMBRIA-MARCHE, ITALY SMR Stations

Site ID 260NCB
NEHRP CLASS: C
Vs30 442 (m/s)
SUB-CLASS C-
Vs100 823 (m/s)
Location

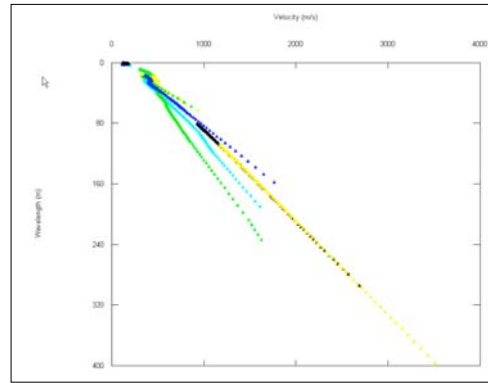
SMR Station NCB
State UMBRIA
Description STATION-B BISCONTIN
POSITION NOCERA UMBRA - B
LAT (N) 43.10358
LON (E) 12.80518

Data Type SWEPT-SINE SASW
Investigators KAYEN, SCASSERRA
Date collected 14-Nov-2006

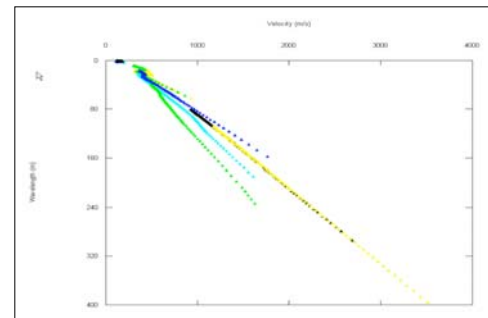
TEST METHODS PARALLEL-ARRAY SOURCES;
 CONTINUOUS HARMONIC
 WAVE-SASW; 3D AMBIENT
 MICROTREMOR ANALYSIS

PROJECT NAME UMBRIA-MARCHE
 SMR CHARACTERIZATION
SPONSOR PEER, UNIV OF ROME

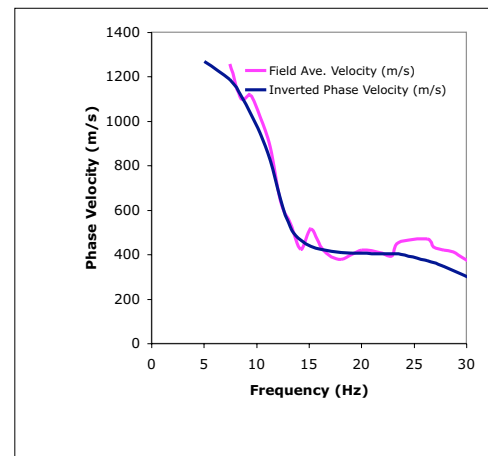
SITE SUB CLASS: Vs30 (m/s)
 A >1500 m/s
 B+ 1080 < Vs30 ≤ 1500 m/s
 B- 720 < Vs30 ≤ 1080 m/s
 C+ 540 < Vs30 ≤ 720 m/s
 C- 360 < Vs30 ≤ 540 m/s
 D+ 270 < Vs30 ≤ 360 m/s
 D- 180 < Vs30 ≤ 270 m/s
 E <180 m/s
 F Special Soil Conditions: Liquefiable soils; quick and high sensitivity clays; collapsible cemented soils; peats>3m; high (>75) PI soils thicker than 8m; soft/medium stiff clays thicker than 36m.



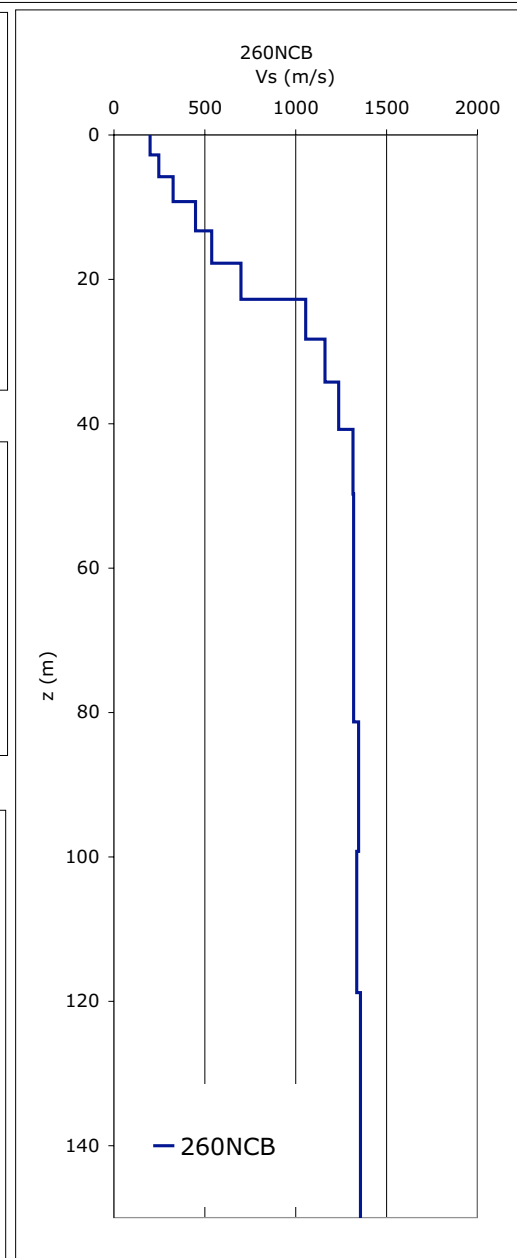
(A) Merged Field-LAMBDA Dispersion Curves



(B) Merged Field-Frequency Dispersion Curves



(C) Inversion-theoretical dispersion curve versus averaged field dispersion curve,



(D) Shear Wave Velocity SASW

260NCB	DISPERSION DATA			INVERSION PROFILE	
Site Disp. Vr (m/s)	Theoretical Disp. Vr (m/s)	Frequency (Hz)		Inversion Vs (m/s)	Depth (m)
				198.1	0.0
1300.0	1271.3	5.0		198.1	2.8
1259.8	1190.7	7.4		246.8	2.8
1103.4	1116.2	8.5		246.8	5.8
1018.9	1037.9	9.4		326.0	5.8
1018.6	946.5	10.3		326.0	9.3
885.3	824.7	11.3		447.2	9.3
646.4	654.2	12.2		447.2	13.3
537.8	522.2	13.2		537.7	13.3
425.6	466.4	14.2		537.7	17.8
517.3	440.2	15.1		699.8	17.8
434.0	424.8	16.1		699.8	22.8
405.0	416.5	17.1		1056.1	22.8
404.0	411.8	18.0		1056.1	28.3
404.3	409.1	19.0		1161.5	28.3
400.0	407.8	20.0		1161.5	34.3
400.0	407.4	20.9		1235.8	34.3
395.0	407.4	22.0		1235.8	40.8
398.9	407.2	22.9		1313.6	40.8
398.9	406.5	23.5		1313.6	49.8
398.9	376.3	26.2		1318.5	49.8
398.9	366.2	26.8		1318.5	64.8
398.9	349.8	27.7		1317.3	64.8
398.9	331.7	28.7		1317.3	81.3
386.2	311.8	29.6		1345.2	81.3
357.2	289.1	30.6		1345.2	99.3
333.0	266.3	31.6		1334.4	99.3
312.5	245.7	32.6		1334.4	118.8
310.0	180.3	33.0		1357.0	118.8
305.0	179.1	35.0		1357.0	99118.8
295.0	177.9	37.0		1357.0	99118.8
285.0	176.7	39.0			
280.0	175.7	40.0		Vs30	441.5

UMBRIA-MARCHE, ITALY SMR Stations

Site ID 261NCS
NEHRP CLASS: C
Vs30 694 (m/s)
SUB-CLASS C+
Vs100 1170 (m/s)

Location

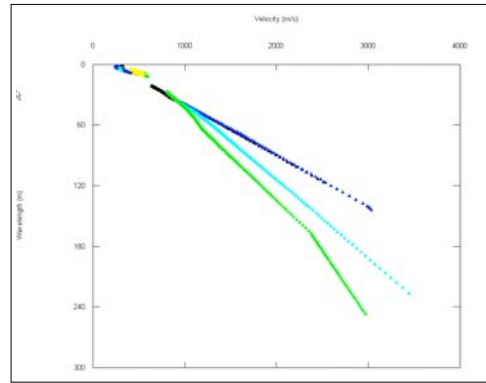
SMR Station NCS
State UMBRIA
Description STATION-C GRAVEL ROAD
POSITION NOCERA UMBRA - C GRAVEL RD
LAT (N) 43.14835
LON (E) 12.79134

Data Type SWEPT-SINE SASW
Investigators KAYEN, SCASSERRA
Date collected 15-Nov-2006

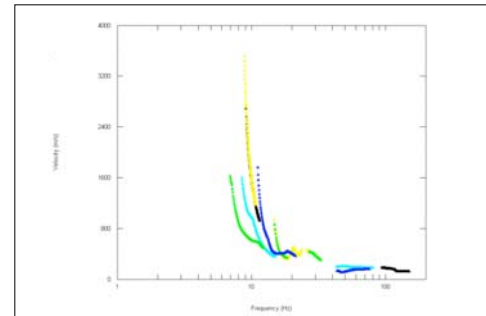
TEST METHODS PARALLEL-ARRAY SOURCES;
 CONTINUOUS HARMONIC
 WAVE-SASW; 3D AMBIENT
 MICROTREMOR ANALYSIS

PROJECT NAME UMBRIA-MARCHE
 SMR CHARACTERIZATION
SPONSOR PEER, UNIV OF ROME

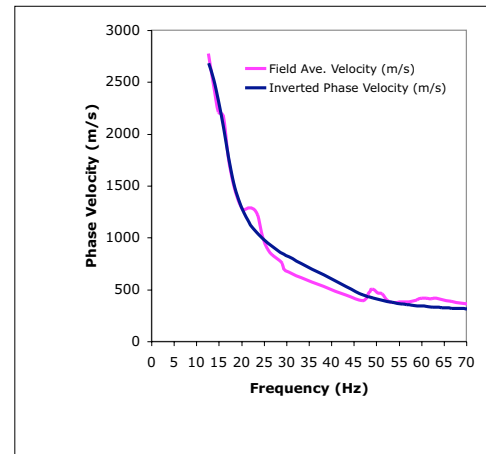
SITE SUB CLASS: Vs30 (m/s)
 A >1500 m/s
 B+ 1080 < Vs30 ≤ 1500 m/s
 B- 720 < Vs30 ≤ 1080 m/s
 C+ 540 < Vs30 ≤ 720 m/s
 C- 360 < Vs30 ≤ 540 m/s
 D+ 270 < Vs30 ≤ 360 m/s
 D- 180 < Vs30 ≤ 270 m/s
 E <180 m/s
 F **Special Soil Conditions:** Liquefiable soils; quick and high sensitivity clays; collapsible cemented soils; peats>3m; high (>75) PI soils thicker than 8m; soft/medium stiff clays thicker than 36m.



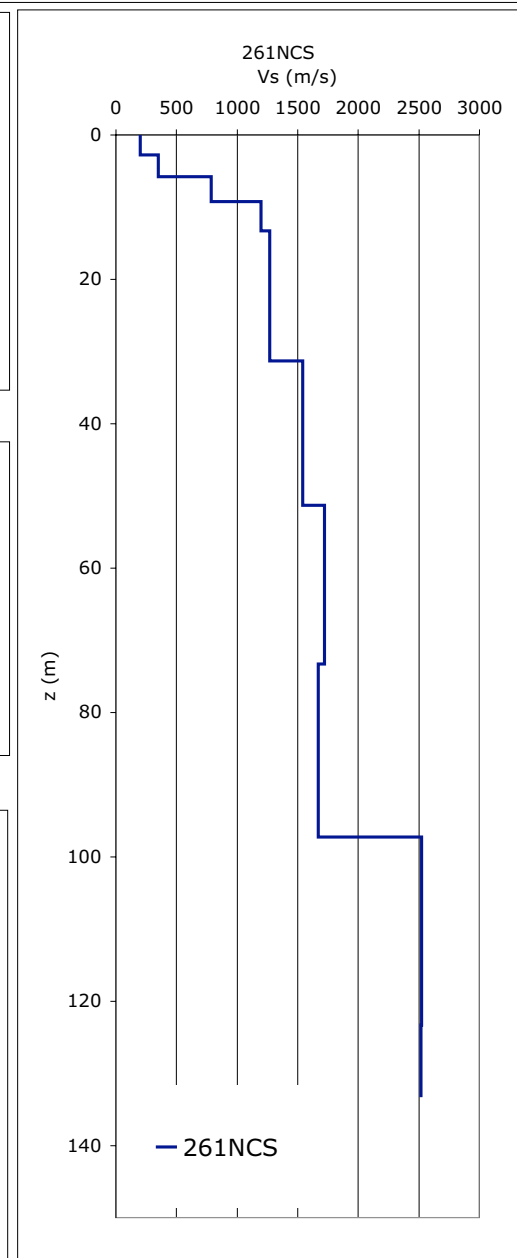
(A) Merged Field-LAMBDA Dispersion Curves



(B) Merged Field-Frequency Dispersion Curves



(C) Inversion-theoretical dispersion curve versus averaged field dispersion curve,



(D) Shear Wave Velocity SASW

261NCS	DISPERSION DATA			INVERSION PROFILE	
Site Disp. Vr (m/s)	Theoretical Disp. Vr (m/s)	Frequency (Hz)		Inversion Vs (m/s)	Depth (m)
				200.6	0.0
2778.8	2689.8	12.6		200.6	2.8
2482.0	2531.5	13.7		350.3	2.8
2213.7	2314.7	14.8		350.3	5.8
2175.0	2062.9	15.9		785.7	5.8
1776.2	1776.8	17.0		785.7	9.3
1526.3	1538.4	18.1		1198.8	9.3
1360.8	1372.2	19.2		1198.8	13.3
1272.1	1255.7	20.3		1270.8	13.3
1188.7	1164.4	21.4		1270.8	31.3
1184.4	1100.8	22.5		1541.1	31.3
1126.9	1043.7	23.6		1541.1	51.3
1015.9	995.1	24.7		1721.9	51.3
894.6	956.3	25.7		1721.9	73.3
832.1	916.0	26.9		1667.9	73.3
795.4	882.2	28.0		1667.9	97.3
754.6	851.2	29.1		2523.5	97.3
686.0	832.3	29.8		2523.5	123.3
593.6	457.0	46.8		2516.8	123.3
497.6	440.4	48.0		2516.8	133.3
511.1	426.9	49.0			133.3
476.5	414.2	50.1			133.3
464.8	403.4	51.1			133.3
402.7	392.3	52.3			133.3
380.5	383.5	53.4			133.3
379.0	375.0	54.5			133.3
386.7	367.7	55.6			133.3
384.5	361.4	56.6			133.3
387.2	355.5	57.8			133.3
387.2	350.2	58.9			150.0
387.2	345.6	60.0			150.0
387.2	341.4	61.1			
387.2	337.6	62.2		Vs30	693.7

UMBRIA-MARCHE, ITALY SMR Stations

Site ID 262GBP
NEHRP CLASS: C
Vs30 492 (m/s)
SUB-CLASS C+
Vs100 864 (m/s)
Location

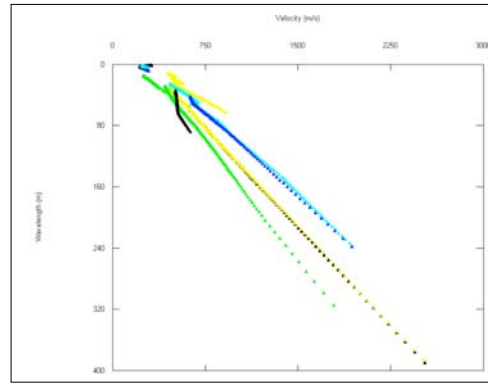
SMR Station GBP
State UMBRIA
Description GUBBIO SOIL SITE PIANA
POSITION GUBBIO
LAT (N) 43.314
LON (E) 12.59

Data Type SWEPT-SINE SASW
Investigators KAYEN, SCASSERRA
Date collected 17-Nov-2005

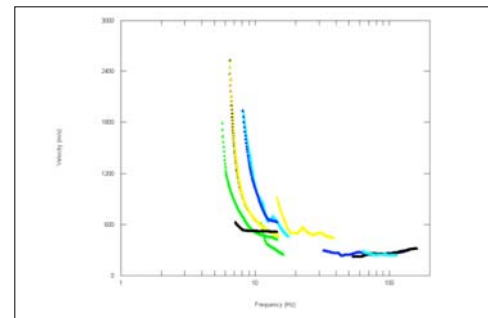
TEST METHODS PARALLEL-ARRAY SOURCES;
 CONTINUOUS HARMONIC
 WAVE-SASW; 3D AMBIENT
 MICROTREMOR ANALYSIS

PROJECT NAME UMBRIA-MARCHE
 SMR CHARACTERIZATION
SPONSOR PEER, UNIV OF ROME

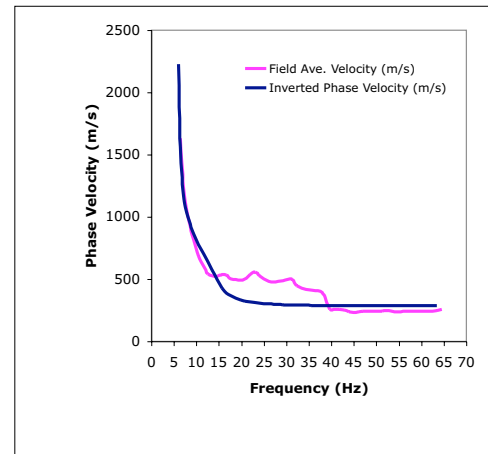
SITE SUB CLASS: Vs30 (m/s)
 A >1500 m/s
 B+ 1080 < Vs30 ≤ 1500 m/s
 B- 720 < Vs30 ≤ 1080 m/s
 C+ 540 < Vs30 ≤ 720 m/s
 C- 360 < Vs30 ≤ 540 m/s
 D+ 270 < Vs30 ≤ 360 m/s
 D- 180 < Vs30 ≤ 270 m/s
 E <180 m/s
 F Special Soil Conditions: Liquefiable soils; quick and high sensitivity clays; collapsible cemented soils; peats>3m; high (>75) PI soils thicker than 8m; soft/medium stiff clays thicker than 36m.



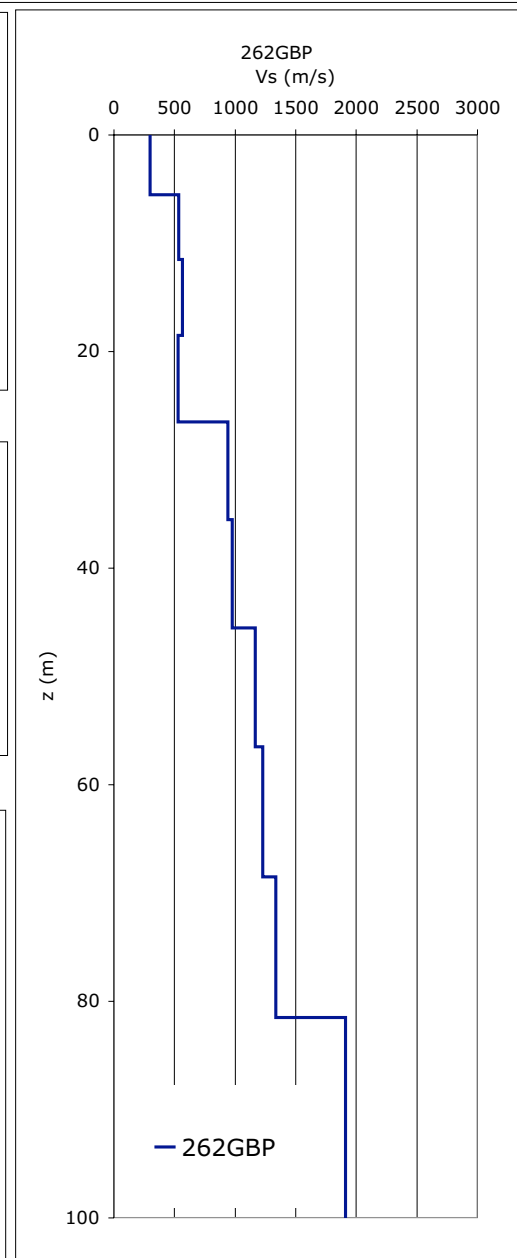
(A) Merged Field-LAMBDA Dispersion Curves



(B) Merged Field-Frequency Dispersion Curves



(C) Inversion-theoretical dispersion curve versus averaged field dispersion curve,



(D) Shear Wave Velocity SASW

262GBP	DISPERSION DATA			INVERSION PROFILE	
Site Disp. Vr (m/s)	Theoretical Disp. Vr (m/s)	Frequency (Hz)		Inversion Vs (m/s)	Depth (m)
				296.0	0.0
2510.0	2229.3	5.9		296.0	5.5
1634.1	1567.2	6.3		531.9	5.5
1193.3	1136.2	7.3		531.9	11.5
963.5	976.1	8.3		567.3	11.5
826.7	867.7	9.3		567.3	18.5
691.5	781.7	10.4		531.2	18.5
608.7	711.6	11.4		531.2	26.5
543.8	646.2	12.4		940.1	26.5
528.4	573.3	13.5		940.1	35.5
525.1	498.4	14.5		976.6	35.5
540.8	431.8	15.6		976.6	45.5
533.1	392.3	16.6		1165.3	45.5
502.5	369.3	17.5		1165.3	56.5
499.8	348.1	18.7		1225.6	56.5
495.0	335.2	19.8		1225.6	68.5
495.0	325.7	20.8		1335.4	68.5
495.0	318.6	21.9		1335.4	81.5
495.0	313.2	22.9		1911.0	81.5
495.0	308.9	24.0		1911.0	100.0
495.0	305.7	25.0			99081.5
487.4	302.9	26.0			99081.5
477.9	300.7	27.0			99081.5
484.8	298.9	28.1			99081.5
484.8	297.4	29.2			99081.5
484.8	296.1	30.2			99081.5
484.8	295.1	31.3			99081.5
452.2	294.2	32.3			99081.5
430.1	293.5	33.3			99081.5
420.0	292.8	34.3			150.0
416.8	292.3	35.4			150.0
408.2	291.8	36.5			
403.9	291.4	37.5		Vs30	491.9

UMBRIA-MARCHE, ITALY SMR Stations

Site ID 263GBB
NEHRP CLASS: C
Vs30 922 (m/s)
SUB-CLASS C+
Vs100 1759 (m/s)

Location

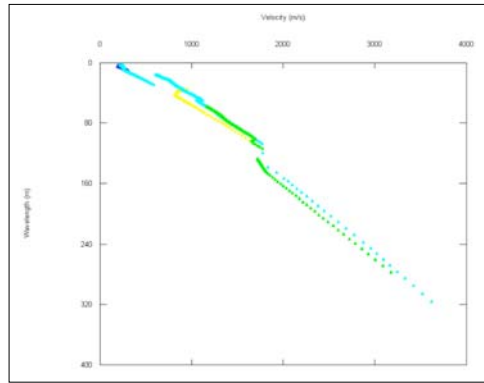
SMR Station GBB
State UMBRIA
Description GUBBIO - PARK COLLO
POSITION GUBBIO
LAT (N) 43.35786
LON (E) 12.5947

Data Type SWEPT-SINE SASW
Investigators KAYEN, SCASSERRA
Date collected 17-Nov-2005

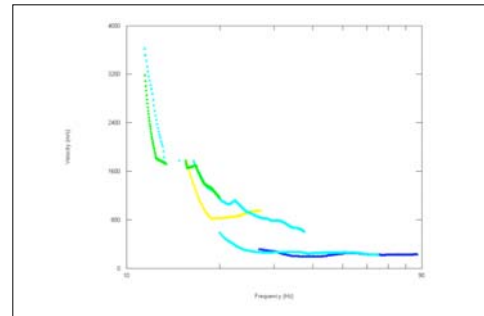
TEST METHODS PARALLEL-ARRAY SOURCES;
 CONTINUOUS HARMONIC
 WAVE-SASW; 3D AMBIENT
 MICROTREMOR ANALYSIS

PROJECT NAME UMBRIA-MARCHE
 SMR CHARACTERIZATION
SPONSOR PEER, UNIV OF ROME

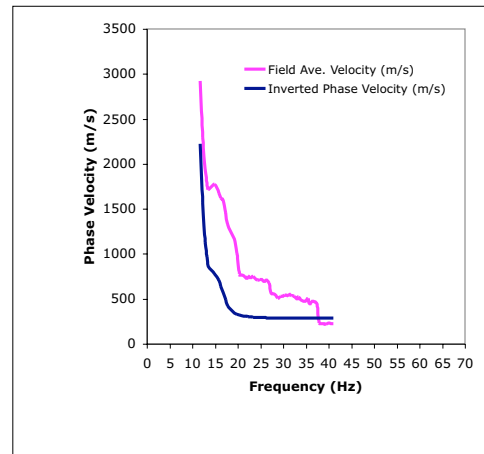
SITE SUB CLASS: Vs30 (m/s)
 A >1500 m/s
 B+ 1080 < Vs30 ≤ 1500 m/s
 B- 720 < Vs30 ≤ 1080 m/s
 C+ 540 < Vs30 ≤ 720 m/s
 C- 360 < Vs30 ≤ 540 m/s
 D+ 270 < Vs30 ≤ 360 m/s
 D- 180 < Vs30 ≤ 270 m/s
 E <180 m/s
 F Special Soil Conditions: Liquefiable soils; quick and high sensitivity clays; collapsible cemented soils; peats>3m; high (>75) PI soils thicker than 8m; soft/medium stiff clays thicker than 36m.



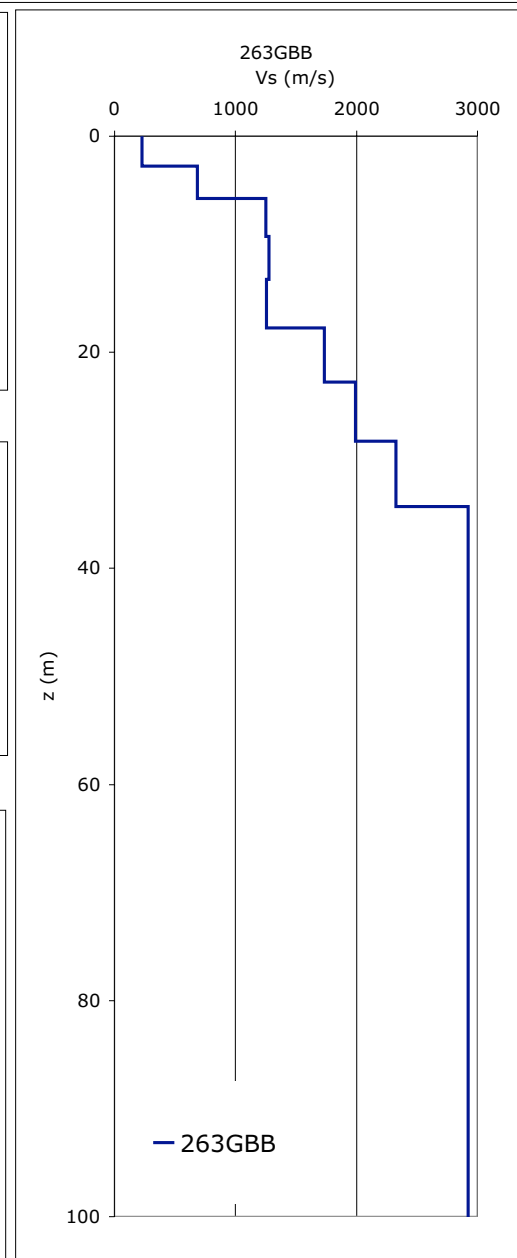
(A) Merged Field-LAMBDA Dispersion Curves



(B) Merged Field-Frequency Dispersion Curves



(C) Inversion-theoretical dispersion curve versus averaged field dispersion curve,



(D) Shear Wave Velocity SASW

263GBB	DISPERSION DATA			INVERSION PROFILE	
Site Disp. Vr (m/s)	Theoretical Disp. Vr (m/s)	Frequency (Hz)		Inversion Vs (m/s)	Depth (m)
				224.8	0.0
2923.5	2229.3	11.7		224.8	2.8
2299.0	1567.2	12.2		683.9	2.8
1943.0	1136.2	12.7		683.9	5.8
1788.4	976.1	13.2		1248.2	5.8
1720.7	867.7	13.5		1248.2	9.3
1776.1	781.7	14.8		1275.4	9.3
1680.6	711.6	15.7		1275.4	13.3
1628.0	646.2	16.2		1254.5	13.3
1597.5	573.3	16.7		1254.5	17.8
1461.5	498.4	17.2		1734.3	17.8
1336.0	431.8	17.7		1734.3	22.8
1266.6	392.3	18.2		1990.2	22.8
1211.3	369.3	18.7		1990.2	28.3
1171.5	348.1	19.2		2327.7	28.3
1011.5	335.2	19.7		2327.7	34.3
981.3	325.7	20.2		2923.5	34.3
867.1	318.6	20.7		2923.5	40.8
758.2	313.2	21.2		2923.5	40.8
760.4	308.9	21.7		2923.5	100.0
754.6	305.7	22.3			
742.3	302.9	22.8			
752.0	300.7	23.3			
728.4	298.9	23.8			
712.0	297.4	24.3			
717.7	296.1	24.8			
716.0	295.1	25.3			
698.7	294.2	25.8			
713.2	293.5	26.3			
674.9	292.8	26.8			
567.1	292.3	27.3			
561.2	291.8	27.8			
539.0	291.4	28.3			
				Vs30	921.7

UMBRIA-MARCHE, ITALY SMR Stations

Site ID 264NCI
NEHRP CLASS: C
Vs30 551 (m/s)
SUB-CLASS C+
Vs100 546 (m/s)
Location

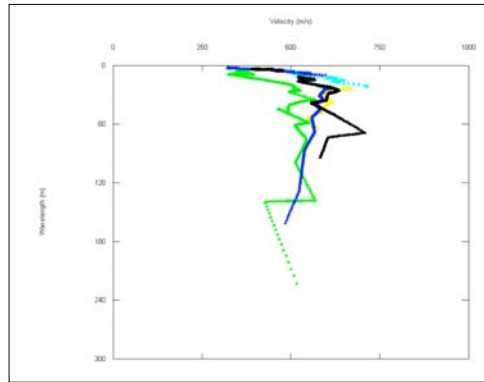
SMR Station NCI
State UMBRIA
Description NORCIA INDUSTRIAL PARK
POSITION NORCIA
LAT (N) 42.77974
LON (E) 13.09729

Data Type SWEPT-SINE SASW
Investigators KAYEN, SCASSERRA
Date collected 18-Nov-2006

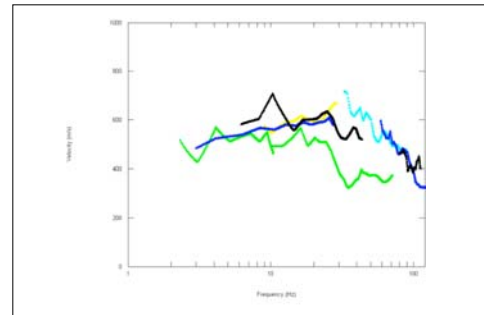
TEST METHODS PARALLEL-ARRAY SOURCES;
 CONTINUOUS HARMONIC
 WAVE-SASW; 3D AMBIENT
 MICROTREMOR ANALYSIS

PROJECT NAME UMBRIA-MARCHE
 SMR CHARACTERIZATION
SPONSOR PEER, UNIV OF ROME

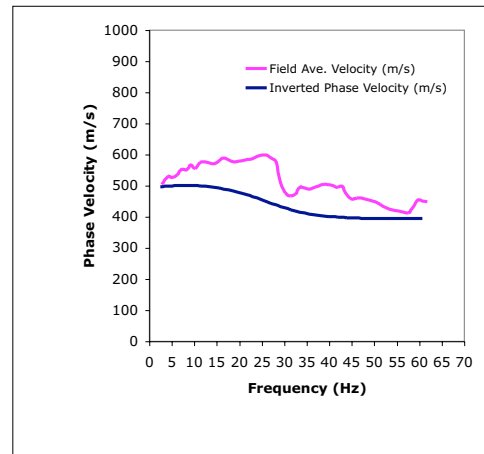
SITE SUB CLASS: Vs30 (m/s)
 A >1500 m/s
 B+ 1080 < Vs30 ≤ 1500 m/s
 B- 720 < Vs30 ≤ 1080 m/s
 C+ 540 < Vs30 ≤ 720 m/s
 C- 360 < Vs30 ≤ 540 m/s
 D+ 270 < Vs30 ≤ 360 m/s
 D- 180 < Vs30 ≤ 270 m/s
 E <180 m/s
 F Special Soil Conditions: Liquefiable soils; quick and high sensitivity clays; collapsible cemented soils; peats>3m; high (>75) PI soils thicker than 8m; soft/medium stiff clays thicker than 36m.



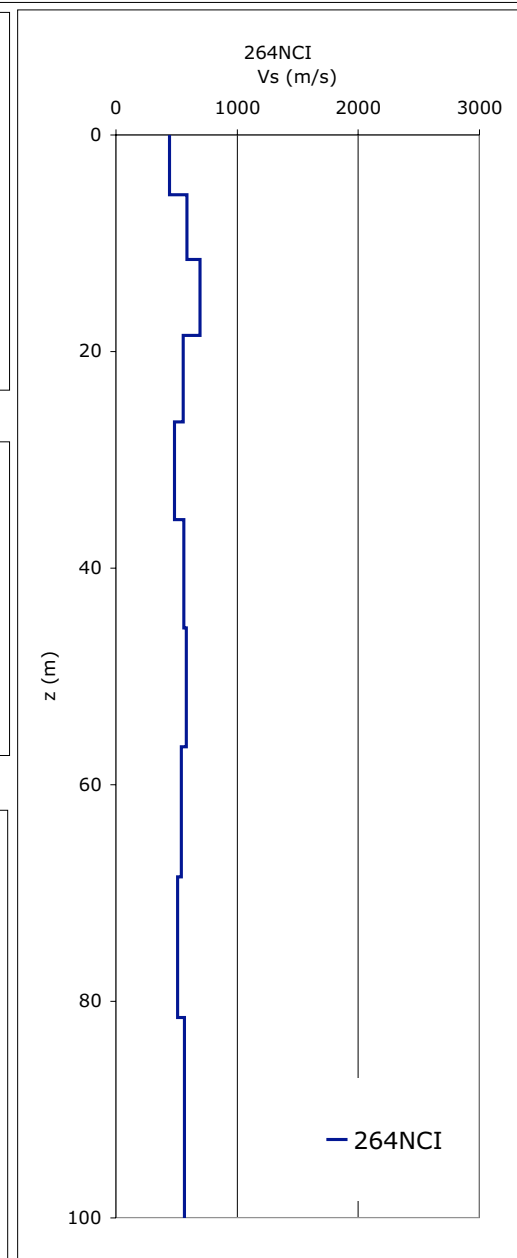
(A) Merged Field-LAMBDA Dispersion Curves



(B) Merged Field-Frequency Dispersion Curves



(C) Inversion-theoretical dispersion curve versus averaged field dispersion curve,



(D) Shear Wave Velocity SASW

264NCI	DISPERSION DATA			INVERSION PROFILE	
Site Disp. Vr (m/s)	Theoretical Disp. Vr (m/s)	Frequency (Hz)		Inversion Vs (m/s)	Depth (m)
				441.5	0.0
550.0	498.0	2.4		441.5	5.5
555.4	498.2	2.6		587.8	5.5
530.4	499.7	4.0		587.8	11.5
527.2	500.6	5.0		693.6	11.5
535.2	501.3	6.0		693.6	18.5
553.7	501.7	7.0		556.7	18.5
551.4	501.8	8.1		556.7	26.5
567.9	501.6	9.2		480.4	26.5
555.9	501.1	10.2		480.4	35.5
576.4	500.3	11.3		558.5	35.5
577.8	499.1	12.3		558.5	45.5
573.4	497.6	13.4		581.3	45.5
571.4	495.8	14.4		581.3	56.5
581.0	493.6	15.5		539.7	56.5
590.1	491.0	16.5		539.7	68.5
583.8	488.0	17.6		509.0	68.5
578.5	484.5	18.6		509.0	81.5
580.5	480.6	19.7		566.8	81.5
582.0	476.4	20.7		566.8	100.0
585.2	471.8	21.8			
587.7	466.8	22.8			
587.7	461.5	23.9			
587.7	456.0	24.9			
587.7	450.4	26.0			
587.7	444.7	27.0			
579.0	439.4	28.0			
511.2	434.1	29.1			
511.2	429.1	30.2			
511.2	424.6	31.2			
511.2	420.4	32.3			
511.2	416.8	33.3			
511.2	413.5	34.4			
				Vs30	551.3

UMBRIA-MARCHE, ITALY SMR Stations

Site ID 265NRC
NEHRP CLASS: C
Vs30 677 (m/s)
SUB-CLASS C+
Vs100 1148 (m/s)
Location

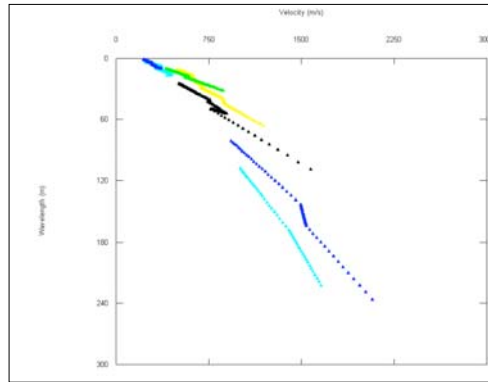
SMR Station NRC
State UMBRIA
Description NORCIA SITE C-CENTRAL DIST.
POSITION NORCIA SITE C-CENTRAL DIST.
LAT (N) 42.79223
LON (E) 13.097

Data Type SWEPT-SINE SASW
Investigators KAYEN, SCASSERRA
Date collected 18-Nov-2006

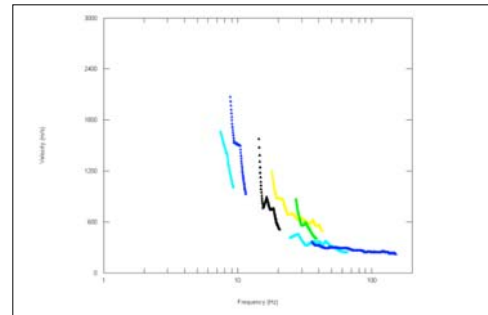
TEST METHODS PARALLEL-ARRAY SOURCES;
 CONTINUOUS HARMONIC
 WAVE-SASW; 3D AMBIENT
 MICROTREMOR ANALYSIS

PROJECT NAME UMBRIA-MARCHE
 SMR CHARACTERIZATION
SPONSOR PEER, UNIV OF ROME

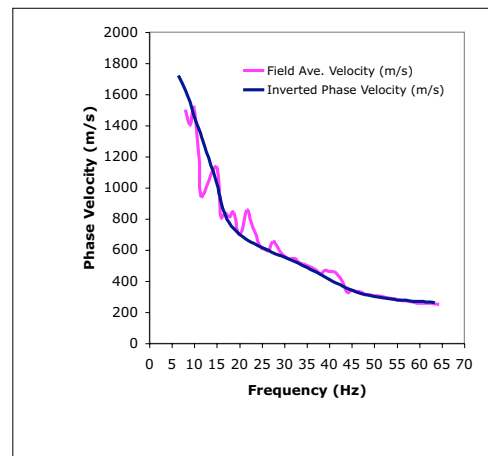
SITE SUB CLASS: Vs30 (m/s)
 A >1500 m/s
 B+ 1080 < Vs30 ≤ 1500 m/s
 B- 720 < Vs30 ≤ 1080 m/s
 C+ 540 < Vs30 ≤ 720 m/s
 C- 360 < Vs30 ≤ 540 m/s
 D+ 270 < Vs30 ≤ 360 m/s
 D- 180 < Vs30 ≤ 270 m/s
 E <180 m/s
 F Special Soil Conditions: Liquefiable soils; quick and high sensitivity clays; collapsible cemented soils; peats>3m; high (>75) PI soils thicker than 8m; soft/medium stiff clays thicker than 36m.



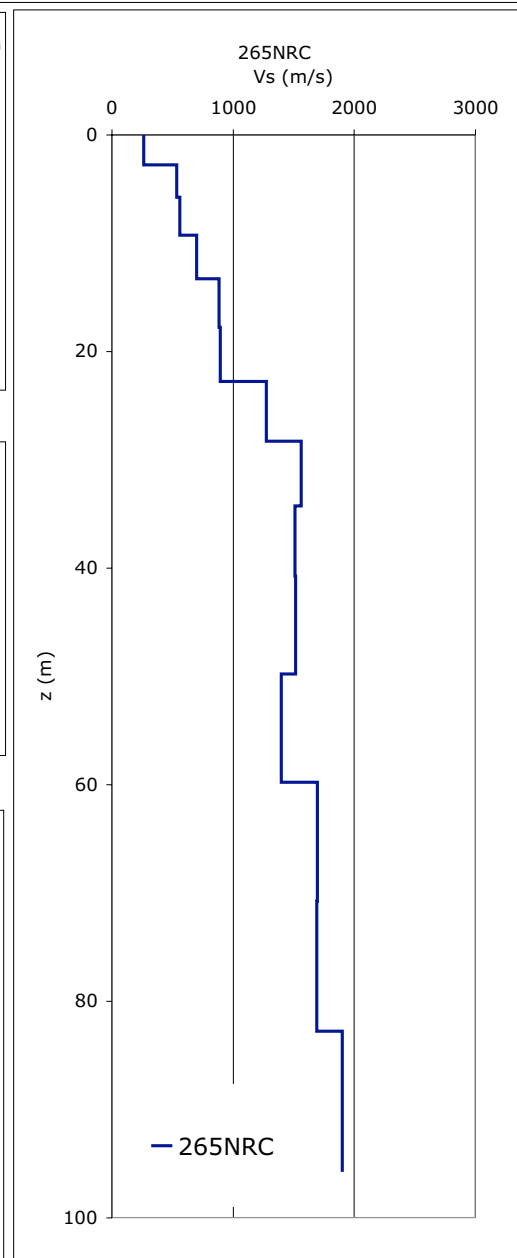
(A) Merged Field-LAMBDA Dispersion Curves



(B) Merged Field-Frequency Dispersion Curves



(C) Inversion-theoretical dispersion curve versus averaged field dispersion curve,



(D) Shear Wave Velocity SASW

265NRC	DISPERSION DATA			INVERSION PROFILE	
Site Disp. Vr (m/s)	Theoretical Disp. Vr (m/s)	Frequency (Hz)		Inversion Vs (m/s)	Depth (m)
				259.8	0.0
1900.0	1723.6	6.3		259.8	2.8
1503.7	1632.0	7.9		531.7	2.8
1408.0	1550.6	9.0		531.7	5.8
1516.3	1465.8	9.9		560.2	5.8
1205.3	1378.1	10.9		560.2	9.3
1145.1	1331.6	11.4		699.0	9.3
1139.9	1040.8	14.8		699.0	13.3
810.7	920.2	15.7		882.4	13.3
841.3	833.4	16.7		882.4	17.8
815.6	776.1	17.7		893.9	17.8
844.5	740.2	18.6		893.9	22.8
708.2	711.6	19.6		1273.6	22.8
725.6	691.0	20.5		1273.6	28.3
725.6	669.7	21.5		1561.2	28.3
725.6	653.3	22.5		1561.2	34.3
706.2	638.6	23.5		1512.6	34.3
629.7	624.1	24.5		1512.6	40.8
609.9	611.8	25.4		1517.0	40.8
598.5	598.9	26.4		1517.0	100.0
657.0	585.5	27.4		1399.8	49.8
625.2	573.9	28.4		1399.8	59.8
578.6	562.1	29.3		1693.8	59.8
558.0	550.3	30.3		1693.8	70.8
544.7	538.5	31.3		1689.4	70.8
546.5	526.4	32.2		1689.4	82.8
521.4	514.0	33.2		1900.0	82.8
513.4	501.2	34.2		1900.0	95.8
501.3	487.9	35.1			
488.3	473.3	36.1			
472.7	458.4	37.1			
447.7	443.4	38.1			
472.6	428.3	39.1			
				Vs30	676.7

UMBRIA-MARCHE, ITALY SMR Stations

Site ID 266NRA
NEHRP CLASS: D
Vs30 218 (m/s)
SUB-CLASS D-
Vs 80 264 (m/s)
Location

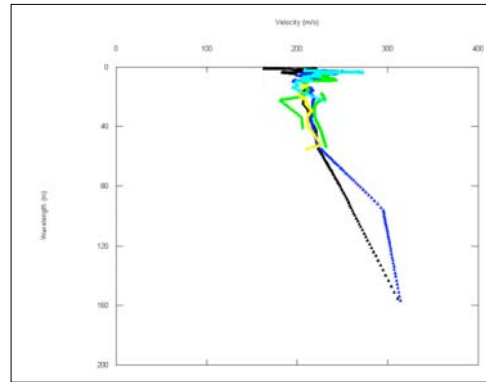
SMR Station NRA
State UMBRIA
Description NORCIA TEMPORARY STATION A
POSITION NORCIA
LAT (N) 42.79556
LON (E) 13.08096

Data Type SWEPT-SINE SASW
Investigators KAYEN, SCASSERRA
Date collected 19-Nov-2006

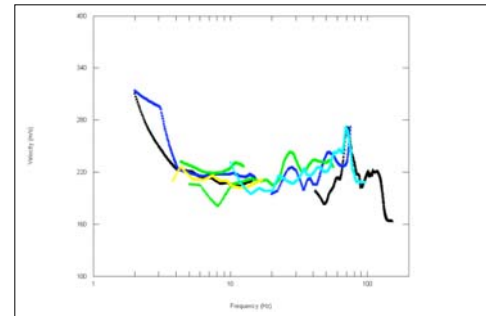
TEST METHODS PARALLEL-ARRAY SOURCES;
 CONTINUOUS HARMONIC
 WAVE-SASW; 3D AMBIENT
 MICROTREMOR ANALYSIS

PROJECT NAME UMBRIA-MARCHE
 SMR CHARACTERIZATION
SPONSOR PEER, UNIV OF ROME

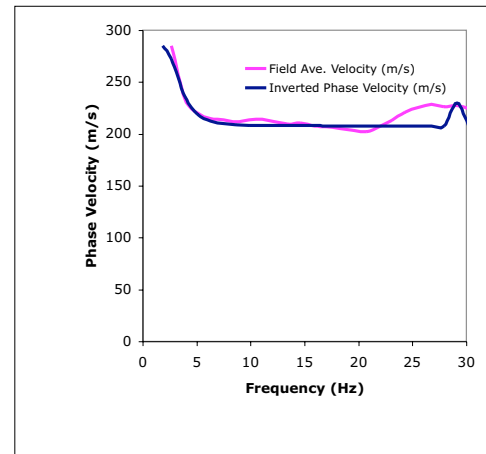
SITE SUB CLASS: Vs30 (m/s)
 A >1500 m/s
 B+ 1080 < Vs30 ≤ 1500 m/s
 B- 720 < Vs30 ≤ 1080 m/s
 C+ 540 < Vs30 ≤ 720 m/s
 C- 360 < Vs30 ≤ 540 m/s
 D+ 270 < Vs30 ≤ 360 m/s
 D- 180 < Vs30 ≤ 270 m/s
 E <180 m/s
 F Special Soil Conditions: Liquefiable soils; quick and high sensitivity clays; collapsible cemented soils; peats>3m; high (>75) PI soils thicker than 8m; soft/medium stiff clays thicker than 36m.



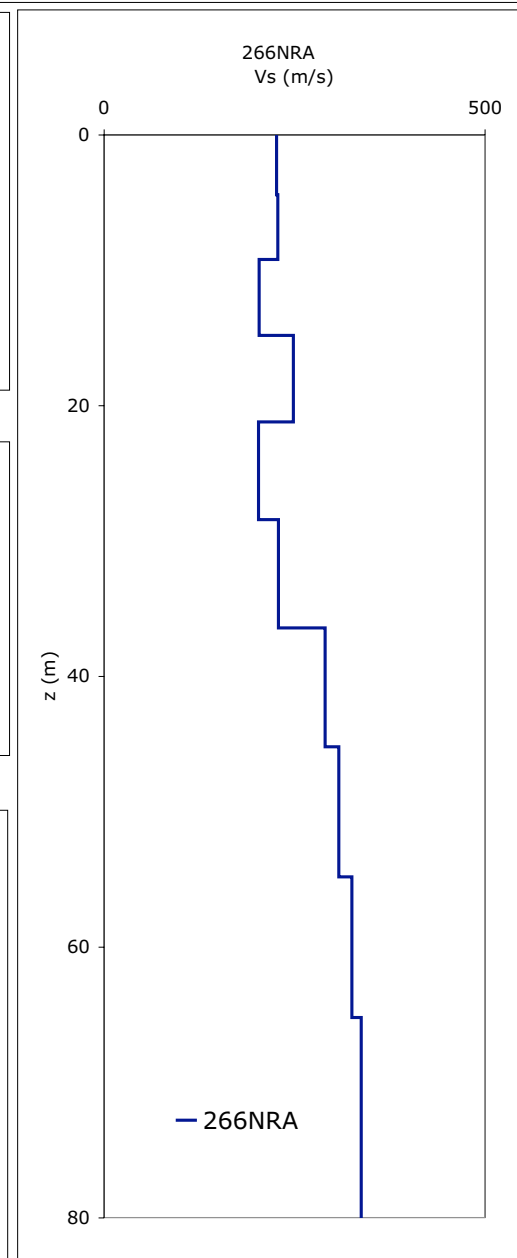
(A) Merged Field-LAMBDA Dispersion Curves



(B) Merged Field-Frequency Dispersion Curves



(C) Inversion-theoretical dispersion curve versus averaged field dispersion curve,



(D) Shear Wave Velocity SASW

266NRA	DISPERSION DATA			INVERSION PROFILE	
Site Disp. Vr (m/s)	Theoretical Disp. Vr (m/s)	Frequency (Hz)		Inversion Vs (m/s)	Depth (m)
				215.0	0.0
310.0	285.5	1.8		215.0	4.4
285.6	273.1	2.6		226.7	4.4
233.8	236.2	3.9		226.7	9.2
221.1	219.7	5.0		193.9	9.2
215.2	213.1	6.2		193.9	14.8
214.1	210.5	7.4		239.5	14.8
212.4	209.3	8.6		239.5	21.2
214.4	208.9	9.8		236.1	21.2
214.7	208.8	11.0		236.1	28.4
212.4	208.7	12.2		230.4	28.4
210.0	208.7	13.4		230.4	36.4
211.1	208.7	14.6		285.2	36.4
207.9	208.6	15.9		285.2	45.2
207.8	208.5	16.9		290.5	45.2
205.5	208.4	18.2		290.5	54.8
203.8	208.4	19.5		318.4	54.8
203.0	208.3	20.7		318.4	65.2
207.7	208.3	21.9		321.5	65.2
213.8	208.3	23.0		321.5	80.0
221.2	208.3	24.3			
226.2	208.3	25.5			
229.1	208.3	26.7			
226.8	208.3	27.9			
227.8	230.3	29.1			
224.2	207.5	30.3			
220.6	206.7	31.5			
218.2	205.9	32.7			
217.0	205.2	33.9			
219.2	204.4	35.1			
219.9	203.7	36.3			
221.8	203.0	37.5			
222.6	202.3	38.7			
				Vs30	223.0

UMBRIA-MARCHE, ITALY SMR Stations

Site ID 267CSC
NEHRP CLASS: C
Vs30 540 (m/s)
SUB-CLASS C+
Vs 80 993 (m/s)
Location

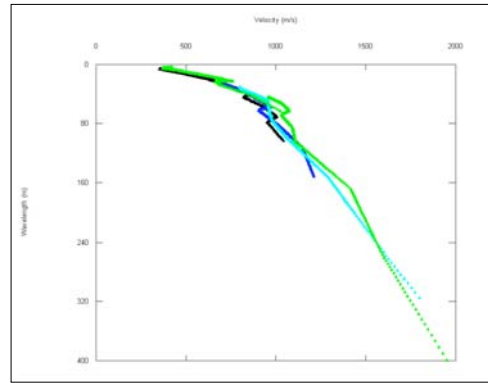
SMR Station CSC
State UMBRIA
Description CASCIA
POSITION CASCIA
LAT (N) 42.71875
LON (E) 13.012

Data Type SWEPT-SINE SASW
Investigators KAYEN, SCASSERRA
Date collected 20-Nov-2006

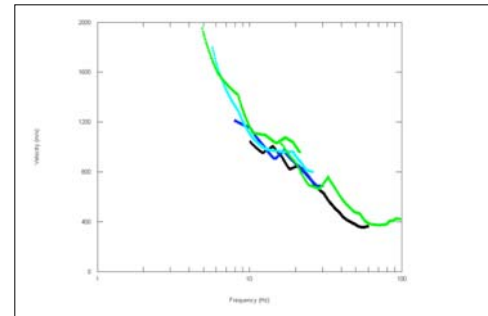
TEST METHODS PARALLEL-ARRAY SOURCES;
 CONTINUOUS HARMONIC
 WAVE-SASW; 3D AMBIENT
 MICROTREMOR ANALYSIS

PROJECT NAME UMBRIA-MARCHE
 SMR CHARACTERIZATION
SPONSOR PEER, UNIV OF ROME

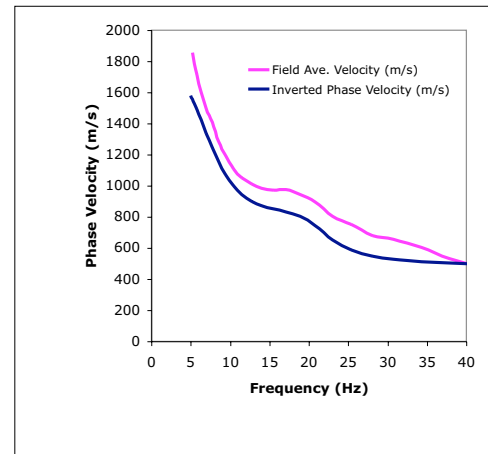
SITE SUB CLASS: Vs30 (m/s)
 A >1500 m/s
 B+ 1080 < Vs30 ≤ 1500 m/s
 B- 720 < Vs30 ≤ 1080 m/s
 C+ 540 < Vs30 ≤ 720 m/s
 C- 360 < Vs30 ≤ 540 m/s
 D+ 270 < Vs30 ≤ 360 m/s
 D- 180 < Vs30 ≤ 270 m/s
 E <180 m/s
 F Special Soil Conditions: Liquefiable soils; quick and high sensitivity clays; collapsible cemented soils; peats>3m; high (>75) PI soils thicker than 8m; soft/medium stiff clays thicker than 36m.



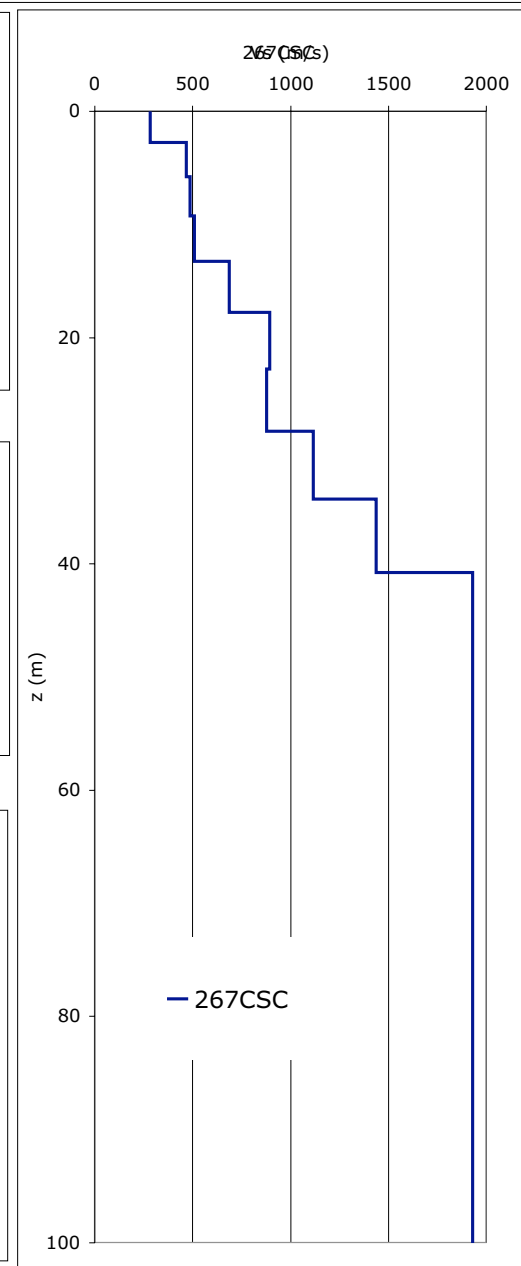
(A) Merged Field-LAMBDA Dispersion Curves



(B) Merged Field-Frequency Dispersion Curves



(C) Inversion-theoretical dispersion curve versus averaged field dispersion curve,



(D) Shear Wave Velocity SASW

267CSC	DISPERSION DATA			INVERSION PROFILE	
Site Disp. Vr (m/s)	Theoretical Disp. Vr (m/s)	Frequency (Hz)		Inversion Vs (m/s)	Depth (m)
				284.2	0.0
1950.0	1695.3	4.9		284.2	2.8
1859.0	1683.4	5.1		496.0	2.8
1718.7	1651.1	5.7		496.0	5.8
1603.5	1615.9	6.3		487.6	5.8
1499.4	1560.8	6.9		487.6	9.3
1410.3	1476.5	7.7		608.6	9.3
1288.8	1356.8	8.5		608.6	13.3
1199.5	1199.8	9.3		486.3	13.3
1111.1	1065.6	10.3		486.3	17.8
1054.4	990.7	11.4		894.5	17.8
1017.7	953.6	12.6		894.5	22.8
988.6	936.8	13.9		878.3	22.8
976.2	931.1	15.4		878.3	28.3
981.5	931.1	17.0		1116.4	28.3
948.8	932.0	18.8		1116.4	34.3
899.2	922.3	20.7		1438.4	34.3
809.1	841.5	23.0		1438.4	54.3
754.4	732.1	25.3		1620.8	54.3
683.2	664.6	28.0		1620.8	76.3
658.3	628.5	30.6		1843.4	76.3
607.3	591.4	34.2		1843.4	100.3
537.4	546.9	37.8		1950.0	100.3
478.5	484.6	41.7		1950.0	126.3
431.7	422.9	46.2		1950.0	126.3
402.0	372.8	51.0		1950.0	
377.3	346.4	56.4			
377.5	346.4	61.6			
217.0	205.2	33.9			
219.2	204.4	35.1			
219.9	203.7	36.3			
0.0	0.0	0.0			
0.0	0.0	0.0		Vs30	575.3

UMBRIA-MARCHE, ITALY SMR Stations

Site ID 268CSP
NEHRP CLASS: D
Vs30 339 (m/s)
SUB-CLASS D+
Vs 80 488 (m/s)
Location

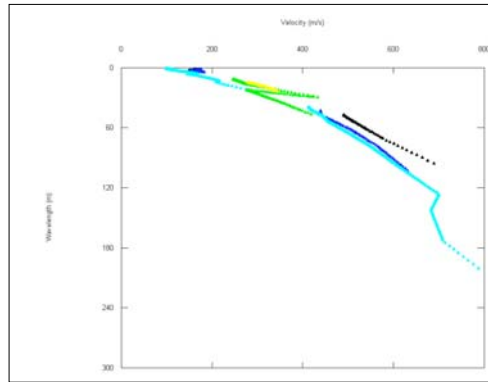
SMR Station CSP
State UMBRIA
Description CASCIA PETRUCCI APARTMENTS
POSITION CASCIA
LAT (N) 42.71788
LON (E) 13.0184

Data Type SWEPT-SINE SASW
Investigators KAYEN, SCASSERRA
Date collected 20-Nov-2006

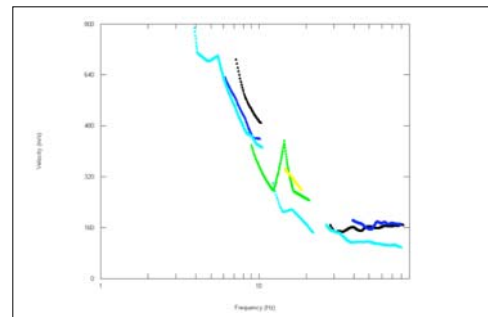
TEST METHODS PARALLEL-ARRAY SOURCES;
 CONTINUOUS HARMONIC
 WAVE-SASW; 3D AMBIENT
 MICROTREMOR ANALYSIS

PROJECT NAME UMBRIA-MARCHE
 SMR CHARACTERIZATION
SPONSOR PEER, UNIV OF ROME

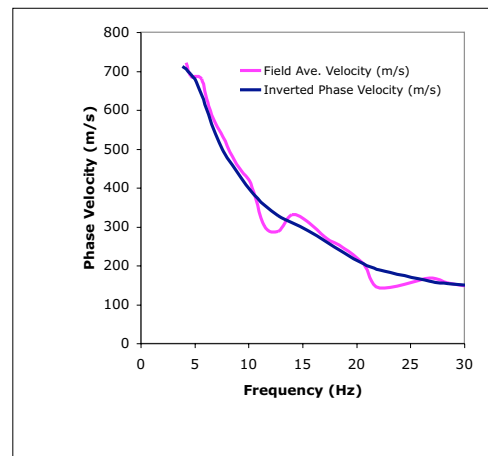
SITE SUB CLASS: Vs30 (m/s)
 A >1500 m/s
 B+ 1080 < Vs30 ≤ 1500 m/s
 B- 720 < Vs30 ≤ 1080 m/s
 C+ 540 < Vs30 ≤ 720 m/s
 C- 360 < Vs30 ≤ 540 m/s
 D+ 270 < Vs30 ≤ 360 m/s
 D- 180 < Vs30 ≤ 270 m/s
 E <180 m/s
 F Special Soil Conditions: Liquefiable soils; quick and high sensitivity clays; collapsible cemented soils; peats>3m; high (>75) PI soils thicker than 8m; soft/medium stiff clays thicker than 36m.



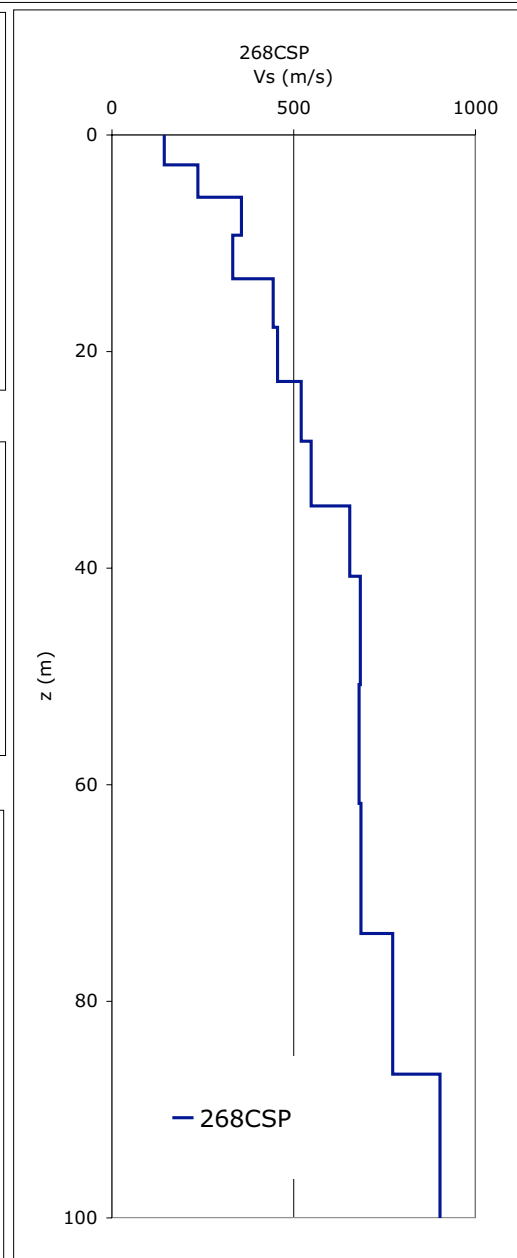
(A) Merged Field-LAMBDA Dispersion Curves



(B) Merged Field-Frequency Dispersion Curves



(C) Inversion-theoretical dispersion curve versus averaged field dispersion curve,



(D) Shear Wave Velocity SASW

268CSP	DISPERSION DATA			INVERSION PROFILE	
Site Disp. Vr (m/s)	Theoretical Disp. Vr (m/s)	Frequency (Hz)		Inversion Vs (m/s)	Depth (m)
				144.4	0.0
800.0	713.3	3.8		144.4	2.8
723.2	706.6	4.1		236.0	2.8
690.2	694.2	4.6		236.0	5.8
688.7	674.5	5.1		356.4	5.8
681.3	640.5	5.6		356.4	9.3
613.1	590.1	6.2		331.9	9.3
567.5	540.8	6.9		331.9	13.3
533.3	497.9	7.6		443.4	13.3
483.7	461.5	8.4		443.4	17.8
445.1	425.6	9.3		455.0	17.8
413.4	394.1	10.2		455.0	22.8
362.7	356.2	11.4		520.2	22.8
349.2	330.3	12.7		520.2	28.3
333.4	311.5	13.9		547.5	28.3
314.1	291.3	15.4		547.5	34.3
273.4	264.2	17.1		653.7	34.3
247.0	234.8	18.8		653.7	40.8
206.2	206.5	20.6		683.4	40.8
184.8	189.9	22.1		683.4	50.8
169.4	161.1	26.7		680.6	50.8
156.9	155.6	28.4		680.6	61.8
145.7	149.4	31.3		685.1	61.8
136.9	145.1	34.6		685.1	73.8
138.6	142.0	38.6		772.6	73.8
146.3	140.2	42.5		772.6	86.8
143.2	138.9	47.0		901.6	86.8
141.9	138.1	51.9		901.6	100.0
145.5	137.5	57.5			
144.8	137.2	63.7			
143.8	137.2	70.5			
0.0	0.0	0.0			
0.0	0.0	0.0		Vs30	338.9

UMBRIA-MARCHE, ITALY SMR Stations

Site ID 269SLW
NEHRP CLASS: C
Vs30 509 (m/s)
SUB-CLASS C-
Vs 80 713 (m/s)
Location

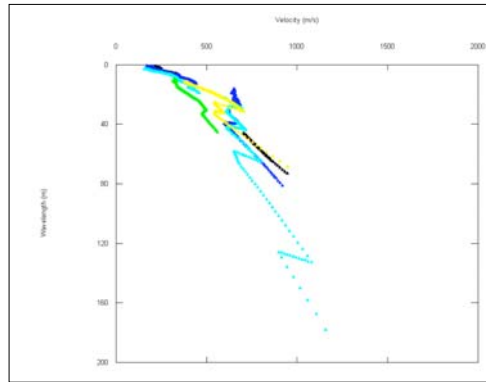
SMR Station SLW
State UMBRIA
Description
POSITION SELLANO WEST
LAT (N) 42.886
LON (E) 12.922

Data Type SWEPT-SINE SASW
Investigators KAYEN, SCASSERRA
Date collected 21-Nov-2006

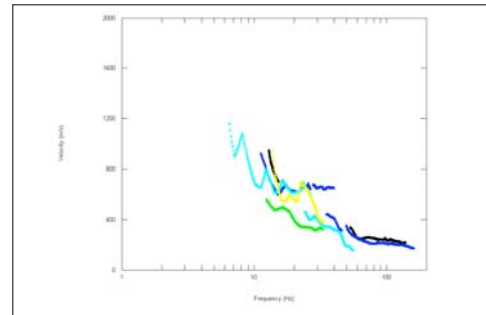
TEST METHODS PARALLEL-ARRAY SOURCES;
 CONTINUOUS HARMONIC
 WAVE-SASW; 3D AMBIENT
 MICROTREMOR ANALYSIS

PROJECT NAME UMBRIA-MARCHE
 SMR CHARACTERIZATION
SPONSOR PEER, UNIV OF ROME

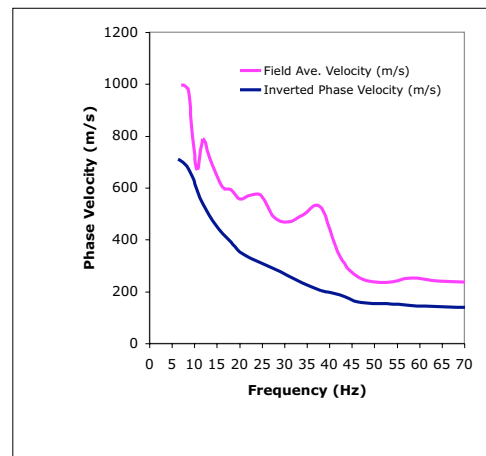
SITE SUB CLASS: Vs30 (m/s)
 A >1500 m/s
 B+ 1080 < Vs30 ≤ 1500 m/s
 B- 720 < Vs30 ≤ 1080 m/s
 C+ 540 < Vs30 ≤ 720 m/s
 C- 360 < Vs30 ≤ 540 m/s
 D+ 270 < Vs30 ≤ 360 m/s
 D- 180 < Vs30 ≤ 270 m/s
 E <180 m/s
 F Special Soil Conditions: Liquefiable soils; quick and high sensitivity clays; collapsible cemented soils; peats>3m; high (>75) PI soils thicker than 8m; soft/medium stiff clays thicker than 36m.



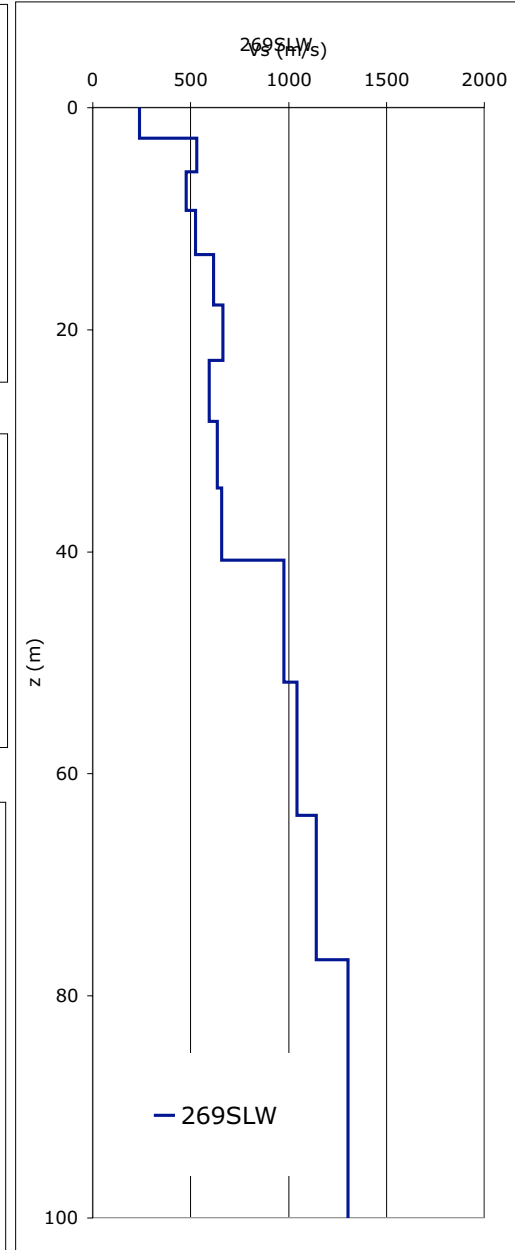
(A) Merged Field-LAMBDA Dispersion Curves



(B) Merged Field-Frequency Dispersion Curves



(C) Inversion-theoretical dispersion curve versus averaged field dispersion curve,



(D) Shear Wave Velocity SASW

269SLW	DISPERSION DATA			INVERSION PROFILE	
Site Disp. Vr (m/s)	Theoretical Disp. Vr (m/s)	Frequency (Hz)		Inversion Vs (m/s)	Depth (m)
1150.0	713.3	6.2		239.9	0.0
998.7	706.6	6.9		239.9	2.8
995.2	694.2	7.7		530.8	2.8
973.9	674.5	8.5		530.8	5.8
785.6	640.5	9.5		476.2	5.8
672.7	590.1	10.6		476.2	9.3
789.0	540.8	11.8		523.9	9.3
721.3	497.9	13.1		523.9	13.3
662.8	461.5	14.5		616.0	13.3
601.9	425.6	16.1		616.0	17.8
595.8	394.1	18.0		664.3	17.8
559.9	356.2	20.0		664.3	22.8
574.2	330.3	22.2		594.8	22.8
570.1	311.5	24.8		594.8	28.3
489.5	291.3	27.5		636.6	28.3
469.4	264.2	30.6		636.6	34.3
496.0	234.8	33.9		659.2	34.3
527.0	206.5	38.0		659.2	40.8
338.1	189.9	42.2		974.9	40.8
254.6	161.1	46.7		974.9	51.8
236.9	155.6	52.5		1041.6	51.8
254.6	149.4	57.8		1041.6	63.8
242.5	145.1	64.6		1141.5	63.8
236.7	142.0	72.0		1141.5	76.8
228.8	140.2	80.0		1304.8	76.8
227.5	138.9	88.9		1304.8	100.0
225.2	138.1	99.1			
220.9	137.5	110.3			
210.9	137.2	122.7			
201.8	137.2	135.6			
0.0	0.0	0.0			
0.0	0.0	0.0		Vs30	509.1

UMBRIA-MARCHE, ITALY SMR Stations

Site ID 270MTL
NEHRP CLASS: C
Vs30 437 (m/s)
SUB-CLASS C-
Vs 80 767 (m/s)
Location

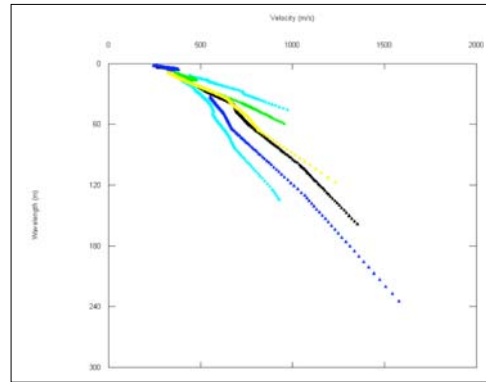
SMR Station MTL
State MARCHE'
Description MATELICA
POSITION
LAT (N) 43.24841
LON (E) 13.0079

Data Type SWEPT-SINE SASW
Investigators KAYEN, SCASSERRA
Date collected 21-Nov-2006

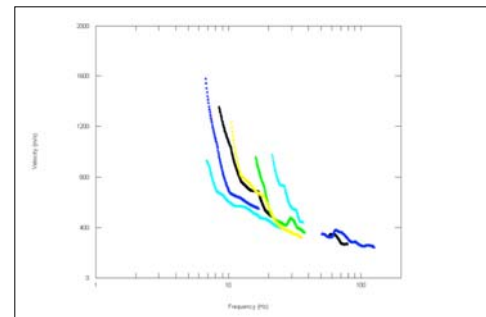
TEST METHODS PARALLEL-ARRAY SOURCES;
 CONTINUOUS HARMONIC
 WAVE-SASW; 3D AMBIENT
 MICROTREMOR ANALYSIS

PROJECT NAME UMBRIA-MARCHE
 SMR CHARACTERIZATION
SPONSOR PEER, UNIV OF ROME

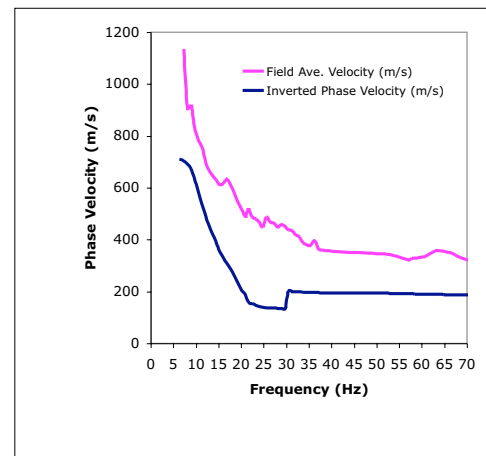
SITE SUB CLASS: Vs30 (m/s)
 A >1500 m/s
 B+ 1080 < Vs30 ≤ 1500 m/s
 B- 720 < Vs30 ≤ 1080 m/s
 C+ 540 < Vs30 ≤ 720 m/s
 C- 360 < Vs30 ≤ 540 m/s
 D+ 270 < Vs30 ≤ 360 m/s
 D- 180 < Vs30 ≤ 270 m/s
 E <180 m/s
 F **Special Soil Conditions:** Liquefiable soils; quick and high sensitivity clays; collapsible cemented soils; peats>3m; high (>75) PI soils thicker than 8m; soft/medium stiff clays thicker than 36m.



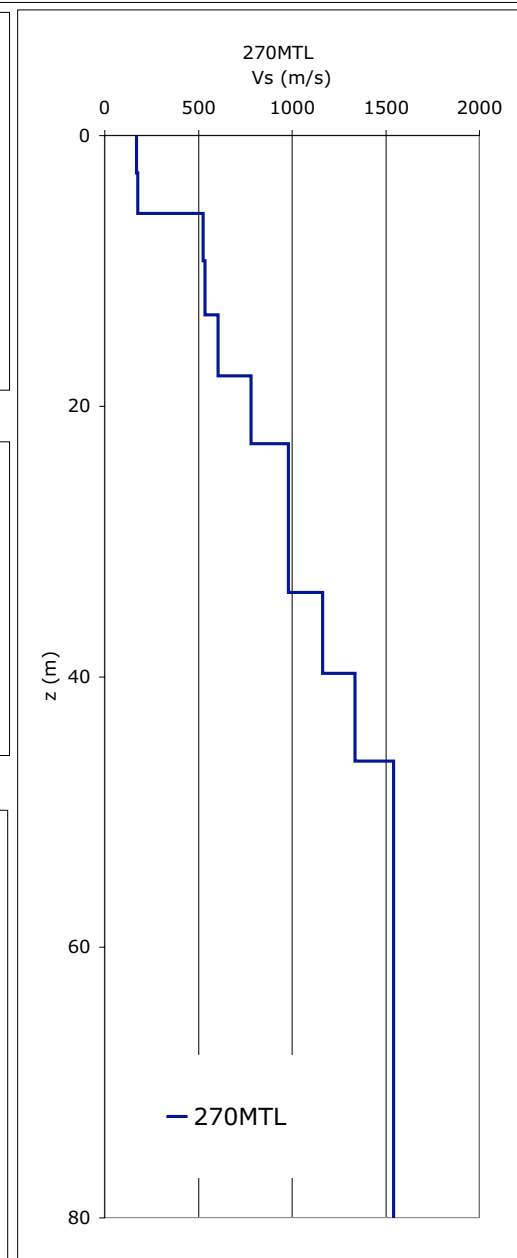
(A) Merged Field-LAMBDA Dispersion Curves



(B) Merged Field-Frequency Dispersion Curves



(C) Inversion-theoretical dispersion curve versus averaged field dispersion curve,



(D) Shear Wave Velocity SASW

270MTL	DISPERSION DATA			INVERSION PROFILE	
Site Disp. Vr (m/s)	Theoretical Disp. Vr (m/s)	Frequency (Hz)		Inversion Vs (m/s)	Depth (m)
				170.7	0.0
1570.0	713.3	6.2		170.7	2.8
1136.8	706.6	7.2		175.4	2.8
909.8	694.2	7.9		175.4	5.8
921.6	674.5	8.8		524.7	5.8
839.2	640.5	9.5		524.7	9.3
789.1	590.1	10.3		535.9	9.3
761.1	540.8	11.1		535.9	13.3
704.2	497.9	11.9		605.2	13.3
672.7	461.5	12.7		605.2	17.8
650.9	425.6	13.5		779.2	17.8
633.2	394.1	14.3		779.2	22.8
615.3	356.2	15.1		978.6	22.8
619.0	330.3	16.0		978.6	28.3
636.5	311.5	16.7		978.6	28.3
614.1	291.3	17.5		978.6	33.8
583.3	264.2	18.3		1164.3	33.8
546.8	234.8	19.1		1164.3	39.8
517.3	206.5	20.0		1336.7	39.8
517.3	189.9	20.8		1336.7	46.3
517.6	161.1	21.5		1541.6	46.3
489.9	155.6	22.3		1541.6	80.0
481.3	149.4	23.2			
467.0	145.1	24.0			
451.9	142.0	24.7			
451.9	140.2	25.6			
451.9	138.9	26.4			
451.9	138.1	27.2			
452.2	137.5	27.9			
459.6	137.2	28.7			
454.4	137.2	29.6			
438.3	203.0	30.4			
436.1	202.3	31.2			
				Vs30	437.2

APPENDIX B

Sample of Recording-Station Information Form

STATION: Auletta

GEOGRAPHICAL LOCATION



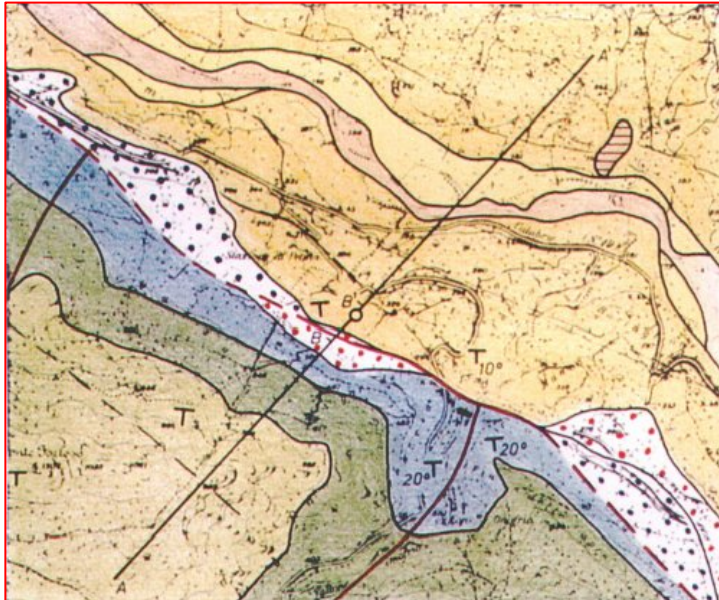
INSTRUMENT INFO

latitude	40° 33' 21.60"
longitude	15° 23' 42.00"
owner	DPC
type	analogue
housing	ENEL cabin
working (Y/N)	N
activated	march 24, 1975
dismissed	?



GEOLOGY

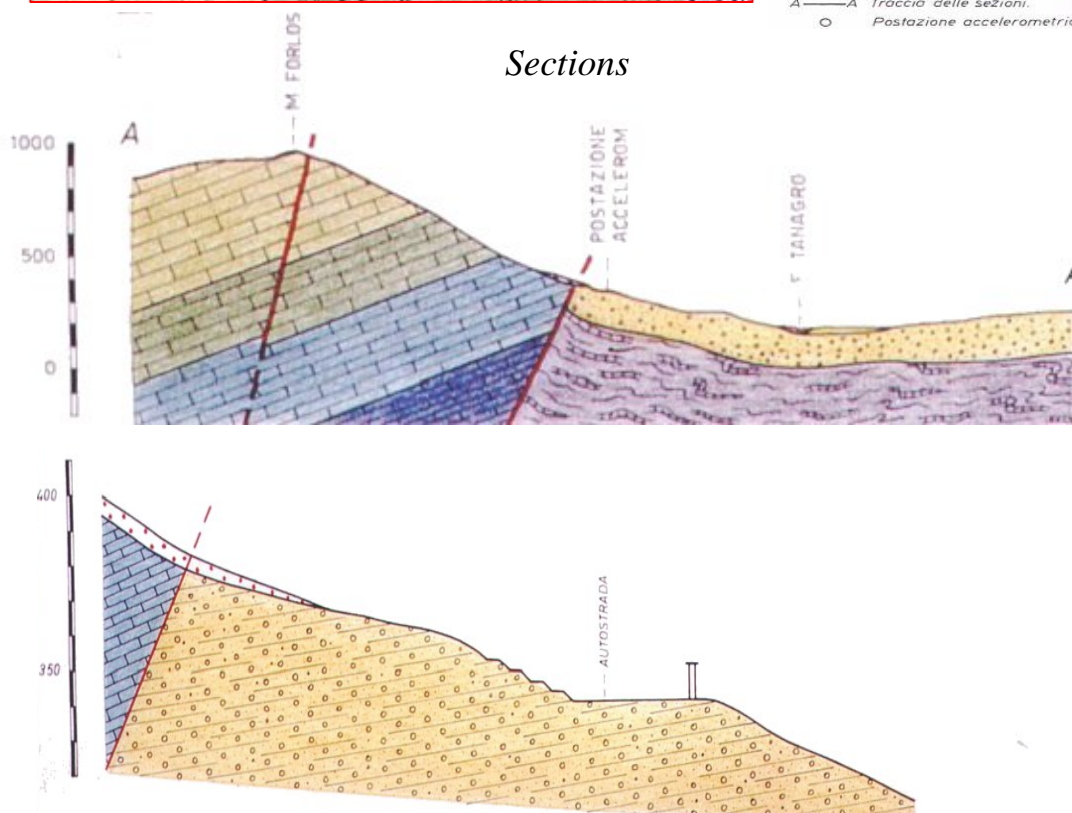
Geologic map (1:100.000)



LEGEND

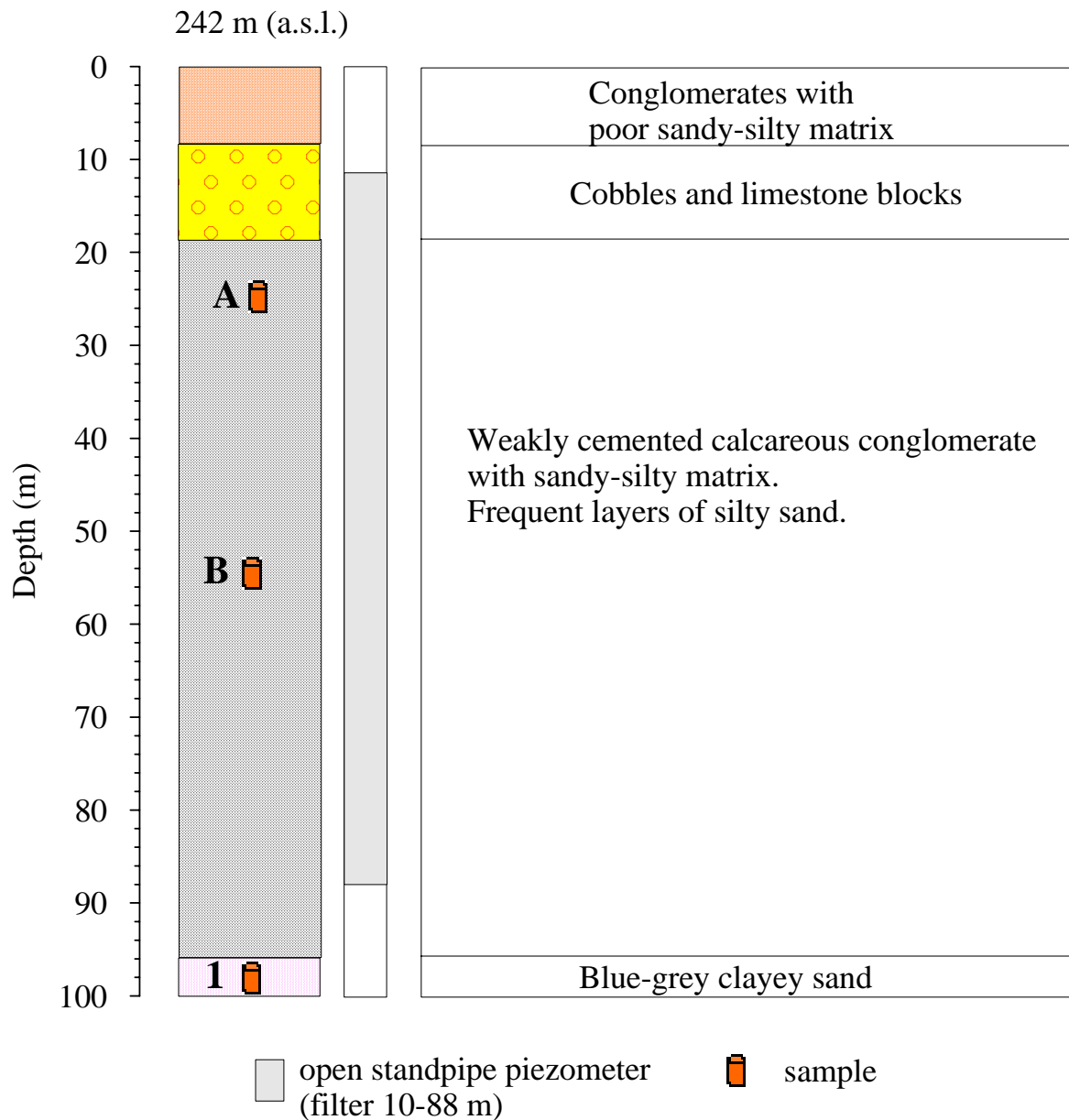
- Alluvioni attuali e di fondovalle (a), alluvioni terrazzate (b) (Olocene)
- Detrito di falda (Olocene).
- Travertino compatto o terroso (Pleistocene).
- Detriti di falda antichi e breccie di pendio cementate (Pleistocene).
- Conglomerati poligenici a cemento sabbioso-argilloso, di origine deltizia e lacustre (Plio-Pleistocene).
- UNITÀ ALBURNO-CERVATI**
(Piattaforma interna campano-lucana)
- Calcare grigio-chiaro con resti di rudiste, in banchi e strati (Senoniano-Turoniano).
- Calcari avana in banchi e strati con intercalazioni di dolomie grigie fetide (Cenomaniano-Neocomiano).
- Calcari pseudocristallini e pseudoolitici, di color grigio, avana e biancastro Giurassico (Malm-Dogger).
- Calcari granulosi grigio-avana, raramente rossicci, nettamente stratificati, talora leggermente siliciferi (Lias).
- COMPLESSO SICILIDE**
- Argille variscali. Alternanze di marnosisti con abbondanti intercalazioni di calcari tipo "Alberese" e "Palombino" e arenarie (Miocene?)
- Faglie.
- A—A' Traccia delle sezioni.
- O Postazione accelerometrica.

Sections



Reference: Geologic monography of ENEL recording stations

SINTHETIC STRATIGRAPHIC PROFILE



Reference: Palazzo S. (1991). PROGETTO IRPINIA. Elaborazione dei risultati delle indagini geotecniche in sito e in laboratorio eseguite nelle postazioni accelerometriche di : Bagnoli Irpino, Calitri, Auletta, Bisaccia, Bovino, Brienza, Rionero in Vulture, Sturmo, Benevento e Mercato San Severino. Ottobre 1991.

LABORATORY TEST

Tested samples

Sample code	Depth (m)	Soil type	Test type*
A	25,9	conglomerates	CL
B	51,4	conglomerates	CL
1	99,1	clayey sands	CL, UU, BE

* CL = Classification; UU = Uncosolidated undrained triaxial; BE = Bender elements

Index properties

Sample	Depth (m)	Gravel (%)	Sand (%)	Silt (%)	Clay (%)	γ (kN/m ³)	w (%)	w _L (%)	PI
A	25,9	59	22	7	10	-	10	55*	38*
B	51,4	90	6	2	1	-	6	-	-
1	99,1	-	26	38	36	21	18	39	21

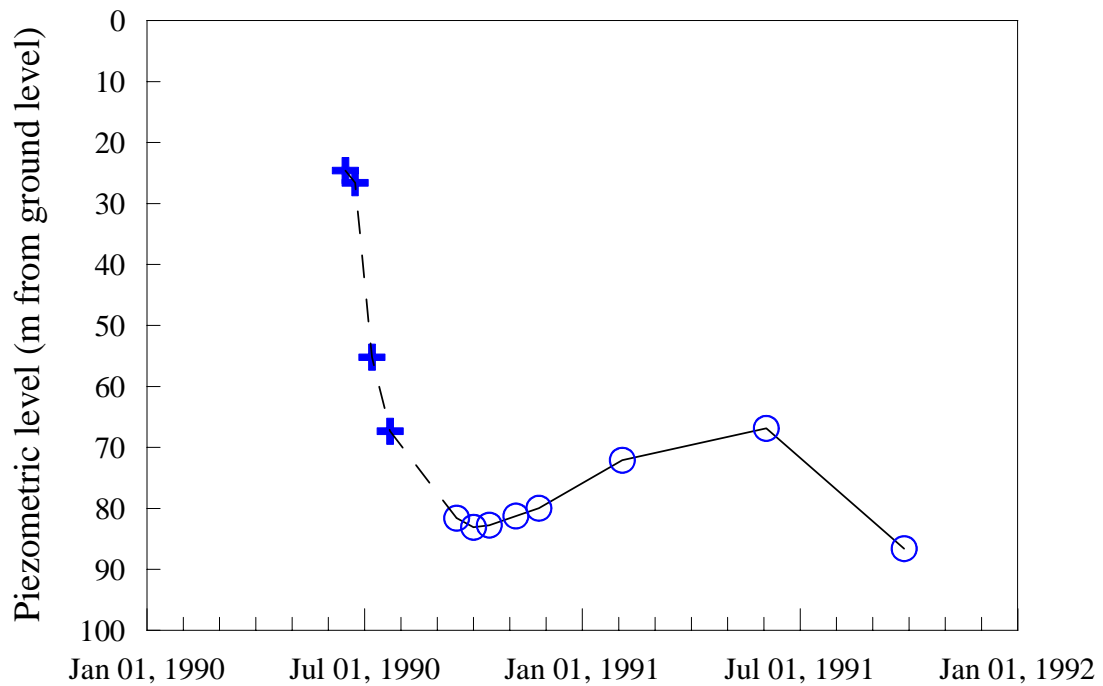
* only on fine fraction

Mechanical properties

Sample	Depth (m)	Test type	c _u (MPa)	G ₀ (MPa)	V _s (m/s)
1	99,1	UU	0,2-0,9	-	-
1	99,1	BE	-	190	302

Reference: Palazzo S. (1991). PROGETTO IRPINIA. Elaborazione dei risultati delle indagini geotecniche in sito e in laboratorio eseguite nelle postazioni accelerometriche di : Bagnoli Irpino, Calitri, Auletta, Bisaccia, Bovino, Brienza, Rionero in Vulture, Sturno, Benevento e Mercato San Severino. Ottobre 1991.

PIEZOMETRIC MEASUREMENTS

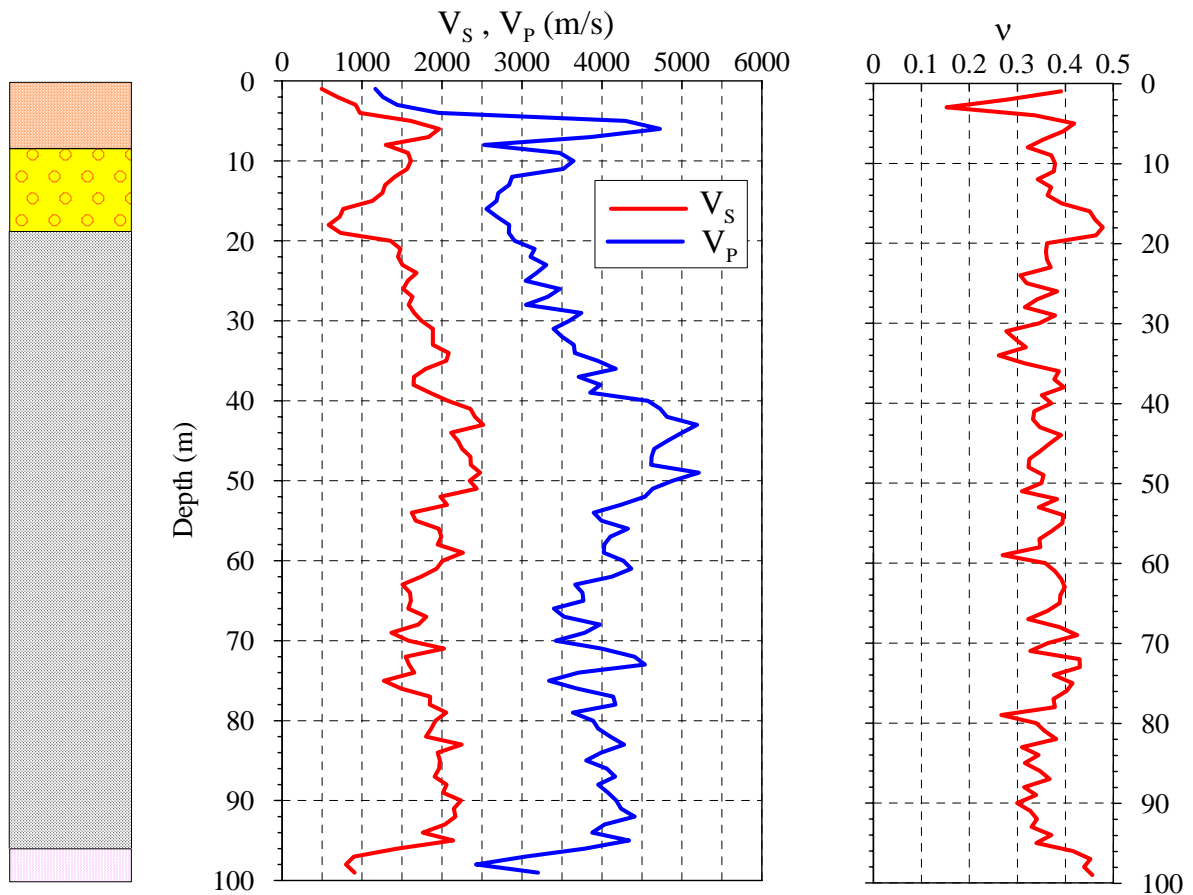


+ Measurements probably affected by disturbance from construction works

Reference: Palazzo S. (1991). PROGETTO IRPINIA. Elaborazione dei risultati delle indagini geotecniche in sito e in laboratorio eseguite nelle postazioni accelerometriche di : Bagnoli Irpino, Calitri, Auletta, Bisaccia, Bovino, Brienza, Rionero in Vulture, Sturmo, Benevento e Mercato San Severino. Ottobre 1991.

IN SITU TEST: CROSS-HOLE

V_S , V_P and ν profiles



Note: The Poisson's ratio ν has been calculated as
$$\nu = \frac{\frac{1}{2} \left(\frac{V_P}{V_S} \right)^2 - 1}{\left(\frac{V_P}{V_S} \right)^2 - 1}$$

Reference: Palazzo S. (1991). PROGETTO IRPINIA. Elaborazione dei risultati delle indagini geotecniche in sito e in laboratorio eseguite nelle postazioni accelerometriche di : Bagnoli Irpino, Calitri, Auletta, Bisaccia, Bovino, Brienza, Rionero in Vulture, Sturno, Benevento e Mercato San Severino. Ottobre 1991.